



**HAL**  
open science

# Predictive control of two synchronous machines in parallel supplied by a standard three phase static converter

Ngoc Linh Nguyen

► **To cite this version:**

Ngoc Linh Nguyen. Predictive control of two synchronous machines in parallel supplied by a standard three phase static converter. Other. Institut National Polytechnique de Toulouse - INPT, 2013. English. NNT : 2013INPT0043 . tel-04286994

**HAL Id: tel-04286994**

**<https://theses.hal.science/tel-04286994>**

Submitted on 15 Nov 2023

**HAL** is a multi-disciplinary open access archive for the deposit and dissemination of scientific research documents, whether they are published or not. The documents may come from teaching and research institutions in France or abroad, or from public or private research centers.

L'archive ouverte pluridisciplinaire **HAL**, est destinée au dépôt et à la diffusion de documents scientifiques de niveau recherche, publiés ou non, émanant des établissements d'enseignement et de recherche français ou étrangers, des laboratoires publics ou privés.



Université  
de Toulouse

# THÈSE

## En vue de l'obtention du DOCTORAT DE L'UNIVERSITÉ DE TOULOUSE

**Délivré par :**  
Institut National Polytechnique de Toulouse (INP Toulouse)

**Discipline ou spécialité :**

Génie Electrique

---

**Présentée et soutenue par :**

M. Ngoc Linh NGUYEN

**le :** Mardi 18 Juin 2013

**Titre :**

Commande Prédicative de deux Machines Synchrones alimentées en parallèle  
par un Onduleur de Tension Triphasé

---

**Ecole doctorale :**  
Génie Electrique, Electronique et Télécommunications (GEET)

**Unité de recherche :**  
Laboratoire LAPLACE - UMR5213

**Directeur(s) de Thèse :**  
Maurice FADEL et Ana LLOR

**Rapporteurs :**  
Santiago Gómez ARNALTES et Emmanuel GODOY

**Membre(s) du jury :**  
Santiago Gómez ARNALTES (Rapporteur)  
Emmanuel GODOY (Rapporteur)  
Mohamed BOUSSAK (Examinateur)  
Maurice FADEL (Directeur de Thèse)  
Ana Maria LLOR (Co-directrice de Thèse)



# Abstract

Nowadays, embedded systems are more and more numerous which strongly impact energy conversion systems. The associated constraints are masses and losses reductions in order to improve energy efficiency in the conversion chain. This is the case in the aeronautics field where the concept of "More Electric Aircraft" now becomes a reality. Therefore, the permanent magnet synchronous machine becomes an excellent actuator due to its high power density, its low maintenance cost and its dynamic qualities.

When these machines are associated to carry out cooperative functions (for example, in flight surfaces) the embedded mass can still be reduced by sharing power electronics. It is precisely in this context where our work has been developed, power reduced structures based in power electronics, able to feed two or more electric machines in parallel and providing control laws to improve energy efficiency.

We have worked more specifically in the Predictive Control of two Synchronous Machines connected in parallel connected to a 2-Level 3-Phase Converter. These machines have identical characteristics and must follow the same speed profile with a load torque which can be different and, in any case, independent.

The predictive control approach leads us to consider the voltage inverter as a device with a finite number of control states. We need to select at each time instant the best control solution to minimize a cost function. This cost function related to one or two machines, is composed of a term representing the quality of the produced torque ( $I_q$  current) and another which represents the quality of the conversion via produced losses ( $I_d$  current).

This approach works naturally in variable switching frequency. Thus, the document considers different studied solutions, showing the limits of such an approach both dynamically and in terms of losses. To improve this basic solution we develop an approach based on virtual vectors. These virtual vectors increase the control possibilities and lead to a constant switching frequency operation through a SVM modulation. The research algorithm of an optimum virtual vector is proposed and applied to a system composed by two low-power machines. The different proposals are validated through numerical simulation and consolidated by experimental results.

---

---

## *Key words:*

- Multi-machine system
- Open loop stability
- Shared structures
- Permanent Magnet Synchronous Machines
- Predictive control
- Direct torque control



# Résumé

De nos jours, les systèmes embarqués sont de plus en plus nombreux ce qui impacte fortement les systèmes de conversion de l'énergie. Les contraintes associées se traduisent par une réduction des masses et des pertes afin d'améliorer l'efficacité énergétique de la chaîne de conversion. C'est le cas dans le domaine de l'aéronautique où le concept "d'avion plus électrique" devient aujourd'hui une réalité. C'est ainsi que la machine synchrone à aimants permanents devient un acteur d'excellence de par sa puissance massique importante, son faible coût de maintenance et ses qualités dynamiques.

Lorsque ces machines sont associées pour remplir des fonctions coopératives (surfaces de vol par exemple) on peut encore réduire la masse embarquée en mutualisant l'électronique de puissance. C'est précisément dans ce cadre que se situe notre travail, en proposant des structures d'alimentation réduites, à base d'électronique de puissance, permettant d'alimenter deux ou plusieurs machines électriques en parallèle et en proposant des lois de commande visant à améliorer le rendement énergétique.

Nous nous sommes intéressés plus particulièrement à la Commande Prédicative de deux Machines Synchrones alimentées en parallèle par un Onduleur de Tension Triphasé. Ces machines ont des caractéristiques identiques et doivent suivre un même profil de vitesse avec un couple de charge différent et en tout cas indépendant.

L'approche commande prédictive nous conduit à considérer l'onduleur de tension comme un dispositif ayant un nombre fini d'états de commande. Nous devons sélectionner à chaque instant la meilleure solution de commande permettant de minimiser une fonction coût. Cette fonction coût, relative à une ou deux machines, est composée d'une partie représentant la qualité du couple produit (courant  $I_q$ ) et d'une autre partie représentant la qualité de la conversion via les pertes produites (courant  $I_d$ ).

Cette approche opère naturellement à fréquence de découpage variable. Ainsi le document fait état de différentes solutions étudiées montrant les limites d'une telle approche tant sur le plan dynamique que sur le plan des pertes. Pour améliorer cette solution de base nous développons une approche basée sur l'utilisation de vecteurs virtuels. Ces vecteurs virtuels augmentent les possibilités de commande et conduisent à un fonctionnement à fréquence constante au travers d'une modulation de type SVM. La recherche d'un vecteur virtuel optimal est proposée et appliquée sur un dispositif composé de deux machines de faible puissance. Les différentes propositions sont validées par la voie de la simulation numérique et consolidées par des résultats expérimentaux.

---

---

## *Mots clés:*

- Système multi-machines
- Machine synchrone à aimants permanents
- Stabilité en boucle ouverte
- Commande prédictive
- Mutualisation
- Commande directe de couple



# DEDICATION

This dissertation is dedicated to my late father, *NGUYEN Xuan Ngoc*, and to my mother, *TRUONG Thi Quynh Mai*, who always had confidence in me and offered me encouragement and support in all my endeavors

It is also dedicated to my darling wife, *THUONG Phuong Nga*, and my lovely unborn child for their care, love, understanding, and patience



# Preface and Acknowledgements

The research study reported in this thesis has been performed in the Laboratory of Plasma and Conversion of Energy (LAPLACE), ENSEEIHT, INP Toulouse. The work has been carried out in the period from April 2010 to April 2013 under the supervision of Professor INPT Maurice FADEL and Associate Professor INPT Ana LLOR.

To achieve these results, besides my own efforts, it is impossible to lack of the assistance, very kind support as well as the encouragements of many people. I would like to thank all of them for their contribution in my work.

I wish to express my deep gratitude to my supervisors, Professor Maurice Fadel and Professor Ana Llor, for the guidance, encouragement and support during my graduate study. Their creative thinking, knowledge and expertise were the “power supply” and “feedback” of my conducted researches.

I would like to thank President of the University of Toulouse – Marie France Barthet, Professor INPT Maria DAVID for their administrative support,

I am also grateful to Dr. Damien Didart for his kind advices and discussions for the experiment in this thesis.

I would like to express my appreciation to the members of the thesis defense committee, Professor Santiago Gómez Añaltes from University of Madrid, Professor Emmanuel Godoy from École Supérieure d'électricité (SUPELEC) for their interest in my research work and the time and effort in considering this thesis.

The USTH program is gratefully acknowledged for its financial support to this research study.

I would like to thank all of my colleagues: Celine, Julie, Etienne, Trung, Ha, Thiet, Think ... who always support, help and encourage me during the past time.

Toulouse, May 2013

NGUYEN Ngoc Linh



# Table of contents

<b>Abstract.....</b>	<b>i</b>
<b>Résumé.....</b>	<b>iii</b>
<b>DEDICATION .....</b>	<b>v</b>
<b>Preface and Acknowledgements .....</b>	<b>vii</b>
<b>Table of contents .....</b>	<b>ix</b>
<b>List of symbols.....</b>	<b>xiii</b>
<b>List of abbreviations .....</b>	<b>xv</b>
<b>General Introduction.....</b>	<b>1</b>
<b>Chapter 1 PMSM with Multi-Machine Systems.....</b>	<b>5</b>
1.1 Introduction .....	6
1.2 Evolution of permanent magnet synchronous machine (PMSM).....	7
1.2.1 Small power applications of PMSM.....	8
1.2.2 Medium power applications of PMSM .....	9
1.2.3 High power applications of PMSM.....	10
1.3 Multi-machine system in aeronautic field .....	11
1.3.1 The idea of sharing structures.....	11
1.3.2 Flight control systems.....	12
1.3.2.1 Introduction .....	12
1.3.2.2 Electromechanical actuators (EMAs).....	14
1.3.2.3 Shared structures .....	15
1.4 Typical structures of multi-machine system.....	16
1.4.1 Classical structure.....	16
1.4.2 Presentation of the shared structures .....	18
1.4.2.1 Sharing common legs structure: n machines with 2n legs .....	18
1.4.2.2 Sharing the midpoint structure: n machines and 2n legs.....	20
1.4.2.3 Mixed structure: $\frac{3n}{2}$ legs for n machines.....	22
1.4.2.4 Parallel structure: 3 legs for n machines .....	23
1.4.2.5 Some other structures .....	24
1.4.2.6 Comparison of these different structures .....	24

1.5	Conclusions.....	26
<b>Chapter 2 Mono-Inverter Dual-Parallel PMSM drive system .....</b>		<b>27</b>
2.1	Introduction.....	28
2.2	Generalities about PMSM drive system .....	29
2.2.1	Principle of operation of PMSM .....	30
2.2.2	Modeling of PMSMs .....	31
2.2.2.1	Electromechanical description.....	31
2.2.2.2	Continuous model of PMSM in d-q reference frame.....	34
2.2.3	Stability analysis of PMSM.....	36
2.2.4	A three-phase two-level voltage inverter.....	39
2.3	Control strategies for PMSM drive.....	39
2.3.1	Field oriented control.....	40
2.3.2	Direct Torque Control (DTC).....	41
2.3.3	Direct Predictive Torque Control (DPTC) .....	44
2.4	Control structure for Mono-inverter Dual-parallel PMSM system .....	46
2.4.1	Master-slave structure.....	46
2.4.1.1	General description.....	46
2.4.1.2	Consequence due to a load variation.....	47
2.4.1.3	The choice of master machine.....	48
2.4.1.4	Conclusions .....	52
2.4.2	Direct torque control (DTC) for mono-inverter dual-parallel PMSM.....	52
2.4.2.1	General description.....	53
2.4.2.2	Optimal switching table for two machines.....	55
2.4.2.3	Simulation tests .....	61
2.5	Conclusions.....	64
<b>Chapter 3 Predictive Torque Control with Mono-Inverter Dual-Parallel PMSM.....</b>		<b>65</b>
3.1	Introduction.....	66
3.2	PMSM under voltage supply mode .....	67
3.2.1	Steady state calculation .....	67
3.2.2	Small deviation model.....	72
3.3	PTC for Mono-Inverter Dual-parallel PMSM .....	74
3.3.1	Description.....	74
3.3.2	R-S-T discrete controller .....	75
3.3.2.1	Introduction .....	75
3.3.2.2	R-S-T anti-windup Speed/Torque controller.....	76

## Table of contents

3.3.3	Predictive Torque Control.....	77
3.3.3.1	Discrete model of considered system.....	78
3.3.3.2	Cost function.....	81
3.3.3.3	Predictive control strategies.....	83
3.4	Direct Predictive Torque Control (DPTC).....	84
3.4.1	Principle.....	85
3.4.2	Simulation results for DPTC.....	86
3.4.3	Relation between the ripple and the sampling time of DPTC.....	90
3.4.4	Optimization problem.....	91
3.4.5	Conclusions.....	94
3.5	Predictive Torque Control – “Split and Seek” (PTC-SS).....	95
3.5.1	Predictive model in ( $\alpha\beta$ ) frame:.....	96
3.5.2	“Split and Seek” approach.....	96
3.5.2.1	Angle seeking.....	97
3.5.2.2	Magnitude seeking.....	99
3.5.3	Simulation results for PTC-SS.....	101
3.5.3.1	A comparison with DPTC.....	101
3.6	Conclusions.....	105
<b>Chapter 4 The experimental platform.....</b>		<b>107</b>
4.1	General description.....	107
4.2	Motor coupling system.....	109
4.3	Power supply system.....	112
4.3.1	Power supply system.....	112
4.3.2	Power converter.....	113
4.4	Measurement and control system.....	113
4.4.1	Measurement interfaces.....	113
4.4.1.1	Current measurement.....	113
4.4.1.2	Mechanical position measurement.....	113
4.4.1.3	Speed calculation.....	115
4.4.2	dSPACE system.....	116
4.4.2.1	dSPACE DS1103 board.....	116
4.4.2.2	MATLAB/Simulink and Control-desk.....	116
4.5	Digital control implementation.....	117
4.5.1	Speed controller.....	118
4.5.2	Predictive torque controller.....	118

4.6	Experiment's results .....	119
4.6.1	Test with one machine.....	119
4.6.2	Test with two machines in parallel.....	122
4.6.3	Test with two machines in parallel under master/slave configuration ..	125
4.7	Conclusions.....	127
<b>Conclusions and Perspectives .....</b>		<b>129</b>
<b>Bibliography .....</b>		<b>133</b>
<b>Résumé en français .....</b>		<b>141</b>
<b>Appendix A "FMINCON" and SVM technique .....</b>		<b>167</b>
A.1	Using FMINCON to solve the optimal problem: .....	168
A.2	Space vector modulation (SVM) .....	169
A.2.1	Determine $V_\alpha$ , $V_\beta$ , $V_{ref}$ and angle $\alpha$ .....	170
A.2.2	Determine time duration $t_1$ , $t_2$ and $t_{0/7}$ .....	170
A.2.3	Determine the switching time of $(s_A, s_B, s_C)$ .....	171
<b>Appendix B Technical data of the experimental.....</b>		<b>175</b>
B.1	The auto-transformer .....	176
B.2	The SEMIKRON device.....	176
B.2.1	The rectifier.....	176
B.2.2	The inverter.....	176
B.3	The PMSM.....	178
B.3.1	The motor .....	178
B.3.2	The holding brake.....	178
B.3.3	The resolver.....	179
B.4	Mechanical properties.....	180
B.4.1	Load machine .....	180
B.4.2	The SEC-AC-305 (Smart Electromotor Controller).....	180
B.4.3	Spindle axes with recirculating ball bearing guide.....	183
B.5	Hardware part of the control.....	185
B.5.1	DS1103 PPC Controller Board.....	185
B.5.2	Current sensors .....	188
B.5.3	Limit switches.....	190
B.6	The Human-Machine Interface.....	191
<b>List of figures.....</b>		<b>193</b>
<b>List of tables.....</b>		<b>197</b>

## List of symbols

$\psi_p$	Permanent magnet flux ( $Wb$ )
$\psi_s$	Flux linkage of machine ( $Wb$ )
$\psi_\alpha$	Flux linkage of machine in $\alpha$ -axis ( $Wb$ )
$\psi_\beta$	Flux linkage of machine in $\beta$ -axis ( $Wb$ )
$\omega_m$	Mechanical speed of motor ( $rad. s^{-1}$ )
$\omega_{m1}$	Mechanical speed of motor 1 ( $rad. s^{-1}$ )
$\omega_{m2}$	Mechanical speed of motor 2 ( $rad. s^{-1}$ )
$\omega_e$	Electrical speed of motor ( $rad. s^{-1}$ )
$\omega_{e1}$	Electrical speed of motor 1 ( $rad. s^{-1}$ )
$\omega_{e2}$	Electrical speed of motor 2 ( $rad. s^{-1}$ )
$\omega_{ref}$	Mechanical reference speed ( $rad. s^{-1}$ )
$\omega_{e\_sl}$	Electrical speed of slave motor ( $rad. s^{-1}$ )
$\omega_{e\_m}$	Electrical speed of master motor ( $rad. s^{-1}$ )
$\alpha$	Argument of the complex impedance $Z$ of the stator PMSM ( $rad$ )
$\delta$	Load angle ( $rad$ )
$\delta_{sl}$	Load angle of slave machine ( $rad$ )
$\delta_m$	Load angle of master machine ( $rad$ )
$\theta_e$	Electrical angle of poled flux ( $rad$ )
$\theta_m$	Mechanical angle of rotor ( $rad$ )
$(\theta)_0$	Initial value of $\theta$ ( $rad$ )
$T_e$	Electromagnetic torque generated by a motor ( $Nm$ )
$T_{load}$	Load torque ( $Nm$ )
$T_f$	Torque caused by the friction ( $Nm$ )
$V_{DC}$	DC voltage ( $V$ )
$u_{sd}, u_{sq}$	Stator voltage in d-q axis ( $V$ )
$i_{sd}, i_{sq}$	Stator current in d-q axis ( $A$ )
$i_{abc}$	Three phase stator current of a machine ( $A$ )
$R_s$	Stator resistance ( $\Omega$ )

$L_s$	Inductance of stator's coil ( $H$ )
$L_d, L_q$	Inductance in d-q frame ( $H$ )
$s_A, s_B, s_C$	Status of IGBT switch (just have two value (0,1))

## List of abbreviations

DPTC	Direct Predictive Torque Control
DTC	Direct Torque Control
EHA	Electro-Hydraulic Actuator
EMA	Electromagnetic Actuator
FOC	Field Oriented Control
IPMSM	Interior Permanent Magnet Synchronous Machine
MEA	More Electric Aircraft
MMS	Multi-Machine System
MS(m,n)	MMS with m-leg inverter and n machines
PMSM	Permanent Magnet Synchronous Machine
PTC	Predictive Torque Control
PTC-SS	Predictive Torque Control – “Split and Seek”
PWM	Pulse Width Modulation
SPMSM	Surface mounted Permanent Magnet Synchronous Machine
SVM	Space Vector Modulation
TTL	Transistor – Transistor Logic
(a,b,c)	Three-phase frame
(d,q)	Rotation frame



# General Introduction

In the conventional aircraft, the non-propulsive aircraft systems are typically distributed by four different secondary power systems: hydraulic, pneumatic, electrical and mechanical. These powers are extracted from the aircraft main engine by different disciplines. For example, mechanical power is obtained from the engine by a driven shaft and distributed to a gearbox to drive lubrication pumps, fuel pumps, hydraulic pumps and electrical generators. Electrical or hydraulic power is distributed throughout the aircraft for driving the subsystems such as flight control actuators, landing gear brakes, utility actuators, avionics, lighting, etc. Over the years, these systems have become more and more complicated and the interactions between different pieces of equipment reduce the efficiency of the whole system.

In order to overcome this complexity, with the aim to improve efficiency and reliability, the aircraft manufacturer trend is toward the "More Electric Aircraft" (MEA) concept [Jon99] [ROAR07] [AF09]. Within the framework of MEA, one of innovations is substituting hydraulic actuators with electromechanical actuators (EA). This reduces weight and decreases maintenance and production costs.

The EA system contains four major components: the electrical motors, the power electronic converters, the control drives and the actuators. The more using of electromechanical actuators (EA) leads to the first demand about an appropriate electrical machine to meet the requirements of aircraft technology. Related to this issue, the permanent magnet synchronous machine (PMSM) is increasingly being used thanks to its high efficiency throughout the full speed range, high power ratio, and ease of refrigeration, compared to classical wound machines. Moreover, the PMSM also satisfies the high requirements of the application in term of volumes and weight minimizations [BMAA11] [CMA+12].

It can be seen that these machines are associated to carry out cooperative functions (for example, in flight control surface or in other mechanical parts such as landing gear, brakes,

fuel pumps defrosting system ...). In order to operate such these systems, each engine needs a power electronic device which consists of a heavy and bulky cooling component. This element will increase the weight and size of the whole system significantly. Moreover, for the aeronautic applications, which require the high fail-safety, it is necessary to have strictly constraint redundant systems. These systems are essentially to ensure the continuous operation of the whole system even when any problem happens. However, they also make the system much heavier and larger. As a result, it is interesting to consider whether possible to use sharing structures to operate individual systems according to the availability of sequencing while respecting the continuous condition of system. It is precisely in this context where our work has been developed, power reduced structures based in power electronics, able to feed two or more electric machines in parallel and providing control laws to improve energy efficiency.

Until recently, together with the development of semiconductor technology, the introduction of powerful microprocessor and the power electronic devices ..., the systems including multi-synchronous machines (especially PMSM) driven by a single inverter begin to be more interested. Some studies have been carried out in order to test and verify the feasibility of these systems [BPD MF08] [APIS08].

We have worked more specifically in the Predictive Control of two Synchronous Machines connected in parallel connected to a 2-Level 3-Phase Converter. These machines have identical characteristics and must follow the same speed profile with a load torque which can be different and, in any case, independent.

The framework of my thesis is presented in four chapters:

- In the first chapter, the evolution of PMSM in many application fields will be presented. Multi-machine systems in the aeronautic field as well as the idea of using sharing power electronic structure are considered. Typical structures of multi-machine system which have been developed in the literature are presented. The features of each structure will be studied. A comparison among these structures will also be synthesized. Finally, the most suitable structure for our application will be selected;
- In the second chapter, before approaching to multi-parallel PMSM drive system, a general description about a PMSM drive system is presented first. In this part, the principle operation and stability analysis of a PMSM are considered. Some control strategies to control this kind of drive system will be presented and analyzed. Finally, two control structures for mono-inverter dual-parallel PMSM will be introduced;

- 
- The third chapter is the main part of this thesis. It will focus on Predictive Control of two Synchronous Machines connected in parallel connected to a 2-Level 3-Phase Converter. A general description about the PTC for mono-inverter dual-parallel PMSM drive system will be presented. Each component of this drive system is studied and explained in detail. Two approaches to predictive control will be described and compared. Some simulations will be done in order to verify the performance of control methods.
  - In the fourth chapter, a new experimental bench has been developed in laboratory LAPLACE with the aim of verifying the operation of the system under proposed control strategies. Experimentation represents a hypothetical displacement of two flaps of an airplane. The studied system converts electrical energy supplied by the EDF network and then distributes it to two mechanical sources. In this mechanism, two PMSMs will be connected in parallel and supplied by a three-phase two-level inverter.
  - The conclusions and perspectives will be pointed out in the final.



# Chapter 1

## PMSM with Multi-Machine Systems

### Table of content

---

1.1. Introduction .....	6
1.2. Evolution of permanent magnet synchronous machine (PMSM).....	7
1.2.1. Small power applications of PMSM.....	8
1.2.2. Medium power applications of PMSM .....	9
1.2.3. High power applications of PMSM.....	10
1.3. Multi-machine system in aeronautic field .....	11
1.3.1. The idea of sharing structures.....	11
1.3.2. Flight control systems.....	12
1.3.2.1. Introduction.....	12
1.3.2.2. Electromechanical actuators (EMAs).....	14
1.3.2.3. Shared structures .....	15
1.4. Typical structures of multi-machine system.....	16
1.4.1. Classical structure.....	16
1.4.2. Presentation of the shared structures .....	18
1.4.2.1. Sharing common legs structure: n machines with 2n legs .....	18
1.4.2.2. Sharing the midpoint structure: n machines and 2n legs.....	20
1.4.2.3. Mixed structure: $\frac{3n}{2}$ legs for n machines.....	22
1.4.2.4. Parallel structure: 3 legs for n machines .....	23
1.4.2.5. Some other structures .....	24
1.4.2.6. Comparison of these different structures .....	24
1.5. Conclusions .....	26

---

## 1.1 Introduction

Nowadays, along with the development of electro-technical technology as well as the economic issues in industries, there are more and more systems consisting of multiple electric machines. A classical structure, which is called multi-machine multi-inverter system (MMS), has been well-developed for these systems. According to this structure, each machine is supplied by its own inverter. As a result, problem of using a large number of power electronic components need to be considered. In addition, classical structure also requires a controller for each machine. Therefore, the requirement of using powerful computers to implement several control modules is unavoidable. Because of these reasons, the price, as well as the size of the whole system, will increase considerably. It is interesting developing sharing structures with a reduction of the number of power components and simplified control algorithm.

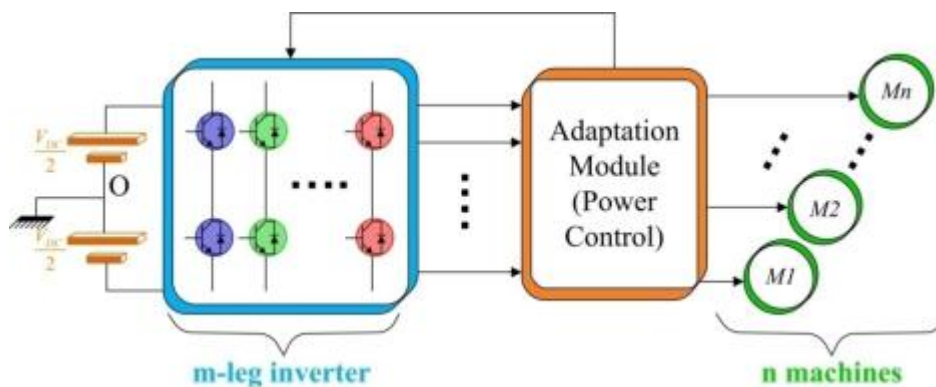


Figure 1.1: Multi-Machine System MS(m,n)

As shown in Figure 1.1, the MMS can be represented as a multi-machine mono-inverter system. According to this configuration, a  $m$ -legs inverter is used to power  $n$  machines. Each leg of inverter is made up of two electronic switches connected in series. This kind of system is marked as multi-machine system – MS(m,n) [Bou95].

Many studies have been carried out to reduce the number of power electronic components by decreasing the number of inverter's legs. It is at the origin of the idea of using the shared structures in multi-machine systems. Such these structures can be found in many applications in the textile industry [Cha03][BBPDdF06], transportation industry such as the traction drives [Kem89][PEPDRdF02][PPN105][BPDD+06], robotic mobile [Bou95][BPDdF96] and other ... However, these studies have just only applied for induction machines. Meanwhile, with the strong development of the semi-conductor and material industry today, the permanent magnet synchronous machines (PMSM) become more and

more popular and appear in many applications. This type of machine shows the superiority in the efficiency, the size and weight, and the flexibility... compared with other machines.

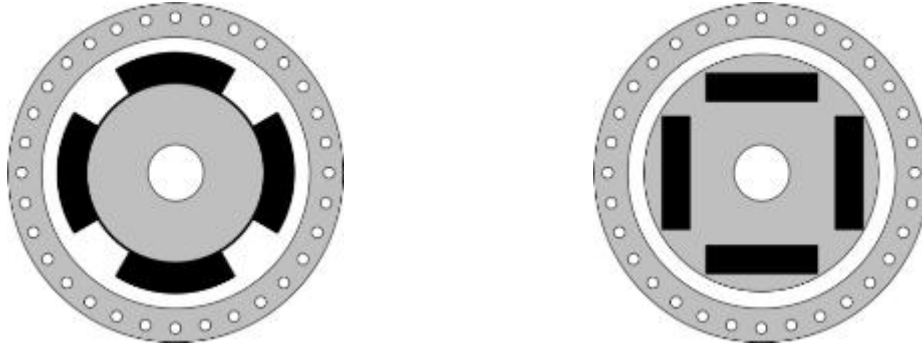
In this chapter, the evolution of PMSM in many application fields will be presented in a first time. After that, a special study of multi-machine system in the aeronautic field is considered. In this part, the possibility and the idea of shared structures are presented and analyzed. Next, the typical structures of multi-machine system which have been developed in the literature are pointed out. The characteristics of each structure will be studied. A comparison among these structures will also be synthesized. Finally, the most suitable structure for our application will be selected in the conclusion.

## 1.2 Evolution of permanent magnet synchronous machine (PMSM)

The permanent magnet synchronous machine (PMSM) drive has emerged as a top competitor for a full range of motion control applications. In specialty, the PMSM is widely used in machine tools, robotics, and actuators and also being considered in high-power applications such as vehicular propulsion and industrial drives. It is also becoming viable for commercial or residential applications. The PMSM is known for having a lot of advantages compared with other types of electric machine:

- + high efficiency: PMSMs use permanent magnets to create a constant rotor magnetic field instead of using a rotor circuit. Therefore, the copper losses are eliminated. Moreover, without the rotor circuit, the only heat is produced on the stator, which is much easier to cool than the rotor;
- + high flux density: Recent advances in high-energy density magnets (NdFeB) have allowed a achievement of very high flux densities. These magnets provide high torques and allow to build the smaller and lighter machines;
- + lower maintenance, great longevity and reliability: Because there are no mechanical commutators and brushes, the friction is lower and the durability is higher. Besides, without brushes and mechanical commutators, the maintenance cost is reduced and the risk of sparking or corrosive environments is eliminated;
- + high torque to inertia ratio: PMSMs use permanent magnets → PMSM will have low inertia; this makes for a fast response under a given electric torque;
- + high power density (it is represented by the ratio  $kW/kg$ );
- + ...

In PMSMs, permanent magnets are mounted inside (interior permanent magnet synchronous machine – IPMSM) or outside (surface mounted permanent magnet synchronous machine – SPMSM) of the rotor (Figure 1.2). Meanwhile, the stator structure is identical to the induction motors as well as other types of AC motor. The windings thus are constructed to produce a sinusoidal flux density in the air gap of the machine.



a) surface mounted permanent magnet synchronous machine (SPMSM)      b) interior permanent magnet synchronous machine (IPMSM)

Figure 1.2: Two main types of PMSM

Today, the PMSMs play an important role in the variable speed applications. These applications have the output capacity ranging from a few hundred  $W$  (brushless DC micro-motor developed in MEMS technology [MKP09]) to more than  $1GW$  (AC synchronous generator [Ber02]). For small power machines, their rotor usually consists of several permanent magnets. These permanent magnet synchronous motors are also called a "brushless motor" because the rotor flux is still created by the magnets, they do not have the brushes collector.

Besides, several high performance applications such as robotics and aerospace actuators in which there is a requirement for high torque per inertia ratio are also the typical applications of PMSM. In the next part, examples in different power ranges using PMSM will be presented.

### 1.2.1 Small power applications of PMSM

In the range of small power (according to the standard NF C 51-200, the power is under  $600W$ ), the brushless motors are mostly used in continuous current mode and called BLDC motors.

In order to control the system with the BLDC motors, an electrical sensor, which are connected to the motor, allows the detection of the rotor position and ensures the



Figure 1.3: Examples of application of brushless motors in small power range continuous switching of the current. The advantage of such a system is no additional speed control is required.

These types of motor are usually used in the systems which are required to control exactly the position (hard disk drives, DVD rewrite ...). They are also used in the systems that need to operate at a fixed speed precisely such as the mechanical timer in the household devices. Other applications which use the small brushless motors are the fans of the micro-computers or the medical instruments such as the drills. All of these examples are illustrated in Figure 1.3.

## 1.2.2 Medium power applications of PMSM

In this section, the studied systems are required in the range of power from 500 W to 100 kW and using or likely to use the PMSM. These machines are mostly poly-phase (usually three-phase) and always associated with a voltage inverter controllable in current in order to ensure the autopilot.

One of the first applications in this power range is supported by the motorization of various electric vehicles. Indeed, current trends lead to the development of electric accumulators (batteries Lithium/ion ...) and the development of electric motors in order to replace the internal combustion engines whose performance is very low while the fossil fuel becomes exhausted. Moreover, brushless motors also possess interesting characteristics which are suitable for embedded systems. Several electrical or hybrid vehicles such as Toyota-Prius or the Citroen-C0 were equipped with PMSM. In the same tendency, the studies on two-wheeled vehicles are also carried out (scooter, electric bikes ...).

Some machine tools and industrial robots also use the brushless motors because they provide good performance (good low-speed torque, strong overload capacity, reliability, speed ...) and require little maintenance.



Figure 1.4: Examples of applications of brushless motors in medium power range

All the examples described above are illustrated in Figure 1.4

Thanks to many advantages, the PMSM can also be used in various driving mechanism for the specialty systems where the weight and volume play an important role. Therefore, if there are already the applications using the PMSM for some systems in cars (ventilations, air conditioning ...), it is also possible to increase their penetration into other areas such as aerospace where the problem "more electric aircraft" is increasingly mentioned.

### 1.2.3 High power applications of PMSM

Despite the high cost of the magnets, PMSMs are increasingly used or considered for higher power applications in which there are strictly requirements about the dimension space such as the electric traction drives or marine propulsion systems.

The AGV (high speed electric railcar), a product of Alstom company, also uses the PMSM for the traction drive and electrodynamic braking systems of the train. The successor of TGV train reconciles also the articulated structure (like TGV) with a distributed drive system throughout the train. This distribution brings to a reduction in consumption of 15% and a division the train into small parts as well as small power units. The power/weight ratio of the train is 22kW/tonne and cruising speed of the train is 360km/h (against 320km/h for the TGV). The used engines have a nominal power of 720kW and the power/weight ratio of 1kW/kg (against the maximum value 0.7kW/kg for asynchronous motor) [AGV07].

Similarly, the PMSM can be used for naval propulsion. In this context, the motors used must be compact, lightweight, reliable and resistant to the marine environment (vibrations, humidity, salinity, temperature ...). In some special cases as military applications, they also are required as discrete as possible. Although PMSM that can generate the high power are quite expensive to manufacture, they still appeared on some submarines and military

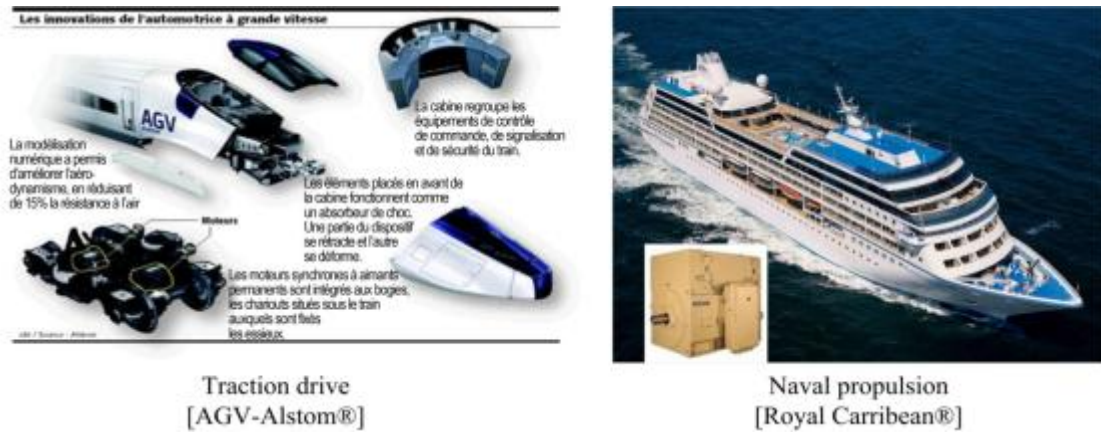


Figure 1.5: Examples of applications of brushless motors in high power range

ships as well as on some cruise ships such as the "Legend of the Seas" (as shown in Figure 1.5).

This section has proposed an overview of the different systems that promote the use of PMSM. These systems mostly use several servo-electric machines and each one is connected to its own electrical converter. These developed systems are of the type multi-machine. It is interesting to see whether it would be possible to optimize the size and weight of such these systems.

## 1.3 Multi-machine system in aeronautic field

### 1.3.1 The idea of sharing structures

Within the framework of the More Electric Aircraft (MEA), there is a trend of using the more and more electric machines [ROAR07][AF09], whether for the flight control actuators (see section 1.3.2), or for other mechanical parts such as the landing gear, brakes, fuel pumps, defrosting systems, air conditioning systems, startup of motors, door locks ...

In order to operate such these systems, each engine needs a power electronic device which consists of a heavy and bulky cooling component. This element will increase the weight and size of the whole systems significantly. Moreover, for the aeronautic applications, which require the high fail-safety, it is necessary to have strictly constraint redundant systems. These systems are essentially to ensure the continuous operation of the whole system even when any problem happens. However, they also make the system much heavier and larger.

On the other hand, during each specific period of the flight, there are just a certain number of drive systems which require the power electronic devices and are used while

many others are in inactive mode. For example, the door opening systems are just used only when the aircraft is at the stop. The landing gear, wing flap or thrust reverser systems also are only used for a few minutes during the whole flight. It is interesting to consider whether possible to use sharing structures to operate individual systems according to the availability of sequencing while respecting the continuous condition of system.

The next part of this section will focus on the flight control system and the actuators which require multiple PMSMs operating with the same function at the same time.

## 1.3.2 Flight control systems

### 1.3.2.1 Introduction

As represented in Figure 1.6, the PMSM can be used for many systems on the airplane. The flight control systems are shown in the Figure 1.7, consists of two actuation parts [Nfo06][Del08]:

- + The primary part is the critical part of each flight which controls the evolution of the aircraft along three axes: roll (by the ailerons on trailing edges of wings), pitch (by the elevators on trailing edge of tail plane), yaw (by the rudder).
- + The secondary part controls the aerodynamic configuration of the aircraft during landing and takeoff processes (lift system, spoilers ...). There are three main parts in the secondary actuation system: the flaps and the slats which are used for take off, landing and increasing lift at low speed, the airbrakes which increase the drag. These components are not actually required for flight but they cannot be omitted.

Figure 1.8 shows an example of secondary flight control of an airbus A300. The two lift devices (slats and flaps) allow their wings to maintain the lift at low speed.

Many studies in science and technology have been developed in order to upgrade the flight control system for the last many years [MGSL09]. At the beginning, flight control systems entirely use mechanical actuators: the pilot controls directly the rudder by taking the effect on the joystick. And then, with the support of the hydro-mechanical technology, the hydraulic actuators allow to operate heavier loads, however, the flight control issue is still always mechanical.

In the 1950s, military aircrafts began to be equipped by electric flight control systems. This technology, which is also called as "fly by wire", allowed reducing the weight of the system as well as improving the response time of the electro-hydraulic servo-system [Sch08].

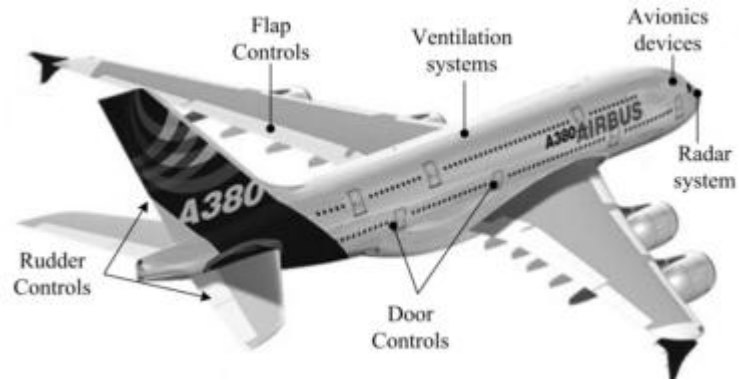


Figure 1.6 The possibility of using PMSM in aeronautics [All95]

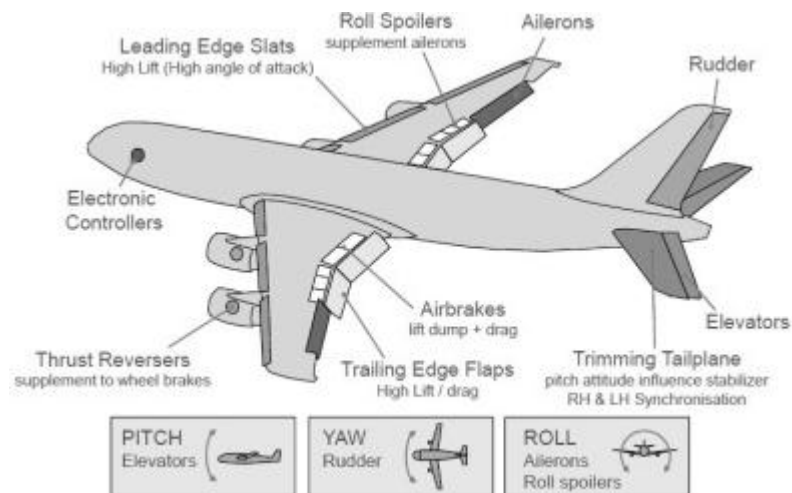


Figure 1.7: Flight control actuation systems [Nfo06]

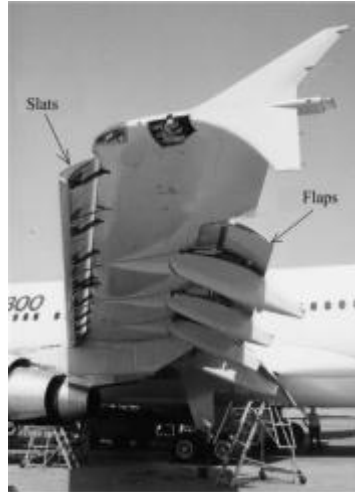


Figure 1.8: Wing of an airbus A300

In 1972, the Concorde is the first commercial aircraft using such flight control system (digital control system). In 1984, the Airbus A320 becomes the first commercial aircraft in which all the electric command signals are processed and generated by a digital computer [BT93].

In the last decade, a lot of research has allowed Electro-Hydrostatic Actuator (EHA) technology to be mastered. One result of this on a new aircraft such as the Airbus A380 is the replacement of the hydraulic circuits by EHA networks. Although there is increasing interest in the use of electric drives to substitute hydraulics and electro-hydraulic system in aircraft, these devices are used just as a back-up for other hydraulic system.



Figure 1.9: An advanced Motor Device EMA

Current airplanes usually use the present hydraulic or electro-hydraulic actuators (EHA) in a centralized system. In the process of building the more electric aircraft, they will be substituted by Electromechanical Actuators (EMAs) in de-centralized systems

(while respecting the conditions of safety). This trend is today of major importance for aeronautic of industry. This improvement will bring the advantages of eliminating completely the hydraulic power, decreasing the production and maintenance cost as well as the weight of the system. An example of such EMA device is presented in Figure 1.9.

### 1.3.2.2 Electromechanical actuators (EMAs)

EMA drives for flight controls are based on direct drive architecture [LD12] built up by an electric motor connected directly to the roller-screw that moves an actuator (Figure 1.10). The complete control block diagram for an EMA drive includes the position, speed torque and flux controls. Besides it also includes the supervisory and communication system.

The more the EMA are used, the electric machines are also becoming more and more important in the general electric aircraft. As mentioned before, thanks to many advantages compared with other types of electric machines such as the high efficiency throughout the full speed range, high power ratio, and ease of refrigeration, the PMSM is increasingly being used for actuator drives. Indeed, the flaps or the slats of both wings must be replaced simultaneously, which means that several PMSMs have to perform the same task at the same time. Therefore, the multi-synchronous machines systems need to be considered.

### 1.3.2.3 Shared structures

The objective of the study developed in this chapter is to look for a suitable structure of multi-synchronous machines mono-inverter system. This structure must meet the requirements of aeronautic applications about weight and volume especially in the case of imposing two or three redundant electronic systems with PMSM. The developed system is composed of several identical PMSMs which move different loads at the same speed. There are two ways to approach to this problem.

- + The first way is just using only one inverter to operate several PMSMs in parallel. According to this method, the weight of system will be decreased.
- + The second way is reusing a classical structure in which an individual inverter can operate just one machine or two machines in parallel.

In the next part of this chapter, the synthesis of existing solutions which have been applied for multi-asynchronous machines system is presented. Then a short comparison is carried out in order to find the most suitable structure which can be applied to the multi-synchronous machines system, especially in aeronautics applications.

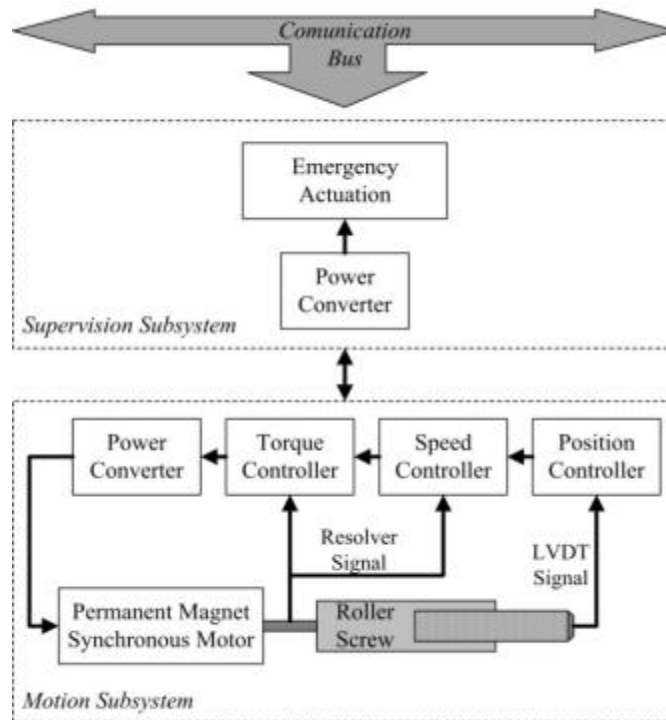


Figure 1.10: Direct drive architecture for EMA [ROAR07]

## 1.4 Typical structures of multi-machine system

### 1.4.1 Classical structure

In the classical structure of a multi-machine system, each phase of a machine is connected and controlled by its own inverter's leg. For  $n$  three-phase machines, so there are  $m = 3n$  inverter's legs. The structure  $MS(3n, n)$  is described in the Figure 1.11.

In this case, as well as the cases which are mentioned afterwards, all the inverter's legs are connected to a DC bus that provides the voltage  $V_{DC}$ .

In the vector representation of the complex voltage,  $O$  is the middle point of the DC bus, ( $A_i$ ,  $B_i$  and  $C_i$ ) represent the phases of the machine  $i$  and  $N_i$  is the neutral point. In general, the voltage resulting from the control of the machines is three-phased and balanced. This relation is true for all machines and is represented by the following equation:

$$V_{A_i N_i} + V_{B_i N_i} + V_{C_i N_i} = 0 \quad (1.1)$$

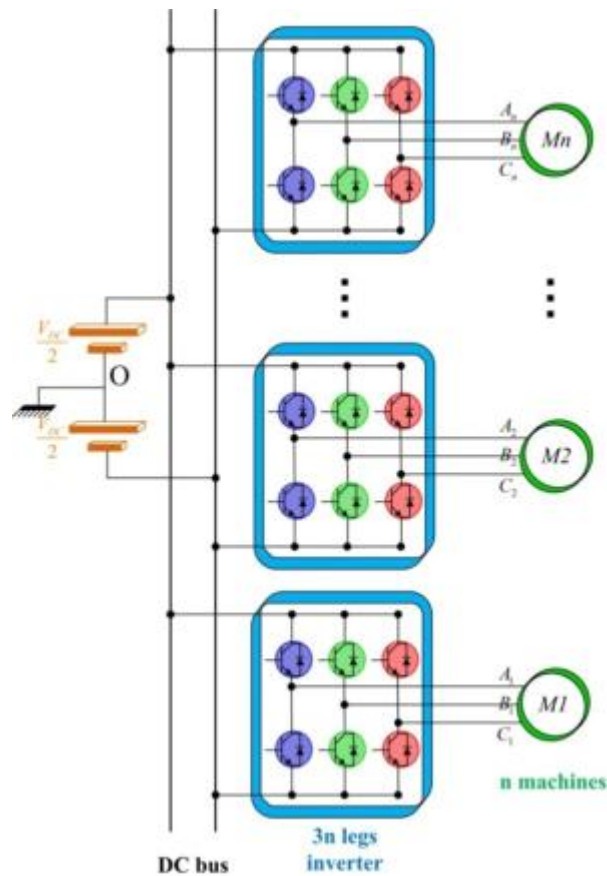


Figure 1.11: The classical structure multi-machine multi-inverter MS(3n,n)

Besides, in the case of the structure MS(3n, n), with a classical pulse width modulation technique (PWM), the average value of the switching voltage  $V_{N_iO}$  can be zero. Therefore, the relations in (1.1) are formed and there is no need of module of a daptation which is shown in Figure 1.1.

The diagram of voltage vectors applied to each different machine is shown in Figure 1.12. Neutral point of each machine and the the mid-point of DC bus are in common.

$$\begin{aligned}
 V_{A_i N_i} &= V_{A_i O} \\
 V_{B_i N_i} &= V_{B_i O} \\
 V_{C_i N_i} &= V_{C_i O}
 \end{aligned}
 \tag{1.2}$$

In this configuration, there is no mutual control between different inverter. All machines operate independently from each others. The synchronism of the system can be obtained easily. However, using one inverter for each machine as well as one drive system needs an individual controller; such system can be expensive and bulky. These problems can be considered as the most negative point of this structure.

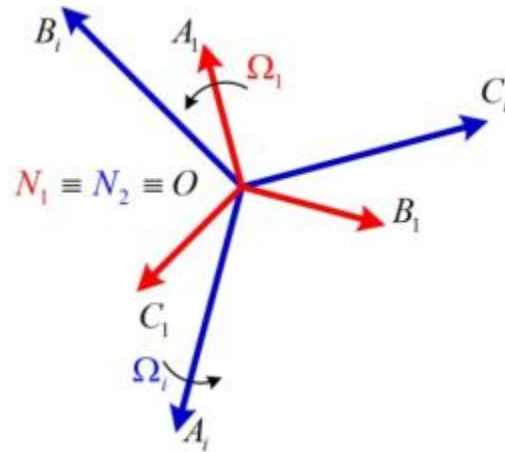


Figure 1.12: Diagram of voltage vectors under structure MS(3n,n)

Shared structures with  $m < 3n$  then have been developed and studied; especially for induction machines. However, according to some specific conditions, it is also possible to apply these structures to the case of synchronous machines.

## 1.4.2 Presentation of the shared structures

In shared structures, several machines can have some common phases. These phases can be connected to the same legs of an inverter or a common point (the neutral point of a DC bus). This is because of the fact that one inverter leg can generate an alternative voltage from the DC voltage, so a multi-phase ( $x$  legs) inverter can feed  $y$  machines. These structures are marked as MS( $x, y$ ) [Bou95].

However, a multi-machine system may include several multi-phase inverters which are independent from each other. Therefore, a system MS( $m, n$ ) will have  $\frac{n}{y}$  multi-phase inverters and can be expressed as MS( $x\frac{n}{y}, n$ ). The number of the machines  $n$  must be multiple of  $y$ . Some different sharing structures will be presented in the following parts of this section.

### 1.4.2.1 Sharing common legs structure: $n$ machines with $2n$ legs

As shown in Figure 1.13, a system which is constructed under this structure consists of a four-leg inverter feeding two machines. The two phases  $B$  and  $C$  of two machines are connected to the same leg of the inverter. The rest phase of each machine is connected individually to its own leg. This structure is denoted as MS( $\frac{4n}{2}, n$ ).

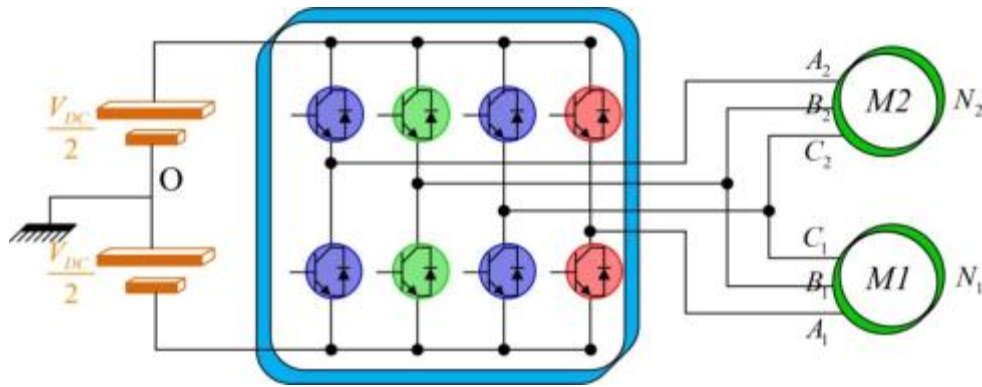


Figure 1.13: The structure using a common leg MS  $(\frac{4n}{2}, n)$

According to this configuration, two machines will run at equal speeds in absolute value. It means that two motors can rotate in the same direction or in opposite directions. It is initially applied for mobile robot applications with the asynchronous machines [Sia92].

Under this configuration, the following relation is always obtained:  $V_{OB_1} = V_{OB_2} = V_{OB}$  and  $V_{OC_1} = V_{OC_2} = V_{OC}$

Figure 1.14 shows the voltage vectors of three phases of two machines under two cases: rotating in the same direction and rotating in the opposite direction.

+  $V_{A_2N_2} = V_{A_1N_1} \Rightarrow \Omega_1 = \Omega_2$  (Figure 1.14(a))

+  $V_{A_2N_1} = -2V_{A_1N_1} \Rightarrow \Omega_1 = -\Omega_2$  (Figure 1.14(b))

The tri-phase voltage obtained will be regulated to follow a reference value by a controller. The control signal is then sent to the inverter. It should be noted that, the voltage applied to the inverter need to refer to the point  $O$ .

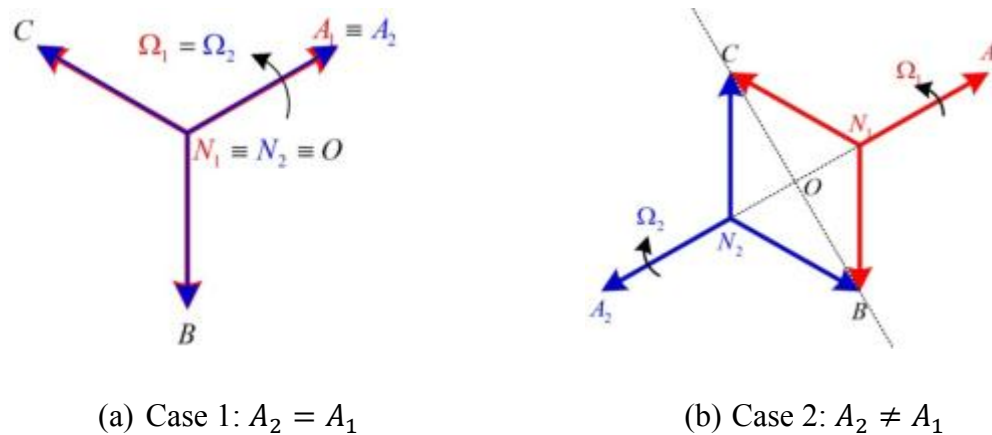


Figure 1.14: Diagram of voltage vectors under structure MS  $(\frac{4n}{2}, n)$

In order to get the well adapted voltage to apply to each leg of the inverter, the potential between the neutral point of inverter  $O$  and the neutral point of each machine  $N_1$  and  $N_2$  need to be considered:  $(V_{N_1O})_{ref}$  and  $(V_{N_2O})_{ref}$ .

Therefore, the reference voltage must be calculated according to the equation in (1.3). This structure can be used to operate multiple machines which are required to rotate at the same speed either in the same direction or in opposite.

The most advantage of this structure is that only a four-leg inverter is used in order to run two three-phase machines (compared with six legs in the case of classical structure). However, with this structure, an adaptation module needs to be used to modulate the midpoint  $O$  of a continuous DC bus. Thanks to this, the two voltages  $(V_{N_1O})_{ref}$  and  $(V_{N_2O})_{ref}$  can be regulated properly. Besides, it should be paid attention that each shared leg of the inverter in this case has to withstand the higher current compared with the case of non-shared leg. It is reasonable because there are two currents who will pass through such these legs.

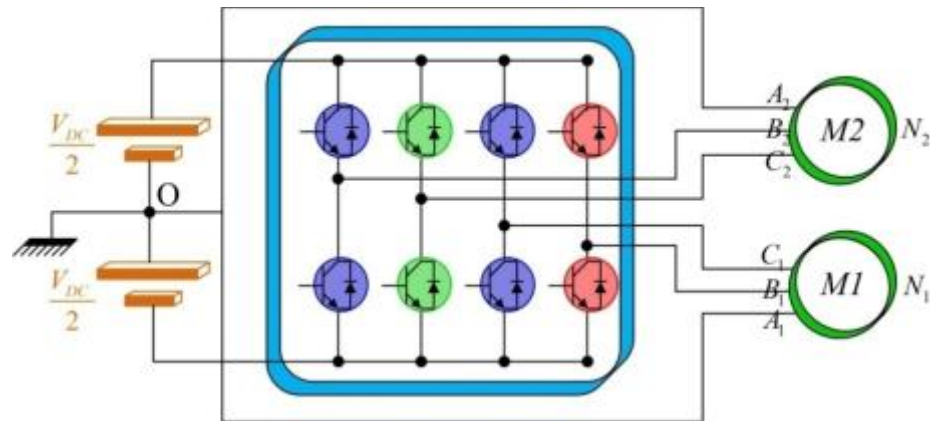
$$\begin{aligned}
 (V_{A_1O})_{ref} &= (V_{A_1N_1})_{reg} + (V_{N_1O})_{ref} \\
 (V_{BO})_{ref} &= (V_{BN_1})_{reg} + (V_{N_1O})_{ref} \\
 (V_{CO})_{ref} &= (V_{CN_1})_{reg} + (V_{N_1O})_{ref} \\
 (V_{A_2O})_{ref} &= (V_{A_2N_2})_{reg} + (V_{N_2O})_{ref}
 \end{aligned} \tag{1.3}$$

Based on the same principle (share the legs of the inverter), another structure expressed as MS(2n + 1, n) is also developed [DJVL09]. A (2n + 1) leg inverter will be used to operate  $n$  machines. This means that there is just one leg is shared by only one phase of all machines. This structure can be used in rolling-up applications in paper industry [JVD+08].

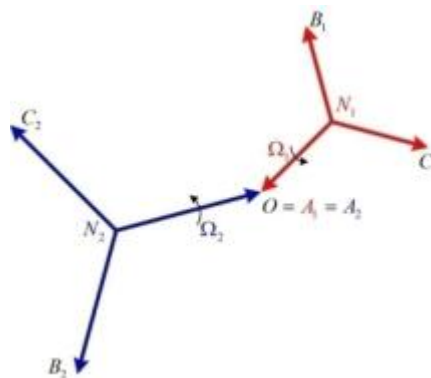
#### 1.4.2.2 Sharing the midpoint structure: n machines and 2n legs

According to this structure, two phases of each machine will be connected to two separated legs of an inverter and the third phase of both machines is shared and connected to the neutral point  $O$  of the continuous DC bus which feed the inverter. This configuration is called MS(2n, n) and shown in Figure 1.15.

Using this structure, the two motors can run at different speed. Figure 1.16 represents the diagram of three-phase voltage vectors of two motors. Each motor can operate independently [Bou95][FOM07].


 Figure 1.15: The structure sharing the midpoint MS( $2n, n$ )

Because the third phase of each machine is fixed to the neutral point  $O$ , for any motor, the relation  $V_{OA_i} = 0$  is always true. At the equilibrium of all machines, the relation  $V_{ON_i} = -V_{A_iN_i}$  is also assured.


 Figure 1.16: Diagram of voltage vectors under the structure MS( $2n, n$ )

As in the case of using the common legs of the inverter, the reference voltage applied to the inverter's legs will differ from the voltage calculated by the regulator. For the  $i^{th}$  machine, the reference voltage will be obtained from the relation in (1.4).

$$\begin{aligned}
 (V_{B_iO})_{ref} &= (V_{B_iN_i})_{reg} + (V_{N_iO})_{ref} \\
 (V_{C_iO})_{ref} &= (V_{C_iN_i})_{reg} + (V_{N_iO})_{ref} \\
 &\text{with } (V_{N_iO})_{ref} = -(V_{A_iN_i})_{reg}
 \end{aligned} \tag{1.4}$$

One of the advantages of this structure is that the motors can operate independently with each others, while the number of power electronic components can be reduced.

However, to implement this structure in applications, the neutral point of the continuous DC bus must be accessible in order to regulate the reference voltage. It is not easy to solve this problem, especially in aeronautics systems.

### 1.4.2.3 Mixed structure: $\frac{3n}{2}$ legs for $n$ machines

In accordance with its name, the mixed structure, which is represented in Figure 1.17, is a combination of two structures which are mentioned above. According to this structure, a three-leg inverter is used to operate two motors. One phase of both motors will be shared and connected to a common leg of inverter (Figure 1.17, two phases  $C_1$  and  $C_2$ ) while another phase of both motors ( $A_1$  and  $A_2$ ) is linked to the neutral point  $O$ . The third phase is connected to its own legs of the inverter. This structure is named as  $MS\left(\frac{3n}{2}, n\right)$ .

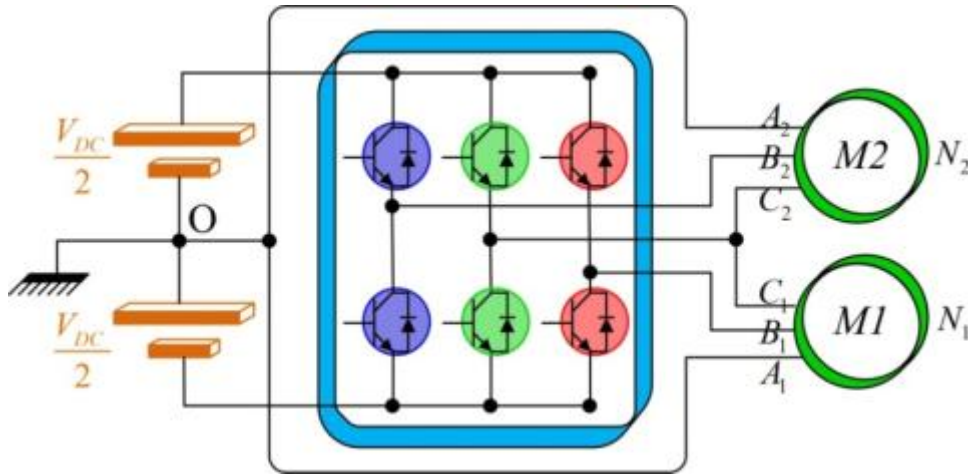


Figure 1.17: Mixed structure  $MS\left(\frac{3n}{2}, n\right)$

As shown in Figure 1.17, the phase A of two machines is connected to the midpoint  $O \Rightarrow V_{OA_1} = V_{OA_2} = 0$  and the phase C of two machines is linked to the same leg  $\Rightarrow V_{OC_1} = V_{OC_2} = V_{OC}$ .

The diagram of voltage vectors of two machines under the mixed structure is shown in the Figure 1.18.

Moreover, like in the structure with common leg, two possibilities can happen:

- + if  $V_{B_2N_2} = V_{B_1N_1} \Rightarrow \Omega_1 = \Omega_2$  (Figure 1.18(a))
- + if  $V_{B_2N_2} = -2V_{B_1N_1} \Rightarrow \Omega_1 = -\Omega_2$  (Figure 1.18(b))
- + Therefore, the reference voltages applied to the inverter will be calculated by the equation (1.5):

$$\begin{aligned}
 (V_{B_1O})_{ref} &= (V_{B_1N_1})_{reg} + (V_{N_1O})_{ref} \\
 (V_{B_2O})_{ref} &= (V_{B_2N_2})_{reg} + (V_{N_2O})_{ref} \\
 (V_{CO})_{ref} &= (V_{CN_1})_{reg} + (V_{N_1O})_{ref}
 \end{aligned} \tag{1.5}$$

with

$$\begin{aligned}
 (V_{N_1O})_{ref} &= -(V_{A_1N_1})_{reg} \\
 (V_{N_2O})_{ref} &= -(V_{A_1N_1})_{reg} \text{ if } B_2 = B_1 \\
 (V_{N_1O})_{ref} &= -(V_{C_1N_1})_{reg} \text{ if } B_2 \neq B_1
 \end{aligned}$$

This structure, like the structures having the midpoint, has the same disadvantage because of having to access to the neutral point of the DC bus to adjust the potential. In spite of decreasing the number of inverter's legs, this structure just is used in some specific applications.

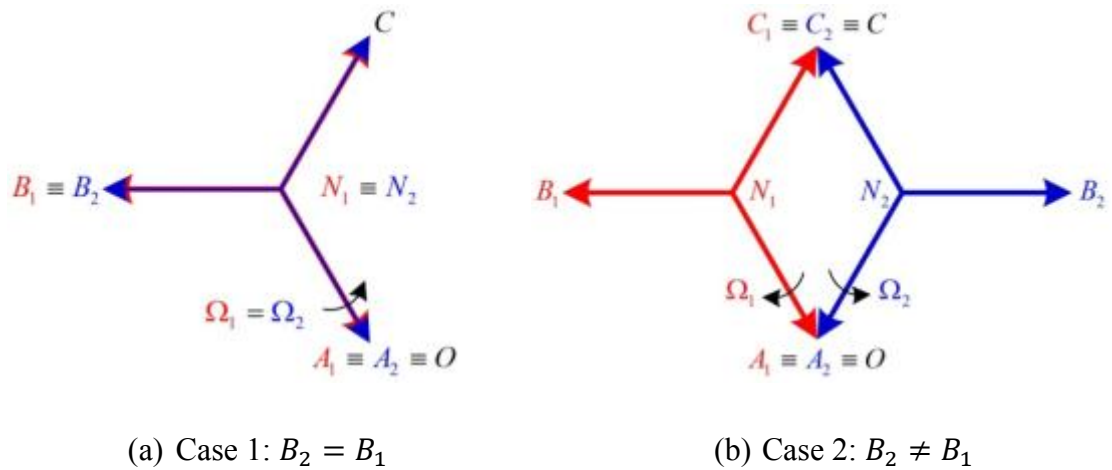


Figure 1.18: Diagram of voltage vectors under mixed structure:  $MS\left(\frac{3n}{2}, n\right)$

#### 1.4.2.4 Parallel structure: 3 legs for n machines

This structure belongs to the type  $MS(3, n)$ , a three-leg inverter will operate n machines simultaneously. Some studies can be found in the literature [KFM00] [PE02]. According to these studies, the case of two machines in parallel is focused. As shown in Figure 1.19, each leg of the inverter is shared by all the machines. Therefore, the dimension of the power electronic components of the inverter must be in accordance to the number of machines in parallel. Besides, these machines must be as similar as possible about electrical parameters.

According to this structure, all the machines will receive exactly same voltages in both frequency and amplitude. These machines will be set up at the same initialization; the same

stator flux is created in each machine. The angular speeds of the machines thus are identical:  $\Omega_i = \Omega_j, \forall (i, j) \in [1, \dots, n]^2$ .

Contrary to those previous structures, it is impossible to control all the phase voltages of these machines. Suitable methods need to be considered and developed in order to guarantee the stability of such these systems.

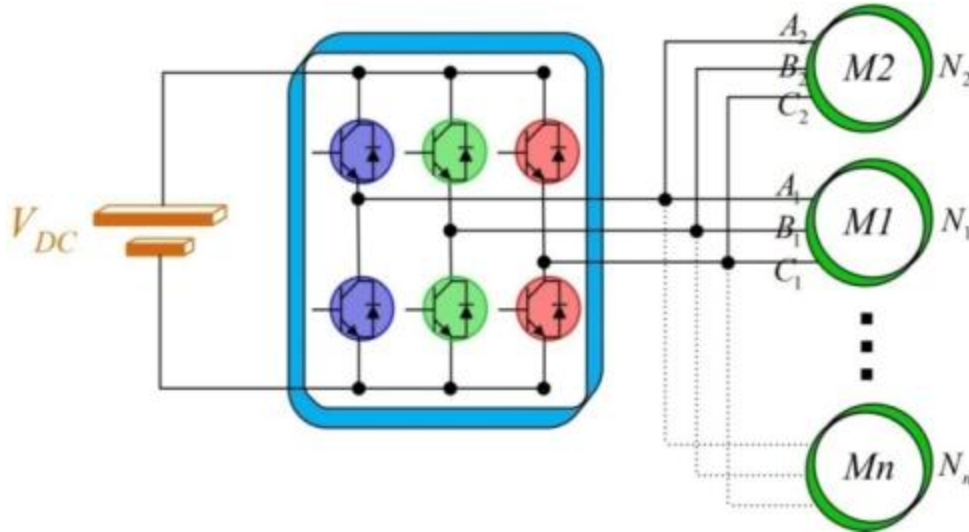


Figure 1.19: Parallel structure MS(3,n)

#### 1.4.2.5 Some other structures

Some other structures, which are more complex such as  $MS\left(\frac{6n}{6}, n\right)$  or  $MS\left(\frac{6n}{4}, n\right)$ , have also been studied [Bou95]. These structures which are based on the same principle of using common legs or mixed structure were used in many applications having more than two machines.

Another principle has been also developed in the field of multi-machine system which is using inverters or machines with special topology [SH07]. However, such these particular systems are not easily adaptable in replacing the redundancy systems.

#### 1.4.2.6 Comparison of these different structures

In previous parts, many different structures developed for multi-machine systems have been presented. To see which structure is more suitable according to the requirements of aeronautic applications in section 1.3.2.3, a comparison of those structures is provided in Table 1.1.

In this table, besides the advantages and disadvantages of these developed structures, several other criteria also are considered and pointed out.

- + The first criterion is the number of the inverter's legs per machine. Normally, a three-phase A C machine will be controlled independently by a three-leg inverter. The structures using common legs will decrease the number of inverter's legs. This means that the number of power electronic components is also reduced. However, using common legs will lead to the problem that the current passing through these legs will be higher. Therefore, there are different electronic devices inside one inverter.
- + The second criterion is the ratio between the maximum voltage that a machine can receive  $(V_{Ni})_{max}$  and the maximum voltage which can be generated from the inverter  $(V_{Oi})_{max}$ . Denote this ratio as  $\eta_V = \frac{(V_{Ni})_{max}}{(V_{Oi})_{max}}$ . For the classical and parallel structure, this ratio is  $\eta_V = 1$  while with other structures this ratio is always smaller than ( $\eta_V < 1$ ). Therefore, for the structures which make the ratio  $\eta_V < 1$ , the value of the DC bus  $V_{DC}$  needs to be regulated.
- + For the structures that can be used for only one machine, it is possible to obtain independent control between different machines easily. However, for sharing structures, it is necessary to look for suitable control structures as well as control algorithms to ensure the stable operation of each machine.

The parallel structure presents the best advantage of using as less as possible number of inverter's legs. Moreover, it is not necessary to modulate the voltage of the DC bus ( $V_{DC}$ ) in order to obtain the same machine voltage when compared with the case of conventional structure. It is not too difficult to apply this structure in real applications. The drawback of this structure comes from sharing all inverter's legs. Because being connected to the same legs, all phases of all the machines will not be controlled independently. In fact, when  $n$  machines are put into parallel, the current passing through each leg will be  $n$  times higher than that of the classical structure. The problem will come from the design of the electronic devices. However, using these oversized components in the redundancy systems, which are inactive most of time, is still an acceptable solution.

Therefore, parallel structure is selected as the most feasible solution for the aeronautic application based in the secondary flight control system. In the case of detecting a failure in an inverter of a machine, it will be possible to switch to this structure to guarantee the continuity of the whole system.

Structure's name	MS(m,n)	Number of legs per machine	Relation $\frac{(V_{Nk})_{\max}}{(V_{Ok})_{\max}}$	Speed	Volume	Notes	
						Advantages	Disadvantages
Classical	MS(3n, n)	3	1	independent	large	Independent machines	Non-sharing
Common legs	MS( $\frac{4n}{2}, n$ )	2	$\frac{2}{3}$	$\Omega_1 = \Omega_2$ or $\Omega_1 = -\Omega_2$	average	Easy to implement	Over current in common legs
Midpoint	MS(2n, n)	2	$\frac{1}{\sqrt{3}}$	independent	average	Can apply for 1 machine	Access to neutral point
Mixed	MS( $\frac{3n}{2}, n$ )	1.5	$\frac{1}{\sqrt{3}}$	$\Omega_1 = \Omega_2$ or $\Omega_1 = -\Omega_2$	small	Inherit from the previous	Inherit from the previous
Parallel	MS(3, n)	$\frac{3}{n}$	1	$\Omega_1 = \Omega_2$	small	Easy to implement	Over current in all legs

Table 1.1: Summary of different structures

## 1.5 Conclusions

The rapid development of semi-conductor and material technology has allowed the use of increasingly the PMSM in industry, replacing the current electric machine types. Along with this, it is the development of embedded systems with the strictly requirements about the performance, quality, weight, size ... This is the case in aeronautics field where the concept of "More Electric Aircraft" now becomes a reality.

When these machines are associated to carry out cooperative functions (for example, in flight surfaces), it is a time that a sharing structure needs to be considered and developed. This concept has already been applied for the applications with induction motors. However, for PMSM, there is still limit. A structure including two or more synchronous machines is really interesting.

In this first chapter, several structures of multi-machine systems has been presented and compared. According to the comparison given and analyzed, parallel structure seems to be the most suitable for the aeronautic applications. It uses the least number of power electronic devices, does not require accessing to the DC voltage bus and so it is quite simple to implement. However, according to this structure, because all machines obtain the same voltage from only one inverter, it is difficult to satisfy independently the requirements of all machines, especially in the case of different loads.

In the next chapter, a two-parallel PMSM system will be described. The solutions used to control this system will be introduced and analyzed.

# Chapter 2

## Mono-Inverter Dual-Parallel PMSM drive system

### Table of Content

---

2.1. Introduction .....	28
2.2. Generalities about PMSM drive system .....	29
2.2.1. Principle of operation of PMSM .....	30
2.2.2. Modeling of PMSMs .....	31
2.2.2.1. Electromechanical description .....	31
2.2.2.2. Continuous model of PMSM in d-q reference frame.....	34
2.2.3. Stability analysis of PMSM.....	36
2.2.4. A three-phase two-level voltage inverter .....	39
2.3. Control strategies for PMSM drive .....	39
2.3.1. Field oriented control .....	40
2.3.2. Direct Torque Control (DTC).....	41
2.3.3. Direct Predictive Torque Control (DPTC).....	44
2.4. Control structure for Mono-inverter Dual-parallel PMSM system .....	46
2.4.1. Master-slave structure .....	46
2.4.1.1. General description .....	46
2.4.1.2. Consequence due to a load variation.....	47
2.4.1.3. The choice of master machine.....	48
2.4.1.4. Conclusions.....	52
2.4.2. Direct torque control (DTC) for mono-inverter dual-parallel PMSM.....	52
2.4.2.1. General description .....	53
2.4.2.2. Optimal switching table for two machines.....	55
2.4.2.3. Simulation tests .....	61
2.5. Conclusions .....	64

---

## 2.1 Introduction

As mentioned in previous chapter, multi-machine systems become more and more popular in variable speed applications. The problem of using many power electronic devices which increases the weight and size of these systems is solved by the idea of sharing structures.

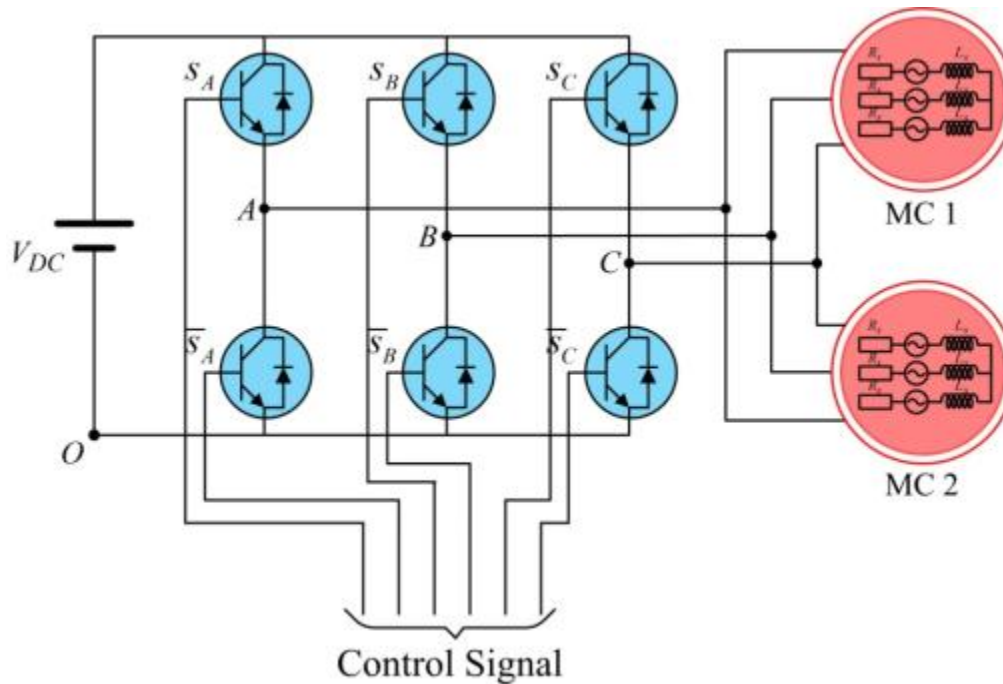


Figure 2.1: Mono-inverter dual-parallel PMSM drive

In addition, the development of the system with multiple machines also leads to a higher attention in selecting suitable electrical machines. In this field, the PMSMs gradually become dominant compared with others such as DC machines, IMs...

In the special field of aeronautic applications where the efficiency as well as the weight and size are the most important things, the parallel structures along with PMSMs seem to be the best choice.

Combining parallel structures with PMSM leads to the idea of multiple PMSMs drive system. Until now, few studies have been developed in order to control this kind of drive systems. These studies focus on a drive system including two PMSMs connected to a three-phase inverter [CSSS02][BPDMF08][PIS10]. Such these systems are also called mono-inverter dual-parallel PMSM (Figure 2.1).

According to Figure 2.1, a drive system including two PMSMs connected in parallel and supplied by a three-phase two-level inverter is presented. In this kind of drive system,

two machines are identical. It means that all parameters of both machines are the same. Besides, both machines will receive the same voltage (magnitude and frequency):

$$\begin{cases} |V_{s1}| = |V_{s2}| = |V_s| \\ \omega_{e1} = \omega_{e2} = \omega_s \end{cases} \quad (2.1)$$

For this system, the aim is to keep the mechanical speeds of two machines equal and follow the speed reference under different load conditions:

$$\begin{aligned} \omega_{m1} &= \omega_{m2} = \omega_{ref} \\ s.t. T_{load1} &\neq T_{load2} \end{aligned} \quad (2.2)$$

In this chapter, a general description about a PMSM drive system will be presented first. In this part, the principle of operation and stability analysis of a PMSM are considered. In order to operate this drive system, some typical methods will be presented in the next part. Finally, two control strategies for mono-inverter dual-parallel PMSM drive will be described.

## 2.2 Generalities about PMSM drive system

PMSM normally is not a self-started motor type. Therefore, in variable speed applications, a PMSM is usually supplied by the variable frequency sources such as voltage source inverter (VSI), current source inverter (CSI)... General structure of such drive system is presented in Figure 2.2.

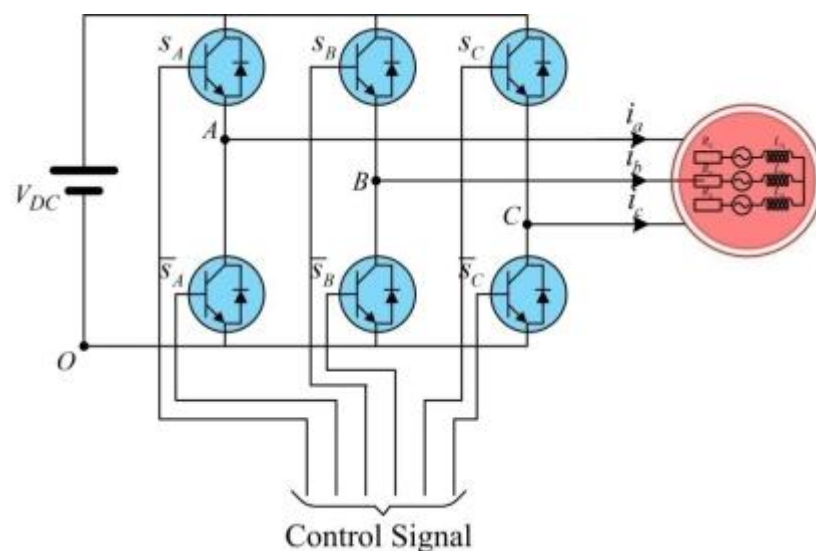


Figure 2.2: Structure of a PMSM drive system

In this figure, a PMSM is supplied by a three-phase two-level voltage inverter. A controller will be used to generate the control signals of the inverter in order to control the PMSM.

### 2.2.1 Principle of operation of PMSM

In the case of a PMSM, the rotor acts as an inductor, containing  $n_p$  pairs of poles (North and South) permanent magnets. Meanwhile, the stator of a three-phase PMSM normally has a sine distributed three-phase winding. When these windings are excited with a three-phase balanced supply, a rotating magnetic field is developed. It is assumed that this field is sinusoidally distributed in the air gap. The mutual impact between the stator and rotor magnetic fields will produce forces to the rotor and will make the rotor rotate.

At steady state, PMSM is a constant speed motor. This speed is calculated by equation (2.3):

$$\omega_m = 60 \frac{f_s}{n_p} \quad (2.3)$$

where  $\omega_m$  is the mechanical speed of the rotor (*rpm*);

$f_s$  is the electrical frequency of the voltage supply (*Hz*);

$n_p$  is the number of pole pairs;

Figure 2.3 is an example of a three-phase motor with  $n_p$  pole pairs ( $n_p = 2$ ). It consists of  $3n_p$  pairs of windings which are spaced  $2\pi/(3 \times 2n_p)$  (*rad*).



Figure 2.3: Stator windings of a three-phase PMSM 2 pole pairs

In order to get the best control performance of a drive system with PMSMs, the characteristic equations which describe the electrical and mechanical relations of the machine will be studied. The modeling and stability analysis have been done in the following parts.

## 2.2.2 Modeling of PMSMs

In a rotating electrical machine, there is always a rotating component and a stationary one. Because of this rotation, the self and mutual inductances, which are responsible for various voltages, become time varying. These time varying inductances sometimes cause difficulties for the analysis. Besides, rotor flux in a PMSM is constant and provided by the permanent magnets. Thanks to this, rotor flux is always polarized and has a clearly and consistently oriented shaft. If using a position sensor (such as resolver, encoder with zero pulse), the position of the rotor flux can be specified precisely and for this reason, the problem of flux oriented always can be ensured.

Therefore, in this section, a model of a three-phase PMSM in d-q reference frame is derived in order to clarify the concept of the axis transformation (Park) and the relation between three-phase quantities and their equivalent two-phase quantities.

Throughout the derivation of the two-phase (d-q) mathematical model of PMSM, the following assumptions are pointed out [Kri01]

- + Stator windings produce sinusoidal EMF distribution. Space harmonics in the air-gap are neglected;
- + Air-gap reluctance has a constant component as well as a sinusoidal varying component;
- + Balanced three-phase sinusoidal supply voltage is considered;
- + Although magnetic saturation is considered, eddy current and hysteresis effect are neglected;
- + Presence of damper windings is not considered because PMSMs used today rarely have that kind of configuration.

As mentioned in previous chapter, there are two types of PMSM depending on the rotor structure. In SPMSM, magnets are mounted on the surface of the rotor. Since the permeability of magnets is close to unity and the saliency is really small, the inductances expressed in the d-q coordinates are approximately equal. In this thesis, just non-silent typed PMSMs are considered. Therefore, the following relation is always confirmed:  $L_d = L_q = L$ .

### 2.2.2.1 Electromechanical description

The space vector form of the stator voltage equation in the stationary reference is given in Equation (2.4):

$$\vec{u}_s = R_s \cdot \vec{i}_s + \frac{d\vec{\psi}_s}{dt} \quad (2.4)$$

where  $R_s$ ,  $\vec{u}_s$ ,  $\vec{i}_s$  and  $\vec{\psi}_s$  are the resistance of the stator winding, complex space vectors of the three phase stator voltages, currents and flux linkages, all expressed in the stationary reference frame fixed to the stator, respectively. They are defined as:

$$\begin{aligned} \vec{u}_s &= \frac{2}{3} [u_{sa}(t) + e^{j120^\circ} u_{sb}(t) + e^{j240^\circ} u_{sc}(t)] \\ \vec{i}_s &= \frac{2}{3} [i_{sa}(t) + e^{j120^\circ} i_{sb}(t) + e^{j240^\circ} i_{sc}(t)] \\ \vec{\psi}_s &= \frac{2}{3} [\psi_{sa}(t) + e^{j120^\circ} \psi_{sb}(t) + e^{j240^\circ} \psi_{sc}(t)] \end{aligned} \quad (2.5)$$

The resultant voltage, current and flux linkage space vector shown in (2.5) for the stator are calculated by multiplying instantaneous phase values by the stator winding orientation in which the stator reference axis for the a-phase is chosen to the direction of maximum emf. Reference axes for b- and c- stator frame are chosen  $120^\circ$  and  $240^\circ$  (electrical angle) ahead of the a-axis, respectively. Next, the direction of permanent magnet flux is chosen as the d-axis, while the q-axis is  $90^\circ$  ahead of the d-axis. The angle between the rotor d-axis and the stator a-axis is defined as  $\theta_e$ . Note that, as the machine operates at steady state, the d-q reference frame also rotates at a speed of  $\omega_e = d\theta_e/dt$ , while the stator a-b-c axes are fixed in space. Figure 2.4 illustrates a conceptual cross-sectional view of a three-phase, two-pole PMSM.

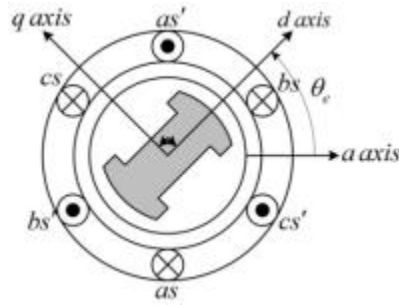


Figure 2.4: Two-pole three-phase PMSM

Equation in (2.4) is a general stator voltage equation and it is true for all kinds of rotating field electrical machines including the PMSM.

In terms of phase variables, the electrical dynamic equation of PMSM can be written as:

$$u_k = R_s \cdot i_k + L \cdot \frac{di_k}{dt} + e_k \quad (2.6)$$

This equation is illustrated through the equivalent circuit of one phase of the machine shown in Figure 2.5(a). At steady state, currents are considered as sinusoidal form. The vector diagram thus is represented in Figure 2.5(b).

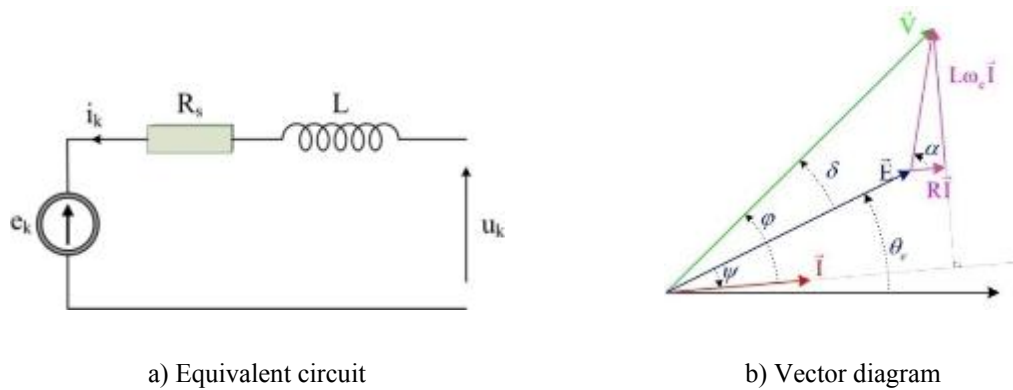


Figure 2.5: Electrical model of one phase of PMSM

In Figure 2.5:

- + the index  $k = (a, b, c)$  corresponds to the phase of a PMSM;
- +  $u_k$  (the RMS value is  $V$ ) is the stator voltage applied between one phase and the neutral point;
- +  $e_k$  (the RMS value is  $E$ ) is the induced electromagnetic force;
- +  $i_k$  (the RMS value is  $I$ ) is the current in the phase  $k$ ;

$L$  is the equivalent cyclic RMS. It is synthesized by the inductance of the phase winding  $L_s$  and the mutual inductances  $L_m$ :

- +  $R_s$  is the resistance of a phase of the stator. Normally, because the impedance of the inductance which depends on the rotating speed ( $Z_L = L\omega_e$ ) is much bigger than the resistance:  $L\omega_e \gg R$ , the resistive drop can be neglected;
- +  $\theta_e$  represents the electrical angle. This value depends on the rotor position  $\theta_m$  and the number of pole pairs  $n_p$ :  $\theta_e = n_p\theta_m$ .

In addition, three other angles are also shown on the vector diagram (Figure 2.5b):

$$\psi = \widehat{(E; I)}, \quad \varphi = \widehat{(V; I)} \quad \text{and} \quad \delta = \widehat{(V; E)}.$$

For a maximum excitation flux  $\Phi_M$  created by the rotor in the gap, the effective value of the electromagnetic force is proportional to speed and is presented in equation (2.7).

$$E = \frac{n_p \Phi_M}{\sqrt{2}} \omega_m = k_e \omega_m \quad (2.7)$$

Based on the electrical dynamic equation described in (2.6), output mechanical torque generated  $T_e$  in a PMSM is related to the mechanical speed  $\omega_m$  as given by Equation (2.8)

$$T_e = \frac{e_a i_a + e_b i_b + e_c i_c}{\omega_m} \quad (2.8)$$

When the machine is connected to a mechanical load (such as a screw shaft for example), the external torques coming from these loads can be denoted as  $T_{load}$ . The mechanical model of a PMSM based on the fundamental principle of dynamics and is represented in (2.9).

$$\begin{cases} \omega_m = \frac{d\theta_m}{dt} \\ J \frac{d\omega_m}{dt} = T_{em} - T_{load} - f_0 \omega_m \end{cases} \quad (2.9)$$

With:

- +  $f_0$ : the coefficient of viscous friction of the machine and load;
- +  $J$ : the total inertia of the machine;
- +  $T_{load}$ : the load torque
- +  $T_{em}$ : the electromagnetic torque generated by the machine.

Calling  $T_{total}$  as the total load applied to the motor. Because the component  $\frac{d\omega_m}{dt} = 0$  at the steady state, the relation in (2.9) will be rewritten as shown in Equation (2.10).

$$T_{em} = T_{total} = f_0 \omega_m + T_{load} \quad (2.10)$$

### 2.2.2.2 Continuous model of PMSM in d-q reference frame

In order to get the model of PMSM, general stator voltage equation in (2.4) will be transformed to the d-q reference frame (flux reference frame - Figure 2.4). This frame rotates at the same speed with the flux vector ( $\omega_e$ ). This relation is shown in Equation (2.11).

$$\vec{u}_s^{dq} = R_s \vec{i}_s^{dq} + \frac{d\vec{\psi}_s^{dq}}{dt} + j\omega_e \vec{\psi}_s^{dq} \quad (2.11)$$

The relationship between the stator and rotor flux can be described as follows:

$$\vec{\psi}_s^{dq} = L_s^{dq} \vec{i}_s^{dq} + \vec{\psi}_p^{dq} \quad (2.12)$$

The index "dq" in the right-upper represents to the flux reference frame (field oriented frame).

In (2.12),  $\vec{\psi}_p^{dq}$  is polar-flux vector. Because the real axis of the coordinate system is directly orientated to the axis of the pole flux, quadrature component (along the q-axis) of  $\vec{\psi}_p^{dq}$  is zero. Accordingly, the pole flux vector just has only the real direct component  $\psi_p$ .

From that, it follows:

$$\vec{\psi}_p^{dq} = \psi_{pd} + j\psi_{pq} = \psi_p \text{ with } \psi_{pq} = 0 \quad (2.13)$$

Substituting the E equation (2.13) and E equation (2.12) into E equation (2.11), we will obtain:

$$\vec{u}_s^{dq} = R_s \vec{i}_s^{dq} + \frac{d(L\vec{i}_s^{dq})}{dt} + j\omega_e(L\vec{i}_s^{dq} + \psi_p) \quad (2.14)$$

Let  $\vec{u}_s^{dq} = u_{sd} + ju_{sq}$  and  $\vec{i}_s^{dq} = i_{sd} + ji_{sq}$ . The equations (2.15) are obtained by separating the real and imaginary parts from the above equation:

$$\begin{cases} u_{sd} = R_s i_{sd} + \frac{d(Li_{sd})}{dt} - \omega_e Li_{sq} \\ u_{sq} = R_s i_{sq} + \frac{d(Li_{sq})}{dt} + \omega_e Li_{sd} + \omega_e \sqrt{\frac{3}{2}} \psi_p \end{cases} \quad (2.15)$$

Where  $u_{sd}$  and  $u_{sq}$  are the d-q axis voltages,  $i_{sd}$  and  $i_{sq}$  is the d-q axis stator currents, and  $\psi_p$  is the polar flux.

The equations of flux components in d-q reference frame also are obtained:

$$\begin{cases} \psi_{sd} = Li_{sd} + \psi_p \\ \psi_{sq} = Li_{sq} \end{cases} \quad (2.16)$$

The equivalent circuits of the machine in d-q rotational frame are illustrated in Figure 2.6.

Based on the general rotating moment equation of the electrical machine, the electromagnetic torque is:

$$T_e = n_p(\psi_{sd}i_{sq} - \psi_{sq}i_{sd}) = n_p\sqrt{3/2}\psi_p i_{sq} \quad (2.17)$$

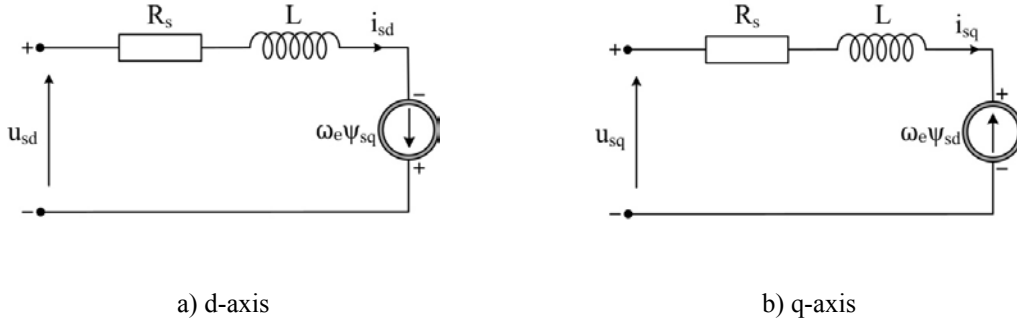


Figure 2.6: Equivalent circuit of a PMSM in d-q frame

Equations (2.15) can be rewritten as follow:

$$\begin{cases} \frac{di_{sd}}{dt} = -\frac{R_s}{L}i_{sd} + \omega_e i_{sq} + \frac{1}{L}u_{sd} \\ \frac{di_{sq}}{dt} = -\omega_e i_{sd} - \frac{R_s}{L}i_{sq} + \frac{1}{L}u_{sq} - \omega_e \sqrt{\frac{3}{2}} \frac{\psi_p}{L} \end{cases} \quad (2.18)$$

With the equations in (2.17) and (2.18), a continuous state model which describes completely a PMSM in d-q coordinate is obtained. Equations (2.18) can be used to create the current state space model of a PMSM as follow:

$$\frac{d\vec{i}_s^{dq}}{dt} = A^{dq}\vec{i}_s^{dq} + B^{dq}\vec{u}_s^{dq} + P^{dq} \quad (2.19)$$

$$A^{dq} = \begin{bmatrix} -\frac{R_s}{L} & \omega_e \\ -\omega_e & -\frac{R_s}{L} \end{bmatrix}; B^{dq} = \begin{bmatrix} \frac{1}{L} & 0 \\ 0 & \frac{1}{L} \end{bmatrix}; P^{dq} = \begin{bmatrix} 0 \\ -\omega_e \sqrt{\frac{3}{2}} \frac{\psi_p}{L} \end{bmatrix}$$

From the mechanical equations of PMSM, we also have:

$$\begin{cases} \frac{d\omega_e}{dt} = \frac{n_p^2 \sqrt{3/2} \psi_p i_{sq}}{J} - \frac{f_0}{J} \omega_e - \frac{n_p}{J} T_{load} \\ \frac{d\delta}{dt} = \omega_s - \omega_e \end{cases} \quad (2.20)$$

### 2.2.3 Stability analysis of PMSM

The equation of the machine in complex domain, which is shown in (2.21), is considered.

$$\underline{V} = \underline{E} + \underline{Z}I \quad (2.21)$$

where  $\underline{Z}$  is the complex stator impedance and follows these equations below:

$$\begin{cases} |Z| = Z = \sqrt{R_s^2 + (L\omega_{re})^2} \\ \arg(Z) = \alpha = \text{atan}\left(\frac{L\omega_{re}}{R_s}\right) \end{cases} \quad (2.22)$$

From equation (2.21), the complex value of the current  $\underline{I}$  can be obtained as shown in equation (2.23)

$$\underline{I} = \frac{V - \underline{E}}{Z} \quad (2.23)$$

The power developed is calculated by:

$$P_e = 3\mathcal{R}e\{\underline{E} \cdot \underline{I}^*\} \quad (2.24)$$

Let the applied voltage be the reference:  $\underline{V} = |V|\angle 0^\circ$  then  $\underline{E} = |E|\angle \delta = |E|\cos \delta + j|E|\sin \delta$ . Therefore, the power can be written as follow:

$$P_e = \frac{3|E||V|}{|Z|^2} (R_s \cos \delta - X \sin \delta) - \frac{3|E|^2 R_s}{|Z|^2} \quad (2.25)$$

$$P_e = \frac{3|E|}{Z} (V \cos(\alpha - \delta) - |E| \cos \alpha)$$

The electromagnetic torque will be expressed as:

$$T_{em} = \frac{P_e}{\omega_{rm}} = \frac{3k_e}{Z} (V \cos(\alpha - \delta) - |E| \cos \alpha) \quad (2.26)$$

where  $k_e$  is the EMF constant of PMSM, which is determined in (2.7).

Finally, an expression of the torque versus the load angle  $\delta$  is represented in Figure 2.7.

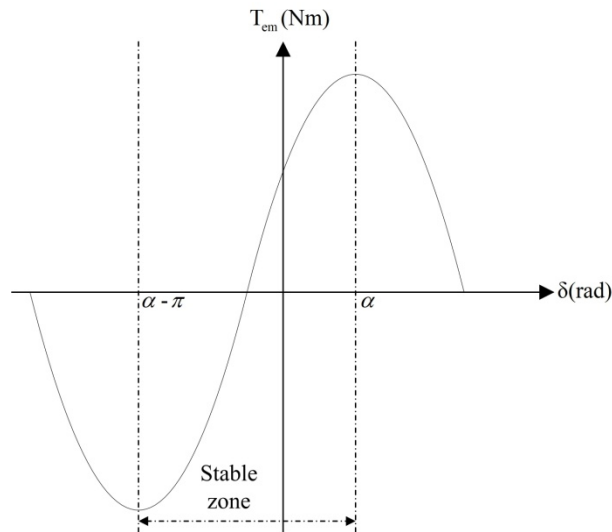


Figure 2.7: Evolution of  $T_{em} = f(\delta)$  with the consideration of  $R_s$

Using the condition of stability of PMSM, which is expressed as  $\frac{\partial T_{em}}{\partial \delta} > 0$ , it can be pointed out that a PMSM is stable in open loop in the values of load angle  $\delta$  respecting the following relation:

$$\alpha - \pi < \delta < \alpha \quad (2.27)$$

In the case of neglecting the value of resistance, the electromagnetic torque can be rewritten as follows:

$$T_e = K \frac{V_s}{\omega_m} \sin(\delta) \quad (2.28)$$

According to the equation (2.28), the torque  $T_e$  evolves as a sinusoidal function of the load angle  $\delta$  (Figure 2.8). In figure, two different zones are defined. The grey zone limited by the dash lines is the stable operating zone and the other (outside the grey zone) are unstable zones.

The stable operation zone of the synchronous machine is characterized by the slope of the curve  $T_e = f(\delta)$ , that is the sign of  $\frac{\partial T_e}{\partial \delta}$ . Therefore, the system is stable if, at constant speed, the load angle is limited in the range as shown in following relation:

$$-\frac{\pi}{2} < \delta < \frac{\pi}{2} \quad (2.29)$$

This angle depends on the position of the rotor flux ( $\theta_e$ ) and the stator flux (the position of  $\vec{V}$ ).

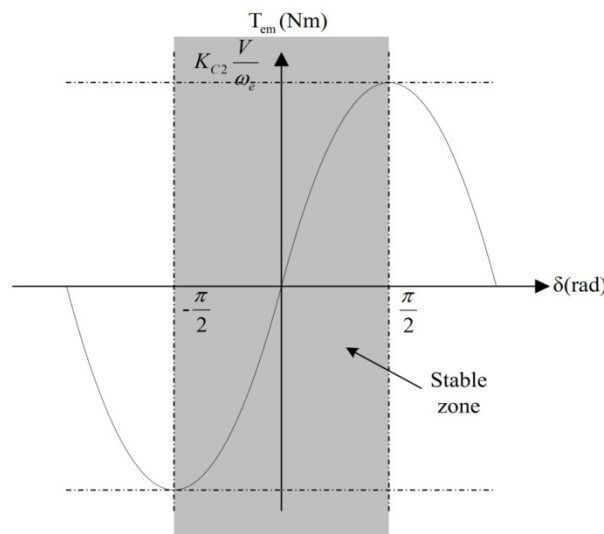


Figure 2.8: Evolution of  $T_{em}=f(\delta)$  without consideration of  $R_s$

### 2.2.4 A three-phase two-level voltage inverter

As mentioned, in order to control a PMSM, either in torque or in speed, it is necessary to supply voltages which have the variable amplitude and frequency at the terminals of machines. To modulate these quantities, a voltage inverter is implemented. In this work, the inverter chosen is a three-phase two-level type which is shown in Figure 2.9

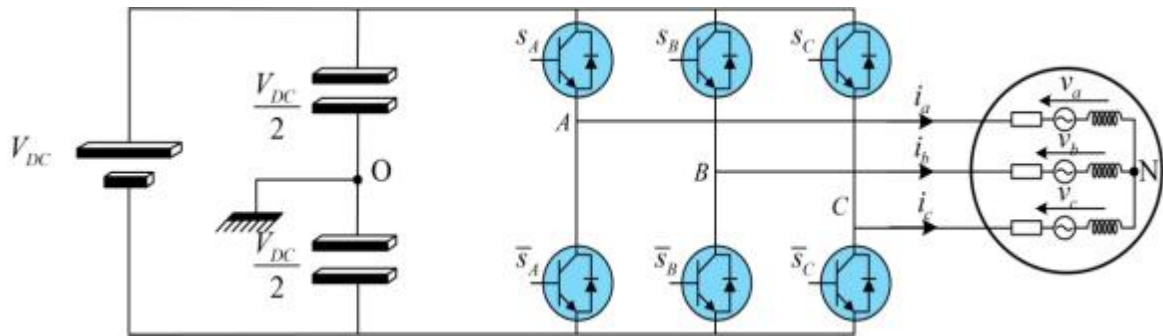


Figure 2.9: Diagram of a three-phase two-level inverter

As represented in this figure, the inverter has three legs composed of two bidirectional switches. In this study, the use switch is IGBT type with diode for anti-parallel.

In the case which the neutral of machine is not connected, we will have the equation in (2.30) always be verified:

$$\begin{aligned} v_a + v_b + v_c &= (v_{AO} + v_{ON}) + (v_{BO} + v_{ON}) \\ &+ (v_{CO} + v_{ON}) = 0 \end{aligned} \quad (2.30)$$

Following this relationship, the phase voltages can be obtained by the equation (2.31)

$$\begin{bmatrix} v_a \\ v_b \\ v_c \end{bmatrix} = \begin{bmatrix} v_{AO} + v_{ON} \\ v_{BO} + v_{ON} \\ v_{CO} + v_{ON} \end{bmatrix} = \frac{1}{3} \begin{bmatrix} 2 & -1 & -1 \\ -1 & 2 & -1 \\ -1 & -1 & 2 \end{bmatrix} \begin{bmatrix} v_{AO} \\ v_{BO} \\ v_{CO} \end{bmatrix} \quad (2.31)$$

## 2.3 Control strategies for PMSM drive

The principle of controlling AC machines is well-known and such structure has been developed in many studies [Leo01][Vas90]. In this section, the basic structure with field-oriented control for PMSM drives will be presented first [QD08]. Some other structures such as Direct Torque Control (DTC) [Vas98], Predictive Torque Control (PTC)... will also be considered after that.

### 2.3.1 Field oriented control

Field Oriented Control (FOC) is one of the most popular vector control methods and gives PMSM high performances. This method allows controlling the flux and the torque in AC machine in similar way as for DC motor. In this method, the motor equations are transformed to a coordinate system that rotates in synchronism with PM flux (d-q frame). In this frame, the stator current vector is split into two current components,  $i_{sd}$  and  $i_{sq}$ , which are flux and torque production currents respectively. Therefore, this method allows, separately and indirectly, to control of the flux and torque quantities by using current control loop with some kinds of controllers such as PI controller, hysteresis controller... Also a speed controller is needed in the outer loop; the speed control can be achieved by closing the loop by a feedback outside the inner torque control loop. The speed feedback can be derived from the same rotor angular position sensor, which is used to obtain the rotor position feedback.

In Figure 2.10, a general scheme of the FOC is presented. The three phase measured stator currents are transformed into d-q frame. This conversion provides the feedback currents  $i_{sd}$  and  $i_{sq}$ . Also a sensing of the DC-link voltage is required in order to feed the space vector algorithm.

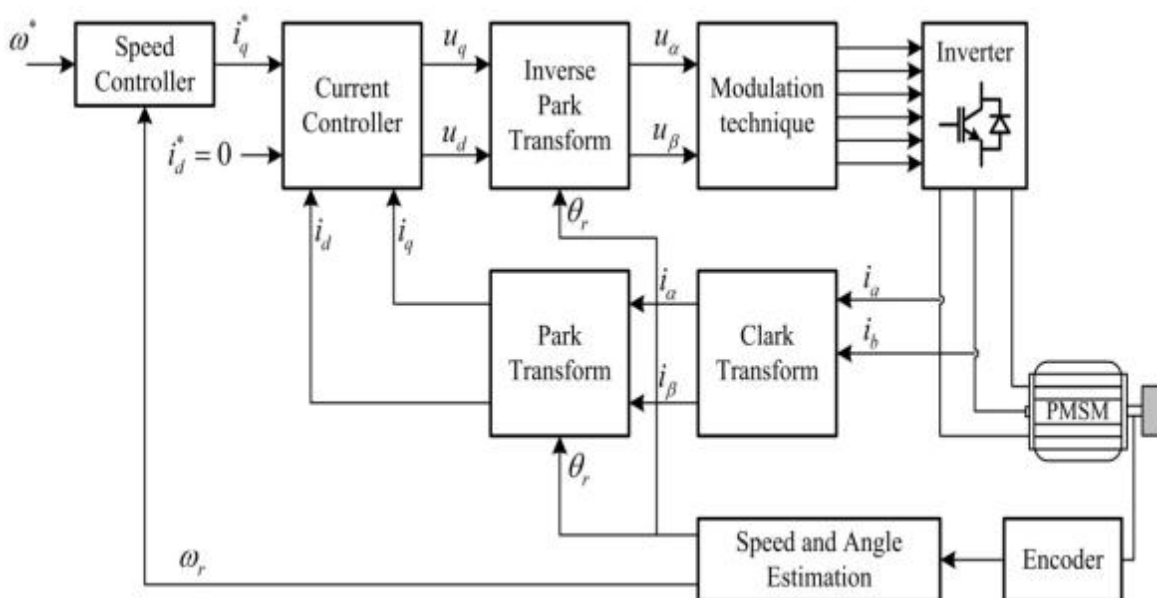


Figure 2.10: General scheme of FOC for a PMSM

One of the easiest strategies and most widely used in the industry is constant torque angle. The torque angle is defined as the angle between the q-axis current  $i_{sq}$  and the rotor permanent flux  $\psi_p$ . This angle will be maintained at  $\pi/2$  according to this control strategy.

It also means that the d-axis current is maintained equal to zero ( $i_{sd} = 0$ ). This means that a linear current controller results in linear control over the torque. This control strategy is not recommended for IPMSM with high saliency ratio ( $L_d/L_q$ ). However, for SPMSM where  $L_d = L_q$ , this strategy is commonly used. The main advantage of this control strategy is that it minimizes the current/torque ratio.

The control system consists of separate controllers for the torque and the current. Measurement or estimation of the rotor angle is needed in the transformation of the d- and q- axis current components into fixed coordinate system and vice versa.

### 2.3.2 Direct Torque Control (DTC)

Direct torque control is another strategy for AC motor control which was introduced in Japan by Takahashi and Noguchi [TN86] and also in Germany by Depenbrock [Dep88]. Their innovative studies depart from the idea of transformation from abc three-phase coordinate to  $\alpha\beta$  coordinate.

The principle of this method relies on a bang-bang control instead of a decoupling control which is the characteristic of vector control. Their technique (bang-bang control) works very well with the on-off operation of inverter with power electronic components.

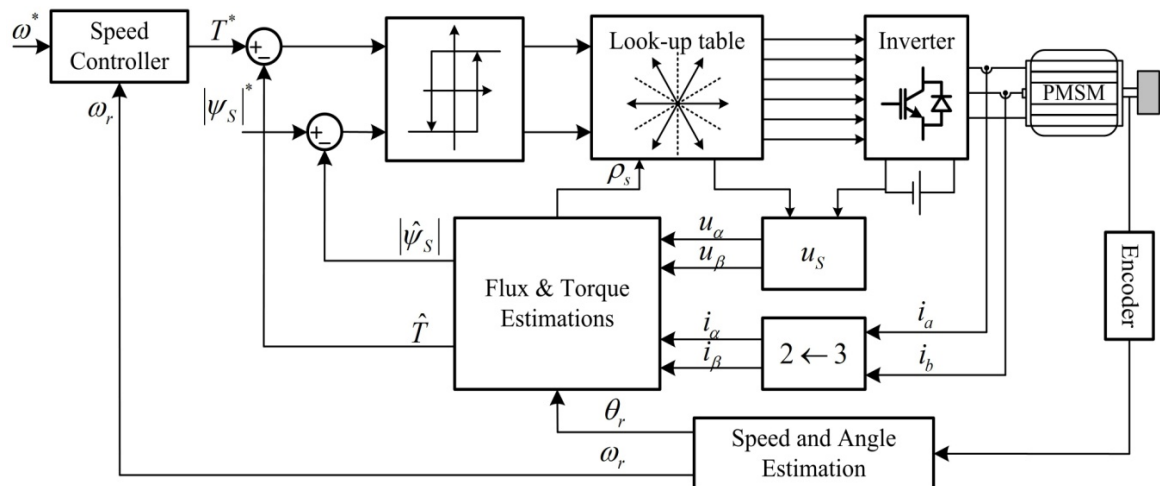


Figure 2.11: General scheme of DTC for a PMSM

A general scheme of DTC is presented in Figure 2.11. According to this scheme, two hysteresis controllers are used, one for torque error correction and one for flux linkage error correction.

The principle of DTC, as its name implies, is to control the electromagnetic torque and flux linkage directly and independently by the use of six or eight voltage space vectors

found in a lookup table based on the position of this flux [ABRA02] [Llo03]. The representation of these voltage vectors and six correlative sectors are shown in Figure 2.12

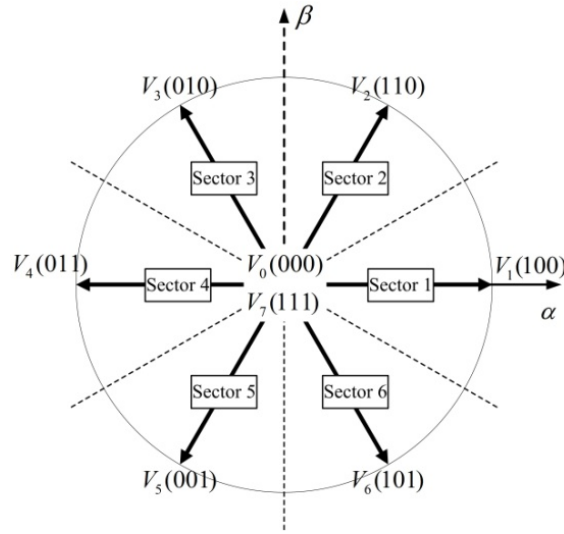


Figure 2.12: The basic voltage vectors and six sectors

As shown in Figure 2.13, the hysteresis flux controller makes the stator flux rotate in a circular fashion and be limited in the reference trajectory.

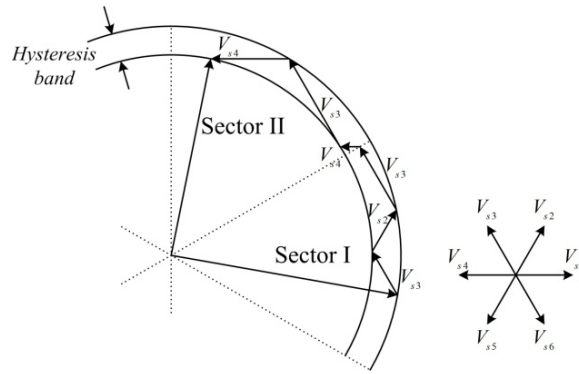


Figure 2.13: Circular trajectory of stator flux linkage in DTC

Rewriting the equation of electromagnetic torque of a PMSM as follow:

$$T_e = \frac{n_p |\psi_s|}{L} \psi_p \sin \sigma \tag{2.32}$$

The torque thus can be controlled by controlling the standard stator flux and the angle  $\sigma$  which is formed by this flux and the flux created by the magnets. However, this flow also can be approximated by the integration of the stator voltages (Equation (2.33)).

$$\psi_s = \int (V - RI)dt \approx \int V dt \quad (2.33)$$

The hysteresis torque controller tries to keep the motor torque within a pre-defined hysteresis band. The evolution of torque under the effect of each voltage vector is illustrated in Figure 2.14.

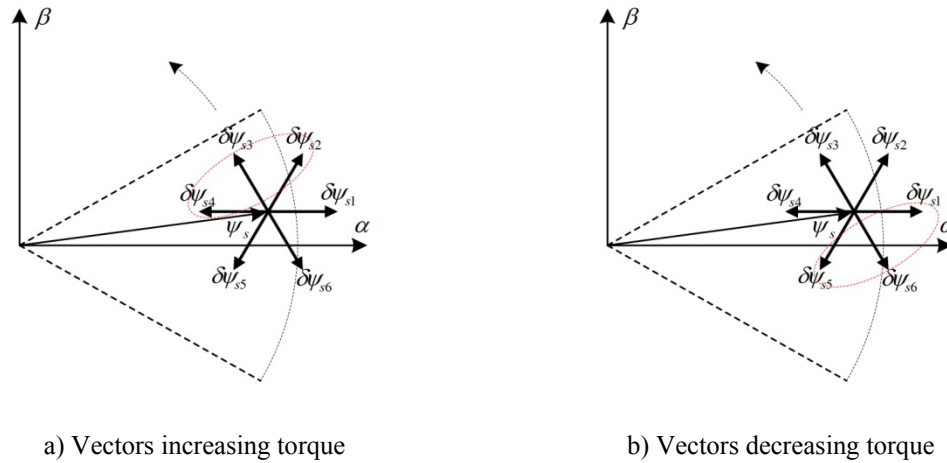


Figure 2.14: The evolution of torque under DTC

At every sampling time the voltage vector selection block decides on one of the six possible inverter switching states ( $s_a, s_b, s_c$ ) to be applied to the motor terminals. The possible outputs of the hysteresis controller and the possible number of switching states in the inverter are finite, so a look-up table can be constructed to choose the appropriate switching state of the inverter. This selection is a result of both the outputs of the hysteresis controllers and the sector of the stator flux vector in the circular trajectory. A conventional optimal switching table is built based on the analysis above.

$\psi_s T$	$S_1$	$S_2$	$S_3$	$S_4$	$S_5$	$S_6$
	$V_5$	$V_6$	$V_1$	$V_2$	$V_3$	$V_4$
	$V_3$	$V_4$	$V_5$	$V_6$	$V_1$	$V_2$
	$V_6$	$V_1$	$V_2$	$V_3$	$V_4$	$V_5$
	$V_2$	$V_3$	$V_4$	$V_5$	$V_6$	$V_1$

Table 2.1: Optimal switching table for DTC control

### 2.3.3 Direct Predictive Torque Control (DPTC)

The first ideas about Predictive Control applied to power converters started in the 1980's [HS83][KS83]. The principle of this strategy is based on the calculation of the future system behaviors and the use of a cost function to evaluate these behaviors. The execution of the predictive algorithm can be divided in three main steps:

- + Updating the states of the system and estimating the variables that cannot be measured;
- + Predicting the future plant behaviors;
- + Optimizing the control signal according to a cost function.

Based on the principle of predictive control and DTC, a Direct Predictive Torque Control (DPTC) strategy is applied to the PMSM drive system. A general scheme of DPTC for PMSM is shown in Figure 2.15.

Due to the pre-calculation of the system behavior up to the prediction horizon [CB07], predictive control is generally inevitable of high computational effort. Especially, in the area of electrical drives, a high sampling frequency is necessary. Therefore, in DPTC for PMSM drive system, the prediction horizon is limited to one step ahead. Besides, the set of tested control signal also is finite. Normally, this set includes the number of configurations

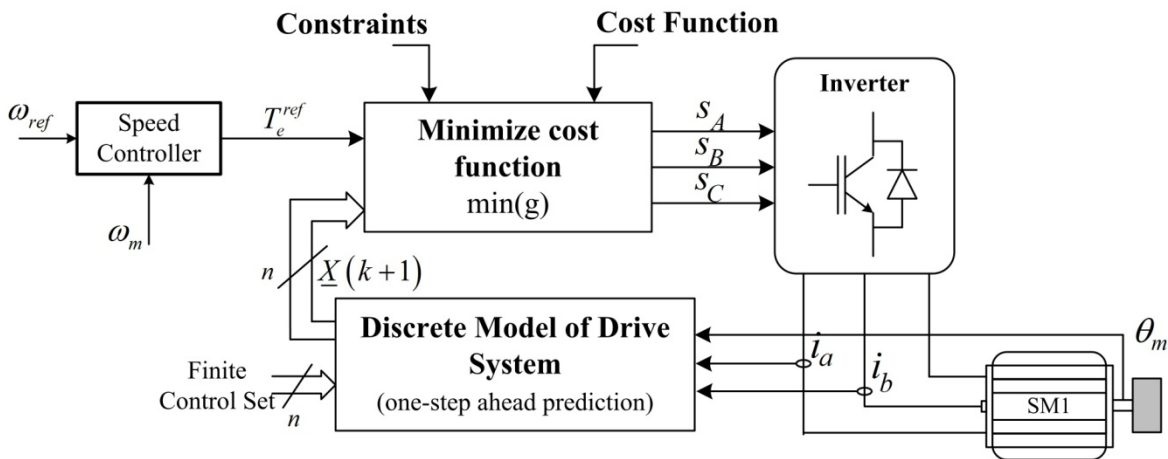


Figure 2.15: General scheme of DPTC for PMSM

generated from an inverter. In Figure 2.15, a general scheme of DPTC for PMSM is illustrated.

The one-step ahead discrete model of drive system will be built. The first component of this model is the discrete state model of PMSM which is derived from the continuous model of PMSM in section 2.2.2.2.

$$\begin{aligned} \begin{bmatrix} i_{sd}(k+1) \\ i_{sq}(k+1) \end{bmatrix} &= \begin{bmatrix} 1 - T_s \frac{R_s}{L} & T_s \omega_e(k) \\ -T_s \omega_e(k) & 1 - T_s \frac{R_s}{L} \end{bmatrix} \begin{bmatrix} i_{sd}(k) \\ i_{sq}(k) \end{bmatrix} + \begin{bmatrix} \frac{T_s}{L} & 0 \\ 0 & \frac{T_s}{L} \end{bmatrix} \begin{bmatrix} u_{sd}(k) \\ u_{sq}(k) \end{bmatrix} \\ &+ \begin{bmatrix} 0 \\ T_s \frac{\psi_p}{L} \omega_e(k) \end{bmatrix} \end{aligned} \quad (2.34)$$

To complete the model of the whole system, a discrete model of the inverter is used:

$$\begin{bmatrix} u_{AN}(k) \\ u_{BN}(k) \\ u_{CN}(k) \end{bmatrix} = \frac{V_{DC}}{3} \begin{bmatrix} 2 & -1 & -1 \\ -1 & 2 & -1 \\ -1 & -1 & 2 \end{bmatrix} \begin{bmatrix} s_A(k) \\ s_B(k) \\ s_C(k) \end{bmatrix} \quad (2.35)$$

where  $s_X (X = A, B, C)$  is the states of inverter's leg. With a standard three-phase two-level inverter, there are eight configurations. Among these configurations, the first state (0,0,0) and the eight one (1,1,1) give the same output voltage. Therefore, the set of control signal is limited to seven different states of inverter.

From this model, the future behaviors of the system under the finite set of control signal can be predicted. The future errors can be pre-calculated through a cost function.

In DPTC control, the torque and the flux linkage will be considered in the cost function:

$$g_T = \|T^{ref} - T_{em}(k+1)\|^2 + \gamma_\psi \|\psi_s^{ref} - \psi_s(k+1)\|^2 \quad (2.36)$$

The factor denotes the so-called weighting factor, which increases or decreases the importance of the torque or flux control. If the same importance is assigned to both control objectives, this factor would correspond to the ratio between the nominal magnitudes of the torque  $T_n$  and the stator flux  $|\vec{\psi}_{sn}|$  [KRET10]:

$$\gamma_\psi = \left( \frac{T_n}{|\vec{\psi}_{sn}|} \right)^2 \quad (2.37)$$

Moreover, with SPMSM whose the inductances in d and q axis are equal  $L_d = L_q = L$ , the torque is directly proportional to the q-current  $i_{sq}$ . Therefore, another cost function including the current components can be considered:

$$g_i = \|i_{sq}^{ref} - i_{sq}(k+1)\|^2 + \gamma_i \|i_{sd}(k+1)\|^2 \quad (2.38)$$

There are also several modified cost functions with other criteria such as the power loss of the machine, the power loss in switching states of inverter...

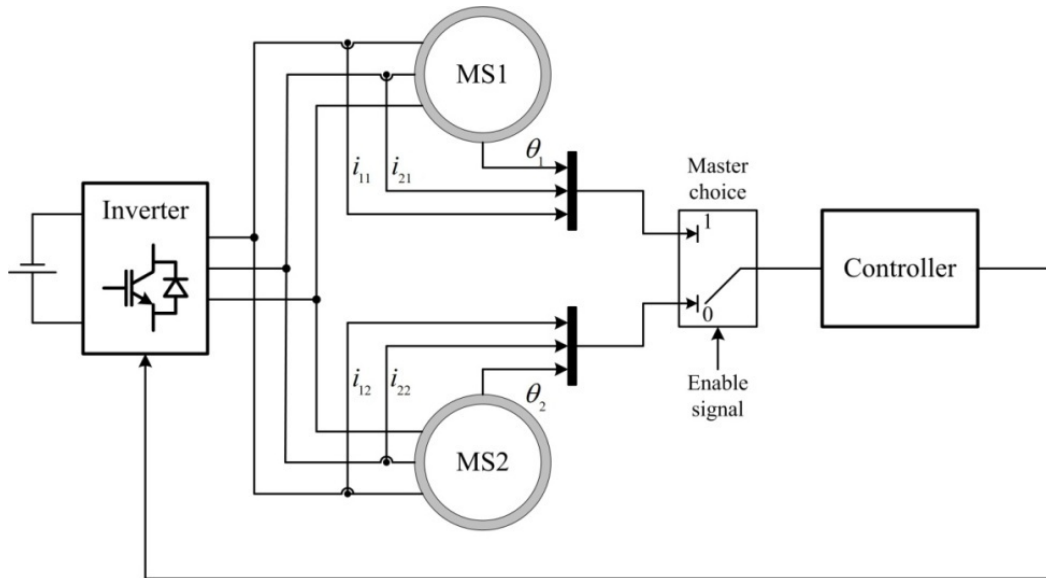


Figure 2.16: Parallel structure under master/slave configuration

## 2.4 Control structure for Mono-inverter Dual-parallel PMSM system

In previous section, general descriptions about a PMSM drive system have been presented. Moreover, the strategies used to control this drive system also are introduced. All these analyses will be very useful for the consideration of mono-inverter dual-parallel PMSM system.

In this section, the structures which are applied for this kind of drive system will be considered.

### 2.4.1 Master-slave structure

#### 2.4.1.1 General description

In this part, a master/slave configuration, which was applied to the mono-inverter dual-parallel PMSM drive system [Bid11], is presented. Some considerations are taken into account:

- + Both machines are identical;
- + Both machines must be operated at the same speed  $\omega_{m1} = \omega_{m2}$ ;
- + The loads applied to each machine are different and not mechanically linked;

As shown in Figure 2.16, this is a block diagram describing the master/slave configuration. A block named “Master choice” is added to the system in order to select the master machine. According to this configuration, at each moment of time, only the machine considered as master is controlled. The other one, the slave machine, will operate in open loop under the voltage supplying mode.

Like this, the value of the voltage supplied by the inverter is entirely due to the control of the master machine. The slave machine does not have any influence on this value.

Practically, according to this structure, it is not different compared with a normal PMSM drive system. Therefore, the stability of the master machine which is always controlled will be assured. However, it is possible that the slave machine, which is in open loop, could be unstable. The problem of choosing the adequate machine to set as the master while respecting the stability condition of the complete system needs to be considered.

#### 2.4.1.2 Consequence due to a load variation

In order to understand and anticipate the operation of two parallel PMSM connected to an inverter, behaviors of master and slave machines will be considered in case of variation of the load of one machine.

Figure 2.17 illustrates the evolution of mono-inverter dual-parallel PMSMs drive system under master/slave configuration with different loads.

According to Figure 2.17, the imposition of a speed  $\Omega_m$  (point A) to the master machine leads to two consequences:

- + First, the self-synchronism of PMSM will impose a pulse with  $\omega_{e_m}$  to voltage applied at the terminals of the machines (point B);
- + Secondly, a load torque  $T_{load_m}$ , which depends on the speed, will be applied (point H)

Two machines are connected in parallel with an inverter, the speed of stator field of the slave machine thus is also imposed:  $\omega_{e_{sl}} = \omega_{e_m}$  (point C).

To assure the synchronism of slave machine  $SM_{sl}$ , its speed has to be the same with the master machine:  $\omega_{m_m} = \omega_{m_{sl}}$  (point D). Similar to the master, a load torque  $T_{load_{sl}}$ , which can be different from  $T_{load_m}$ , is also applied to the slave machine (point E).

At steady state, both machines must provide respectively the electromagnetic torque  $T_{e_m}$  (point I) and  $T_{e_{sl}}$  (point F). In order to obtain this torque along with a current angle  $\psi_m = 0$ , for master machine it is necessary to provide a certain voltage  $V$  (point J). Under this voltage, a load angle  $\delta_m$  is defined (point K).

This voltage (with amplitude  $V$  and frequency  $\omega_e$ ) is also applied to the slave machine. A load angle  $\delta_{sl}$  is also defined and correlative to a load torque  $T_{e_{sl}}$  (point G).

From the steady state, the stability of the slave machine in the presence of a load change from one machine is then studied. And the choice of master machine will be pointed out.

### 2.4.1.3 The choice of master machine

At steady state, because the two machines are identical and supplied by the same voltage source with same value of voltage  $V_s$  and frequency  $f_s$ , they will have the same torque characteristic  $T_e = f(\delta)$ . The comparison of two loads applying to two motors gives the following relationship:

$$\frac{T_{load_{sl}}}{T_{load_m}} = \frac{T_{e_{sl}}}{T_{e_m}} = \frac{\sin(\delta_{sl})}{\sin(\delta_m)} \quad (2.39)$$

Referring to the stability analysis of PMSM, the condition of  $\delta_m$  is always guaranteed for the load angle of the master machine because the value of  $I_m$  is limited. To investigate the stability of the slave motor, two cases comparing the loads of two machines are pointed out:

- + If  $T_{load_{sl}} \leq T_{load_m} \Rightarrow \delta_{sl} \leq \delta_m \Rightarrow$  The stability is ensured for both machines;
- + If  $T_{load_{sl}} > T_{load_m} \Rightarrow \delta_{sl} > \delta_m \Rightarrow$  It is possible for the load angle of the slave machine to be out of the stability condition. The stability of the system then is not guaranteed.

To illustrate this, a vector diagram showing the positions of the two machines at steady state is represented in Figure 2.19. Both studies are then considered:  $T_{load_{sl}} > T_{load_m}$  (Figure 2.19a) and  $T_{load_{sl}} < T_{load_m}$  (Figure 2.19b). These figures are shown for a given electrical value of motor angle of master machine  $\theta_{e_m}$ . This value varies over time, and when the steady state is reached, the trend is the same as the angle of slave machine  $\theta_{e_{sl}}$ .

In these diagrams, comparisons between two load angle ( $\delta_m, \delta_{sl}$ ) are consistent with the theory described above.

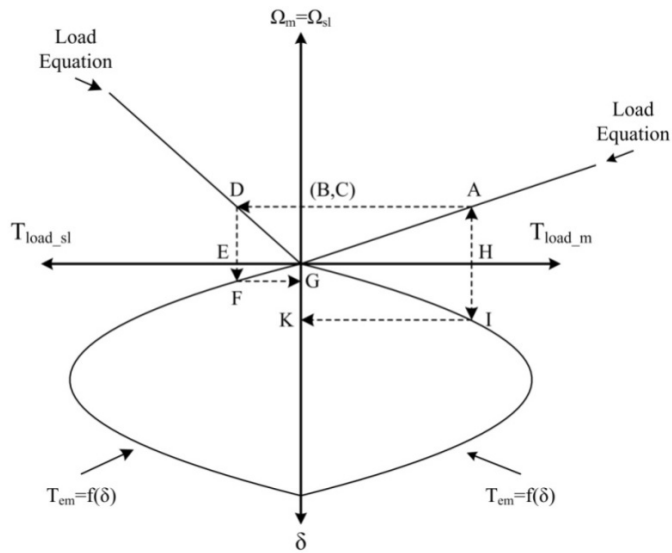
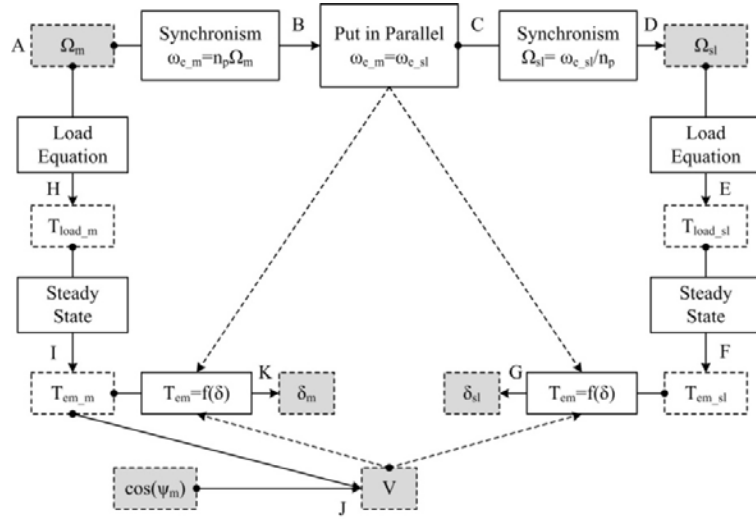


Figure 2.17: Evolution of system under master/slave configuration with different loads

For such these systems, therefore, in order to ensure the stability of whole system, it is necessary to control the machine which has the highest mechanical load (the master machine). The machine with the higher load also has the bigger load angle, thus, it is possible to compare the load angle of each machine ( $\delta_1$  and  $\delta_2$ ) to determine which machine is the master one.

However, when the same voltages  $\vec{V}_g$  are applied to the two machines, the following relationship always is verified:

$$\theta_{e1} + \delta_1 = \theta_{e2} + \delta_2 \quad (2.40)$$

From the relation in Equation (2.40), another relation can be brought out as follows:  $\delta_1 < \delta_2 \Leftrightarrow \theta_{e1} > \theta_{e2}$ . As a result, to determine which machine is the master one and to be controlled, it must be compared the electrical position  $\theta_{e1}$  and  $\theta_{e2}$ : the machine with the smaller electrical position will be chosen as the master one. This solution, proposed in a patent [FBM+07], is presented in Figure 2.18. The value of  $\theta_e$  is already used for the autopilot, no additional sensor is needed.

As shown in Figure 2.16, the position and currents of the two machines are continuously recorded. A logic signal "Enable" allows choosing the master machine in order to carry out the speed and current control. This signal is created by calculating the difference ( $\theta_{e2} - \theta_{e1}$ ) and passing this difference through a hysteresis comparator. If "Enable = 1" the master machine is MS1 and MS2 is the slave, on the contrary, if "Enable = 0" MS2 is the master and MS1 is the slave one. The master selector block is presented in Figure 2.18.

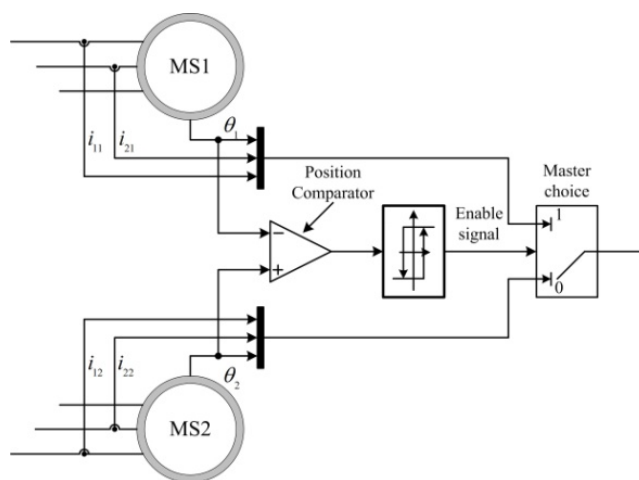


Figure 2.18: Master choice block

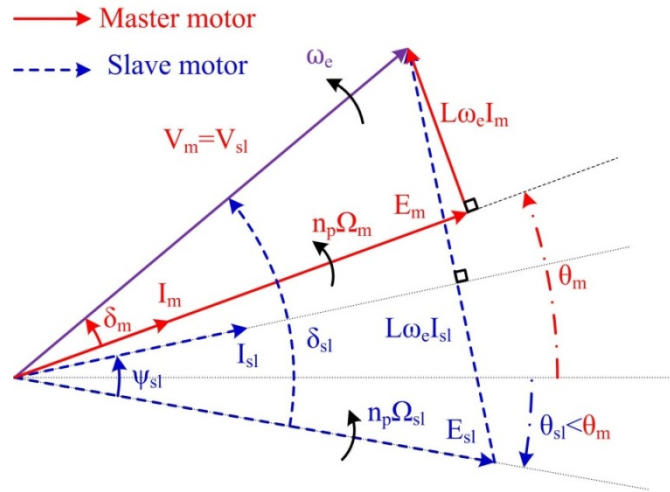
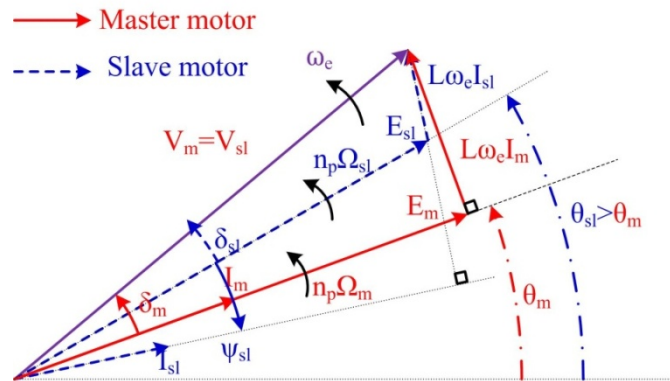
a) Case 1:  $T_{load\_m} < T_{load\_sl}$ b) Case 2:  $T_{load\_m} > T_{load\_sl}$ 

Figure 2.19: Voltage vector diagram of two PMSM under different loads

According to the analysis above, the selection of the master machine has been developed. However, this principle is just appropriate to the case of positive speed. In the case where the speed of the motors is negative, the value of load angle  $\delta$  is also negative and the machine that is in open loop will be stable as its angle  $\delta > -\frac{\pi}{2}$  (or  $(\alpha - \pi)$  in the case of consideration of  $R_s$ ).

Applying the same principle as above, the slave machine is stable if the absolute value of the load torque applied to the master machine respects the following relations:

- + If  $|T_{load\_sl}| \leq |T_{load\_m}| \Rightarrow |\delta_{sl}| \leq |\delta_m| \Rightarrow \delta_{sl} \geq \delta_m \Rightarrow$  the stability is guaranteed for both machines;
- + If  $|T_{load\_sl}| > |T_{load\_m}| \Rightarrow |\delta_{sl}| > |\delta_m| \Rightarrow \delta_{sl} < \delta_m \Rightarrow$  it is possible for the load angle of the slave machine be out of the stability zone. The stability of the system is not guaranteed.

In this case, the master machine will be the one that has the smallest value of load angle  $\delta$ , i.e the highest value of  $\theta_e$ . Besides, when selecting the master machine, the value of the speed, represented by the reference speed  $\omega_{ref}$  is a parameter need to be taken into account.

#### 2.4.1.4 Conclusions

Based on the method of choosing the master machine like in paragraph **Error! Reference source not found.**, the stability of the whole system is assured although only master machine is controlled. The slave machine in many conditions still follows the master one and the synchronism of both machines is obtained.

To improve the performance of the system under master/slave structure, the value of the hysteresis can be modulated in the "master choice block". This issue has been also considered in [BPDFM09] [Bid11].

Moreover, because just only one machine is controlled in this structure, other control strategies for high performance of PMSM drive system such as DTC, PTC...can be applied for the master machine.

In the next part of this chapter, another approach with mono-inverter dual-parallel PMSM will be considered. This consideration is carried out based on the principle of DTC.

### 2.4.2 Direct torque control (DTC) for mono-inverter dual-parallel PMSM

DTC has been well-adapted to electric drive systems in general, as well as PMSM drive system in particular. In the following paragraphs, DTC strategy continues to be

considered with mono-inverter dual-parallel PMSM. The aim of this approach is to construct an optimal lookup table to meet the demands of two PMSMs connected in parallel.

The configuration of this DTC drive system is set up as shown in Figure 2.20.

### 2.4.2.1 General description

In this part, DTC method will be considered with the mono-inverter dual-parallel PMSM structure [Ndi09] [FNL13]. All the characteristic of this drive system as mentioned in the previous section are respected.

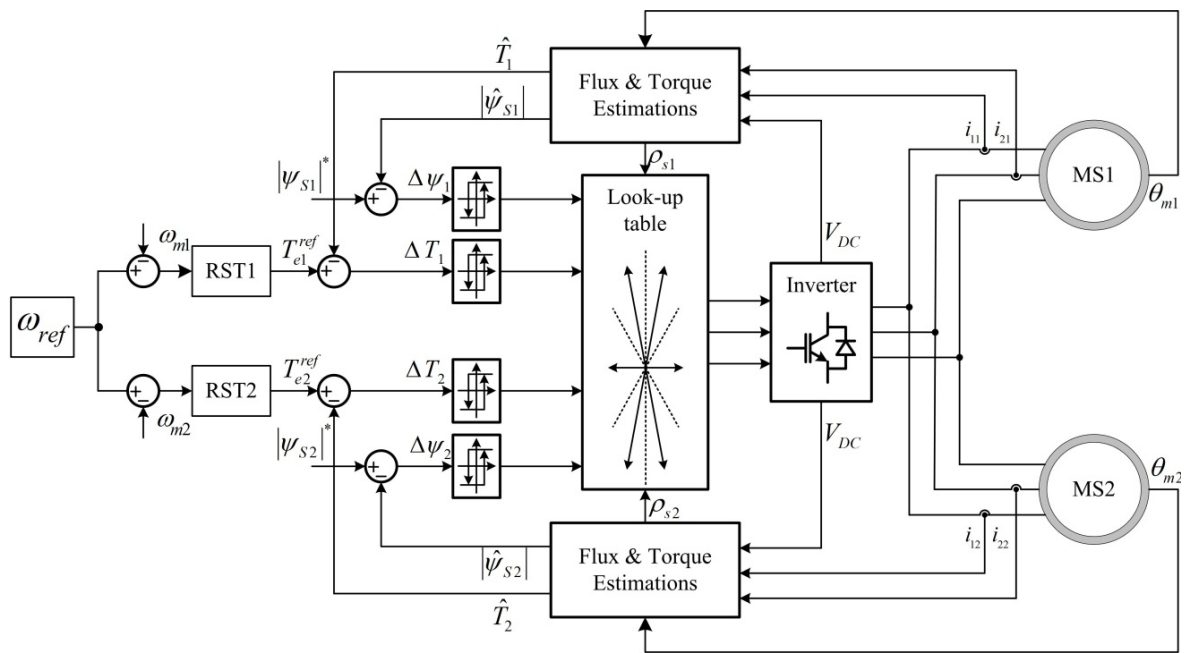


Figure 2.20: General scheme of DTC for dual-parallel PMSM drive system

The principle is preserved as in the case of one machine. However, with one machine, there are just two error components  $\Delta T$  and  $\Delta\psi_s$  which are considered by two hysteresis controllers. Just four cases can then happen as shown in Table 2.1. Therefore, it is easy to find just only one suitable voltage to meet the control demand.

In the case two machines operating in parallel, the number of error component increases to four  $\Delta T_1$ ,  $\Delta T_2$ ,  $\Delta\psi_{s1}$  and  $\Delta\psi_{s2}$ . Four hysteresis comparators have to be used in order to control the torque and flux linkage of two machines. Now, there are sixteen cases can be synthesized from four states of two machines (Table 2.2).

$\Delta T_1 \Delta T_2$ $\Delta \psi_{s1} \Delta \psi_{s2}$	00	01	11	10
00				
01				
11				
10				

Table 2.2: Table of the evolution of torque and flux of two PMSMs in parallel

Following the Table 2.2, sixteen cases can be separated into three groups. In the first group (denoted as **I**), both machines have the same requirements for torque and flux. The second group (denoted as **II**), just the requirements of either torque or flux of both machines are identical, the other one is different. In the last group (denoted as **III**) the requirements of torque and flux for both machines are completely different. For example, if for the first machine, both the torque and flux need to be increased, meanwhile for the second machine, they need to be decreased.

According to the DTC, each requirement pair of torque and flux will be correlative to a voltage vector (Table 2.1). However, the choice of this voltage vector also depends on the position of the stator flux vector in space vector. Under different load conditions, the stator flux vectors of two machines can be located in different sectors. This problem is also illustrated in Figure 2.21.

In this figure (Figure 2.21a), the flux vectors of two machines are in the same sector. The signals from all hysteresis comparators require the reduction of both the torque and flux of two machines. The suitable voltage vector in this case for both machines is the same. However, the problem will happen when the demands, which depends on the output of the hysteresis regulators of each machine, are different (Figure 2.21b) or when two flux vectors are located in different sectors (Figure 2.21c).

Therefore, it is necessary to build a new optimal switching table to adapt to both machines in parallel configuration. It will be discussed in the next part.

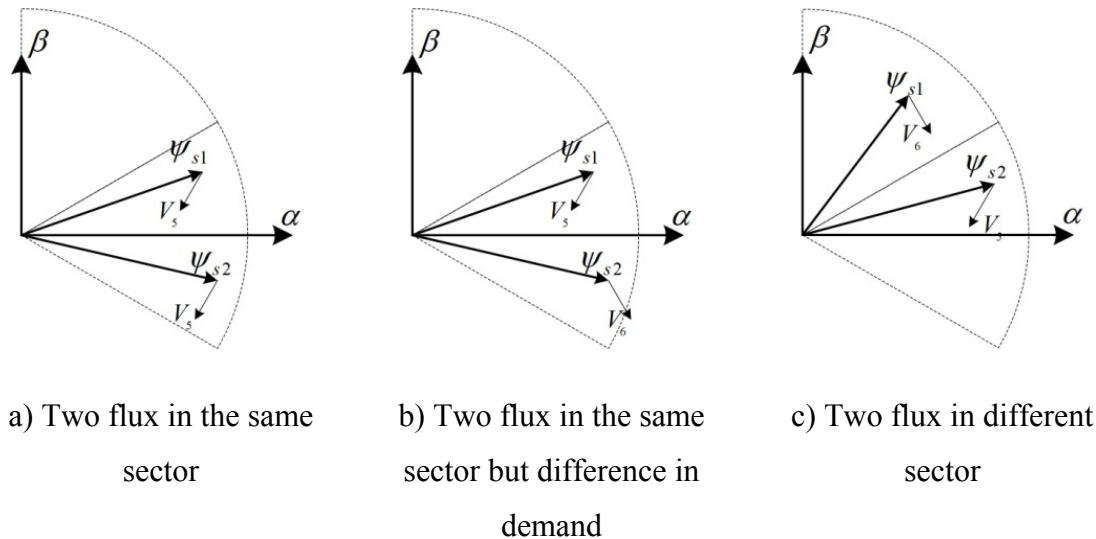


Figure 2.21: Different situation for selecting a suitable voltage vector

#### 2.4.2.2 Optimal switching table for two machines

In this part, an optimal switching table, which allows selecting a suitable voltage vector to apply to the dual-parallel PMSM system, will be created. The two cases will be considered:

##### a) Two stator flux vectors are in the same sector

The principle used to determine the voltage vector with the aim of meeting the requirements of both machines is pointed out as follows:

- + In the case of **III** (Table 2.2), the requirements of two machines are absolutely different. Therefore, the null vector is chosen;
- + In the second case (**II**), two machines have one requirements in common, either the torque or the flux evolution. In this case, the suitable voltage of each machine will not be of different sign. Let's suppose that the suitable vector for the first machine is noted as  $V^1$  and for the second machine is  $V^2$ . If there is an average vector located in the middle of  $V^1$  and  $V^2$ , this vector will be chosen (Figure 2.22).
- + If the two vectors are in adjacent sectors and the requirements for the torque of both machines are the same, but requirements for the flux will be different. The optimal voltage will be chosen depending on the position of flux vector of each machine (as shown in Figure 2.23).
- + The final case is the easiest case. Because the two machines have the same requirements for the torque and the flux, the same voltage vector will be the optimal for both of them.

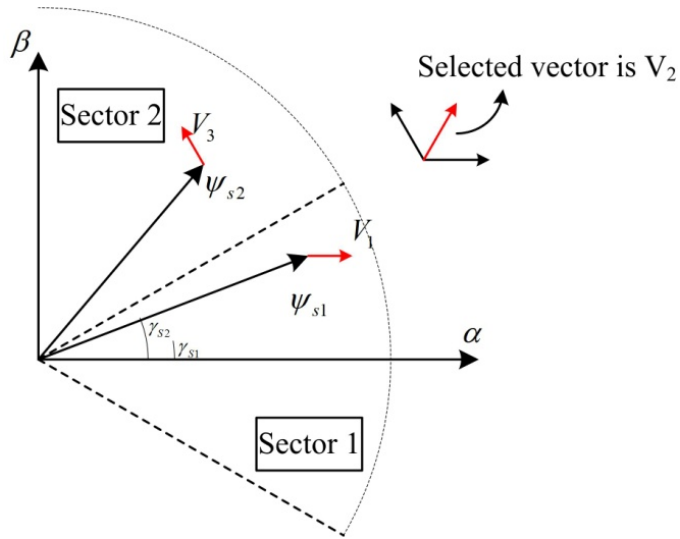


Figure 2.22: Average rule

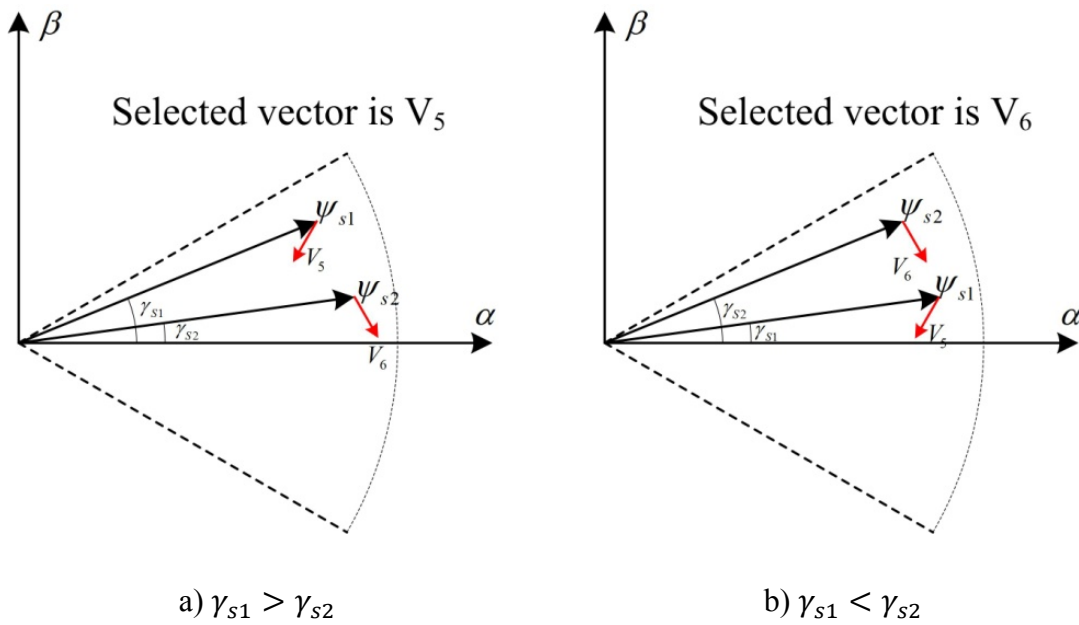


Figure 2.23: Two vectors are adjacent

According to these analyses, an optimal table is built and represented in Table 2.3.

$\Delta\psi_{s1}$	$\Delta\psi_{s2}$	$\Delta T_{e1}$	$\Delta T_{e2}$	$S_1$	$S_2$	$S_3$	$S_4$	$S_5$	$S_6$
0	0	0	0	$V_5$	$V_6$	$V_1$	$V_2$	$V_3$	$V_4$
0	0	0	1	$V_4$	$V_5$	$V_6$	$V_1$	$V_2$	$V_3$
0	0	1	0	$V_4$	$V_5$	$V_6$	$V_1$	$V_2$	$V_3$
0	0	1	1	$V_3$	$V_4$	$V_5$	$V_6$	$V_1$	$V_2$
0	1	0	0	$V_5/V_6$	$V_6/V_1$	$V_1/V_2$	$V_2/V_3$	$V_3/V_4$	$V_4/V_5$
0	1	0	1	$V_{0/7}$	$V_{0/7}$	$V_{0/7}$	$V_{0/7}$	$V_{0/7}$	$V_{0/7}$
0	1	1	0	$V_{0/7}$	$V_{0/7}$	$V_{0/7}$	$V_{0/7}$	$V_{0/7}$	$V_{0/7}$
0	1	1	1	$V_3/V_2$	$V_4/V_3$	$V_5/V_4$	$V_6/V_5$	$V_1/V_6$	$V_2/V_1$
1	0	0	0	$V_6/V_5$	$V_1/V_6$	$V_2/V_1$	$V_3/V_2$	$V_4/V_3$	$V_5/V_4$
1	0	0	1	$V_{0/7}$	$V_{0/7}$	$V_{0/7}$	$V_{0/7}$	$V_{0/7}$	$V_{0/7}$
1	0	1	0	$V_{0/7}$	$V_{0/7}$	$V_{0/7}$	$V_{0/7}$	$V_{0/7}$	$V_{0/7}$
1	0	1	1	$V_2/V_3$	$V_3/V_4$	$V_4/V_5$	$V_5/V_6$	$V_6/V_1$	$V_1/V_2$
1	1	0	0	$V_6$	$V_1$	$V_2$	$V_3$	$V_4$	$V_5$
1	1	0	1	$V_1$	$V_2$	$V_3$	$V_4$	$V_5$	$V_6$
1	1	1	0	$V_1$	$V_2$	$V_3$	$V_4$	$V_5$	$V_6$
1	1	1	1	$V_2$	$V_3$	$V_4$	$V_5$	$V_6$	$V_1$

Table 2.3: Table of optimal voltage vectors for two PMSMs

*b) Two stator flux vectors are in two adjacent sectors*

In this case, with 6 basic sectors, there are twelve combination sectors. According to these sectors and requirements about the voltage vector of each machine, another table will be built. Some general conditions also are inferred:

- + Although locating in two adjacent sectors, in some case, requirements of both machines can be the same for torque and flux.
- + Meanwhile, in the critical case shown in Table 2.2, the requirements for torque and flux of both machines are completely opposed to each other. The voltage vector will be chosen according to the average rule (Figure 2.22). It means that an average vector located in the middle of two vectors will be chosen.
- + Another special case can be happened, the two suitable voltage vectors for two machines are also two adjacent vectors. The vector will be determined based on the position of the two flux vectors (as shown in Figure 2.23).

As a result, an optimal voltage vector is defined for each case. They are summarized in Table 2.4 and Table 2.5

$\psi_{s1}$	$\Delta\psi_{s2}$	$\Delta T_{e1}$	$\Delta T_{e2}$	$S_{12}$	$S_{16}$	$S_{21}$	$S_{23}$	$S_{32}$	$S_{34}$
0	0	0	0	$V_5$	$V_4$	$V_5$	$V_6$	$V_6$	$V_1$
0	0	0	1	$V_5$	$V_{0/7}$	$V_{0/7}$	$V_6$	$V_{0/7}$	$V_1$
0	0	1	0	$V_{0/7}$	$V_4$	$V_5$	$V_{0/7}$	$V_6$	$V_{0/7}$
0	0	1	1	$V_3$	$V_2$	$V_3$	$V_4$	$V_4$	$V_5$
0	1	0	0	$V_6$	$V_5$	$V_6$	$V_1$	$V_1$	$V_2$
0	1	0	1	$V_4$	$V_6$	$V_1$	$V_5$	$V_2$	$V_6$
0	1	1	0	$V_2$	$V_4$	$V_5$	$V_3$	$V_6$	$V_4$
0	1	1	1	$V_3$	$V_2$	$V_3$	$V_4$	$V_4$	$V_5$
1	0	0	0	$V_6$	$V_5$	$V_6$	$V_1$	$V_1$	$V_2$
1	0	0	1	$V_5$	$V_1$	$V_2$	$V_6$	$V_4$	$V_1$
1	0	1	0	$V_1$	$V_3$	$V_4$	$V_2$	$V_5$	$V_3$
1	0	1	1	$V_3$	$V_2$	$V_3$	$V_4$	$V_4$	$V_5$
1	1	0	0	$V_6$	$V_5$	$V_6$	$V_1$	$V_1$	$V_2$
1	1	0	1	$V_{0/7}$	$V_1$	$V_2$	$V_{0/7}$	$V_3$	$V_{0/7}$
1	1	1	0	$V_2$	$V_{0/7}$	$V_{0/7}$	$V_3$	$V_{0/7}$	$V_4$
1	1	1	1	$V_2$	$V_1$	$V_2$	$V_3$	$V_3$	$V_4$

Table 2.4: Table of optimal voltage vectors for two PMSMs ( $S_{12} \rightarrow S_{34}$ )

$\Delta\psi_{s1}$	$\Delta\psi_{s2}$	$\Delta T_{e1}$	$\Delta T_{e2}$	$S_{43}$	$S_{45}$	$S_{54}$	$S_{56}$	$S_{61}$	$S_{65}$
0	0	0	0	$V_1$	$V_2$	$V_2$	$V_3$	$V_4$	$V_3$
0	0	0	1	$V_{0/7}$	$V_2$	$V_{0/7}$	$V_3$	$V_4$	$V_{0/7}$
0	0	1	0	$V_1$	$V_{0/7}$	$V_2$	$V_{0/7}$	$V_{0/7}$	$V_3$
0	0	1	1	$V_5$	$V_6$	$V_6$	$V_1$	$V_2$	$V_1$
0	1	0	0	$V_2$	$V_3$	$V_3$	$V_4$	$V_5$	$V_4$
0	1	0	1	$V_3$	$V_1$	$V_4$	$V_2$	$V_3$	$V_5$
0	1	1	0	$V_1$	$V_5$	$V_2$	$V_6$	$V_1$	$V_3$
0	1	1	1	$V_5$	$V_6$	$V_6$	$V_1$	$V_2$	$V_1$
1	0	0	0	$V_2$	$V_3$	$V_3$	$V_4$	$V_5$	$V_4$
1	0	0	1	$V_4$	$V_2$	$V_5$	$V_3$	$V_4$	$V_6$
1	0	1	0	$V_6$	$V_4$	$V_1$	$V_5$	$V_6$	$V_2$
1	0	1	1	$V_5$	$V_6$	$V_6$	$V_1$	$V_2$	$V_1$
1	1	0	0	$V_2$	$V_3$	$V_3$	$V_4$	$V_5$	$V_4$
1	1	0	1	$V_4$	$V_{0/7}$	$V_5$	$V_{0/7}$	$V_{0/7}$	$V_6$
1	1	1	0	$V_{0/7}$	$V_5$	$V_{0/7}$	$V_6$	$V_1$	$V_{0/7}$
1	1	1	1	$V_4$	$V_5$	$V_5$	$V_6$	$V_1$	$V_6$

Table 2.5: Table of optimal voltage vectors for two PMSMs ( $S_{43} \rightarrow S_{65}$ )

### 2.4.2.3 Simulation tests

In order to verify the optimal table of DTC for mono-inverter dual-parallel PMSM drive system, a simulation is carried out under the Matlab/Simulink environment. The parameters of PMSM using in this test are summarized in Table 2.6.

$R_s$	2.06( $\Omega$ )
$L_{sd} = L_{sq} = L$	9.15 $\times 10^{-3}(H)$
$\psi_p$	0.29(Wb)
Numbers of pole pairs ( $n_p$ )	3
Inertia ( $J$ )	$7.2 \times 10^{-4}(kg.m^2)$

Table 2.6: Parameters of machine using in simulation

The test is carried out under these following conditions. Three set points of speed will be considered:

- + From  $t = 0(s) \rightarrow 0.4(s)$ : the reference speed is set at  $\omega_{ref1} = 25\pi(rad/s)$ ;
- + From  $t = 0.4(s) \rightarrow 0.8(s)$ : the motor is reversed and run at  $\omega_{ref2} = -25\pi(rad/s)$ ;
- + From  $t = 0.8(s) \rightarrow 1.2(s)$ : the motor is kept standstill.

These set-points are plotted in Figure 2.24.

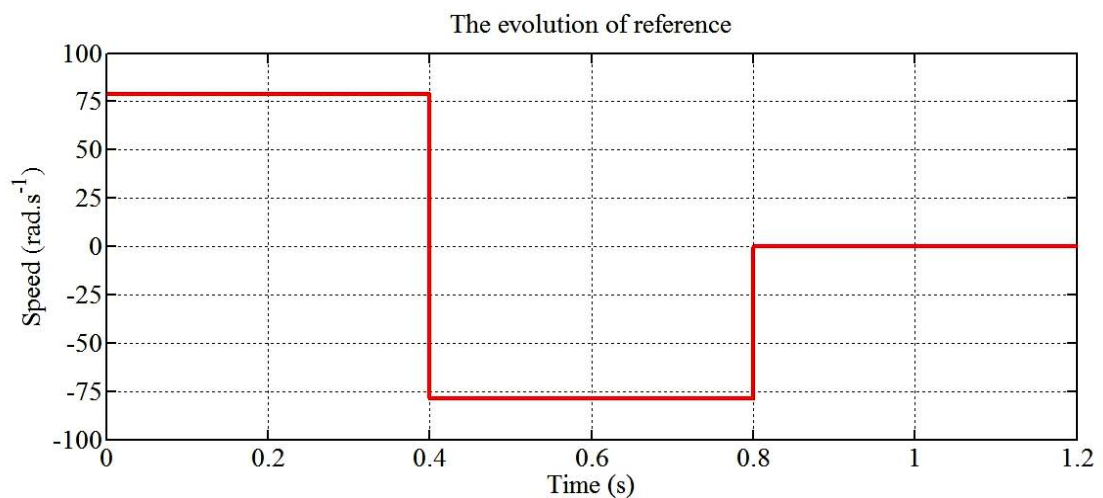


Figure 2.24: The evolution of reference value

At each reference speed, the loads applied to each machine are always different. The load of the first machine  $T_{load1}$  is kept constant during the simulation:  $T_{load1} = 2.5Nm$ . Meanwhile, the load of second machine varies:

- + From  $t = 0(s) \rightarrow 0.2(s)$ :  $T_{load2} = 1(Nm)$ ;
- + From  $t = 0.2(s) \rightarrow 0.6(s)$ :  $T_{load2} = 4(Nm)$ ;
- + From  $t = 0.6(s) \rightarrow 1.0(s)$ :  $T_{load2} = 1(Nm)$ ;
- + From  $t = 1.0(s) \rightarrow 1.2(s)$ :  $T_{load2} = 4(Nm)$ .

The varies of load of two machine are represented in Figure 2.25.

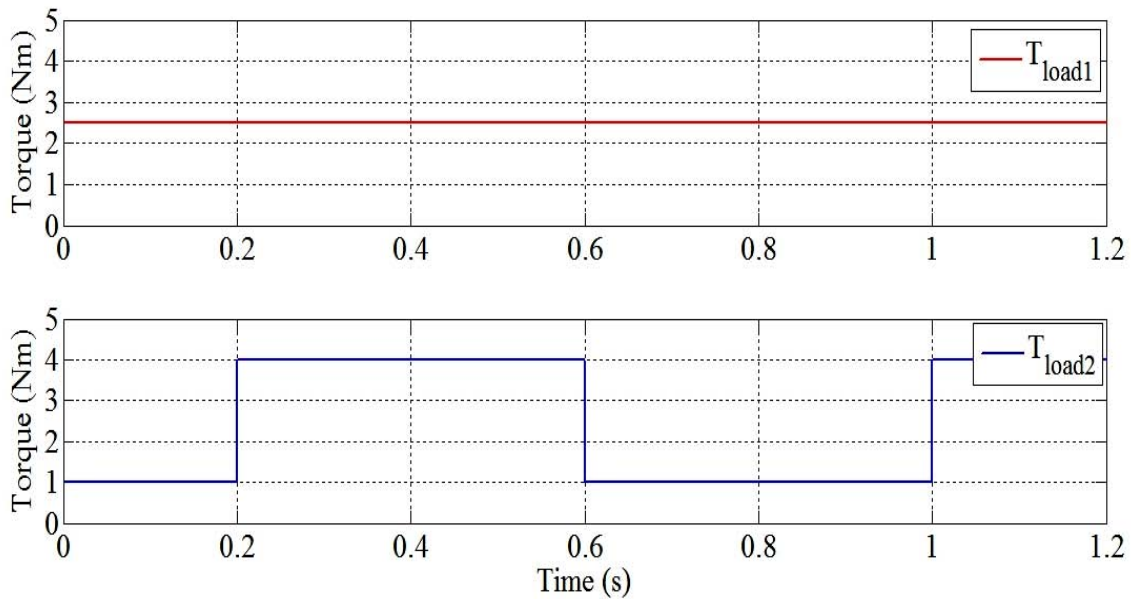


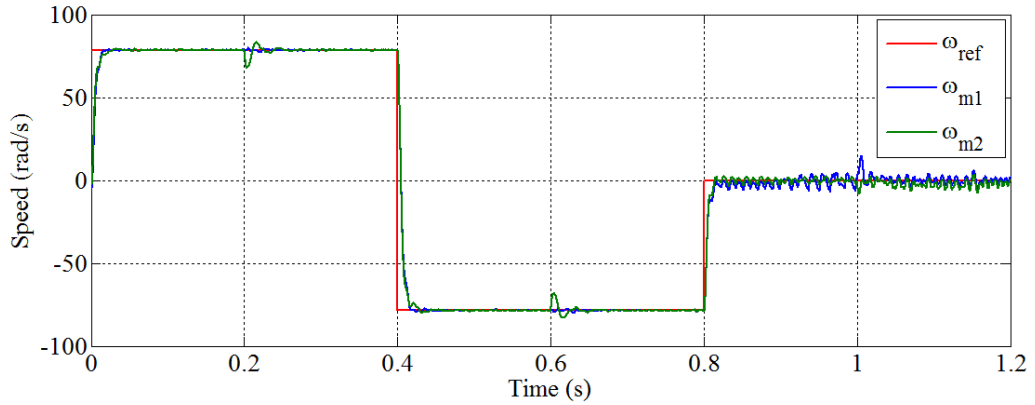
Figure 2.25: The variation of load of each machine in simulation

All the simulation results are shown in Figure 2.26

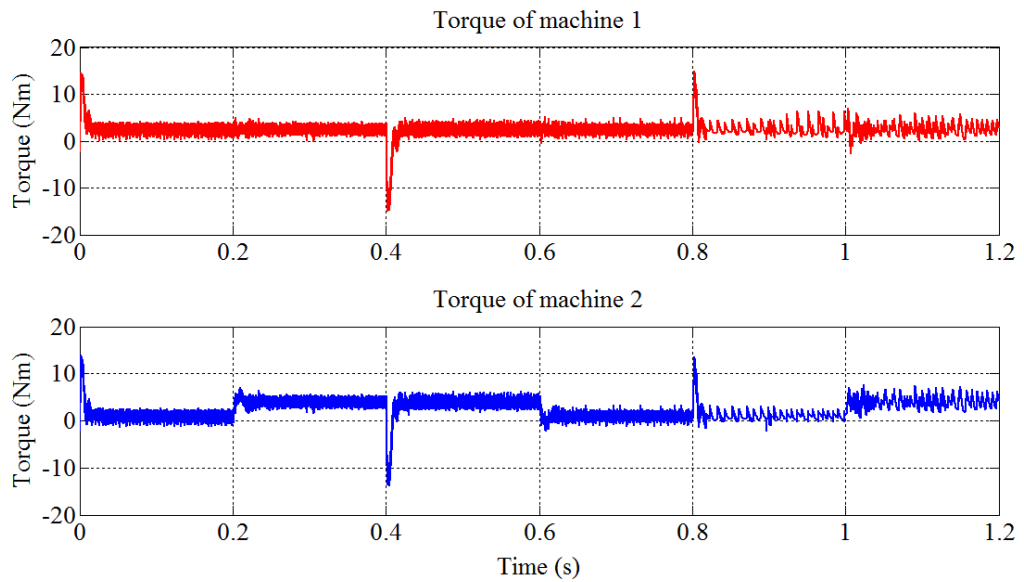
From the simulation results, it can be seen that the speeds of two machines can follow the set point (Figure 2.26a). Dynamic response of the system is very fast ( $\sim 0.02s$ ). However, the responses at standstill are not good. There is a ripple in speed. System is also stable with the load variations. The steady state is reestablished in a short time ( $\sim 0.03s$ ).

The electromagnetic torques of two machines are shown in Figure 2.26b. At steady state, their values are correlative to the value of the total load applied  $T_{total} = T_{load} + f_0\omega_m$ .

In Figure 2.26c, the flux linkage of both machines in  $(\alpha\beta)$ -frame is presented. Those fluxes evolve in a circular trajectory and are limited by a hysteresis band (amplitude  $\approx 0.02Wb$ ).



a) Speed response of two machines



b) Electromagnetic torque of two machines

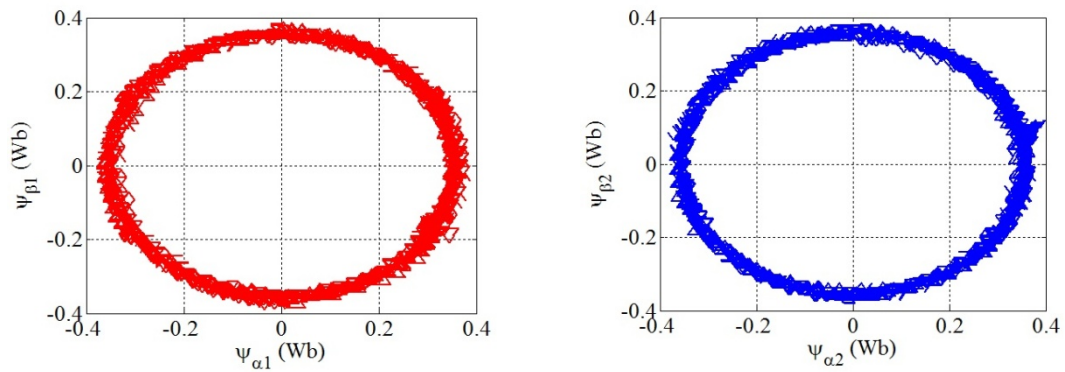
c1) Flux of MC1 in  $(\alpha\beta)$ c2) Flux of MC2 in  $(\alpha\beta)$ 

Figure 2.26: Responses of system under DTC

## 2.5 Conclusions

In this chapter, the mono-inverter dual-parallel PMSM drive system has been described and analyzed. The main components of this system are presented and considered in detail. The first component is the PMSM. Through this part, a model as well as the problems concerned to PMSM such as stability, control is studied.

The structure master/slave applying to this kind of system has been presented. The principle to determine the master machine is proposed and proved based on the studies about the stability of PMSM in open loop.

Another method also has been developed in this chapter is based on the principle of direct torque control. DTC is an effective method for high performance motion control thanks to the fast torque response. It also can be applied for a mono-inverter dual-parallel PMSM drive system. DTC for two machines leads to the issue of building another optimal switching table. This table will allow controlling the two PMSMs at the same time under different condition of loads. Simulation results show that with an optimal lookup table we can find a solution for the control of mono-inverter dual-parallel PMSM.

However, in practical application, this table cannot satisfy absolutely the requirements of both machines under different load conditions. The system still operates in stable partly because of the self-synchronism ability of synchronous machine. In order to build a good optimal lookup table of voltage vector, it needs further studies.

The use of DTC method for two machines also leads to the idea of considering another method to control the mono-inverter dual-parallel PMSM drive system. This method is based on the principle of predictive control. Instead of using hysteresis comparators to find the requirements for two machines, an optimization issue will be solved in order to satisfy all the requirements. The analysis and testing of this method will be presented in the next chapter.

# Chapter 3

## Predictive Torque Control with Mono-Inverter Dual-Parallel PMSM

### Table of contents

---

3.1. Introduction .....	66
3.2. PMSM under voltage supply mode .....	67
3.2.1 Steady state calculation .....	67
3.2.2 Small deviation model .....	72
3.3. PTC for Mono-Inverter Dual-parallel PMSM .....	74
3.3.1 Description .....	74
3.3.2 R-S-T discrete controller .....	75
3.3.2.1 Introduction .....	75
3.3.2.2 R-S-T anti-windup Speed/Torque controller .....	76
3.3.3 Predictive Torque Control .....	77
3.3.3.1 Discrete model of considered system .....	78
3.3.3.2 Cost function .....	81
3.3.3.3 Predictive control strategies .....	83
3.4. Direct Predictive Torque Control (DPTC) .....	84
3.4.1 Principle .....	85
3.4.2 Simulation results for DPTC .....	86
3.4.3 Relation between the ripple and the sampling time of DPTC .....	89
3.4.4 Optimization problem .....	91
3.4.5 Conclusions .....	94
3.5. Predictive Torque Control – “Split and Seek” (PTC-SS) .....	95
3.5.1 Predictive model in $(\alpha\beta)$ frame: .....	96
3.5.2 “Split and Seek” approach .....	96
3.5.2.1 Angle seeking .....	97
3.5.2.2 Magnitude seeking .....	99

---

3.5.3	Simulation results for PTC-SS .....	101
3.5.3.1.	A comparison with DPTC .....	101
3.6	Conclusions.....	105

---

### 3.1 Introduction

As analyzed in previous chapter, in the progress of looking for a control strategy for mono-inverter dual-parallel PMSM drive system, two solutions which are master-slave structure with PI controllers and Direct Torque Control (DTC), have been pointed out.

In master-slave structure with PI controller, operation of whole system is fairly well. The stability can be assured according to the choice of master machine. However, the slave machine will not be regulated in this case.

DTC is another solution for such kind of drive system. Purpose of this solution is considering the information (electromagnetic torque and flux linkage) of both machines. Based on this principle, a suitable voltage vector will be chosen and defined in a look-up table. Nevertheless, how to choose only one vector suitable for both machines will be a difficult question and sometimes there is no solution.

Based on the principle of DTC, the idea of Predictive Torque Control (PTC) has been proposed. In DTC, an estimation model is used to estimate the current torque and flux linkage of each machine. Meanwhile, PTC uses a discrete model of the whole system to predict its evolution in the future. Requirements for all the variables which need to be controlled such as torque, flux and currents ... are considered in a cost function. This cost function will help us choosing the most suitable state of an inverter to apply to the system. For this kind of drive system, we just change the cost function as well as the optimization algorithm in order to get the different performance of the system.

However, it is difficult for either DTC or PTC to satisfy absolutely the requirements of each machine. They just try to harmonize in the best way the demands of both machines.

Because each voltage vector found in the optimization process might be not meet exactly the demands of each machine, the two PMSMs will sometimes operate in voltage supply mode. Therefore, the responses of the PMSMs under voltage supply will be considered first in this chapter. After that, a general description about the PTC for mono-inverter dual-parallel PMSM drive system will be presented. Each component of this drive system is studied and explained in detail. Two approaches to predictive control will be

described and compared. Some simulations will be done in order to verify the performances of control methods.

## 3.2 PMSM under voltage supply mode

As mentioned above, a PMSM in voltage supply mode will be considered. In this case, amplitude ( $V_s$ ) and frequency ( $\omega_s$ ) of voltage supply and load torque ( $T_{load}$ ) will be the known parameters. At each value of ( $V_s, \omega_s, T_{load}$ ), we will obtain a specific steady state of a PMSM. In the next paragraph, the calculation of variables of a PMSM at steady state will be presented.

### 3.2.1 Steady state calculation

Steady states of PMSM will be calculated by considering the continuous model of PMSM (section 2.2.2.2). It is noted that, at steady state all the differential components will equal to zero. As a result, all equations will be rewritten as in (3.1).

$$\begin{cases} u_{sd} = R_s i_{sd} - \omega_e L i_{sq} \\ u_{sq} = R_s i_{sq} + \omega_e L i_{sd} + \omega_e \sqrt{\frac{3}{2}} \psi_p \\ T_{em} = n_p \sqrt{\frac{3}{2}} \psi_p i_{sq} \\ T_{em} - T_{load} = \frac{f_0 \omega_e}{n_p} \end{cases} \quad (3.1)$$

At steady state, we have  $\omega_e = \omega_s$ .

From the third and the fourth equation in (3.1), q-current of PMSM at steady state will be obtained:

$$i_{sq} = \frac{f_0 \left( \frac{\omega_e}{n_p} \right) + T_{load}}{n_p \sqrt{\frac{3}{2}} \psi_p} \quad (3.2)$$

From the first and the second equation in (3.1) and using the relationship between the d-q voltages and  $V_s$  and the load angle  $\delta$ :  $\begin{cases} u_{sd} = -V_s \sin \delta \\ u_{sq} = V_s \cos \delta \end{cases}$ , we have:

$$R_s V_s \cos \delta + \omega_e L V_s \sin \delta = (R_s^2 + (\omega_e L)^2) I_{sq} + \omega_e R_s \sqrt{\frac{3}{2}} \psi_p \quad (3.3)$$

From this equation, the load angle  $\delta$  will be calculated by the following equation:

$$\delta = \alpha - \arccos \left( \frac{(R_s^2 + (\omega_e L)^2) I_{sq} + \omega_e R_s \sqrt{\frac{3}{2}} \psi_p}{V_s \sqrt{R_s^2 + (\omega_e L)^2}} \right) \quad (3.4)$$

with  $\alpha = \text{atan} \left( \frac{\omega_e L}{R_s} \right)$ . In (3.4), the appearance of “arccos” function can be lead to double value of load angle. Therefore, the condition of stability of a PMSM, which is presented in section 2.2.3, will be used to eliminate an unsuitable value:  $\alpha - \pi < \delta < \alpha$ .

Besides, it is necessary to satisfy the condition of “arccos” function. It means that in order to let this function be meaningful, the relation in (3.5) must be respected.

$$\sqrt{R_s^2 + (\omega_e L_s)^2} i_{q0} + \frac{\omega_e R_s \sqrt{\frac{3}{2}} \psi_f}{\sqrt{R_s^2 + (\omega_e L_s)^2}} < V_s \quad (3.5)$$

Condition in (3.5) shows us a limit in operation of a PMSM. Under a specific value of  $V_s$  and  $T_{load}$ , speed of a PMSM cannot exceed a specific value. This limitation is illustrated in Figure 3.3.

The d-current then can be calculated as in (3.6):

$$I_{sd} = \frac{-V_s \sin \delta + \omega_e L I_{sq}}{R_s} \quad (3.6)$$

To illustrate these theoretical equations, the calculations above will be applied to a PMSM. Parameters of this PMSM are summarized in Table 2.6

$R_s$	2.06( $\Omega$ )
$L_{sd} = L_{sq} = L$	$9.15 \times 10^{-3}$ (H)
$\psi_p$	0.29(Wb)
Numbers of pole pairs ( $n_p$ )	3
Inertia ( $J$ )	$7.2 \times 10^{-4}$ (kg.m <sup>2</sup> )

Table 3.1: Parameters of PMSM

The three known parameters will be chosen as follow:

- + the voltage  $V_s$  is considered from 0 to  $V_{max} = V_{DC}/\sqrt{3} \approx 312(V)$ ;
- + the frequency  $\omega_s$  is considered from 0 to nominal value  $\omega_{nominal} = 300 \times \pi \approx 942(rad.s^{-1})$ ;
- + three load condition: 
$$\begin{cases} T_{load} = 0(Nm) \\ T_{load} = 5(Nm) ; \\ T_{load} = 10(Nm) \end{cases}$$

In Figure 3.1, currents in dq-axis of this PMSM are shown. Under the same values of  $(\omega_s, T_{load})$ , although the voltage  $V_s$  increase, q-current does not change. The q-current at steady state just depends on frequency  $\omega_s$  and load torque  $T_{load}$ . Otherwise, the increase of  $V_s$  makes d-current change. At small range of speed, the change of d-current is very big. Under standstill condition ( $\omega_s = 0 rad.s^{-1}$ ) and load torque equals to zero ( $T_{load} = 0Nm$ ), the change is from 0 to  $\approx 150 A$ . At higher speed, the change is smaller. Moreover, when the speed increases (with the same  $V_s$  and  $T_{load}$ ), the d-current has a tendency toward negative value (the field weakening region).

On the other hand, meanwhile q-current much depends on the load because it represents for electromagnetic torque, d-current changes a little under three values of load.

In Figure 3.2, load angle is shown. As its name, value of load angle  $\delta$  will change according to the load torque. At a specific pair of value  $(\omega_s, V_s)$ , load angle correlative to heavier load will bigger.

The limit in operation of this PMSM is illustrated in Figure 3.3. As mentioned above, under specific values of  $V_s$  and  $T_{load}$ , speed of PMSM will be limited according to the condition in (3.5). According to Figure 3.3, with the same load, the voltage increases, the speed limit also are increased. In order to operate in full nominal range of speed, for this machine, the voltage must be larger than  $\approx 150$ .

In this part, we just calculate the steady state of a PMSM. It is carried out under the supposition that these states existed. It is also necessary to consider if these states really can be obtained and stable or not. Therefore, a small deviation model of PMSM will be built and analyzed.

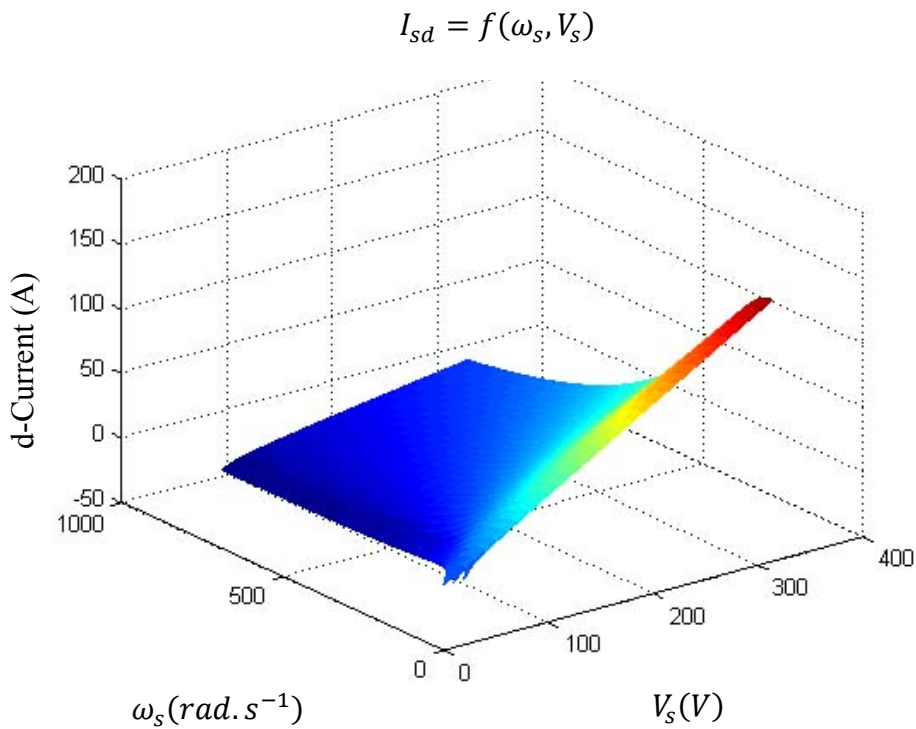
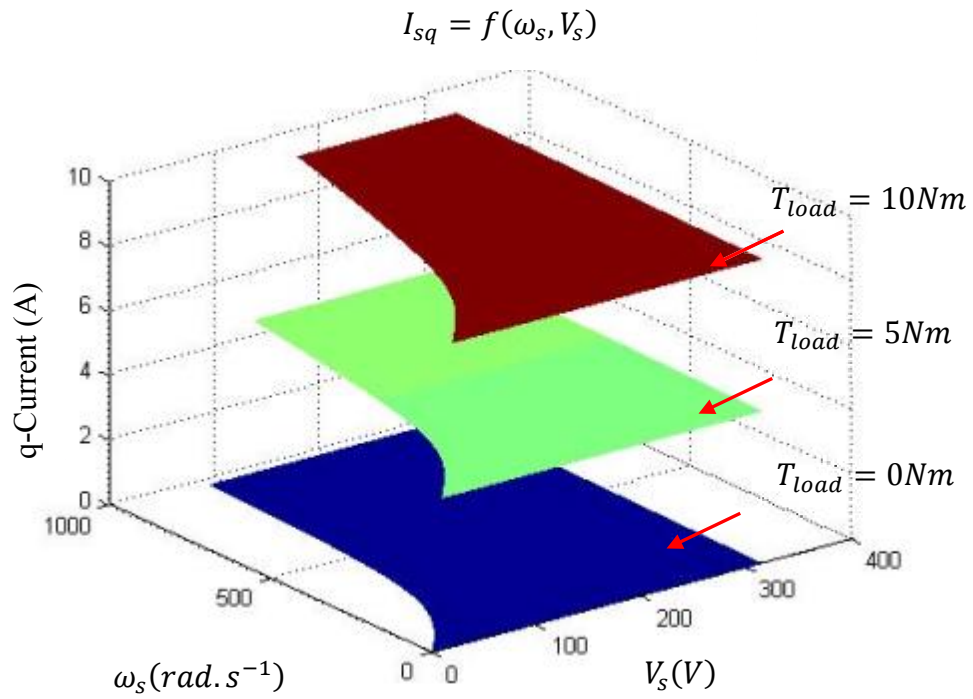


Figure 3.1: dq-current at steady state of a PMSM

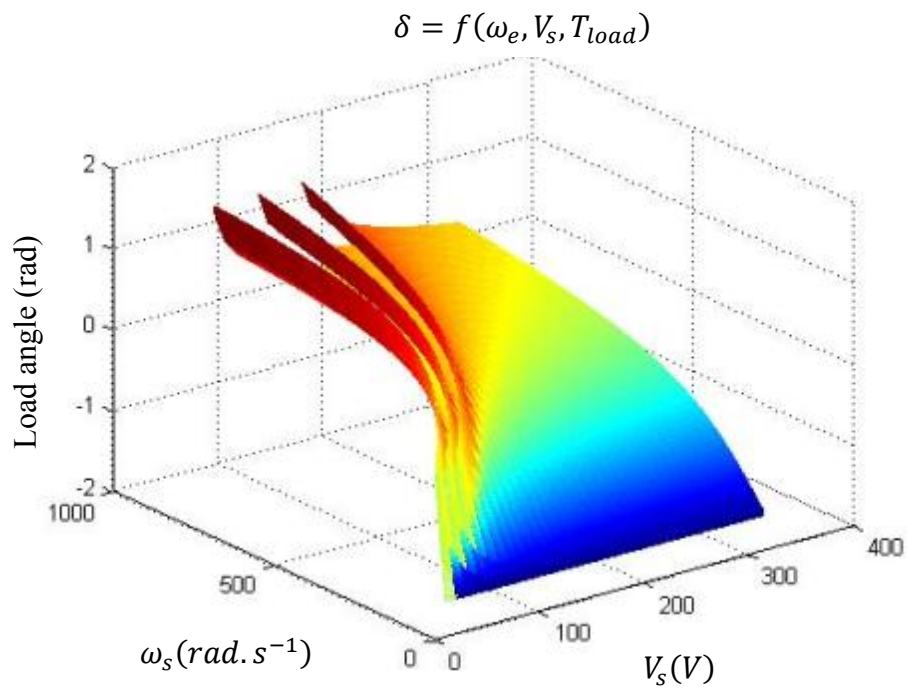


Figure 3.2: Load angle at steady state

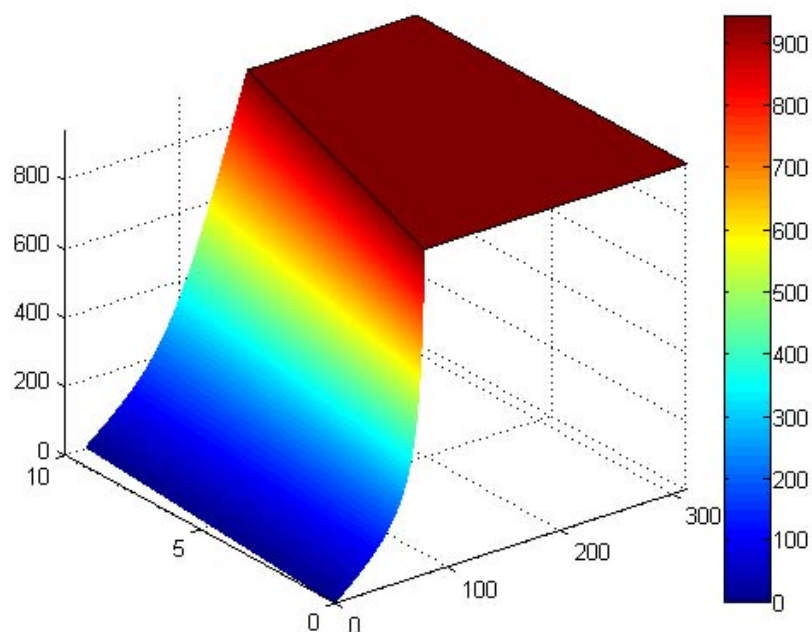


Figure 3.3: Limit in operation of a PMSM

### 3.2.2 Small deviation model

In the previous part, the calculation about steady state of a PMSM has been established. It can be seen that to operate a PMSM at a given speed under a constant load, several values of voltage can be supplied. However, thinking about if all these voltage values are really suitable or not. Will a PMSM operate stably? As a result, a small deviation model of PMSM will be considered in order to know which one is stable operating point [PBPT03].

Considering that a PMSM is operating at a steady state with specific components:  $V_s$ ,  $I_{sd0}$ ,  $I_{sq0}$ ,  $\omega_e$  and  $\delta_0$ . Proposed that there is a small change of load  $\delta T_{load}$ . This change makes all steady states also change in small quantities as in (3.7):

$$\begin{cases} i_{sd} &= I_{sd0} + \delta i_{sd} \\ i_{sq} &= I_{sq0} + \delta i_{sq} \\ u_{sd} &= U_{sd0} + \delta u_{sd} \\ u_{sq} &= U_{sq0} + \delta u_{sq} \\ T_{em} &= T_{em0} + \delta T_{em} \\ \omega_e &= \omega_{e0} + \delta \omega_e \\ \delta &= \delta_0 + \delta \delta \end{cases} \quad (3.7)$$

By linearizing and omitting the 2-order differential component, a small deviation model of PMSM can be obtained as shown in (3.8).

$$\begin{bmatrix} \delta \dot{i}_d \\ \delta \dot{i}_q \\ \delta \dot{\omega}_e \\ \delta \dot{\delta} \end{bmatrix} = \underbrace{\begin{bmatrix} -\frac{R_s}{L_s} & \omega_e & i_{d0} & -\frac{V_s}{L_s} \cos \delta_0 \\ -\omega_e & -\frac{R_s}{L_s} & -\left(i_{d0} + \frac{\sqrt{\frac{3}{2}}\psi_p}{L_s}\right) & -\frac{V_s}{L_s} \sin \delta_0 \\ 0 & \frac{p^2 \sqrt{\frac{3}{2}}\psi_p}{J} & -\frac{f_0}{J} & 0 \\ 0 & 0 & -1 & 0 \end{bmatrix}}_A \begin{bmatrix} \delta i_d \\ \delta i_q \\ \delta \omega_e \\ \delta \delta \end{bmatrix} + \begin{bmatrix} 0 \\ 0 \\ -\frac{p}{J} \\ 0 \end{bmatrix} \delta T_{load} \quad (3.8)$$

In (3.8), a characteristic matrix  $A$  is defined. From this matrix, we can build a four-order polynomial characteristic  $P(s)$ . The root of polynomial characteristic  $P(s)$  will give us the information about the stability of a PMSM. By using a built-in function in Matlab, we can obtain all the roots of this polynomial. In general, a four-order polynomial will give us four roots. At a steady state at which the real part of all roots is negative, it will be a stable state. Otherwise, if any root has a positive real part, this point will be unstable.

In Figure 3.4, an example of a map of roots of PMSM is represented. These roots in Figure 3.4 are calculated from a specific steady state of PMSM (the state with  $I_{sd0} = 0A$  and  $T_{load} = 0Nm$ ). We also have the following values:

$$\begin{cases} I_{sd0} = 0 \\ I_{sq0} = \frac{f_0 \left( \frac{\omega_e}{n_p} \right)}{n_p \sqrt{\frac{3}{2}} \psi_p} \\ V_s = \sqrt{\left( (\omega_e L_s I_{sq0})^2 + \left( R_s I_{sq0} + \omega_e \sqrt{\frac{3}{2}} \psi_p \right)^2 \right)} \\ \delta_0 = \arctan \left( \frac{\omega_e L_s I_{sq0}}{R_s I_{sq0} + \omega_e \sqrt{\frac{3}{2}} \psi_p} \right) \end{cases} \quad (3.9)$$

An input parameters  $\omega_e$  are varied and the roots of  $P(s)$  will evolve as shown in this map. According to this map, a limit value of  $\omega_e$  is determined:  $\omega_{limit} \approx 380(\text{rad. s}^{-1})$ .

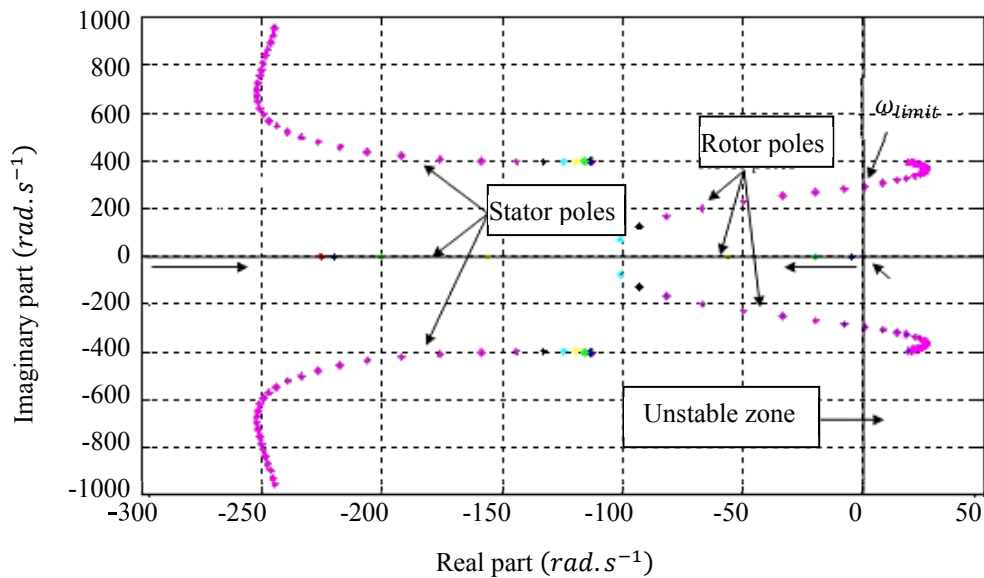


Figure 3.4: Map of roots of  $P(s)$

From the analysis above, all three parameters  $V_s$ ,  $\omega_e$  and  $T_{load}$  will vary as in section (3.2.1). At each steady state we will have a correlative small deviation model as well as a polynomial characteristic  $P(s)$ . Solving  $P(s)$  and considering the roots of  $P(s)$  give us a limit value of stable operation point of PMSM. The limit surface is shown in Figure 3.5.

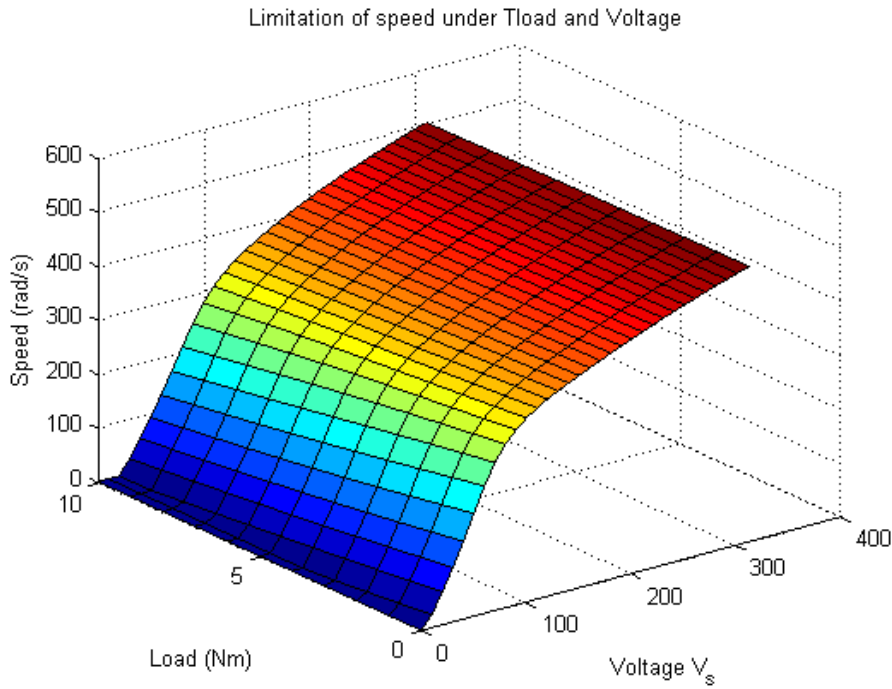


Figure 3.5: Example of limitation of stable zone of a PMSM

### 3.3 PTC for Mono-Inverter Dual-parallel PMSM

#### 3.3.1 Description

The structure of this kind of drive system is represented in Figure 3.6. All conditions of a mono-inverter dual-parallel PMSM are preserved as described in Section 2.1.

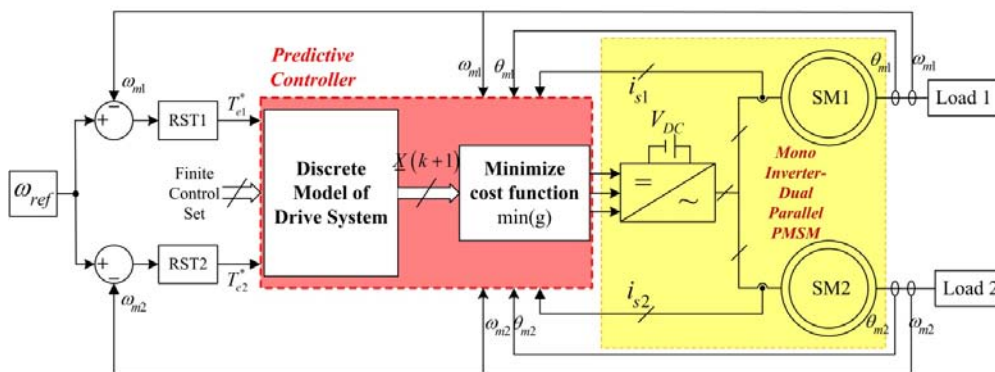


Figure 3.6: PTC for Mono-Inverter Dual-parallel PMSM drive system

Inside this structure, two control loops are used:

- + The outer control loop uses two speed controllers: controllers will calculate the reference torque for each machine based on the difference between the two speeds of two PMSMs ( $\omega_{m1}, \omega_{m2}$ ) and the set speed ( $\omega_{ref}$ ). In this work, R-S-T discrete controller will be used [NFL11];

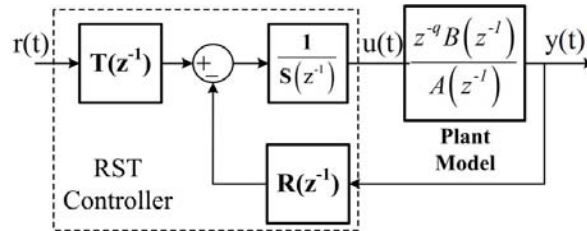


Figure 3.7: The R-S-T digital controller [Lan98]

- + The inner loop uses a predictive torque controller: the main objective is controlling directly the torque of both PMSMs. The core of the predictive torque controller consists of a discrete model of this drive system, a defined cost function and an optimal procedure which minimizes the cost function. In this thesis, a one-step ahead predictive control method is considered.

The two control loops will be considered in detail in the following part of this chapter. Firstly, the outer loop with R-S-T discrete controller will be presented.

### 3.3.2 R-S-T discrete controller

#### 3.3.2.1 Introduction

In the context of computer control, which is now widespread in industry, it is necessary to develop an efficient design and implementation methodology for digital controller. Based on these aspects, the two-degrees-of-freedom R-S-T controller is becoming a standard and plays a crucial role [Lan98] [OG05] [LZ06]. The canonical structure of R-S-T controller was represented in Figure 3.7.

This structure has two degrees of freedom: the digital filters  $R$  and  $S$  are designed in order to achieve the desired regulation performances and the digital filter  $T$  is designed afterwards in order to achieve the desired tracking performance. This structure thus allows obtaining different levels of performance in tracking and regulation. The case of a controller operating on the regulation error corresponds to  $T = R$ . Digital PID can also be represented in this form leading to particular choices of  $R$ ,  $S$  and  $T$ .

Consider a plant model with  $G(z^{-1}) = \frac{z^{-d}B(z^{-1})}{A(z^{-1})}$ , the equation of the R-S-T controller is given by:

$$S(z^{-1})u(t) + R(z^{-1})y(t) = T(z^{-1})y^*(t + d + 1) \quad (3.10)$$

where  $u(t)$  and  $y(t)$  are the input and output of the plant and  $y^*(t + d + 1)$  is the desired tracking trajectory, which is either generated by a tracking reference model ( $B_m/A_m$ ) or stored in the computer memory.

The polynomial characteristic of closed loop control is then written as follows:

$$P(z^{-1}) = A(z^{-1})S(z^{-1}) + z^{-d}B(z^{-1})R(z^{-1}) \quad (3.11)$$

Solving this equation allows the determination of  $S(z^{-1})$  and  $R(z^{-1})$ . In order to do that, a pole placement strategy is usually used [IGL+08]. This technique can be used for plant models of any order, with or without time delay and featuring stable or unstable zeros.

In the following paragraph, a R-S-T digital controller with anti-windup for speed/torque control in the case of PMSM will be presented.

### 3.3.2.2 R-S-T anti-windup Speed/Torque controller

From the electromechanical description of a PMSM, the relationship between the speed and torque in Laplace domain is built as follows:

$$G(s) = \frac{\omega_m(s)}{T_{em}(s)} = \frac{1}{Js + f_0} \quad (3.12)$$

Performing Z-Transform, a PMSM model in Z-domain will be obtained:

$$G(z^{-1}) = \frac{b_1 z^{-1}}{a_0 + a_1 z^{-1}} = \frac{\frac{1}{f} (1 - e^{-T_s/\tau_m}) z^{-1}}{1 - e^{-T_s/\tau_m} z^{-1}} \quad (3.13)$$

where  $\tau_m = \frac{J}{f_0}$  is the mechanical time constant.

Based on the coefficients  $a_0$ ,  $a_1$  and  $b_1$  obtained from the model of PMSM in Z-domain, along with the support of pole placement technique, the parameters of RST speed controller will be calculated as follow:

$$\begin{cases} s_0 = 1 \\ s_1 = 1 \\ r_0 = \frac{p_1 - a_1 + 1}{b_1} \\ r_1 = \frac{p_2 + a_1}{b_1} \end{cases} \quad (3.14)$$

where  $p_1, p_2$  are the desired poles:

$$\begin{cases} p_1 = -2e^{-\xi\omega_n T_s} \cos(\omega_n T_s \sqrt{1-\xi^2}) \\ p_2 = e^{-2\xi\omega_n T_s} \end{cases} \quad (3.15)$$

With the setting  $s_0 = 1$  and  $s_1 = 1$ , the RST controller is digital equivalent form of PI controller. The structure of RST Anti-Windup controller is shown in Figure 3.8. In (3.15),  $\xi$  and  $\omega_n$  are damper factor and natural frequency. These parameters will be chosen according to the desired dynamic response of the system.

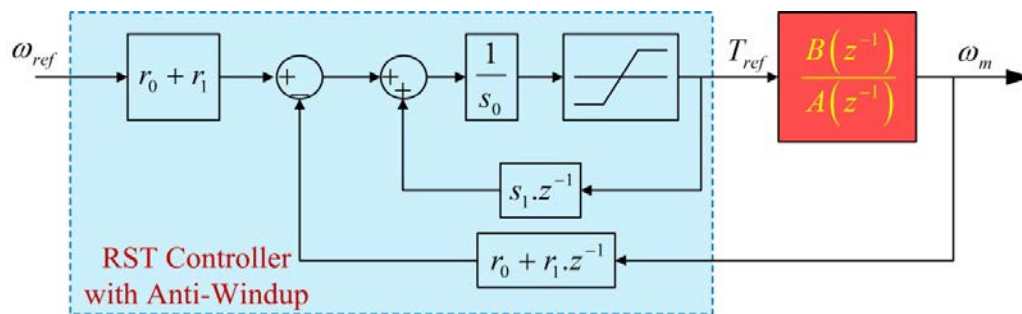


Figure 3.8: RST anti-windup Speed/Torque controller for a PMSM

### 3.3.3 Predictive Torque Control

Predictive Torque Control strategy has been studied and applied in many applications with both induction machines [CPR07] [RKE+10]... and permanent magnet synchronous machines [GBPM10] [MD11]... A torque magnitude control along with a complement criterion will evaluate a cost function for each switching state available in a two-level inverter. The voltage vector with the lowest value of the cost function is selected to be applied in the next sampling interval.

Based on the principle of Model Predictive Control (MPC) [CB04], a model which pre-calculates the future behavior of the system is one of the crucial points of a Predictive Control scheme. Generally, most systems to be controlled are continuous-time systems, so the description of the system should be made in time or Laplace domain. In contrast to the controlled systems, the controllers, which usually are realized with the help of digital computers, are often discrete-time controllers. For the controller design, it is in most cases sufficient to replace it by a continuous-time model, parameterize it and afterwards realize it as a discrete-time digital controller. Nevertheless, it is more advantageous to consider the discrete character of the controller already in the first approach of the controller design and hence to use a discrete-time system description. This also implies that the controlled

system is described in the discrete-time domain too. It is especially true in power electronics applications or control of electrical machines where control elements are usually the power converters [VRAGL12]. Those devices just have discrete states (for example a two-level inverter has 8 different states).

In the following part, a discrete model of considered system will be constructed step by step.

### 3.3.3.1 Discrete model of considered system

#### 3.3.3.1.1 One-step predictive model of dual-parallel PMSM

In this part, the continuous model of PMSM in d-q reference frame which has already been presented in section 2.2.2.2 will be used to build the discrete model of dual-parallel PMSM. For a PMSM, we already have:

$$\frac{di_s^{dq}}{dt} = A^{dq}i_s^{dq} + B^{dq}u_s^{dq} + P^{dq} \quad (3.16)$$

$$A^{dq} = \begin{bmatrix} -\frac{R_s}{L} & \omega_e \\ -\omega_e & -\frac{R_s}{L} \end{bmatrix}; B^{dq} = \begin{bmatrix} \frac{1}{L} & 0 \\ 0 & \frac{1}{L} \end{bmatrix}; P^{dq} = \begin{bmatrix} 0 \\ -\sqrt{\frac{3}{2}}\frac{\psi_p}{L}\omega_e \end{bmatrix}$$

Considering a linear, time-variant system, the values of the elements of the matrices  $A^{dq}$ ,  $B^{dq}$  and  $P^{dq}$  are constant. However, in the case of a rotating electric machine, this is not true for the rotating speed  $\omega_{re}$ , as it changes its values during the operation of the machine. Moreover, the rotating speed is also multiplicatively linked with different state variables resulting in nonlinearity.

With a small enough sampling time  $T_s$ , it can be considered that the rotating speed  $\omega_{re}$  does not change in one sampling period. Thank to this, a first order approximation will be used to generate the discrete time model of a PMSM as shown in (3.17)

$$i_s^{dq}(k+1) = A_d^{dq}(k)i_s^{dq}(k) + B_d^{dq}(k)u_s^{dq}(k) + P_d^{dq}(k)$$

where:

$$A_d^{dq}(k) = \begin{bmatrix} 1 - T_s \frac{R_s}{L} & T_s \omega_e(k) \\ -T_s \omega_{re}(k) & 1 - T_s \frac{R_s}{L} \end{bmatrix}; B_d^{dq}(k) = \begin{bmatrix} \frac{T_s}{L} & 0 \\ 0 & \frac{T_s}{L} \end{bmatrix} \quad (3.17)$$

$$P_d^{dq}(k) = \begin{bmatrix} 0 \\ T_s \sqrt{\frac{3}{2}} \frac{\psi_p}{L} \omega_e(k) \end{bmatrix}$$

As mentioned above, this drive system includes two identical machines. Therefore, using equation from (3.17), the discrete current model of dual-parallel PMSM will be obtained.

$$\begin{aligned}
 \begin{bmatrix} i_{sd1}^{k+1} \\ i_{sq1}^{k+1} \\ i_{sd2}^{k+1} \\ i_{sq2}^{k+1} \end{bmatrix} &= \underbrace{\begin{bmatrix} 1 - T_s \frac{R_s}{L} & T_s \omega_{e1}^k & 0 & 0 \\ -T_s \omega_{e1}^k & 1 - T_s \frac{R_s}{L} & 0 & 0 \\ 0 & 0 & 1 - T_s \frac{R_s}{L} & T_s \omega_{e2}^k \\ 0 & 0 & -T_s \omega_{e2}^k & 1 - T_s \frac{R_s}{L} \end{bmatrix}}_{\mathbb{F}(k)} \begin{bmatrix} i_{sd1}^k \\ i_{sq1}^k \\ i_{sd2}^k \\ i_{sq2}^k \end{bmatrix} \\
 &+ \underbrace{\begin{bmatrix} \frac{T_s}{L} & 0 & 0 & 0 \\ 0 & \frac{T_s}{L} & 0 & 0 \\ 0 & 0 & \frac{T_s}{L} & 0 \\ 0 & 0 & 0 & \frac{T_s}{L} \end{bmatrix}}_{\mathbb{G}(k)} \begin{bmatrix} u_{sd1}^k \\ u_{sq1}^k \\ u_{sd2}^k \\ u_{sq2}^k \end{bmatrix} + \underbrace{\begin{bmatrix} 0 \\ T_s \sqrt{\frac{3}{2}} \frac{\psi_p}{L} \omega_{e1}^k \\ 0 \\ T_s \sqrt{\frac{3}{2}} \frac{\psi_p}{L} \omega_{e2}^k \end{bmatrix}}_{\mathbb{H}(k)}
 \end{aligned} \tag{3.18}$$

The d-q voltages which are used in (3.18) are calculated from the phase-to-neutral voltages from the inverter by using the Park's transformation. This relation is presented in (3.19)

$$\begin{bmatrix} u_{sd1}(k) \\ u_{sq1}(k) \\ u_{sd2}(k) \\ u_{sq2}(k) \end{bmatrix} = \sqrt{\frac{2}{3}} \begin{bmatrix} \cos \theta_{e1}(k) & \cos \left( \theta_{e1}(k) - \frac{2\pi}{3} \right) & \cos \left( \theta_{e1}(k) - \frac{4\pi}{3} \right) \\ -\sin \theta_{e1}(k) & -\sin \left( \theta_{e1}(k) - \frac{2\pi}{3} \right) & -\sin \left( \theta_{e1}(k) - \frac{4\pi}{3} \right) \\ \cos \theta_{e2}(k) & \cos \left( \theta_{e2}(k) - \frac{2\pi}{3} \right) & \cos \left( \theta_{e2}(k) - \frac{4\pi}{3} \right) \\ -\sin \theta_{e2}(k) & -\sin \left( \theta_{e2}(k) - \frac{2\pi}{3} \right) & -\sin \left( \theta_{e2}(k) - \frac{4\pi}{3} \right) \end{bmatrix} \begin{bmatrix} V_{AN}(k) \\ V_{BN}(k) \\ V_{CN}(k) \end{bmatrix} \tag{3.19}$$

In (3.19),  $\theta_{e1}(k)$  and  $\theta_{e2}(k)$  are the electrical positions of d-q reference frame of each machine at time  $k$ . In this work, these positions are measured by resolvers. The  $V_{AN}(k)$ ,  $V_{BN}(k)$  and  $V_{CN}(k)$  voltage will be calculated from the discrete state model of the inverter in next section.

### 3.3.3.1.2 A three-phase two-level inverter

A simple diagram of a three-phase two-level inverter is shown in Figure 3.9. The vector  $[V_{AN}(k) V_{BN}(k) V_{CN}(k)]^T$ , which is represented by the phase-to-neutral voltages will be expressed as functions of inverter's leg states (Equation (3.20)):

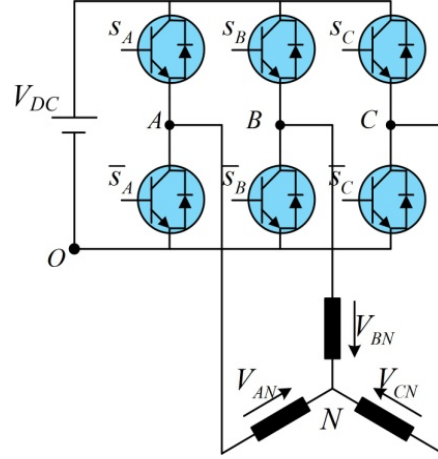


Figure 3.9: A standard three-phase two-level inverter

$$\begin{bmatrix} V_{AN}(k) \\ V_{BN}(k) \\ V_{CN}(k) \end{bmatrix} = \frac{V_{DC}}{3} \underbrace{\begin{bmatrix} 2 & -1 & -1 \\ -1 & 2 & -1 \\ -1 & -1 & 2 \end{bmatrix}}_{\mathbb{D}} \begin{bmatrix} s_A(k) \\ s_B(k) \\ s_C(k) \end{bmatrix} \quad (3.20)$$

where  $s_X$  ( $X = A, B, \text{ or } C$ ) is represented for two states of the inverter's legs.

$$s_x = \begin{cases} 0 \Leftrightarrow V_{XO} = 0 \\ 1 \Leftrightarrow V_{XO} = V_{DC} \end{cases} \quad (3.21)$$

With a three-phase two-level voltage inverter, there are two switching states for each leg, so there are eight possible switching states represented by eight different real vectors  $[s_A \ s_B \ s_C]^T$  (Table 3.2). Configurations 0 and 7 lead both to zero voltages, therefore there is usually only one configuration is really used.

$i$	0	1	2	3	4	5	6	7
$s_A$	0	1	1	0	0	0	1	1
$s_B$	0	0	1	1	1	0	0	1
$s_C$	0	0	0	0	1	1	1	1

Table 3.2: Eight real states of a three-phase two-level inverter

### 3.3.3.1.3 Synthesized model

Finally, one-step ahead predictive model of the mono-inverter dual-parallel PMSM structure is obtained by applying (3.20) into (3.18)

$$\begin{bmatrix} i_{sd1}^{k+1} \\ i_{sq1}^{k+1} \\ i_{sd2}^{k+1} \\ i_{sq2}^{k+1} \end{bmatrix} = \mathbb{F}(k) \begin{bmatrix} i_{sd1}^k \\ i_{sq1}^k \\ i_{sd2}^k \\ i_{sq2}^k \end{bmatrix} + \mathbb{G}(k) \sqrt{\frac{2}{3}} \mathbb{P}(k) \mathbb{D} \begin{bmatrix} s_A(k) \\ s_B(k) \\ s_C(k) \end{bmatrix} + \mathbb{H}(k) \quad (3.22)$$

This model allows predicting the behaviors after a sampling period if a specific configuration of  $[s_A(k) \ s_B(k) \ s_C(k)]^T$  is used.

### 3.3.3.2 Cost function

Besides the model, one vital factor of predictive control is the cost function. The main objective of it is to reduce the error between the predicted and the reference value. Moreover, the cost function also admits an y necessary term that could represent a prediction for system variables, system constraint or system requirement. This flexibility allows achieving easier more control targets to increase system performance (efficiency, power quality ...). Since these terms can be of different physical nature (current, voltage, reactive power, switching losses, torque, flux, etc.), they can lead to coupling effects between variables, or to overestimate the importance of one term respecting to the others in the cost function, making their presence not worth, and even not controllable. This issue has been commonly dealt with by including weighting coefficients or weighting factors  $\lambda$ , for each term of the cost function:

$$g = \lambda_x |x^* - x^p| + \lambda_y |y^* - y^p| + \dots + \lambda_z |z^* - z^p| \quad (3.23)$$

Depending on the nature of the different terms involved in the formulation of the cost function, some typical types will be presented in the next section.

#### 3.3.3.2.1 Typical cost functions

##### A. Cost functions without weighting factors

In these cost functions, only one, or the components of one variable, are controlled. This is the simplest case, and since only one type of variable is controlled, no weighting factors are necessary. The typical cost function for this case is the predictive current control [RPS+07]. In this cost function, all the terms are composed of variables of the same nature (same unit and order of magnitude). Moreover, some are a decomposition of a single variable into two components. Therefore, no weighting factors and their corresponding tuning process is necessary.

Application	Cost function
Predictive current control	$\ i_{sq}^* - i_{sq}^p\  + \ i_{sd}^* - i_{sd}^p\ $

### B. Cost functions with secondary terms

Some systems have a primary goal or a more important control objective that must be achieved in order to provide an adequate system behavior, and additional secondary constraints or requirements that should also be accomplished to improve system performance, efficiency or power quality. In these cases, the cost function presents a primary and secondary terms, where the importance of the secondary term can vary within a wide range, depending on the application and its specific needs. Some examples are: predictive current control with reduction of the switching frequency to improve efficiency [VCA+07], predictive current control with reduction of common mode voltage to prevent motor damage [VRRE08], and predictive current control with reactive power reduction to improve power quality [MAR05][VARP08]. The corresponding cost functions are listed in Table 3.3.

Application	Cost function
Switching frequency reduction	$ i_{s\alpha}^* - i_{s\alpha}^p  +  i_{s\beta}^* - i_{s\beta}^p  + \lambda_{sw} n_{sw}^p$
Common mode voltage reduction	$ i_{s\alpha}^* - i_{s\alpha}^p  +  i_{s\beta}^* - i_{s\beta}^p  + \lambda_{cw} V_{cw}^p$
Reactive power reduction	$ i_{s\alpha}^* - i_{s\alpha}^p  +  i_{s\beta}^* - i_{s\beta}^p  + \lambda_Q  Q^p $

Table 3.3: Cost functions with secondary terms

### C. Cost functions with equivalent important terms

Unlike the previous case, there are systems in which several variables need to be controlled simultaneously with the same priority. In these cases, the cost function can include several terms with equivalent importance, and it is the job of the weighting factors to compensate the difference in nature of the variables. Such in the case of torque and flux control [NFL11], where both variables need to be controlled accurately in order to have proper system performance.

Application	Cost function
Torque and flux control	$\frac{1}{T_{en}^2} (T_{em}^* - T_e^p)^2 + \lambda_\psi \frac{1}{\psi_{sn}^2} ( \psi_s ^* -  \psi_s^p )^2$

### 3.3.3.2.2 Cost function for two parallel PMSMs system

In the case of parallel PMSM, in order to control the speed of both machines, it is necessary to control the torque applied to each machine. This is because of the relationship between the torque and the speed presented in the mechanical equation of PMSM. However, PMSM which is considered in this work, is a non-silent type ( $L_{sd} = L_{sq} = L$ ). The electromechanical torque  $T_e$  is proportional directly to the q-axis component of the current:  $T_e = n_p \sqrt{3/2} \psi_p i_{sq}$ . Therefore, instead of considering the torque, the q-axis current of two machines will be added to the cost function.

However, if only the q-axis currents of two machines are considered, the d-axis currents will be free. The power losses in term of ( $R_s i_{sd}^2$ ) might be large. This is the reason why the d-axis currents will be also added to the cost function.

Finally, the cost function chosen for this system will be built as follows:

$$g = \left( i_{sq1}^{ref} - i_{sq1}(k+1) \right)^2 + \left( i_{sq2}^{ref} - i_{sq2}(k+1) \right)^2 + \left( i_{sd1}(k+1) \right)^2 + \left( i_{sd2}(k+1) \right)^2 \quad (3.24)$$

This cost function will be considered throughout this work. Along with this cost function, it is also necessary to choose a suitable solving algorithm in order to optimize it. Several algorithms have been studied and synthesized in [LKKS10]. However, in this work, the considered predictive control is along with a finite control set. It means that only a limit number of discrete control signals is tested with model of the system. The question here is how to choose the most suitable control signals into this set.

In the next paragraph, predictive control strategies will be presented.

### 3.3.3.3 Predictive control strategies

The techniques for optimum control of electrical machine drive are based on the principle that an optimum voltage space vector determined will be applied to the machine in the next switching cycle. As described before, commonly a two-level inverter fed from a DC voltage bus is used as voltage source for the machine. Hence, only a finite number of possible voltage space vectors  $u_s$  can really exist.

An optimum control which considered the fact that a two-level inverter just can realize only eight naturally output states is also called as Direct Predictive Control. It allow direct inverter control, the control algorithm directly determines the optimum inverter switching state for the next sampling cycle. There is no modulation technique and so the switching frequency is variable. This strategy is shown in Figure 3.10a.

Another approach is using a modulation technique which discretizes the reference space voltage vector generated from the controller (Figure 3.10b) before applying to the inverter. In this approach, along with the real vectors from a two-level inverter, a group of virtual vectors will be created and considered thanks to special strategies.

There is another technique in which the on-off time of switches of inverter is calculated directly based on the error between predicted and reference values. This error will be predefined based on desired performance of the system [PW05]

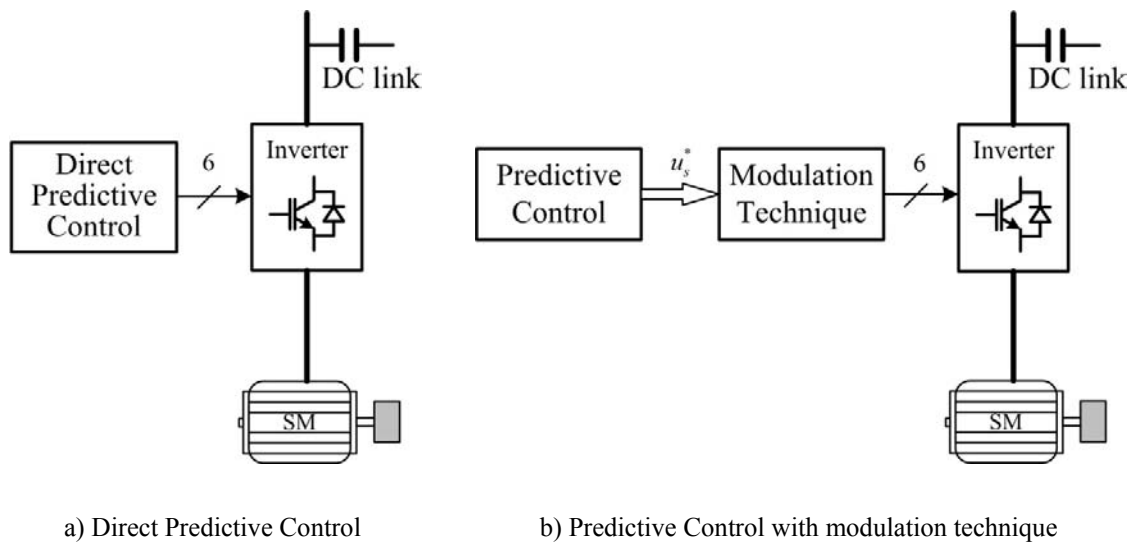


Figure 3.10: Two strategies for predictive control [LKKS10]

From the above analyses, two approaches to predictive torque control (PTC) will be considered and verified. The first one based on the principle of Direct Predictive Control and can be named as Direct Predictive Torque Control (DPTC). The second one is along with modulation technique.

We will consider firstly the “Direct Predictive Torque Control (DPTC)” in the next section.

### 3.4 Direct Predictive Torque Control (DPTC)

As mentioned in previous section, one simple method called Direct Predictive Control is presented. According to this strategy, only eight natural states of a three-phase two-level inverter are considered in optimization process during each control cycle. Each

configuration found in this process will be applied directly to the inverter. No modulation technique needs to be used. So, it also belongs to variable switching frequency methods.

The scheme of this control structure is shown in Figure 3.11.

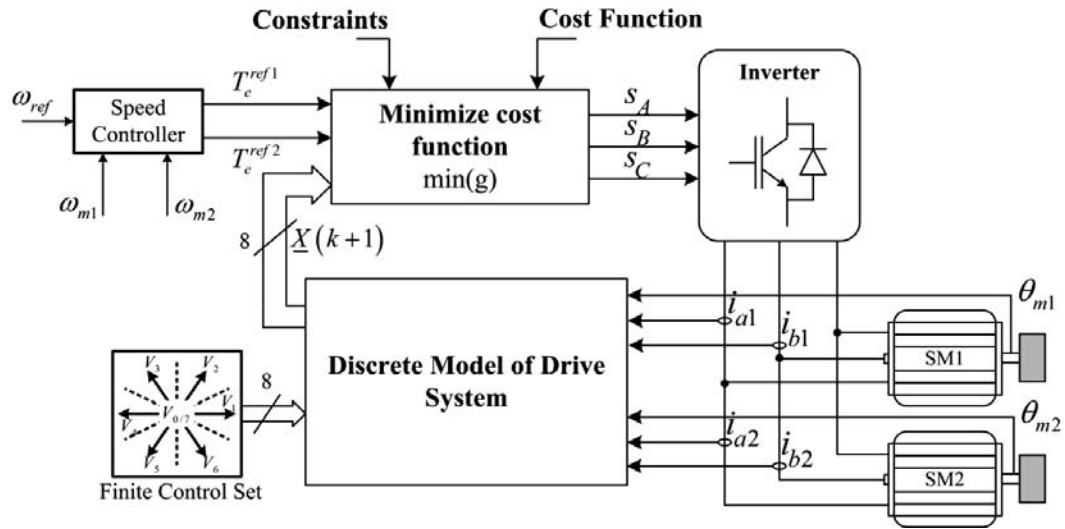


Figure 3.11: Direct predictive torque control (DPTC) scheme

### 3.4.1 Principle

The principle of DPTC is followed these steps:

- + At  $k$  instant time, the system states including the positions  $(\theta_{m1}(k), \theta_{m2}(k))$ , the phase currents  $(i_{abc1}(k), i_{abc2}(k))$  are updated into the controller;
- + Along with the set of eight real states of inverter  $\{(s_A, s_B, s_C)\}_{1...8}$ , all of these quantities are considered in the discrete model of drive system (as presented in (3.22)) in order to predict all the possible system transitions:  $X_i(k+1) = f\{x(k), (s_A, s_B, s_C)_i\}$ , for  $i = 1 \dots 8$ . This prediction function is directly derived from the discrete model and system parameters;
- + To determine which of the control actions must be selected, the cost function built in (3.24) will be evaluated with all the predictions above and the desired reference values  $x^*(k+1)$ . The references here are the desired torques for both machines generated from the two RST speed controller. The future reference value needed  $x^*(k+1)$  can be assumed equal to the actual value  $x^*(k)$  because the sampling time  $T_s$  is small enough and it can be considered constant over  $T_s$ ;
- + The evaluation of the cost function for the eight predictions will lead to eight different cost values. The control action leading to the minimum cost value

$(\min\{g_i\})$ , for  $i = 1 \dots 8$ , is selected to control the system during the next sampling period.

A diagram of the control algorithm is shown in Figure 3.12.

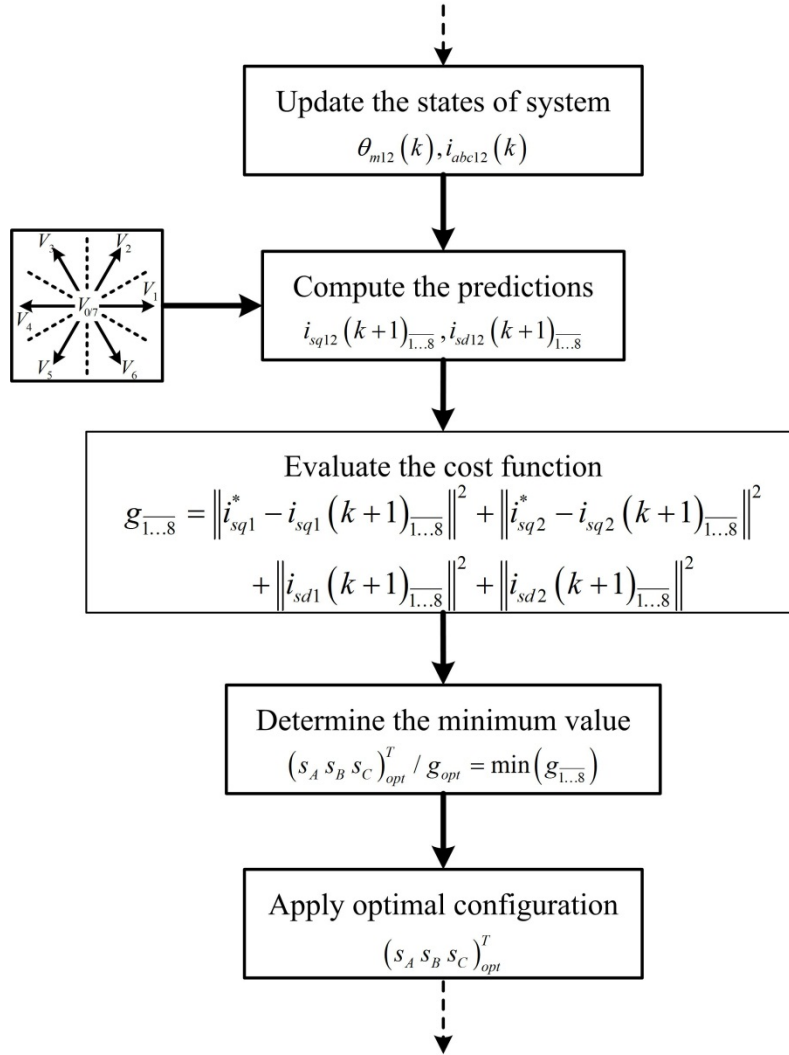


Figure 3.12: Flow chart of direct predictive control algorithm

### 3.4.2 Simulation results for DPTC

In order to verify the performances of the system under direct predictive torque control strategy, a simulation has been built in the Matlab/Simulink environment. PMSM presented in Table 2.6 continues to be used.

The test is carried out under these following conditions. Three set points of speed will be considered:

- + From  $t = 0(s) \rightarrow 0.4(s)$ : the reference speed is set at  $\omega_{ref1} = 75(rad/s)$ ;
- + From  $t = 0.4(s) \rightarrow 0.8(s)$ : the motor is reversed and run at  $\omega_{ref2} = -75(rad/s)$ ;

- + From  $t = 0.8(s) \rightarrow 1.2(s)$ : the motor is kept standstill.

These set-points are plotted in Figure 2.24.

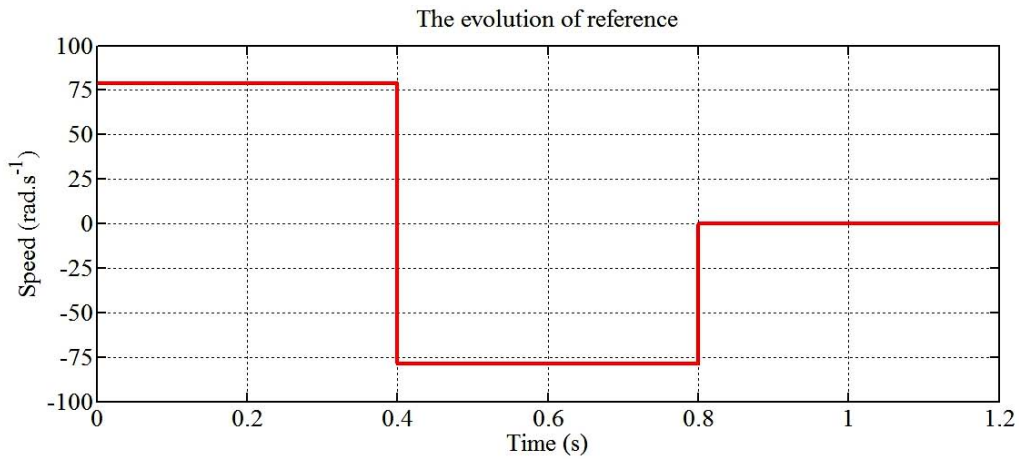


Figure 3.13: The evolution of reference value

At each reference speed, the loads applied to each machine are always different. The load of the first machine  $T_{load1}$  is kept constant during the simulation:  $T_{load1} = 2.5Nm$ .

Meanwhile, the load of second machine varies:

- + From  $t = 0(s) \rightarrow 0.2(s)$ :  $T_{load2} = 1(Nm)$ ;
- + From  $t = 0.2(s) \rightarrow 0.6(s)$ :  $T_{load2} = 4(Nm)$ ;
- + From  $t = 0.6(s) \rightarrow 1.0(s)$ :  $T_{load2} = 1(Nm)$ ;
- + From  $t = 1.0(s) \rightarrow 1.2(s)$ :  $T_{load2} = 4(Nm)$ .

The varies of load of two machine are represented in Figure 2.25.

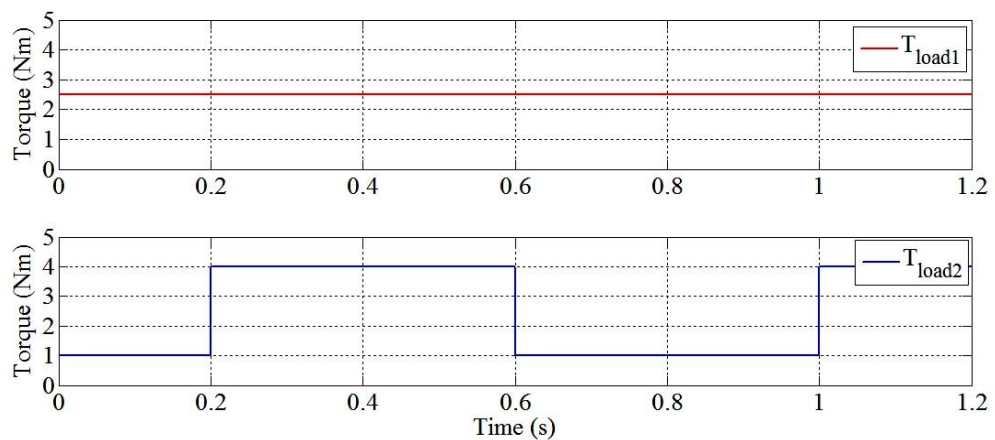


Figure 3.14: The variation of load of each machine in simulation

In this simulation, two sampling times are used. For the speed control loop, due to the slower mechanical response time, the sampling time is chosen equal to  $T_{sc} = 1 \times 10^{-3}(s)$ . Meanwhile, for the predictive controller, in order to impose the dynamic response of system as well as reduce the ripple of system's states (torque, currents ...), a faster sampling time is used:  $T_{pc} = 5 \times 10^{-5}(s)$ .

All the simulation results (speed, torque, and current responses) will be presented and analyzed in the next paragraphs.

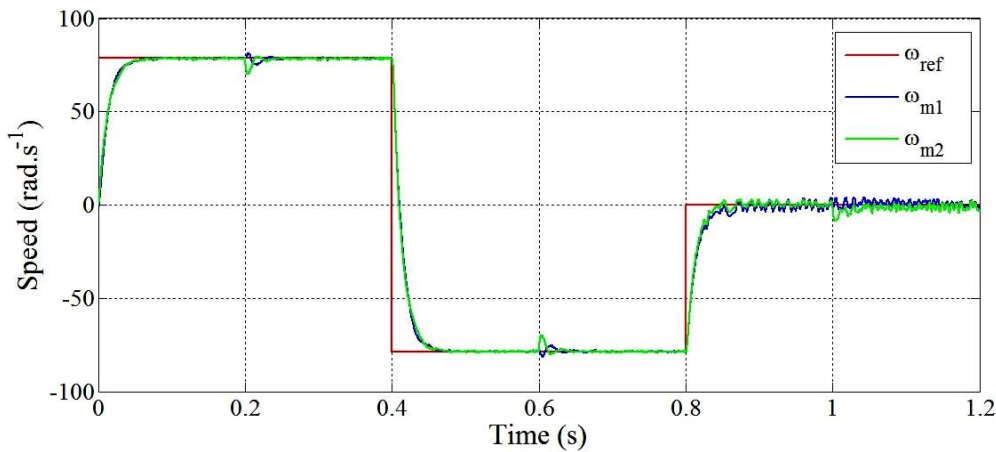


Figure 3.15: Speed of two machines

According to the Figure 3.15, the speed responses of two machines (a blue for the first machine and a green for the second) are presented and compared with the reference speed which is drawn in red. It can be seen that the speeds of two machines follow the reference value. Dynamic response of system is quite fast. The transient time when there is a step change in set point is very small ( $\approx 0.05s$ ).

Moreover, the system is also stable. At several points of time  $t = 0.2(s), 0.6(s)$  and  $1(s)$ , the load applied to the second machine is changed between two values:  $1(Nm)$  and  $4(Nm)$  while the load applied to the first machine is constant. This change makes the system be out of the steady state, however, the steady state immediately is re-established in  $\approx 0.03(s)$ . The speed response at standstill is not good. There is a ripple in both motors. This problem is inevitable with DPTC because it is a feature of variable switching frequency method where low speed operation is not encouraged.

The torque responses of two machines are shown in Figure 3.16. At steady state, the torque of each machine corresponds to the load applied in order to guaranty the following relation:

$$T_e = T_{total} = T_{load} + f_0 \omega_m \quad (3.25)$$

However, the ripple in the torque is important. The peak to peak value of ripple is approximate  $2.8(Nm)$ . This ripple can be reduced if the sampling time used in DPTC strategy is smaller. This issue will be discussed in the next section.

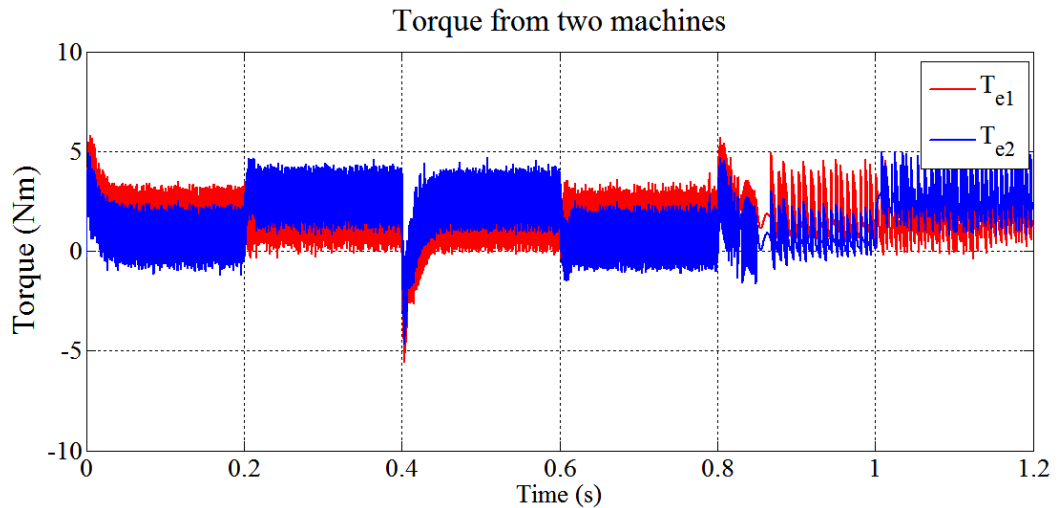


Figure 3.16: Electromagnetic torque of two machines

The representation of machine currents in d-q axis is expressed in Figure 3.17. The q-current is directly proportional to the electromagnetic torque of each machine. Therefore, the machine with heavier load will have bigger q-current. Meanwhile, the d-current of the machine with heavier load is always smaller.

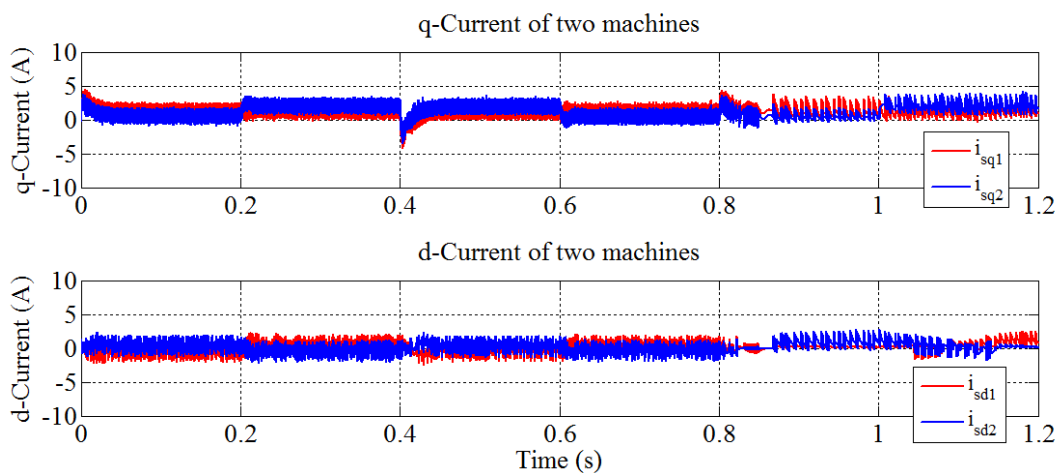


Figure 3.17: Currents in d-q frame for two machines

As shown in this figure, the two d-currents have the same absolute value but with the opposite sign. It can be explained by re-considering the cost function. The criteria

represented by the term of sum square of both d-current:  $(i_{sd1}^2 + i_{sd2}^2)$  was included. Optimal process lets this term come to minimum also respected the following relation:

$$i_{sd1}^2 + i_{sd2}^2 \geq \frac{(i_{sd1} + i_{sd2})^2}{2} \quad (3.26)$$

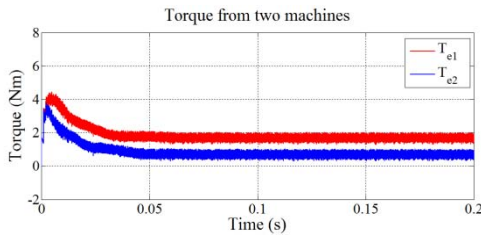
As results, when optimal process makes the left side of (3.26) come to the minimum value, it also does nearly the same thing with the right side. We can see that it will be happened when  $i_{sd1} = -i_{sd2}$ .

### 3.4.3 Relation between the ripple and the sampling time of DPTC

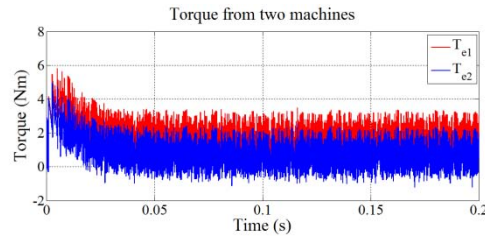
Sampling time applied to DPTC is also the time used in discrete model of the drive system. The smaller the sampling time is the higher accuracy the model has. Moreover, this sampling time is also the shortest time that each voltage vector found in optimization process will be applied. In some cases, optimization process can find the same voltage for several control cycles. This voltage with high amplitude ( $= \frac{2V_{DC}}{3}$ ) will make the system goes further from the steady state and so the ripple is large. In the following consideration, two sampling frequencies will be studied:

- + Figure 3.18a:  $T_{pc} = 1 \times 10^{-5}(s)$ ;
- + Figure 3.18b:  $T_{pc} = 5 \times 10^{-5}(s)$

Results are shown in Figure 3.18.



a)  $T_{pc} = 1 \times 10^{-5}(s)$



b)  $T_{pc} = 5 \times 10^{-5}(s)$

Figure 3.18: Ripple in torque under different sampling time for DPTC

It is easy to realize that with smaller sampling time the ripple is decreased considerably. Theoretically, the amplitude of this ripple can be calculated by the following equation:

$$\Delta i = \frac{V_{DC} \times T_s}{L} \quad (3.27)$$

In Figure 3.18(a), the peak to peak value of ripple is around  $0.5(Nm)$  (compared with  $2.8(Nm)$  in Figure 3.18(b)). This result can be also found with the relation in (3.27).

Reducing the sampling time can improve the performance of the system. However, it will be affected a lot because of the computational cost. Today, many strong computers with high speed processor allow setting up the sampling time at  $10\mu s$ . Nevertheless, with the problem of price, it is not an optimal solution.

Simulation results showed that it is possible to control with DPTC strategy

### 3.4.4 Optimization problem

Optimization process will let the value of cost function come to an optimal value. Normally, this value is close to zero. However, from the simulation results, it can be realized that with DPTC value of cost function  $g$  is not equal to zero. The torque from the machine is different compared with the reference value from speed controller. It leads to the problem that values of q-currents  $i_{sq1}$ ,  $i_{sq2}$  are different with their references  $i_{sq1}^{ref}$ ,  $i_{sq2}^{ref}$ . It is the same with d-currents whose values do not come to zero. A problem pointed out here is whether the cost function which is presented in (3.3.3.2.2) can come to zero or not.

To consider this issue, the optimization problem will be announced as follows:

$$\begin{aligned} & \min(g) \\ s. t \quad & \begin{cases} V_{amin} \leq V_{\alpha} \leq V_{amax} \\ V_{\beta min} \leq V_{\beta} \leq V_{\beta max} \\ 0 \leq V_{\alpha}^2 + V_{\beta}^2 \leq V_{max}^2 \end{cases} \end{aligned} \quad (3.28)$$

We will consider the case when optimization process lets cost function  $g$  come to zero value. It means that, under different load conditions, when the two different reference values will be generated  $i_{sq1}^{ref}$ ,  $i_{sq2}^{ref}$  and  $i_{sq1}^{ref} \neq i_{sq2}^{ref}$ , the two currents  $i_{sq1}^p$ ,  $i_{sq2}^p$  must run to these values. Moreover, the sum  $(i_{sd1}^p)^2 + (i_{sd2}^p)^2$  must come to zero value too  $\Leftrightarrow$

$$\begin{cases} i_{sd1}^p \rightarrow 0 \\ i_{sd2}^p \rightarrow 0 \end{cases}$$

Now, this state will be represented by following features:

$$+ \begin{cases} i_{sd1} = 0; i_{sd2} = 0 \\ i_{sq1} = i_{sq1}^{ref}; i_{sq2} = i_{sq2}^{ref} \end{cases}$$

+ because the load of each machine is different  $\rightarrow i_{sq1}^{ref} \neq i_{sq2}^{ref}$ ;

+ at steady state, the load angles of both machines are constant and different:

$$\begin{cases} \delta_1 = const; \delta_2 = const \\ \delta_1 \neq \delta_2 \end{cases}$$

+ mechanical speeds of two machines are equal:  $\omega_{m1} = \omega_{m2}$  and so the electrical speeds are:  $\omega_{e1} = \omega_{e2}$ ;

The basic electrical equations at steady state of PMSM can be rewritten to calculate the magnitude of voltage vector  $V_s$ :

$$+ \begin{cases} -V_s \sin(\delta_1) & = -\omega_{e1}L_1i_{sq1}^{ref} \\ V_s \cos(\delta_1) & = R_{s1}i_{sq1}^{ref} + \omega_{e2}\sqrt{3/2}\psi_{p1} \end{cases} \Rightarrow V_s^2 = (\omega_{e1}L_1i_{sq1}^{ref})^2 + (R_{s1}i_{sq1}^{ref} + \omega_{e1}\sqrt{3/2}\psi_{p1})^2;$$

$$+ \begin{cases} -V_s \sin(\delta_2) & = -\omega_{e2}L_2i_{sq2}^{ref} \\ V_s \cos(\delta_2) & = R_{s2}i_{sq2}^{ref} + \omega_{e2}\sqrt{3/2}\psi_{p2} \end{cases} \Rightarrow V_s^2 = (\omega_{e2}L_2i_{sq2}^{ref})^2 + (R_{s2}i_{sq2}^{ref} + \omega_{e2}\sqrt{3/2}\psi_{p2})^2$$

In this work, the two considered machines are identical. It means that, the parameters of both machines are the same. Therefore, from two equations above, we will obtain two different values of the voltages supply: the first one is  $(\omega_{e1}Li_{sq1}^{ref})^2 + (R_s i_{sq1}^{ref} + \omega_{e1}\sqrt{3/2}\psi_p)^2$ , and the second one is  $(\omega_{e2}Li_{sq2}^{ref})^2 + (R_s i_{sq2}^{ref} + \omega_{e1}\sqrt{3/2}\psi_p)^2$ . It is clear that two expressions give us two different values. It is unreasonable because we just have only one voltage supply.

With DPTC, for each control cycle, only eight real possibilities from a two-level inverter are considered. Optimization process thus can come to a local minimum. To consider this problem theoretically, optimization process will be carried out by using “FMINCON” function in optimization toolbox of Matlab program.

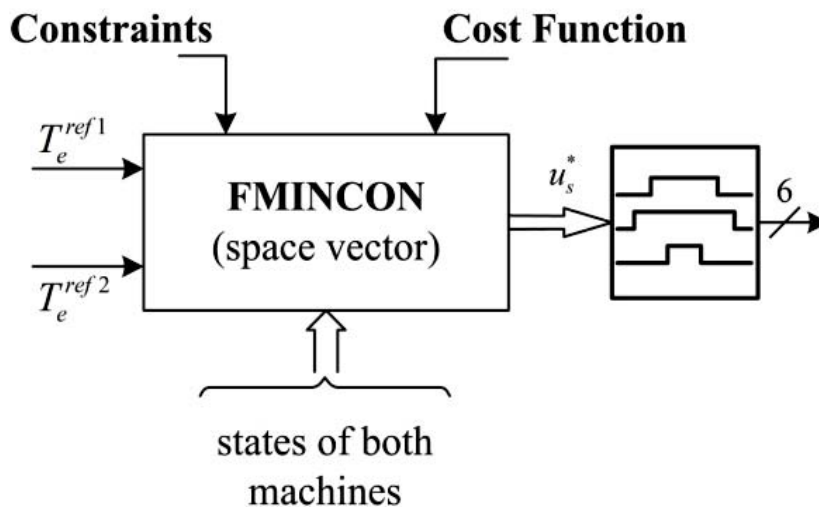
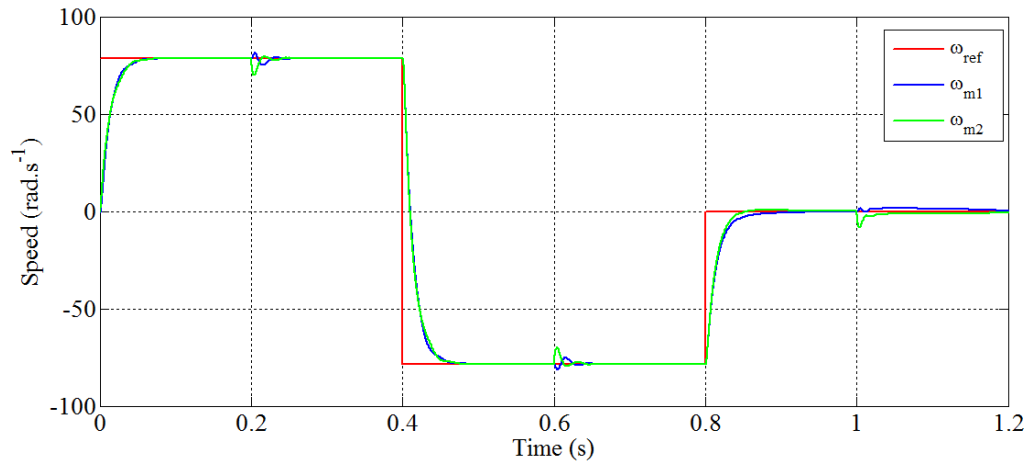
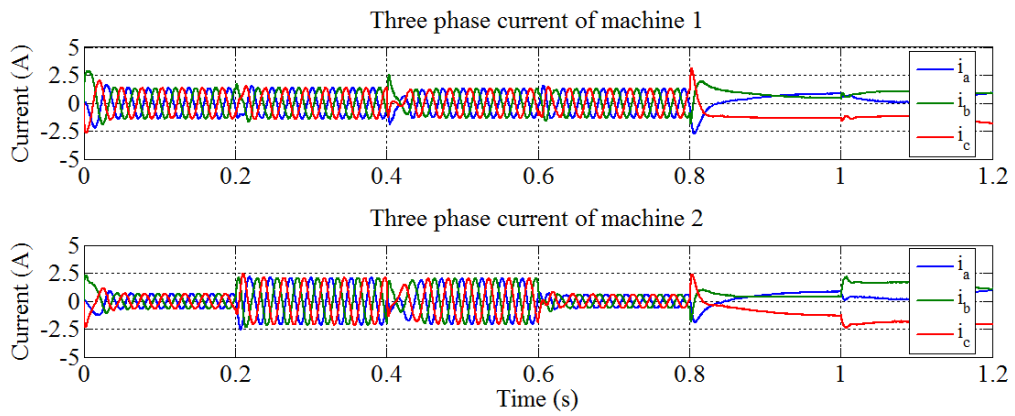


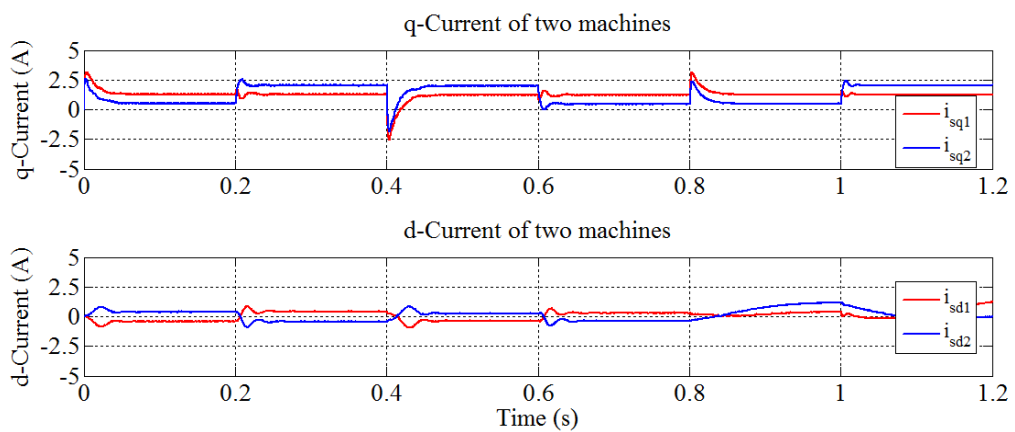
Figure 3.19: “FMINCON” procedure



a) Speed response of two machines



b) Three-phased current of two machines



c) d-q current of two machines

Figure 3.20: Simulation results after optimization process

“fmincon” procedure will search through the whole space vector under the constraints as pointed out in equation (3.28). All voltage vectors which satisfy these conditions will be tested with the cost function  $g$ . The optimal voltage found by “fmincon” procedure is represented in  $\alpha\beta$ -frame:  $V_\alpha^*, V_\beta^*$ . These voltages will be transformed into  $abc$ -frame and synthesized by a modulation technique before being applied to machines. A detailed description of “fmincon” procedure is presented in Appendix A.1

The machines in Table 2.6 will be used to consider the operation of “fmincon” under Matlab/Simulink environment. Simulation results are shown in Figure 3.20.

It can be seen that optimization with “fmincon” function give us nearly the same results about dynamic responses. The time response for speed, current is fast ( $\sim 0.05s$ ). Moreover, the ripple of speed at standstill is improved considerably (Figure 3.20a).

In Figure 3.20b, it is clearly that the three phase current of both machine is smooth. The ripple is also improved.

Using “fmincon” function, the amplitude and phase angle of voltage vector are searched throughout the whole converter control space. Therefore, the ripples in d-q currents are quite small ( $\approx 0.1A$ ) (Figure 3.20c). However, it is clearly that the d-current of both machines are different from zero. It means that cost function  $g$  does not come to zero. Moreover, the ripple is improved but their average values are not much different compared with DPTC. It means that the more exactly reference voltage in “fmincon” procedure just reduces the amplitude of ripple; it does not create a new steady state.

### 3.4.5 Conclusions

The simulation results show that DPTC can be used to control this drive system. The principle of this solution is simple to understand and has easy visualization. If using a small enough sampling time ( $T_{pc} \approx 1 \times 10^{-5}s$ ), a good performance of the whole system can be obtained.

However, it will be difficult to reduce the sampling time to such value as small as  $T_{pc} \sim 1 \times 10^{-5}(s)$ . This problem depends much on the hardware. In such small sampling time, some hardware limitations, due to the high computational cost, can appear. The computational time thus can affect to the operation of the whole system.

As mentioned above, the limitation of sampling time along with the use of only eight real voltage vectors from a two-level inverter leads to a problem of strong in. These vectors have large amplitude of  $\frac{2V_{DC}}{3}$  and are separated with each other by an angle step of  $\frac{\pi}{3}$ . This

issue is also verified with “fmincon” function where the amplitude and the phase angle of the reference voltage can be placed anywhere in the whole control region of the converter.

Based on theoretical analyses, the idea of using more voltage vectors, which are also called virtual voltage vectors, with variable amplitude and smaller angle steps is proposed. A strategy with such a group of virtual voltage vectors will be studied in the next section. As results, a Predictive Torque Control – “Split and Seek” (PTC-SS) strategy is obtained [NFL13].

### 3.5 Predictive Torque Control – “Split and Seek” (PTC-SS)

The advantages of using not only the discrete real states of an inverter but also the virtual voltage vectors placed anywhere in the whole control region of an inverter is mentioned in some documents [VLF+09] [RVAB06]. Moreover, this strategy will be associated with the SVM technique to generate the virtual vectors. It will lead to a constant switching frequency operating mode.

As shown in Figure 3.21, the virtual voltage vectors can be located in any position in the inverter control region. Each virtual vector is considered in the  $(\alpha\beta)$  plane and represented by a pair of values: the angle (in comparison with  $\alpha$ -axis) and the magnitude. In this figure, the real vectors are represented by solid line vectors while the virtual vectors are illustrated by the dash lines. These real ones divide space vector into six sectors. The control region of a standard inverter under space vector modulation technique is limited by a circle with the radius equals to  $V_{DC}/\sqrt{3}$ .

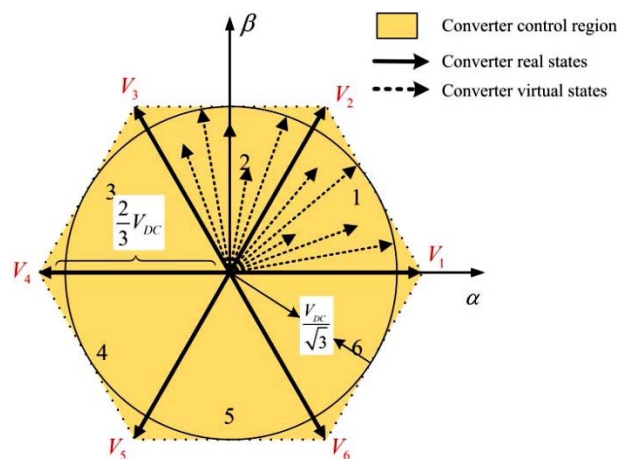


Figure 3.21: Control region of a three-phase two-level inverter including the virtual states

Because all virtual voltage vectors are considered in the  $(\alpha\beta)$  plane, the model of this system needs to be described in  $\alpha\beta$  frame too.

### 3.5.1 Predictive model in $(\alpha\beta)$ frame:

Firstly, voltages in the  $(dq)$  rotor flux reference frame must be rewritten in  $(\alpha\beta)$  plane.

$$\begin{bmatrix} u_{sd1}(k) \\ u_{sq1}(k) \\ u_{sd2}(k) \\ u_{sq2}(k) \end{bmatrix} = \underbrace{\begin{bmatrix} \cos \theta_{re1}(k) & \sin \theta_{re1}(k) \\ -\sin \theta_{re1}(k) & \cos \theta_{re1}(k) \\ \cos \theta_{re2}(k) & \sin \theta_{re2}(k) \\ -\sin \theta_{re2}(k) & \cos \theta_{re2}(k) \end{bmatrix}}_{\mathbb{M}(k)} \begin{bmatrix} V_{\alpha}(k) \\ V_{\beta}(k) \end{bmatrix} \quad (3.29)$$

The voltage in  $(\alpha\beta)$  frame can be calculated from three-phased voltage by using Clark's transformation.

$$\begin{bmatrix} V_{\alpha}(k) \\ V_{\beta}(k) \end{bmatrix} = V_{DC} \sqrt{\frac{2}{3}} \begin{bmatrix} 1 & -\frac{1}{2} & -\frac{1}{2} \\ 0 & \frac{\sqrt{3}}{2} & -\frac{\sqrt{3}}{2} \end{bmatrix} \begin{bmatrix} s_A(k) \\ s_B(k) \\ s_C(k) \end{bmatrix} \quad (3.30)$$

The model of system will be obtained as shown in (3.31)

$$\begin{bmatrix} i_{sd1}^{k+1} \\ i_{sq1}^{k+1} \\ i_{sd2}^{k+1} \\ i_{sq2}^{k+1} \end{bmatrix} = \mathbb{F}(k) \begin{bmatrix} i_{sd1}^k \\ i_{sq1}^k \\ i_{sd2}^k \\ i_{sq2}^k \end{bmatrix} + \mathbb{G}(k) \mathbb{M}(k) \begin{bmatrix} V_{\alpha}(k) \\ V_{\beta}(k) \end{bmatrix} + \mathbb{H}(k) \quad (3.31)$$

The aim of this approach, with the support of SVM technique, is to find the more exactly voltage vector at each control period. Thank to this, the performance of the system can be improved. The ripple in the states such as torque, currents will be reduced.

However, how to define these virtual vectors effectively is really a problem. In the next part of this section, a method which is called “Split and Seek” will be considered and described in order to solve this problem [NFL13].

### 3.5.2 “Split and Seek” approach

As mentioned above, this approach uses virtual voltage vectors to be added to the finite control set (with only eight real vectors) defined in DPTC. However, if all the virtual vectors are considered in each control cycle, the computational effort will be increased considerably. Let's consider an inverter which is supplied by a DC voltage of  $V_{DC} = 540V$ . Under SVM technique, the maximum voltage which can be generated in the linear region is:

$$V_{max} = \frac{V_{DC}}{\sqrt{3}} = \frac{540}{\sqrt{3}} \approx 312(V) \quad (3.32)$$

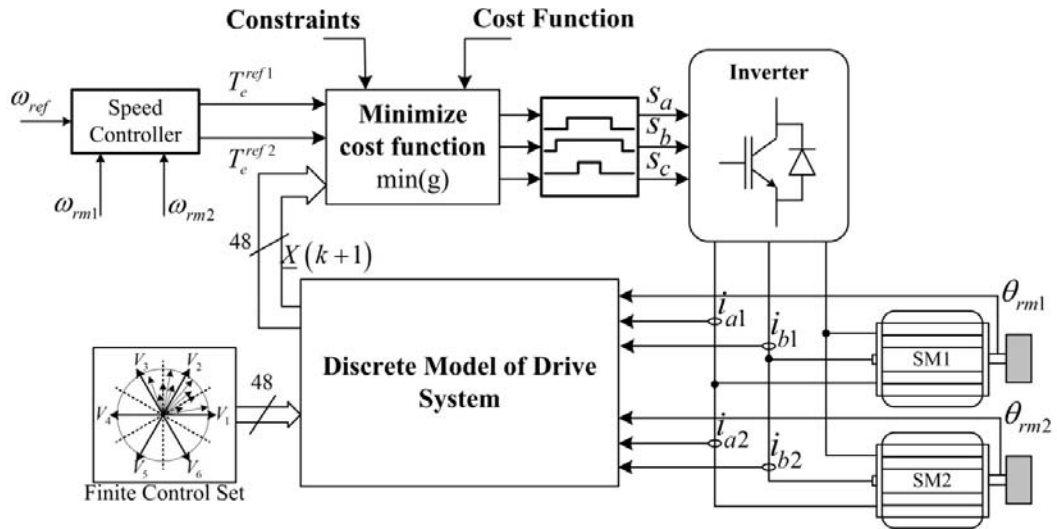


Figure 3.22: PTC – “Split and Seek” approach

If we consider, for instance, a case where the difference between any two virtual vectors is  $\Delta\alpha = 10^\circ$  and  $\Delta V = 10V$ , there will be  $\left(\left\lceil \frac{360}{10} \right\rceil\right) + \left(\left\lceil \frac{312}{10} \right\rceil + 1\right) = 36 \times 32 = 1152$  virtual voltage vectors which need to be evaluated at each sampling time. It is too large compared with the eight real configurations of the inverter.

To overcome this problem, a new solution is proposed. Instead of considering all the virtual vectors in each control cycle, the searching process will be divided into two steps:

- + The first step will look for the angle, around one chosen “real” vector;
- + The second step will look for the magnitude of the vector.

### 3.5.2.1 Angle seeking

This idea is based on the fact DPTC strategy with only eight real vectors can operate the system. Only one problem with DPTC is that such a real vector with large magnitude can be repeated for several sampling periods or jumps directly to another one with an angle step of  $\frac{\pi}{3}$ .

Therefore, the entire voltage space will be firstly divided into six sectors by six real active voltage vectors (as shown in Figure 3.21). These six basic vectors will compose the first considered control set. This control set will be evaluated into the model in (3.31) to calculate the prediction. A value of the cost function will be obtained corresponding to each vector. The vector which gives us the minimum value of the cost function will be chosen as the starting point for the next algorithm step (step 2 in Figure 3.24).

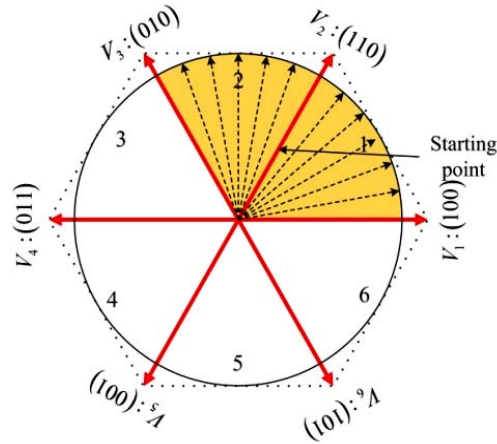


Figure 3.23: Two adjacent sectors with virtual voltages

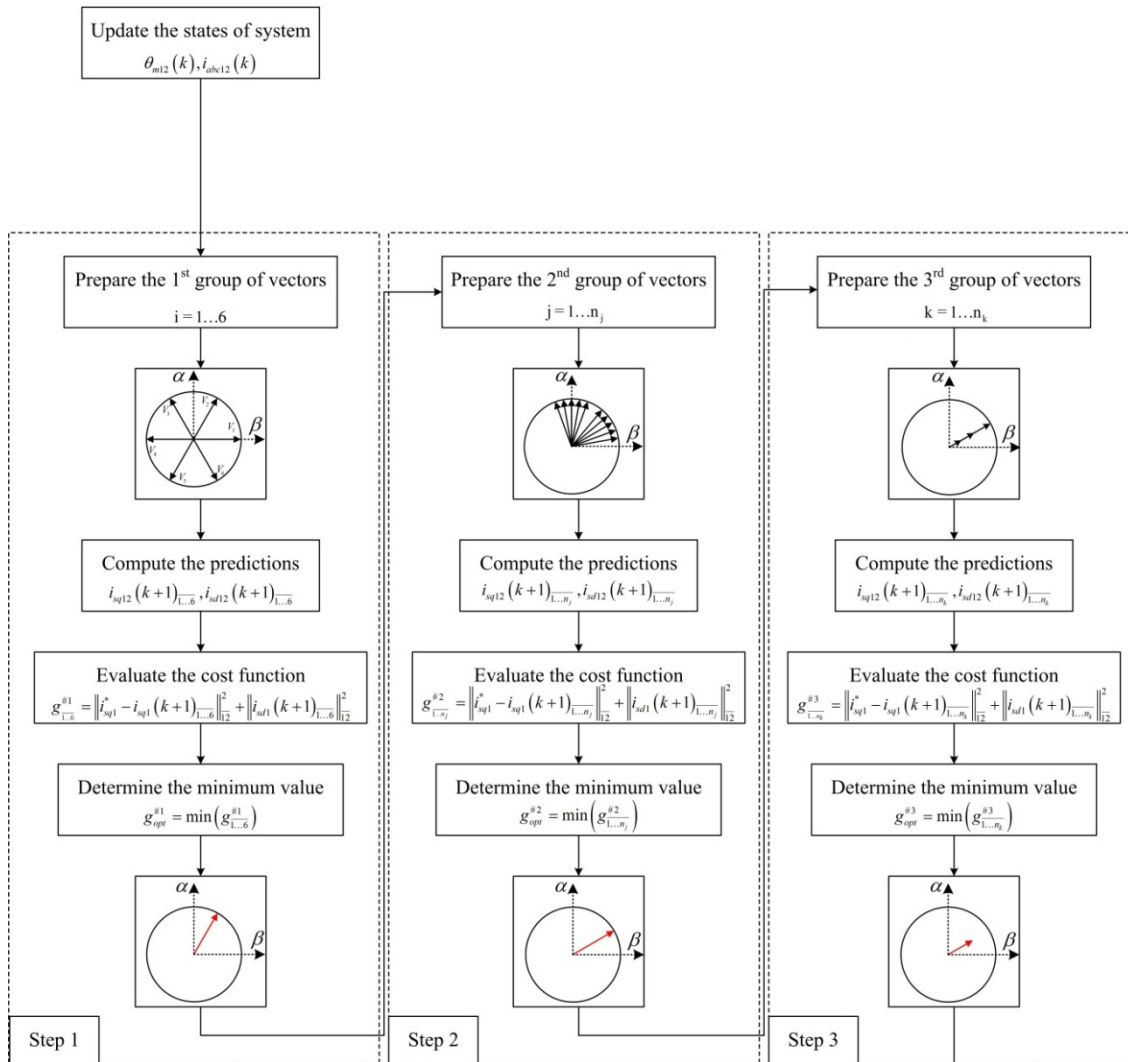


Figure 3.24: Diagram of the new solution

Here, from the basic vector found in the previous search, a group of virtual voltage vector defined in two adjacent sectors (left and right side of the basic vector) will be considered. If we define the difference of the angle between two consecutive vectors  $\Delta\alpha = 10^\circ$ , we will obtain a group of ten voltage vector (as shown in Figure 3.23). These vectors have the same magnitude, equal to the  $V_{max}$ . We will continue evaluating these vectors through the cost function and we will choose the one with minimum value of  $g$ . This vector will give us the best value of angle.

With this process, the number of virtual vectors need to be considered is sixteen (six basic vectors and ten virtual around the basic one).

This is the end of step 2. Through this step, we can eliminate the problem in which a reference voltage vector can jump a large angle ( $\pi/3$ ) between two sampling period. Now, we continue considering a step 3 with magnitude seeking.

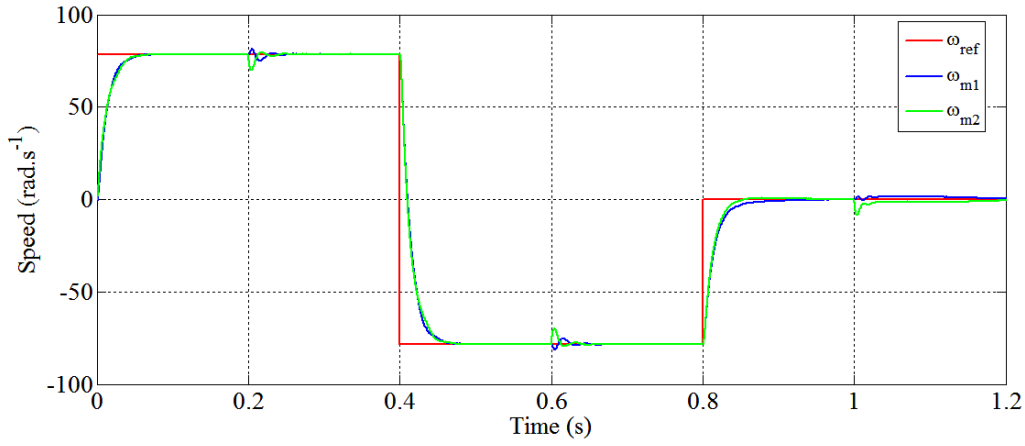
### 3.5.2.2 Magnitude seeking

After positioning the best voltage vector by angle seeking process, we continue looking for the best magnitude of this vector in order to reduce the overshoot which can happen when a maximum voltage vector is applied to the machine.

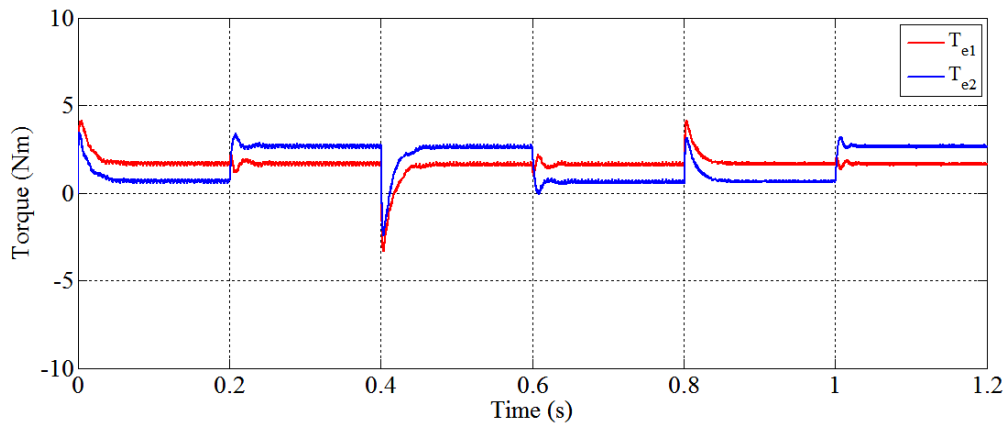
Therefore, the voltage vector found in the angle seeking process will be passed through the optimal magnitude searching algorithm. In this process, a group of voltage vectors which are represented by the optimal angle, will be varied in their magnitude. With the range of voltage from 0 to  $V_{max} = \frac{V_{DC}}{\sqrt{3}} \approx 312V$ , a magnitude step will be defined as:  $\Delta V = 10V$ . So, the number of virtual voltage vectors to be tested is:  $\left\lceil \frac{312}{10} \right\rceil + 1 = 32$ .

Through the two consecutive searching process, an appropriate virtual voltage vector will be selected. The SVM technique will be responsible of modulating this voltage vector and generating pulses for the inverter. With this method, the total number of voltage vectors is reduced from 1152 to  $16+32=48$ .

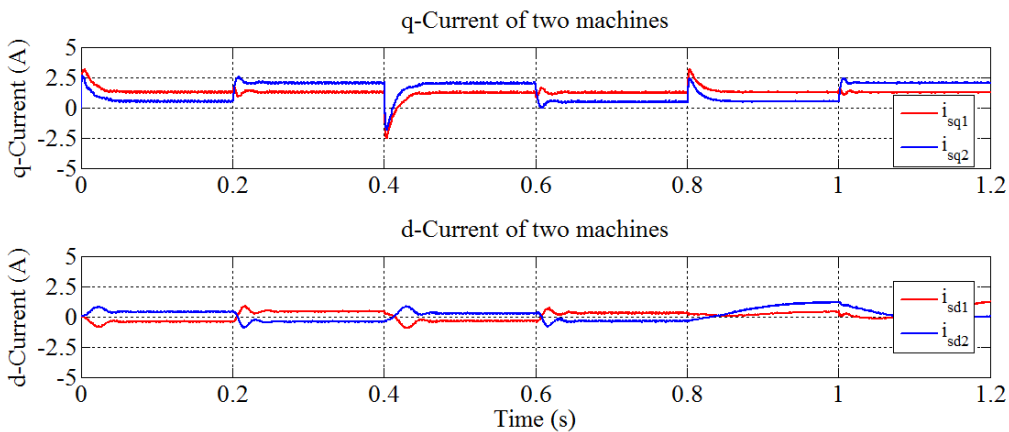
As introduced, voltage vectors found by “SS” algorithm are not the real states of a two-level inverter. It is a pair of values of voltage vector in  $\alpha\beta$  frame and will be transformed into three-phase voltages. These voltages have to be synthesized by a modulation technique. Two typical techniques which have been known are pulse width modulation (Sine PWM) and space vector modulation (SVM). In this work, SVM technique will be used to generate the desired voltage.



a) Speed response of two machines



b) Electromagnetic torque of two machines



c) d-q current of two machines

Figure 3.25: Responses of system under PTC-SS

### 3.5.3 Simulation results for PTC-SS

In order to verify the ability as well as the improvement of this solution compared with the DPTC, the same test is carried out with the PTC-SS. The machine in Table 2.6 continues to be used. The testing conditions are repeated, the reference speed and loads of two machines are represented as in Section 3.4.2.

In this simulation, the two sampling times applied for speed control and predictive control are kept as the same as the case of DPTC. All simulation results are shown in Figure 3.25. In general, the dynamic responses of the two machines are still good. The small transient time and the stability of system under the change of loads as well as under the difference of loads between two machines are maintained. Response time is fast ( $\sim 0.05s$ ). The system is stable under the change of set point as well as of load. When having a suddenly change of load, steady state is reestablished after a short time ( $\sim 0.05s$ ). Besides, the speed response of two machines at standstill is also improved. There is no ripple compared with DPTC (Figure 3.25a). In addition, through Figure 3.25(b) and (c), it is easy to realize that the ripple in torque and current is reduced considerably. The torque ripple is approximate  $0.3(Nm)$ .

A comparison about the spectrum and the THD of one phase current of two machines in both predictive solutions will be carried out in the following parts to evaluate the performance of proposed algorithm.

#### 3.5.3.1 A comparison with DPTC

*a) About the losses:*

According to the electromagnetic torque equation of PMSM, the torque is directly proportional to the q-current. It means that the d-current does not play any role in producing the torque and so is not transformed to mechanical energy. It will cause the losses in the resistance of winding of PMSM.

The total losses of two operating machines are calculated by the following equation:

$$W_{loss} = R_s \sum_{t=0}^{t_{sim}} (i_{sd1}^2 + i_{sd2}^2) \Delta t \quad (3.33)$$

The value of  $W_{loss}$  is shown in Table 3.4. Losses are decreased considerable thank to the new solution. At three range of speed, the losses of PTC-SS are just a half of this in DPTC. It can be recognized that the smaller ripple in the current brings to this improvement.

Speed range ( $rad.s^{-1}$ )	DPTC	PTC-SS
$-18 \times \pi \rightarrow 18 \times \pi$	3.0887 (J)	1.4634 (J)
$-25 \times \pi \rightarrow 25 \times \pi$	2.7210 (J)	1.0362 (J)
$-32 \times \pi \rightarrow 32 \times \pi$	2.7425 (J)	0.8630 (J)

Table 3.4: The total losses of two machines

In the next point, the spectrum and THD factor of phase current will be studied.

b) *Spectrum and the THD of one-phase current:*

The simulation will be carried out with both methods under several reference speeds:

$$\omega_{ref} = \begin{cases} \omega_1 = 18 \times \pi \text{ (rad.s}^{-1}\text{)} \\ \omega_2 = 25 \times \pi \text{ (rad.s}^{-1}\text{)} \\ \omega_3 = 32 \times \pi \text{ (rad.s}^{-1}\text{)} \end{cases} \quad (3.34)$$

with the different load conditions:  $T_{load1} = 2.5(Nm)$  and  $T_{load2} = 5(Nm)$ .

The fundamental frequencies which are correlated with each reference speed are calculated by:

$$f_{fund} = \frac{n_p \times \omega_{ref}}{2 \times \pi} = \begin{cases} f_1 = 27 \text{ (Hz)} \\ f_2 = 37.5 \text{ (Hz)} \\ f_3 = 48 \text{ (Hz)} \end{cases} \quad (3.35)$$

The sampling time for predictive controller is set at  $T_{pc} = 5 \times 10^{-5}(s)$ .

In Figure 3.26, the A-phase current of each machine under is illustrated. It can be realized that under DPTC approach (Figure 3.26a), the phase current ripples a lot with an amplitude is up to  $\sim 1(A)$ . Meanwhile, in PTC-SS, the ripple almost disappears. The current is so smooth (Figure 3.26b)

Normally, it cannot identify the frequency components of a signal buried in a noisy time domain (A-phase current in Figure 3.26b is an example). Therefore, to check this, the Discrete Fourier Transform (DFT)

$$X(m\omega_s) = \sum_{k=0}^{N-1} x_k e^{-jm\omega_s k} \quad ; \omega_s \triangleq \frac{2\pi}{N} \quad (3.36)$$

could be computed to see if a spectral peak is present or not. For this purpose, Matlab has the FFT analysis tool, which performs the computation DFT. We will use this tool to get the spectrum and total harmonic distortion (THD) of these phase currents.

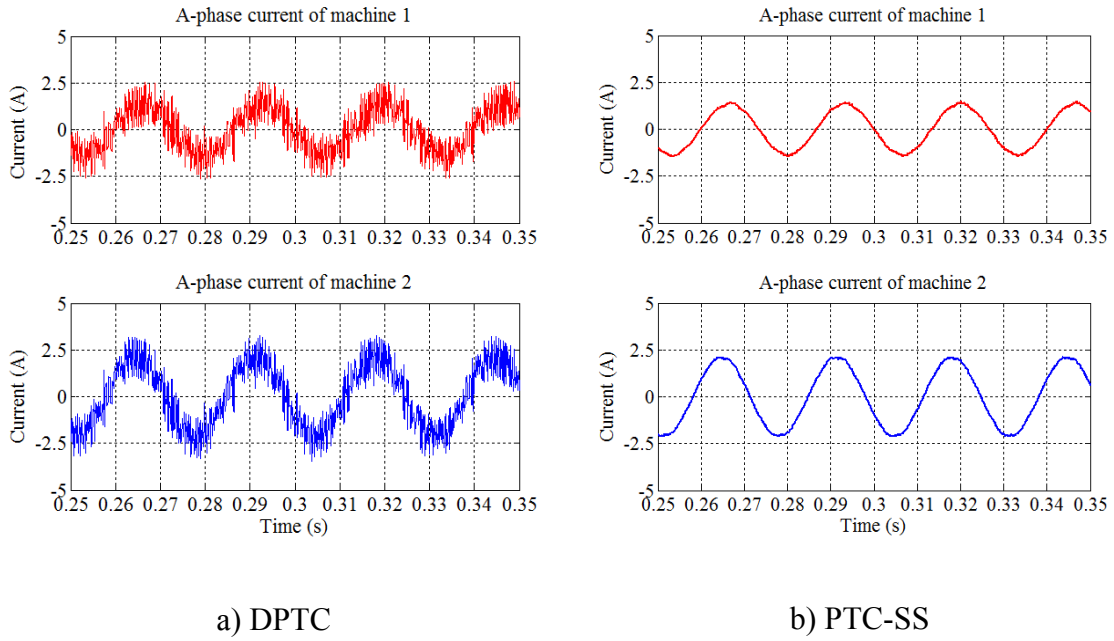


Figure 3.26: A-phase current of two machines

The frequency spectrums of A-phase current of two machines are represented in Figure 3.27 and Figure 3.28. In both figure, there are always the highest peaks which represent for the fundamental frequencies in (3.35). These are fundamental components of signal and are not the noise. However, in the case of DPTC, we can see many smaller peaks. They show a low harmonic content in the current. It also means that the noise buried in these currents is big.

On the contrary, frequency spectrums of A-phase current of two machines under PTC-SS just have one clear spectral peak. The noise underlying sinusoidal current signal is almost absent.

The THD values corresponding to each considered case are also summarized in Table 3.5. This value defines the level of harmonic content in alternating signal. The smaller this value is the better the quality is. For current harmonics, the equation of THD is:

$$THD_i = \frac{\sqrt{\sum_{h=2}^{h=H} I_h^2}}{I_1} \quad (3.37)$$

where  $I_1$  represents for the fundamental component,  $I_h$  is stand for the higher or der harmonic components.

It can be seen that in DPTC, the THD is very high (>20%). Meanwhile, PTC-SS gives us the small THD values (<1%). It means that the quality of system under PTC-SS approach is improved. The ripple is reduced respectively.

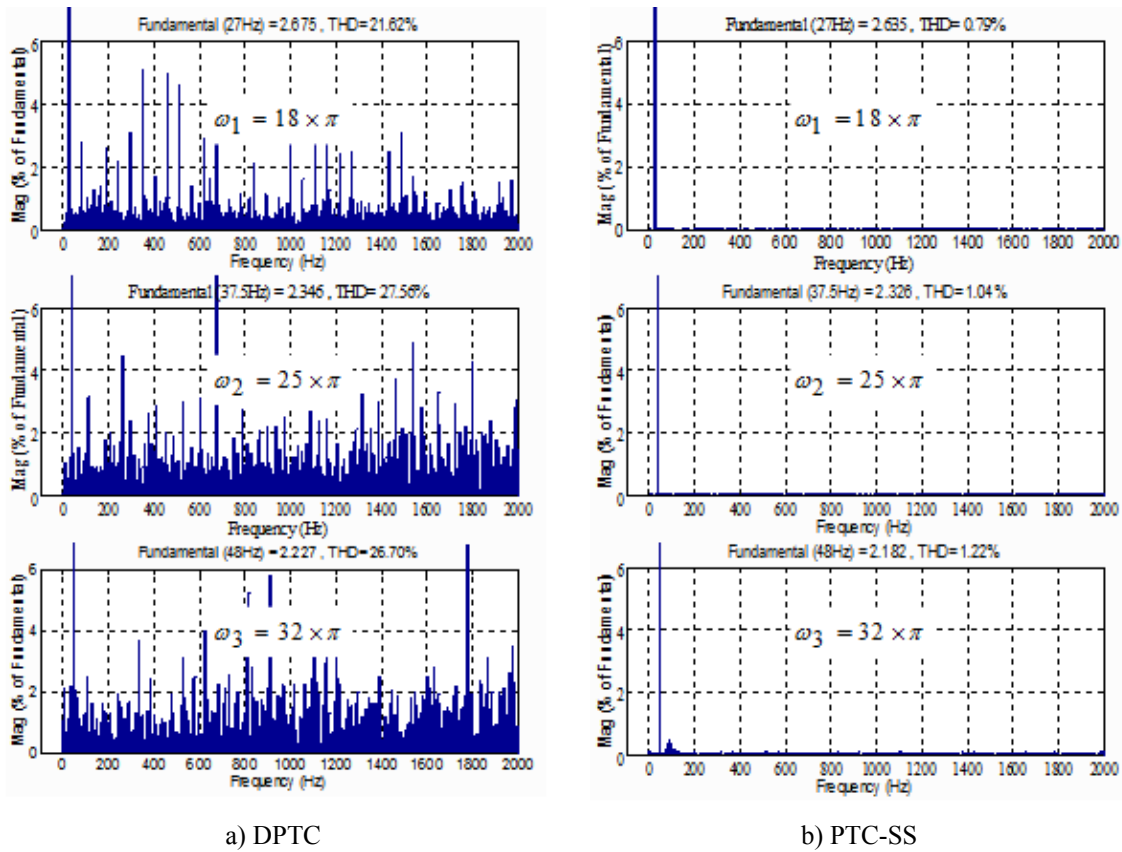


Figure 3.27: Spectrum of A-phase current of machine 1

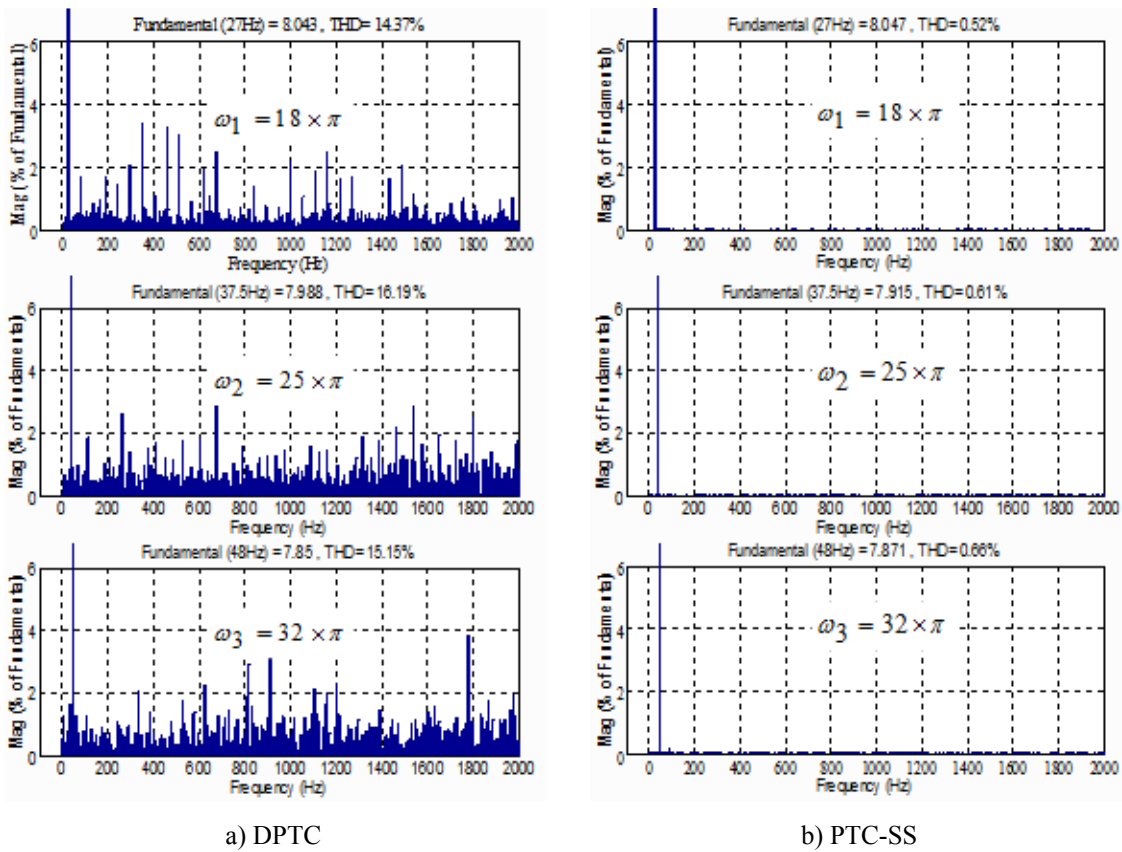


Figure 3.28: Spectrum of A-phase current of machine 2

About the fundamental values, both methods give us nearly the same results. The difference is small (<2%). It can be explained by the fact that the tests applied for both cases are the same and the dynamic responses of the system are also nearly the same (the response time under the change of set point or load).

	Fundamental Value (A)				THD (%)			
	DPTC		PTC-SS		DPTC		PTC-SS	
	MC1	MC2	MC1	MC2	MC1	MC2	MC1	MC2
$\omega_1$	2.675	8.043	2.635	8.028	21.62	14.37	0.79	0.52
$\omega_2$	2.346	7.988	2.326	7.896	27.56	16.19	1.04	0.61
$\omega_3$	2.227	7.85	2.182	7.851	26.70	15.15	1.22	0.66

Table 3.5: The fundamental and THD values

Through this section, a new approach to the predictive control named as PTC-SS is presented and tested with the mono-inverter dual-parallel PMSM drive system. The simulation results have shown that PTC-SS applied in this work has positive effect. The searching algorithm does not increase much the computation effort but gives the much better results. The ripple of system's variables is reduced considerably. Consequently, the losses represented in term ( $R_s i_{sd}^2$ ) are also reduced.

### 3.6 Conclusions

In this chapter, the predictive torque control for mono-inverter dual-parallel PMSM drive system is presented. Two approaches have been studied and applied to this system. After the theoretical analyses, simulations are carried out to verify the performances of two approaches.

The simulation results have initially shown that predictive torque control can be applied to this drive system. Just using an inverter to operate two PMSMs in parallel, the two methods are simple in design and give the good performances.

Under the simulation environment, results are correct and satisfactory. The system can operate stable in many ranges of speed as well as under the load change. However, with a real system, there are many issues which need to be considered. The inverter is not ideal any more. The computation time also has an effect to the performance of the system. The error in measurement process and so on. Therefore, it is very interesting to verify the algorithm with a real system.

In the next chapter, an experimentation bench will be constructed. The predictive torque controller will be tested in this bench.

# Chapter 4

## The experimental platform

### Table of contents

---

4.1. General description.....	107
4.2. Motor coupling system.....	109
4.3. Power supply system.....	112
4.3.1. Power supply system.....	112
4.3.2. Power converter.....	113
4.4. Measurement and control system.....	113
4.4.1. Measurement interfaces.....	113
4.4.1.1. Current measurement.....	113
4.4.1.2. Mechanical position measurement.....	113
4.4.1.3. Speed calculation.....	115
4.4.2. dSPACE system.....	116
4.4.2.1. dSPACE DS1103 board.....	116
4.4.2.2. MATLAB/Simulink and Control-desk.....	116
4.5. Digital control implementation.....	117
4.5.1. Speed controller.....	118
4.5.2. Predictive torque controller.....	118
4.6. Experiment's results.....	119
4.6.1. Test with one machine.....	119
4.6.2. Test with two machines in parallel.....	122
4.6.3. Test with two machines in parallel under master/slave configuration..	125
4.7. Conclusions.....	127

---

### 4.1 General description

An experimental bench based on the principle of DSP-based electric drives system has been designed and constructed to verify the theoretical analyses presented in previous

---

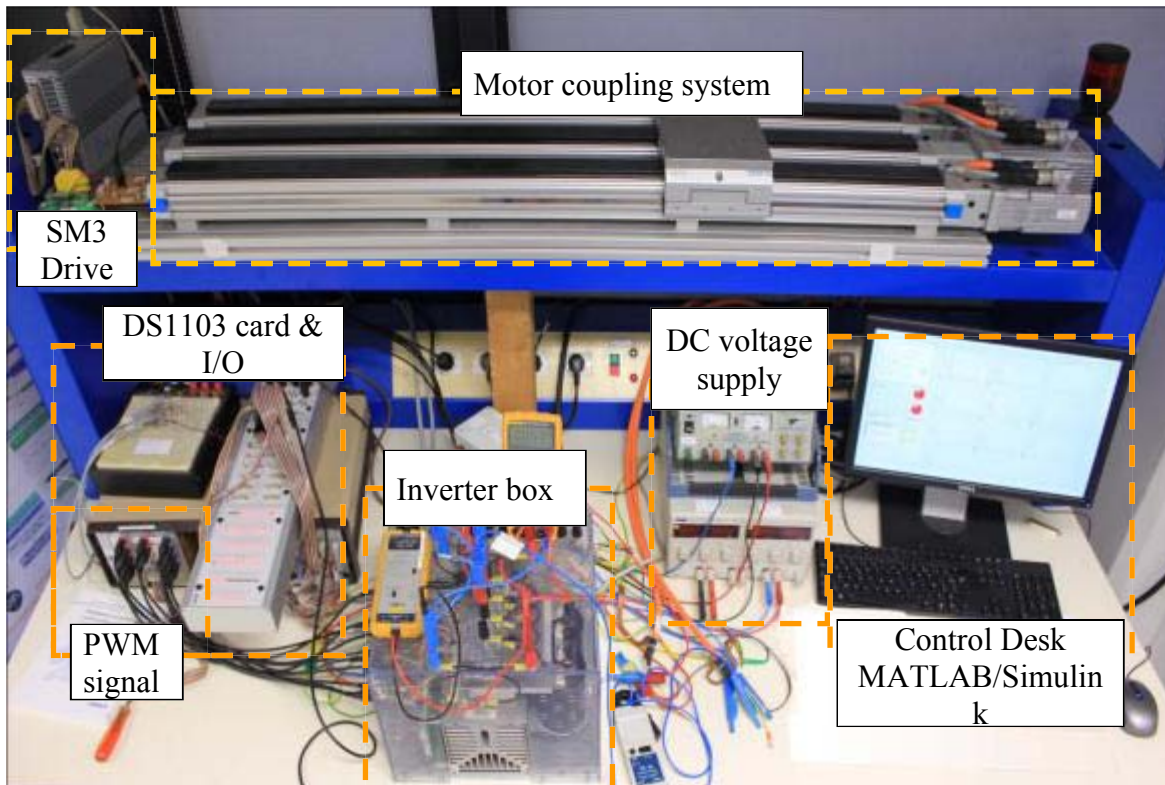


Figure 4.1: Presentation of the experimental bench

chapters. This system is composed of four major parts: 1) Motor coupling system, 2) Power Electronics Drive Board, 3) dSPACE based DS1103 R & D controller card and CP1103 I/O board and 4) MATLAB/Simulink and Control desk software.

All the equipments are installed and organized in the following way:

- Motor coupling system: composed of two identical PMSMs with a resolver already installed. Resolver coils are available from the motor through a 12-pin connector in the motor housing.
- Measurement system:
  - Hall effect sensors type LEM LA 25-S for current measurements;
  - Resolver-to-digital converter that measures the position of the rotor;
  - A multi-meter displays the DC voltage bus.
- Power supply system:
  - An auto-transformer to control the electrical energy from EDF network;
  - A voltage source that provides DC voltage bus for the inverter;
  - A three leg switch-mode inverter that uses IGBT switches.
- Control system:

- A CP1103 dSPACE board including 50 bit-I/O channels, 36 A/D channels, and 8 D/A channels;
- A CLP1103 dSPACE board with LEDs that show the state of different signals;
- A computer with MATLAB/Simulink and Control Desk software.

These entire elements are shown in Figure 4.1.

This experimental bench has been developed in laboratory LAPLACE with the aim of creating a system representing the hypothetical displacement of two flaps of an airplane [Bid11]. In mechanical part, the parallel structure of two PMSMs will be set up. Detailed descriptions of each part of the whole system will be discussed in the next parts of this chapter.

## 4.2 Motor coupling system

This system contains two permanent magnet synchronous machines, which are denoted as SM1 and SM2. They have identical characteristics and are connected in parallel to a voltage inverter. Their technical specifications are shown in Appendix 0.

According to Figure 4.2, each of these machines pulls a plate through a ballscrew axis (axis1 and axis2) which allows obtaining the very smooth motion as well as a good positioning accuracy. In addition, to create a different load between two motors, a third machine which is denoted SM3 or "load machine" is linked with the first machine SM1 through an aluminum plate. Torque generated from SM3 is controlled by a smart electromotor controller (Appendix B.4.2) and take effect on SM1. In consideration of the axis1 and axis3, they are perfectly parallel thanks to an embedded link [Bor81], so a rigid connection is created between these two axes.

In fact, the aim of this experiment is to move the two plates horizontally along axis1 and axis2. To do so, it is necessary to transform a rotational movement of the shaft of the motor into translational movement. Therefore, ballscrew axes are used in this case. The conversion is thus made possible by rolling balls, which are arranged in precision grooves between a screwed shaft and nut. Owing to these characteristics, ballscrews for all applications are essential, with which high speeds, accuracies and reliability are requested over a long service life. The structure of a ballscrew axis is shown in Figure 4.3. Besides, all technical specifications of this axis are summary in Appendix B.4.3

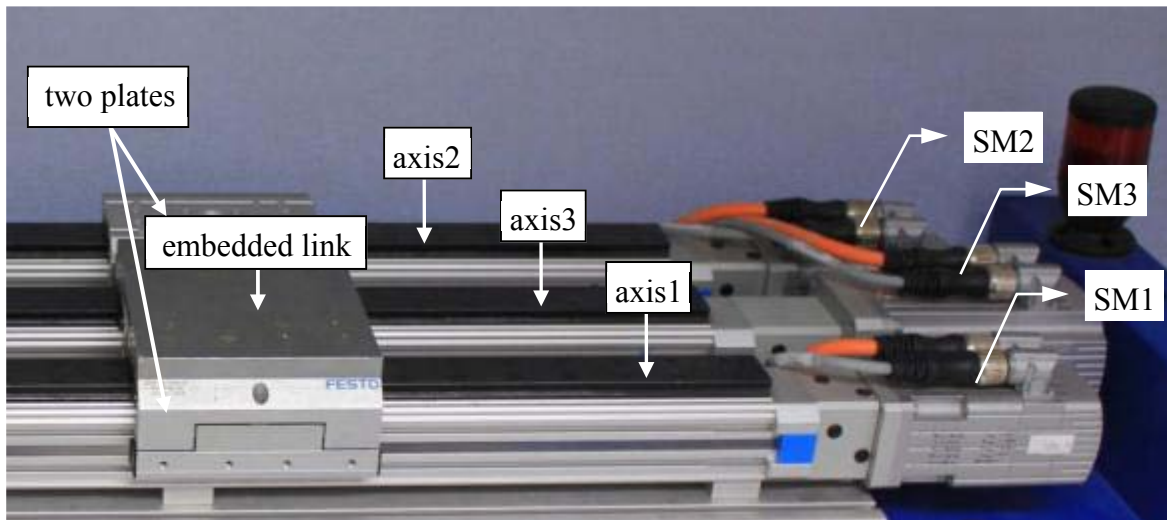
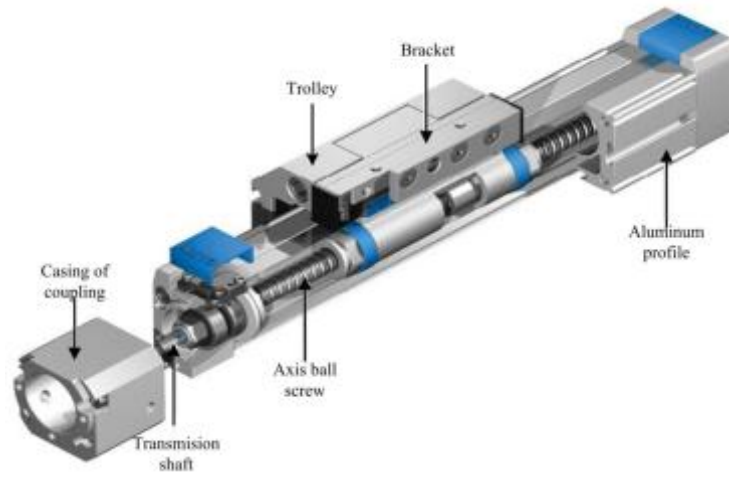


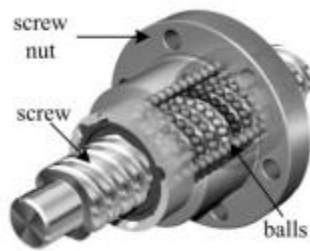
Figure 4.2: Motor coupling system

Besides, for the best representation of motion of the flaps, the axes chosen have a maximum 1 meter length and the speed of movement of the plates is limited to  $1m \cdot s^{-1}$ . At the terminals of axis1 and axis2, there are latches. If a plate passes through the limit of the axis, the latches will send a signal to control the card to stop the system immediately. The used sensors are inductive type whose principle of operation and characteristics are described in Appendix B.5.3

The system also has two resolvers which are mounted on SM1 and SM2. They are used to measure the absolute position of the rotors. In Figure 4.2, the grey cable is used to transfer the information of the position, and the orange is the power cable.



a) Screwed shaft [Fes]



b) Balls bearing [Rex02]

Figure 4.3: Structure of a ballscrew axis

## 4.3 Power supply system

The power supply system is represented in Figure 4.4. It includes the EDF network, a three-phase variable auto-transformer and a power converter which is composed of a rectifier, a filter and a three-leg IGBT inverter.

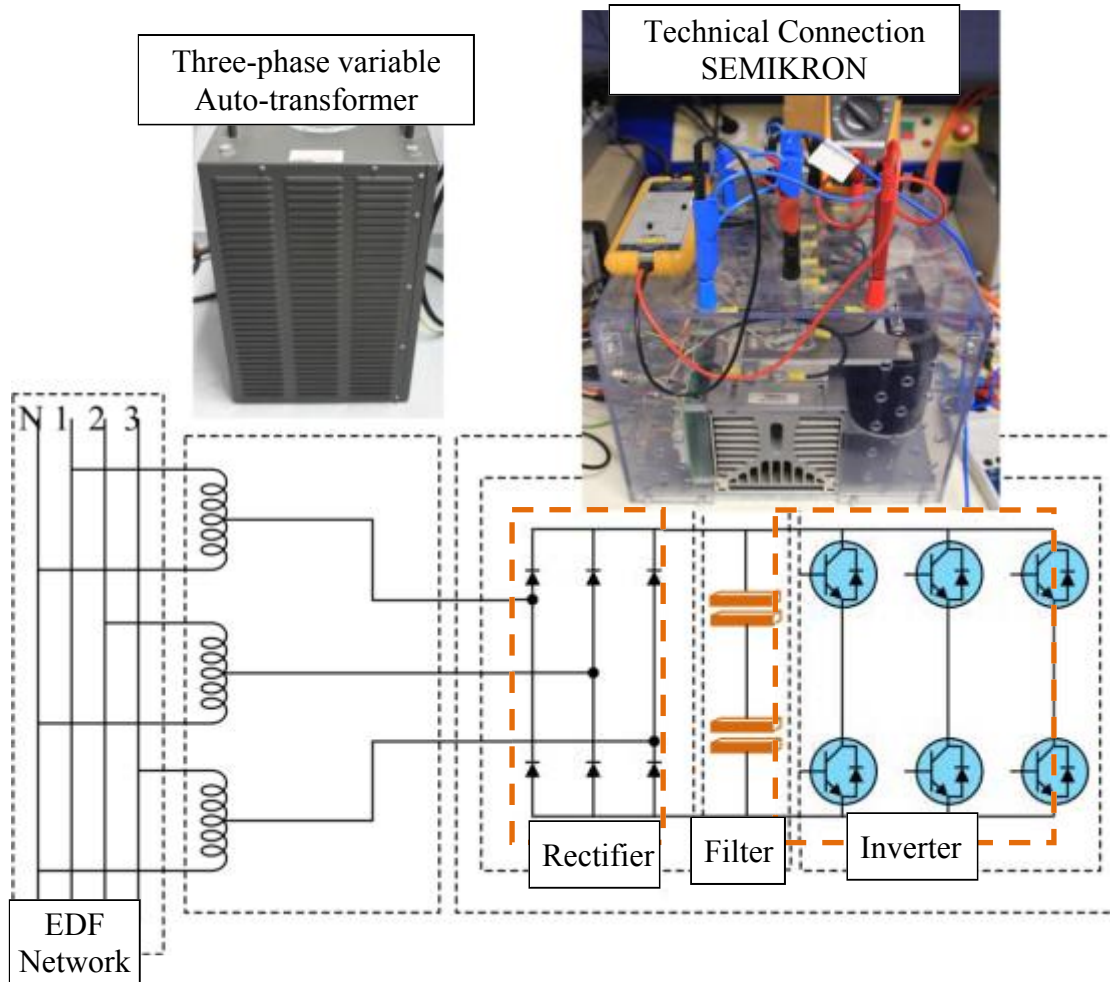


Figure 4.4: Power supply system

### 4.3.1 Power supply system

The power supplied by EDF network is three-phase,  $400V/50Hz$ . In order to adjust the value of the DC voltage ( $V_{DC}$ ) imposed by the continuous DC bus, and to avoid a sudden change of the voltage on the capacitors during the startup, a three-phase variable auto-transformer (400/450/20 AUTC of Automelec) is used. In this way, the voltage applied to the terminals of the rectifier can be adjusted. In addition, thanks to its inductive nature, the current returning to EDF network will be thus smoother.

The characteristics of the auto-transformer are given in Appendix 0.

### 4.3.2 Power converter

Adjustable three-phase voltage from transformer is imposed to a power converter of SEMIKRON, whose technical specifications are presented in Appendix B.2. A bridge rectifier will rectify the three-phase voltages. Two capacitors are also used to smooth the DC voltage.

A three-leg inverter is used to modulate the three-phase voltage whose amplitude and frequency are controlled. These voltages will drive the two PMSMs. The signals controlling the inverter are calculated and sent to each IGBT switch through an interface adapter. The SVM signals are generated under TTL technology (0-5V) by the control card and in order to control IGBTs it is necessary to use C-MOS technology (0-12V).

## 4.4 Measurement and control system

### 4.4.1 Measurement interfaces

#### 4.4.1.1 Current measurement

In order to measure the stator currents  $i_{a1}$ ,  $i_{b1}$ ,  $i_{a2}$  and  $i_{b2}$ , Hall effect sensors type LEM LA-25-P, whose datasheet is given in Appendix B.5.2, are connected to the analog inputs of the card. The neutral points of motors are not linked; the currents  $i_{c1}$  and  $i_{c2}$  which circulate in the third phase are obtained by the equation in (4.1)

$$i_c = -(i_a + i_b) \quad (4.1)$$

To compensate any offset value in the measurement process (due to sensors or CAN bus), a procedure for initializing the values of current to zero is carried out. Thus, while the electric power is not yet applied to the system, an average value of the current measurement is calculated through a large number of sampling periods. The four measured average values are then stored and the obtained offset values are then subtracted from the measured current.

In addition, as will be explained in the following paragraph, in the step of initialization, the absolute values of position of the two machines are measured.

#### 4.4.1.2 Mechanical position measurement

As described in Appendix B.3.3, the encoders associated with the resolvers on SM1 and SM2 create the signals  $V_{\cos 1}$  and  $V_{\sin 1}$  for SM1 and  $V_{\cos 2}$  and  $V_{\sin 2}$  for SM2. Two electronic cards analyze these signals in order to deduce the positions of two PMSM:  $\theta_{m1}$

and  $\theta_{m2}$ . These cards work mainly around the component AD2S1200 developed by Analog Devices [Ana03]. This is a complete 12-bit resolution tracking resolver-to-digital converter, integrating an on-board programmable sinusoidal oscillator that provides sine wave excitation for resolvers.

The system allows obtaining the values of  $\theta_{m1}$  and  $\theta_{m2}$  is represented through the scheme in Figure 4.5.

The measures of absolute positions  $\theta_{num}$  which are obtained by the resolvers are coded by 12 bits. However, the card DS1103 does not allow linking a 20-bit digital Input/Output. It is noted that the I/O is needed to activate the read of the AD2S1200 and also to capture the signals CLCK. Therefore, the two position  $\theta_{m1}$  and  $\theta_{m2}$  can not be read simultaneously.

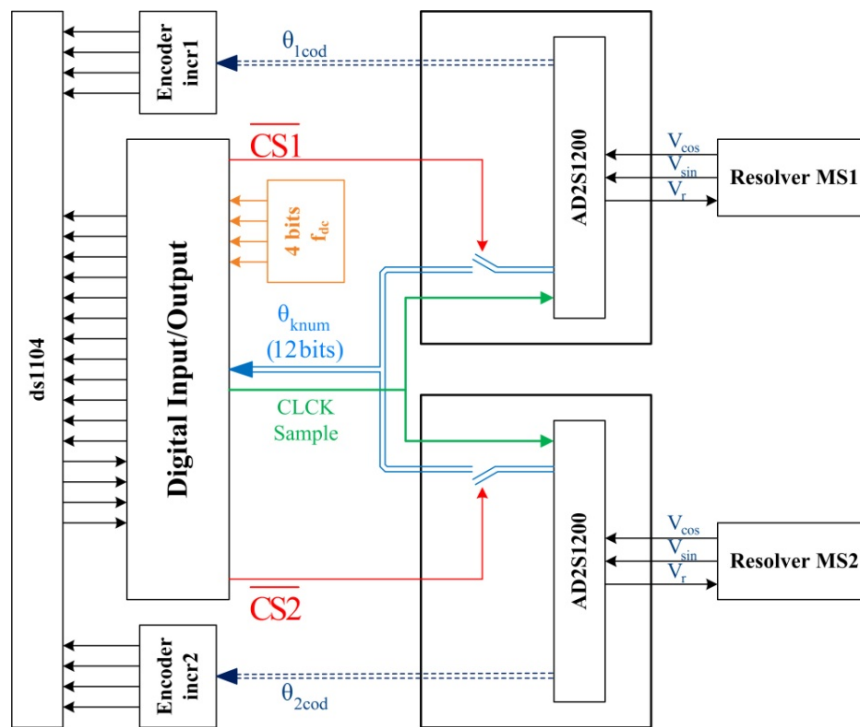


Figure 4.5: Reading of  $\theta_{m1}$  and  $\theta_{m2}$ : Hardware part

Each resolver card also creates an incremental encoder signal which gives the information allows to obtain the relative position of the motor  $\theta_{cod}$ , it is also encoded by 12 bits. Because the card DS1103 has two different interfaces to analyze these signals, the values  $\theta_{1cod}$  and  $\theta_{2cod}$  can be read in the same sampling period. This value is relative position because when powering up the system, the initial values recorded ( $\theta_{cod} = 0$ ) do not necessarily correspond to the actual position value. To obtain the actual values  $\theta_{m1}$  and

$\theta_{m2}$ , the inputs of these incremental encoders need to be initialized by the values  $\theta_{1num}$  and  $\theta_{2num}$ , read through the absolute position encoders.

In the next part, these positions of two motors will be used to calculate their speeds.

#### 4.4.1.3 Speed calculation

The rotational speeds of the two machines SM1 and SM2, respectively denoted as  $\omega_{m1}$  and  $\omega_{m2}$ , can be calculated from the position  $\theta_{m1}$  and  $\theta_{m2}$ .

$$\omega_m = \left. \frac{d\theta}{dt} \right|_{digital} \approx \frac{\Delta\theta}{t_{k+1} - t_k} = \frac{\Delta\theta}{T_s} \quad (4.2)$$

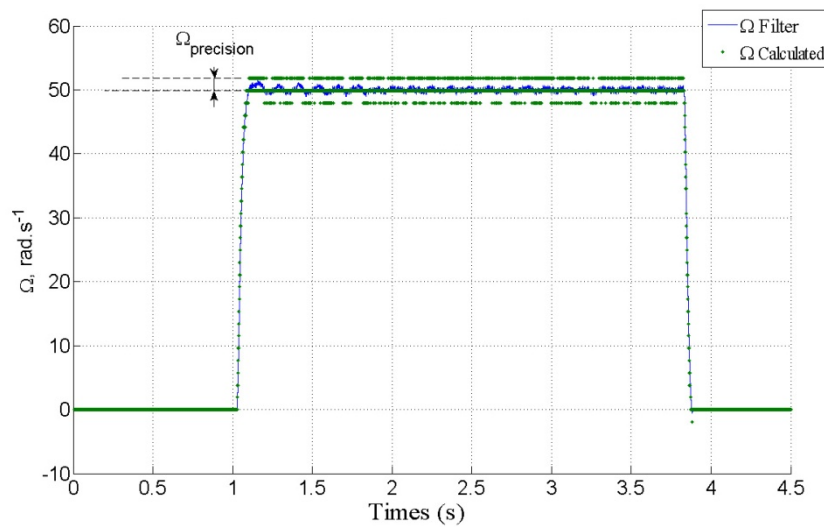


Figure 4.6: Example of filtering speed

In order to eliminate the residual oscillations in a magnitude  $\omega_m$ , a low-pass filter is added to speed calculation block.

$$L = \frac{1}{1 + \frac{s}{\omega_0}} \quad (4.3)$$

Presenting Laplace operator in Z-domain like:  $s = \frac{z-1}{T_e z+1}$  and using the bandpass frequency  $\omega_0 = 500(\text{rad/s})$ , we obtain:

$$L(z) = \frac{T_s \omega_0 (z+1)}{T_e \omega_0 (z+1) + 2(z-1)} = \frac{250(z+1)}{250(z+1) + (z-1)} \quad (4.4)$$

An example of the speed obtained with and without this filter at steady state  $\omega_{ref} = 50 \text{ rad. s}^{-1}$  is presented in Figure 4.6.

## 4.4.2 dSPACE system

dSPACE system is a tool used to build real-time control systems. It is used to connect different kind of signals (analogue or digital) that measurement devices obtain to a computer, as well as send signals from the computer to the device in order to control them.

dSPACE system is an interface between the physical world (motors, inverter, measure sensors ...) and the computer, from where the lab tests is controlled and the results are displayed. dSPACE system model used in this thesis is CP1103 system with different analogue I/O and digital I/O.

Controllers have to be programmed and then, by means of the analogue and digital I/O, command signals are sent to the system and measured values are received.

### 4.4.2.1 dSPACE DS1103 board

Real-time simulation hardware DS1103 is based on power PC microprocessor supplemented by Texas Instruments TMS320F240 DSP processor. The TMS320F240 slave DSP is loaded with firmware that allows access to the different peripheral devices of the slave DSP. Functions needed for motor control (SPI, PWM or SVM) are already pre-defined in slave DSP so there was no need to compile custom code.

Programs for master power PC can be compiled directly from the C-code using RTI library containing the functions provided by the DS1103 processor or Simulink Real-Time Workshop. Besides the PWM/SVM module and SPI interface provided by slave processor, the encoder interface and A/D modules which are controlled by master power PC are used for closed loop motor control to measure the rotor position and stator currents.

Detailed technical specifications of dSPACE DS1103 are described in Appendix B.5.1 [dSP03]

### 4.4.2.2 MATLAB/Simulink and Control-desk

The dSPACE programming has been carried out using MATLAB/Simulink. The model is equal to the one used in chapter 3 for the simulation with the exception of some modifications:

- A measurement block is added for receiving the DC voltage, currents and positions. In this block, the initialization procedure is also done;

- The model of the inverter and two PMSM is removed. They are replaced by the real inverter and motor coupling system;
- The SVM block is changed for the SVM three-phase generation included in the RTI library in Simulink;
- The controller blocks remain in the system.

The system has been organized in two main parts: measurements and controller. The measurement block needs to be synchronized by a PWM interrupt block. The interrupt signal will be generated at the middle of a modulation period. With a SVM symmetric, middle point of a modulation period will be zero voltage vector. There is no state switch in any IGBT as well as the state of system is the most stable. Therefore, the measurement will give the most exactly values.

This process is illustrated in Figure 4.7.

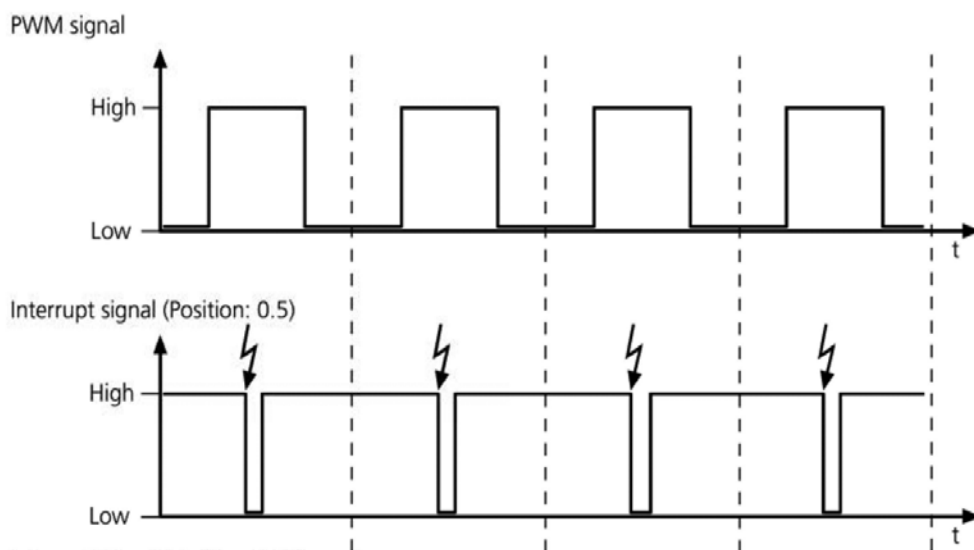


Figure 4.7: Interrupt signal

After all the programming is compiled and downloaded to dSPACE card, a Control-Desk interface software program provides all the necessary functions for control, data acquisition and modification of the parameters of Simulink blocks in real time.

## 4.5 Digital control implementation

The used Simulink structure comprises several tasks:

- + Performing the measurement of variables (currents, positions ...) and calculates the speeds of the two machines;
- + Regulating these parameters in order to achieves the autopilot of the two machines.

In this section, the command structure used for the control of the variables of both PMSMs and the parameters selected for the numerical control are presented.

### 4.5.1 Speed controller

The speed controller as presented in previous chapter is RST type. In this thesis, anti-windup function is also added to the controller. The parameters of this type of controller are calculated base on the model of object in Z-domain.

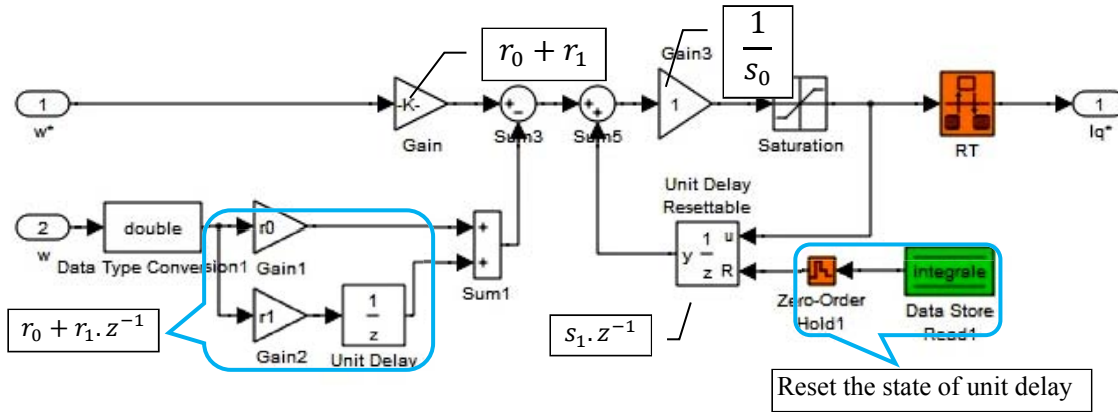


Figure 4.8: RST controller block with anti-windup

During initialization process, the unit delay block always takes a saturation value from a saturation block. Therefore, it is necessary to reset the state of this block at each starting time to zero (Figure 4.8).

The parameters of this controller are summarized in Table 4.1

### 4.5.2 Predictive torque controller

In this work, PTC-SS algorithm has been verified in the real system. The controller will update the measured variables (currents, positions ...) to apply to the discrete model of mono-inverter dual-parallel PMSMs, to calculate the evolution of system in the next sampling period. Besides, the two references from the two RST speed controllers are also used to build the cost function.

In addition, to meet the requirement of fast response, the sampling time used for this controller is set up at  $T_{tc} = 10^{-4}s$ . It is about twenty times faster compared with the electrical time constant of the motor:

$$\tau_e = \frac{L_s}{R_s} \approx 1.8 \times 10^{-3}(s) \quad (4.5)$$

Parameters	Value
Sampling time $T_{sc}$	$10^{-3}(s)$
Damper factor $\xi$	0.95
Natural frequency $\omega_n$	$120(rad. s^{-1})$
$s_0$	1
$s_1$	1
$r_0$	0.04
$r_1$	-0.0376

Table 4.1: Parameters of speed controller

The core of this controller is an S-function. This function will carry out the ‘‘Split & Seek’’ strategy to optimize the cost function to find the suitable voltage vector for the operation of two machines. According to this S-function, six basic vectors ( $V_{1...6}$ ) placed at  $\pi/3$  intervals in space vector will be considered first. Next, a group of ten virtual vectors placed at  $\pi/18$  intervals around the chosen basic vector will be created and tested.

In this experiment, the DC voltage is set up at value  $V_{DC} = 50V$ . The maximum voltage which can be modulated by SVM technique is:

$$V_{max} = \frac{V_{DC}}{\sqrt{3}} = \frac{50}{\sqrt{3}} \approx 29(V) \quad (4.6)$$

Therefore, the amplitude of the steady voltage vectors will be discrete with the PTC-SS algorithm, and set to a 5V step from 0 to  $V_{max}$ .

## 4.6 Experiment's results

### 4.6.1 Test with one machine

In a first time, PTC-SS will be verified with one PMSM. The used machine here is SM1, since it is possible to vary its load.

Diagram of control drive is shown in Figure 4.9.

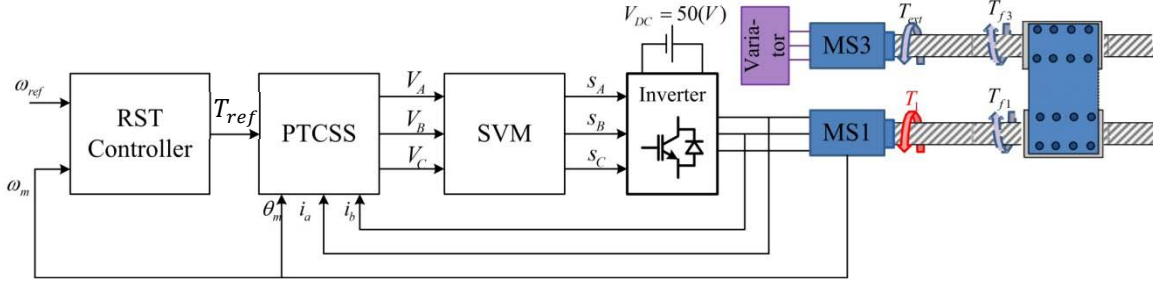


Figure 4.9: PTC-SS applied to one PMSM

In this test, the profile of load torque generated from SM3 is set up as follows:

- From  $t = 0(s) \rightarrow t = 1.5(s)$  and  $t = 9.0(s) \rightarrow t = 10(s)$ : load torque is set at zero. It means that total load applied to SM1 is  $T_{total} = T_{f1} + T_{f3}$ ;
- From  $t = 1.5(s) \rightarrow t = 3.0(s)$ : load is set at  $T_{ext} = 0.1Nm$ . So, the total load will be decreased:  $T_{total} = T_{f1} + T_{f3} - T_{ext}$ ;
- From  $t = 3.0(s) \rightarrow t = 5.0(s)$ : load is set at  $T_{ext} = -0.1Nm$ . So, the total load will be  $T_{total} = T_{f1} + T_{f3} + |T_{ext}|$ ;
- From  $t = 5.0(s) \rightarrow t = 6.5(s)$ : load is set at  $T_{ext} = -0.1Nm$ , however, the motor is reversed. So, the total load will be  $T_{total} = -(T_{f1} + T_{f3} - |T_{ext}|)$ . The absolute value of load is the same with (b);
- From  $t = 6.5(s) \rightarrow t = 9.0(s)$ : load is set at  $T_{ext} = 0.1Nm$ , however, the motor is reversed. So, the total load will have absolute value as in (c);
- From  $t = 9.0(s) \rightarrow 10.0(s)$ : load torque is equal to zero. The total load is the same as (a)

This profile is illustrated in Figure 4.10.

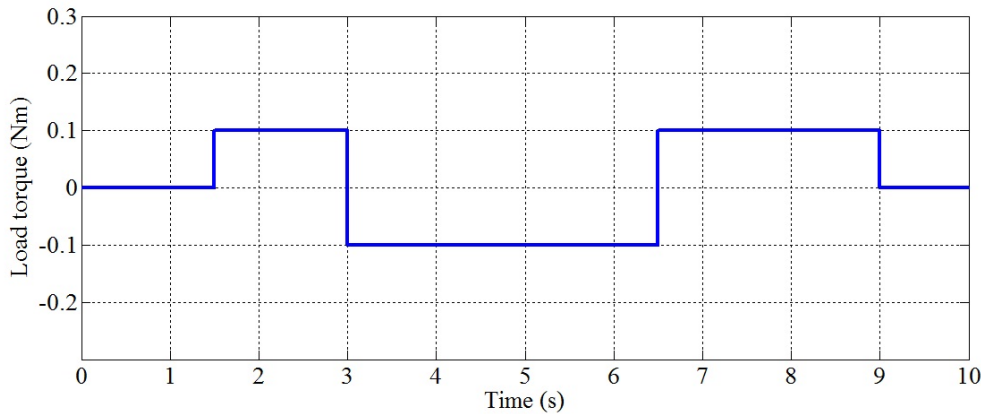


Figure 4.10: Variation of load during the test

The value of torque is updated by user through a human-machine interface to dSPACE. Control signal then will be sent to a variable speed drive which controls the torque of SM3.

Speed response of motor is presented in Figure 4.11. This result shows that the motor follows the set-point and also satisfies the change of set-point. When motor goes to the end of the first half of road, it is reversed. Because of design of the system, the motor operates like starting. We can see the same phenomenon happened at two moments: the starting and at  $t = 5(s)$ .

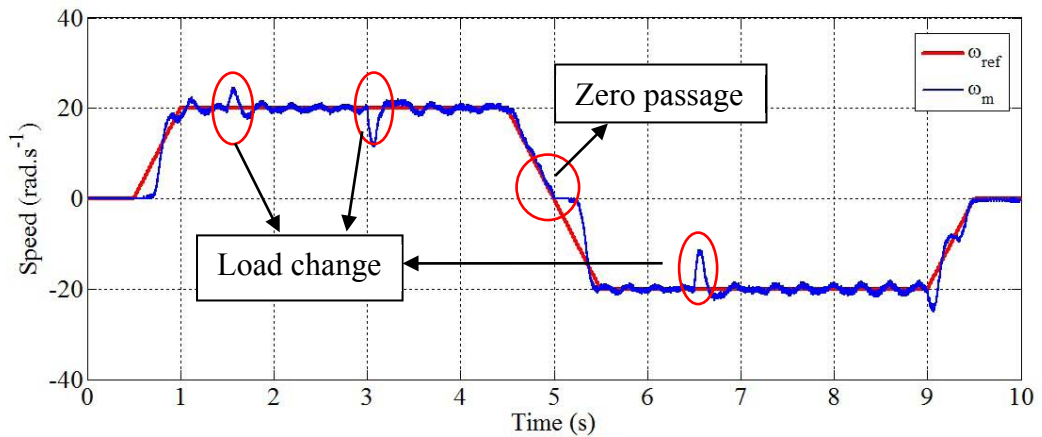


Figure 4.11: Speed response of PMSM

There are some peaks in speed of motor during the test. It is because of the change in load applied to the machine. Besides, it can be seen that under variation of load, system is still stable. Steady state is reestablished in a short time ( $\sim 0.2s$ ).

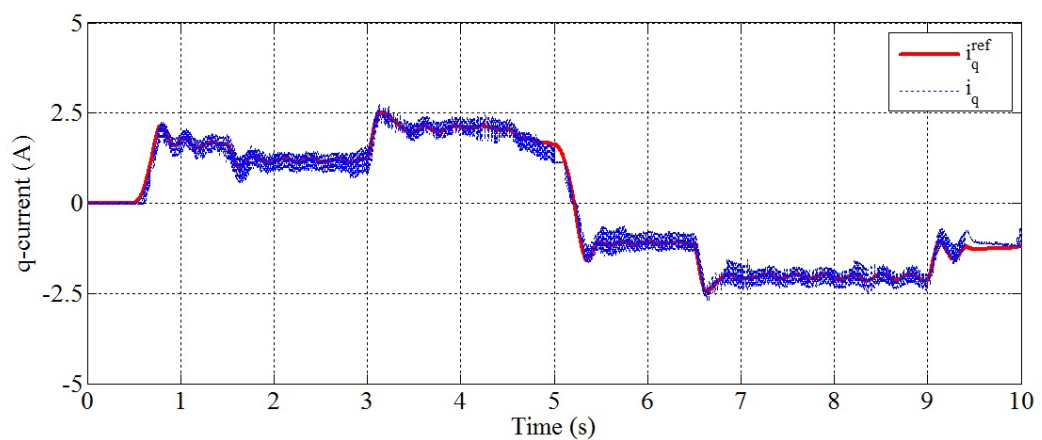


Figure 4.12: Current in q-axis

In Figure 4.12, current of PMSM in q-axis  $i_{sq}$  and its reference value  $i_{sq}^{ref}$  are plotted. With considered PMSM, this current is proportional directly with electromagnetic torque. It can be seen that under the changes of set-point as well as the variation of load, the value of  $i_{sq}$  follows its reference accurately.

In Figure 4.13, the d-current  $i_{sd}$  of PMSM is shown. Its value oscillates around zero. The amplitude of ripple is around 0.4A.

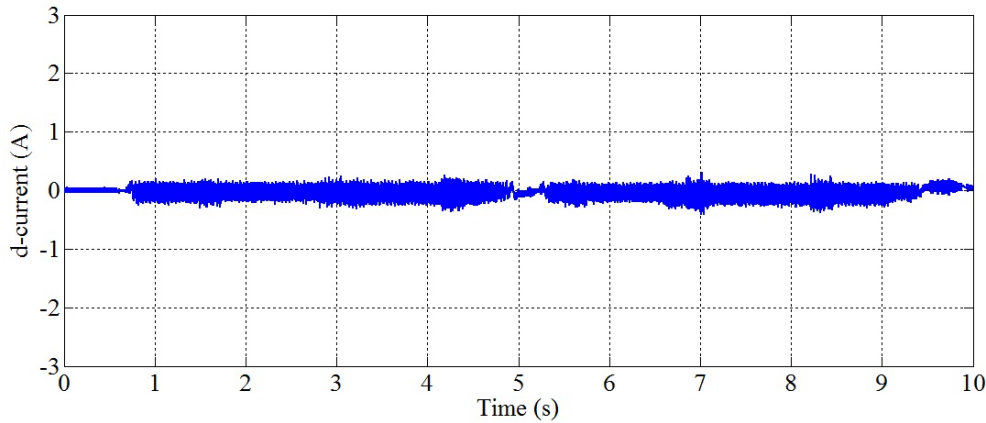


Figure 4.13: Current in d-axis

It is clear that the predictive controller operates quite well with PTC-SS algorithm for only one machine. The cost function considers two criteria  $i_{sd}$  and  $i_{sq}$  as follows:

$$g = \left( i_{sq}^{ref} - i_{sq}(k+1) \right)^2 + \left( i_{sd}(k+1) \right)^2 \quad (4.7)$$

As results, both components are well controlled. Next, the test thus will be continued with two machines in parallel.

#### 4.6.2 Test with two machines in parallel

In this test, information of both machines is considered in only one cost function:

$$g = \left( i_{sq1}^{ref} - i_{sq1}(k+1) \right)^2 + \left( i_{sq2}^{ref} - i_{sq2}(k+1) \right)^2 + \left( i_{sd1}(k+1) \right)^2 + \left( i_{sd2}(k+1) \right)^2 \quad (4.8)$$

Position and phase-currents of two PMSMs are updated to PTC-SS control block every sampling time. These variables will be used to predict the evolution of both machines in the next period. Diagram of control drive is shown Figure 4.14.

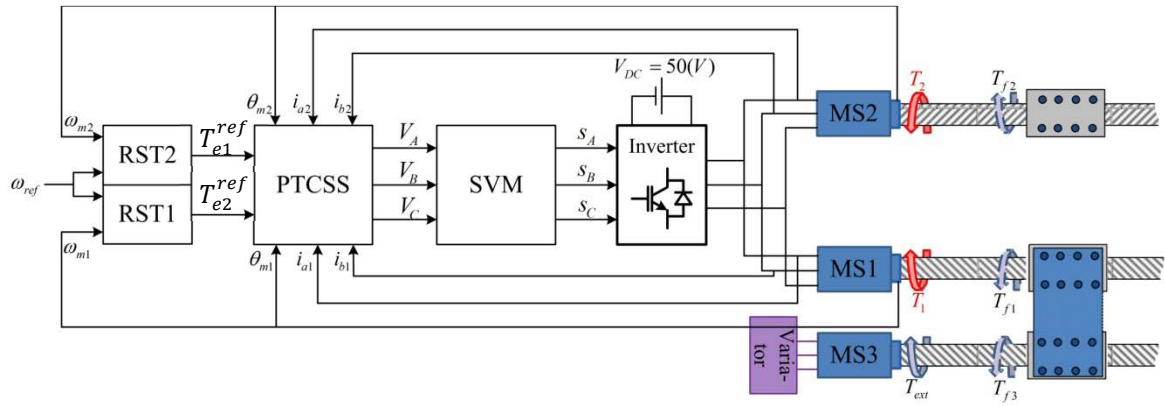


Figure 4.14: PTC-SS with two PMSMs

From Figure 4.14, the load applied to SM2 is  $T_{f2}$  while the load applied to SM1 is  $T_{f1} + T_{f3}$ . In this test, torque from SM3 is set equal to zero ( $T_{ext} \approx 0Nm$ ). Therefore, loads between two machines are always slightly different. The test is carried out under the same set-point  $\omega_{ref} = 20(rad.s^{-1})$ . Two machines will be reversed at  $t = 5s$ .

The speed response is presented in Figure 4.15. According to this, the speed of both PMSMs follows the reference. Response during transient time is not really good. There are some overshoots during this period of time. Although there is also the oscillation, the steady state is still obtained.

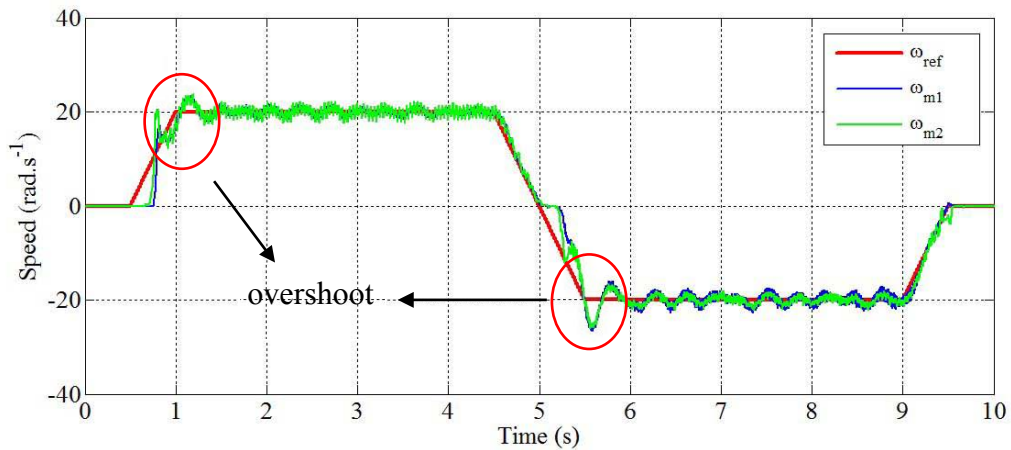


Figure 4.15: Speed response of two PMSMs

In Figure 4.16, q-current of both machines and its reference are shown. There is a difference between the real value from the motor and reference value. Theoretically, q-current determines the torque of the machine and so the speed indirectly. In this case, the real value is not equal to reference but the speed of two machines still comes to the set-

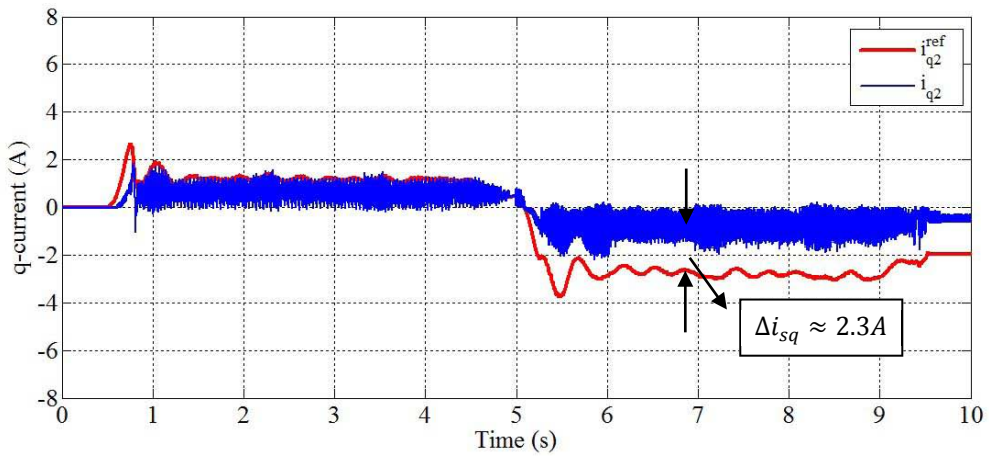
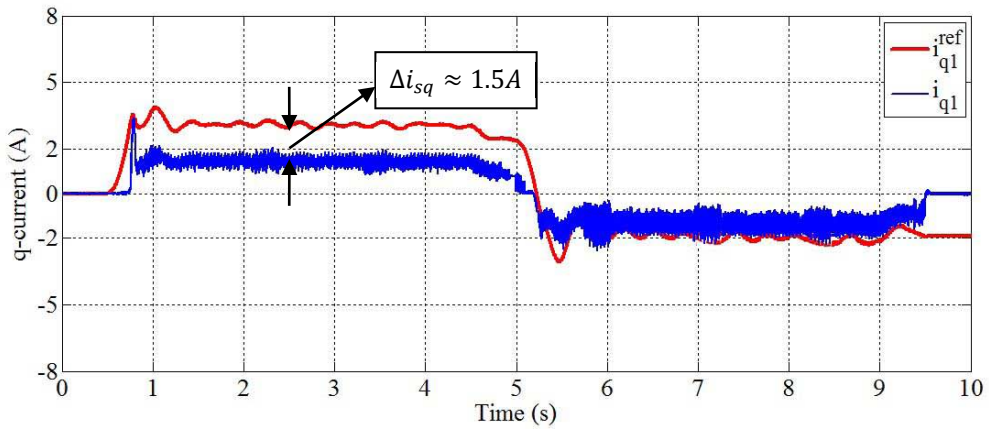


Figure 4.16: Current in q-axis of both machines

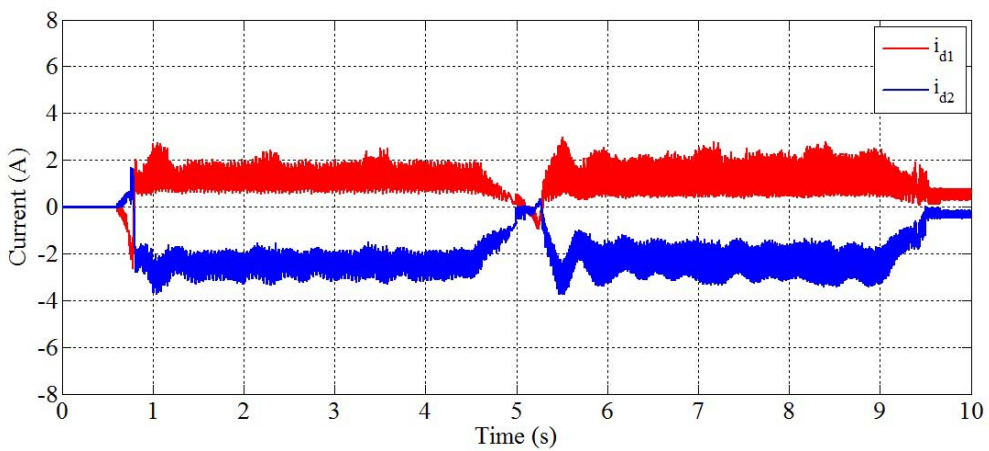


Figure 4.17: Current in d-axis of both machines

point. It can be explained by considering the current in d-axis of both machines from Figure 4.17. Both d-currents are different from zero. This fact allows the machines come to the speed reference.

Results presented in Figure 4.16 and Figure 4.17 show the limitations of the PTC-SS method. Since both machines are considered in the cost function that means the optimal voltage vector found by the algorithm should satisfy the requirements of both machines. This is, in general case, difficult, since requirements can be different due to the different load torque applied to the machines. This is showed by the fact that the cost function is minimized but not equal to zero.

The optimal vector found by the algorithm will be then a compromise of requirements of both machines. This will lead to d-currents different from zero (reference value) and q-current with values corresponding to the values which will allow providing the correct torque.

In fact, when considering the information of both machines, it is sure that the amount of computation will be increased considerable compared with the case of only one machine. This is a really problem with real time application. Therefore, PTC-SS will be tested with master/slave structure.

### 4.6.3 Test with two machines in parallel under master/slave configuration

In this test, master/slave structure is reused but instead of using classical PI controller, predictive controller with “Split and Seek” algorithm is applied. Diagram of control drive is shown in Figure 4.18.

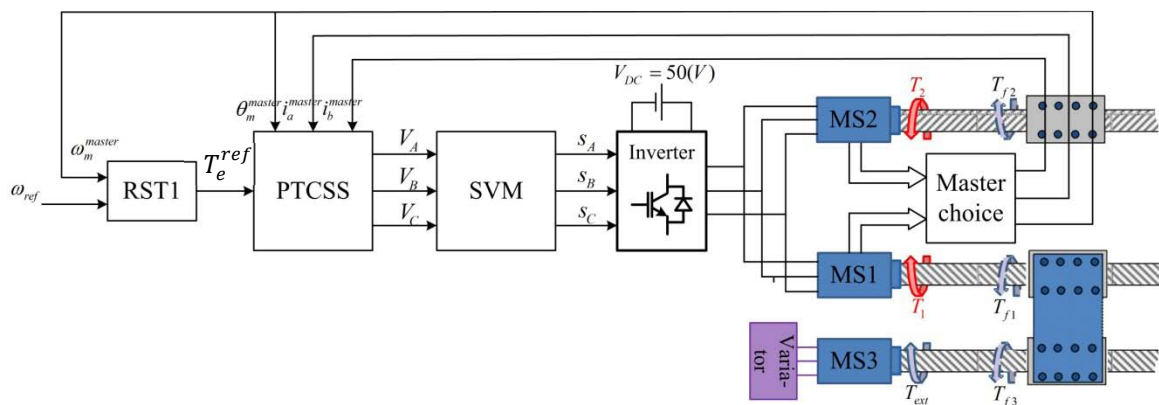


Figure 4.18: PTC-SS with two PMSMs under master/slave

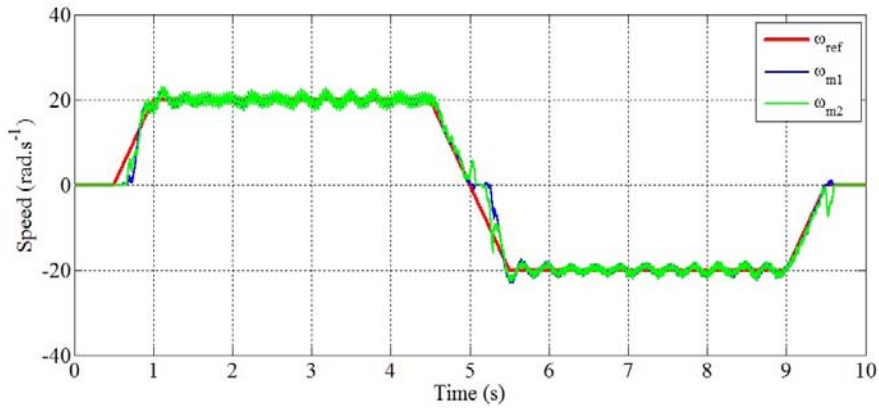


Figure 4.19: Speed response of two PMSMs under master/slave configuration

According to this structure, there is always just one machine controlled at a moment. Therefore, the amount of computation will be the same with the case of one machine and will be smaller than that in the case of both machines.

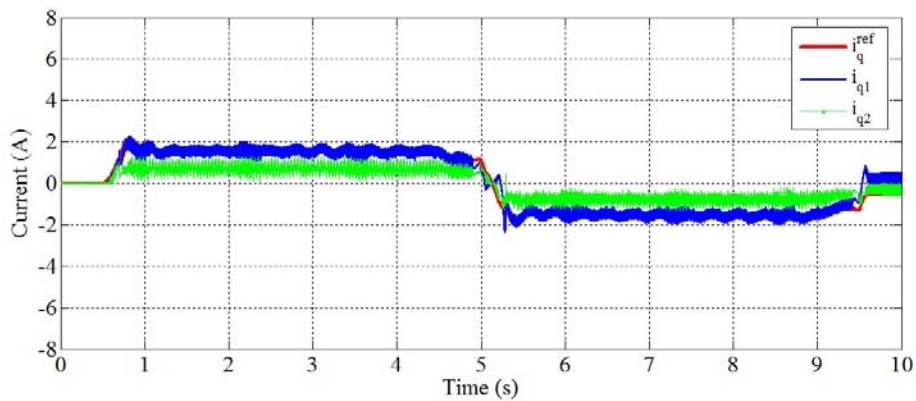


Figure 4.20: Current in q-axis of both machines

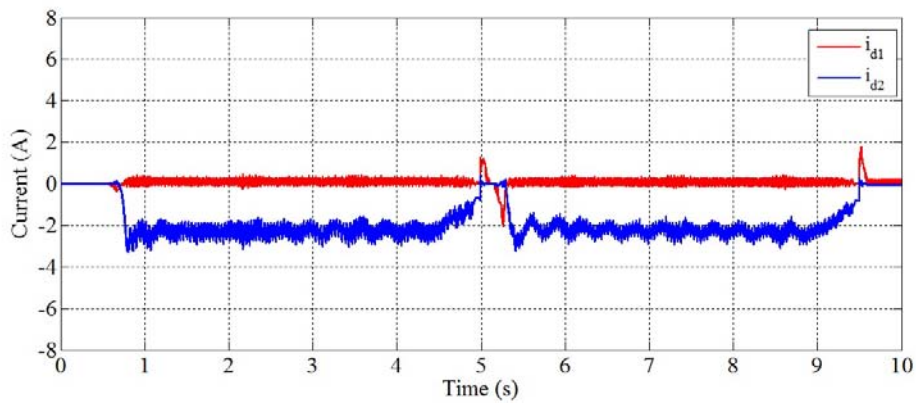


Figure 4.21: Current in d-axis of both machines

In this test, the load condition is the same as in previous test. Therefore, the first machine SM1 always has heavier load. It will be then chosen as master machine and its requirements will be considered in the cost function.

In Figure 4.19, speed response of two PMSMs and reference value are plotted.

According to Figure 4.19, the speed response of both machines is better with no overshoot during the transient time ( $<5\%$  set-point). However, the oscillation still exists at steady state. It might be a result of using discrete control signal in control algorithm.

The dq-currents of both machines are represented in Figure 4.20 and Figure 4.21. Because of being the master one and controlled, the responses of SM2 is quite good. We can see that q-current of SM1 always follows the reference; meanwhile, its d-current is kept close to zero.

However, unlike the SM1, the slave machine (SM2) does not follow the references. The d-current value is different from zero.

## 4.7 Conclusions

In this chapter, predictive control with “Split and Seek” algorithm has been verified with a real experimental bench under three tests:

- Control one PMSM;
- Control two PMSMs in parallel;
- Control two PMSMs in parallel under master/slave configuration.

From the obtained results, some conclusions can be pointed out:

- The oscillation and ripple always exist because of the controller just considered the limit number of discrete control signal. However, in all test, steady state of whole system is obtained.
- In the drive system with one PMSM, PTC-SS give us the interesting results. The system responses very fast (response time  $\approx 0.05s$ ) under the changes of exterior conditions such as set point or loads. It is also stable with the vary of load. The steady state will be reestablished after  $\approx 0.05s$ ;
- For a test with both machines (no master/slave configuration), the system also can obtain desired steady state. However, the performance is just acceptable. In fact, a large amount of computation affected to the quality of system. Besides, it is also difficult to guaranty the stability of the system if the loads of two machines are much different.

- Considering PTC-SS with master/slave structure, there are some advantages. The amount of computation is reduced considerably. Besides, the stability of system can be assured based on the choice of master machine.

In conclusion, the initial results show that predictive control strategy can be developed and adapts to this drive system.

## Conclusions and Perspectives

The principle objective of this thesis is applying predictive control strategy to a drive system which consists of two permanent magnet synchronous machines (PMSM) connecting in parallel with a three-phase two-level inverter.

Related to the control of multi PMSM system, in Chapter 1, the evolution of PMSM with multi-machine systems, especially in aeronautic fields, was presented. Several structures of multi-machine systems has been introduced and compared. Among them, the parallel structure composed of one inverter and several PMSMs showed many advantages. This structure thus is selected to be studied in this thesis.

In chapter 2, the mathematic model of PMSM, stability analyses as well as studies about the response of PMSM under voltage supplying mode are considered in detailed. Typical control methods for this kind of drive system are also introduced. Moreover, some works in the literature with a mono-inverter dual-parallel PMSM were introduced. A control structure which uses Master/Slave configuration gave us a very good performance for the master machine. Besides, thanks to the master-choice technique, the stability of the slave machine is also guaranteed.

Another approach is applying Direct Torque Control strategy to this system. With this method, a new optimal look up table is built in order to meet the requirements of both machines, even in the case of different load.

Model Predictive Control (MPC) theory has been used in many field of science. Recently, this control method also applied more and more in variable speed applications where power electronic devices are used a lot. It gradually becomes competitive to the well known controls as: Field Oriented Control (FOC), Direct Torque Control (DTC). Therefore, in Chapter 3, Predictive Control strategy is paid attention to apply to the mono-inverter dual-parallel PMSM drive system.

In this thesis, the author has concentrated on Finite Set Model Predictive Control (FS-MPC), which meets very well discrete nature of power converters. In view of switching frequency, the FS-MPC methods are considered in two approaches:

- Variable Switching Frequency (VSF) – Section 3.4: Direct Predictive Torque Control (DPTC);
- Constant Switching Frequency (CSF) – Section 3.5: Predictive Torque Control – “Split and Seek” (PTC-SS).

Both approaches are described in detail in Chapter 3 of this thesis. Several theoretical analyses and simulation results have been carried out in order to verify the effect of each approach. In general, they give the satisfactory results which prove the capability of controlling our kind of drive system with predictive control. Taking into consideration advantages of constant switching frequency for converter operation, approach with the use of Virtual Voltage Vector in PTC-SS has shown some advantages compare with DPTC:

- lower line current THD factor;
- requiring lower sampling frequency (as DPTC with the same performance);

Therefore, this approach is chosen to test with a real drive system in Chapter 4. The first experiment results also show that the drive system can operate with this method. However, these results are not really as good as in simulation. It is reasonable because there are many conditions which are idealized in simulation such as: no computation time, all responses are immediately, no error in computation, no noise ... Therefore, it is necessary to have more studies to improve the performance of the system.

In the author's opinion, although the obtained results are not as well as desired, PTC-SS is still a new approach for predictive control strategy.

- First, it is necessary to find solutions in order to optimize the research of the best voltage vector as well as improving the calculation time. It is possible using a dynamic step size in angle and magnitude instead of using the fixed steps as in Section 3.5. It can be carried out based on the following principle: when the system is far from the steady state, the step needs to be large in order to cover all the space vector. When the system is close to the steady state, the step will be small to narrow the range of consideration. As results, the voltage vector will get the more exact value;
- Moreover, with two machines, when considering the states of both machines, the computational efforts show the bad effect to performance of the system. When the number of machines is increased more, it really becomes a serious problem. Besides, the issues of including the criteria of each machine will make the cost

---

function become complex and bulky. Sometimes, a criterion may be not suitable or does not play any role in control problem. Therefore, it is necessary to extend this work to control more than two machines.



## Bibliography

- [ABRA02] S. Arnalte, J. Burgos, and J. Rodriguez-Amenedo. Direct torque control of a double fed induction generator for variable speed wind turbines. In *Electric Power Component and Systems*, volume 30, February 2002.
- [AF09] A. Abdelhafez and A. Forsyth. A Review of More-Electric Aircraft. *International Conference on Aerospace Sciences and Aviation Technology*, May 2009.
- [AGV07] AGV technical document in the site internet Alstom Transport. *AGV Performance et modularité*, June 2007.
- [All95] S. Allano. *Petits moteurs électrique*. Techniques de l'ingénieur, Génie électrique, D 3720, 1995.
- [Ana03] Analog Device. *AD2S1200 12 -Bit R /D C onverter with Reference Oscillator*, Datasheet of A2DS1200 edition, 2003.
- [APIS08] M. S. D. Acampa, D. Pizzo, A. Iannuzzi, and D. Spina. Predictive control technique of single inverter dual motor AC-brushless drives. In *18th International IEEE Conference on Electrical Machines*, pages 1 – 6, September 2008.
- [BBPDdF06] J. Belhadj, I. Belkhdja, M. Pietrzak-David, and B. de Fornel. Direct torque control with an optimized observer for multi-machine systems. *The European Physical Journal Applied Physics*, 33 (1):22–33, 2006.
- [Ber02] F. Bernot. *Alternateurs synchrones de grande puissance (partie 1)*. Technique de l'ingénieur d3550 edition, 2002.
- [Bid11] D. Bidart. *Commande coopérative de systèmes monoconvertisseurs multimachines synchrones*. PhD thesis, National Polytechnic Institute of Toulouse, June 2011.
- [BMAA11] J. W. Bennett, B. C. Mecrow, D. J. Atkinson, and G. J. Atkinson. Safety aircraft design of electromechanical actuation systems in commercial aircraft. *IET Electric Power Application*, 5 (1):37 – 47, January 2011.

- [Bor81] C. Bortoulussi. *Étude des interefforts. Modification des comportement de liaison*, November 1981.
- [Bou95] A. Bouscayrol. *Structures d'alimentation et stratégies de commande pour des systèmes multimachines à synchrones. Application à la motorisation d'un robot mobile*. PhD thesis, National Polytechnic Institute of Toulouse, 1995.
- [BPDD<sup>+</sup>06] A. Bouscayrol, M. Pietrzak-David, P. Delarue, R. Pena-Eguiluz, and X. K. P. E. Vidal. Weighted control of traction drives with parallel connected AC machines. *IEEE Transactions of Industrial Electronics*, 53(6):1799–1806, December 2006.
- [BPDdF96] A. Bouscayrol, M. Pietrzak-David, and B. de Fornel. Comparative studies of inverter structures for a mobile robot asynchrone motorisation. *IEEE International Symposium on Industrial Electronics*, 1: 447–452, 1996.
- [BPDFM09] D. Bidart, M. Pietrzak-David, M. Fadel, and P. Maussion. Stratégie de contrôle d'un système bi machines synchrone monoconvertisseur: connection en parallèle sur un onduleur mutualisé. In *Colloque Electrotechnique du futur, UTC Compiègne*, 2009.
- [BPDFM08] D. Bidart, M. Pietrzak-David, P. Maussion, and M. Fadel. Mono inverter dual parallel PMSM - structure and control strategy. In *34th Annual Conference of IEEE on Industrial Electronics*, pages 268 – 273, November 2008.
- [BT93] D. Briere and P. Traverse. Airbus A 320/A330/A340 electric flight controls - A family of fault-tolerant systems. In *Proceedings of 23rd International Symposium on Fault-Tolerant Computing*, pages 616–623, Toulouse, France, June 1993.
- [CB04] E. F. Camacho and C. Bordons. *Model Predictive Control*. Springer London Limited, 2004.
- [CB07] E. Camacho and C. Bordons. *Model Predictive Control*. Springer-Verlag, 2007.
- [Cha03] S. Charlemagne. *Modélisation et commande d'un système de transport de bande textile, Application des concepts multimachines*. PhD thesis, Lille University of Science and Technology, 2003.
- [CMA<sup>+</sup>12] W. Cao, B. C. Mcrow, G. J. Atkinson, J. W. Bennet, and D. J. Atkinson. Overview of Electric Motor Technologies Used for More Electric Aircraft (MEA). *IEEE Transactions on Industrial Electronics*, 59(9):3523 – 3531, September 2012.

- [CPR07] P. Correa, M. Pacas, and J. Rodriguez. Predictive Torque Control for Inverter-Fed Induction Machines. *IEEE Transactions on Industrial Electronics*, 54(2):1073 – 1079, April 2007.
- [CSSS02] J. Chiasson, D. Seto, F. Sun, and A. Stankovic. Independent control of two pm motors using a single inverter: application to elevator doors. In *IEEE American Control Conference*, pages 3093–3098, 2002.
- [Del08] A. Delehelle. *Étude d'un concept innovant d'actionneur électromécanique linéaire à effets magnétique et piézoélectrique en vue d'applications dans le domaine de la commande de vol*. PhD thesis, Toulouse University, 2008.
- [Dep88] M. Depenbrock. Direct self-control (dsc) of inverter-fed induction machine. In *IEEE Transactions on Power Electronics*, volume 3, pages 420 – 429, October 1988.
- [DJVL09] D. Dujic, M. Jones, S. Vukosavic, and E. Levi. A General PWM Method for a (2n+1)-Leg Inverter Supplying n Three-Phase Machines. *IEEE Transactions on Industrial Electronics*, 56 (10):4107–4118, October 2009.
- [dSP03] dSPACE. *DS1103 PPC Controller Board*, 2003.
- [FBM<sup>+</sup>07] E. Foch, G. Bisson, P. Maussion, M. Pietrzak-David, and M. Fadel. Power system comprising several synchronous machines synchronously self controlled by a converter and control method for such a system, November 2007.
- [Fes] Festo. *Axe à vis à billes électrique DGE-SP*, Product short information provenant du site de festo: [www.festo.com](http://www.festo.com) edition.
- [FNL13] M. Fadel, L. Nguyen, and A. Llor. Direct Torque Control - A Solution for Mono Inverter - Dual Parallel PMSM System. In *21st Mediterranean Conference on Control and Automation*, 25-27 June 2013 (Publication in progress).
- [FOM07] A. Furuya, K. Oka, and K. Matsuse. A characteristic analysis of four-leg inverter in two ac motor drives with independent vector control. In *International Conference on Electrical Machines and Systems*, pages 619–624, October 2007.
- [GBPM10] T. Geyer, G. Beccuti, G. Papafotiou, and M. Morari. Model Predictive Direct Torque Control of permanent magnet synchronous motors. In *IEEE Conference on Energy Conversion Congress and Exposition*, pages 199 – 206, September 2010.

- [HS83] J. Holtz and S. Stadtfeldt. A predictive control for the stator current vector of ac machines fed from a switched voltage source. In *International Power Electronics Conference IPEC*, volume 2, pages 1665 – 1675, 1983.
- [IGL<sup>+</sup>08] M. Iftikhar, E. Godoy, P. Lefranc, D. Sadarnac, and C. Karimi. A Control Strategy to Stabilize PWM DC-DC Converters with Input Filter Using State-Feedback and Pole-Placement. In *In Proceeding of INTELEC 2008*, pages San Diego, USA, September 2008.
- [Jon99] R. Jones. The More Electric Aircraft: the past and the future? In *IEEE Colloquium on Electrical Machines and Systems for the More Electric Aircraft*, pages 1 – 4, 1999.
- [JVD<sup>+</sup>08] M. Jones, S. Vukosavic, D. Dujic, E. Levi, and P. Wright. Five-leg inverter PWM technique for reduced switch count two-motor constant power applications. *IET Electric Power Application*, 2( 5):257–287, September 2008.
- [Kem89] R. Kemp. Developments in electric traction. *Power engineering journal*, March 1989.
- [KFM00] Y. Kono, T. Fushimi, and K. Matsuse. Speed sensorless vector control of parallel connected induction motors. In *3rd International Conference on Power Electronics and Motion Control*, volume 1, pages 278–283, 2000.
- [KRET10] R. Kennel, J. Rodriguez, J. Espinoza, and M. Trincado. High performance speed control methods for electrical machines: An Assessment. In *2010 IEEE International Conference on Industrial Technology (ICIT)*, pages 1793 – 1799, March 2010.
- [Kri01] R. Krishnan. *Electric Motor Drives - Modeling, Analysis, and Control*. Prentice Hall, 2001.
- [KS83] R. Kennel and D. Schoder. A predictive control strategy for converters. In *3rd IPAC Symposium*, pages 415 – 422, 1983.
- [Lan98] I. Landau. The R-S-T digital controller design and applications. *Control Engineering Practice* 6, pages 155 – 165, 1998.
- [LD12] J. Lemmens and J. Driesen. Synchronization and efficiency analysis of a direct-drive multi-motor application. In *6th IET International Conference on Power Electronics, Machines and Drives*, pages 1–6, March 2012.
- [Leo01] W. Leonhard. *Control of Electrical Drives*. Springer, Third edition, 2001.

- [LKKS10] A. Linder, R. Kanchan, R. Kennel, and P. Stolze. *Model-Based Predictive Control of Electrical Drives*. Cuvillier Verlag Göttingen, 2010.
- [Llo03] A. Llor. *Commande directe de couple à fréquence de modulation constante des moteurs synchrones à aimants permanents*. PhD thesis, Research Laboratory: CEGELY - INSA - Lyon, April 2003.
- [LZ06] I. D. Landau and G. Zito. *Digital Control Systems - Design, Identification and Implementation*. Springer-Verlag London Limited, 2006.
- [MAR05] S. Müller, U. Ammann, and S. Rees. New time-discrete modulation scheme for matrix converters. *IEEE Transactions on Industrial Electronics*, 52(6):1607 – 1615, December 2005.
- [MD11] T. Maeda and S. Doki. Improvement of torque control system of PMSM based on model predictive control. In *37th Annual Conference on IEEE Industrial Electronics Society*, pages 1891 – 1896, November 2011.
- [MGSL09] S. Ménio, S. Grand, S. Sandler, and B. Legrand. Transition dans la commande des vol électriques. In *Congres SEE 'Vers des aéronefs plus électrique'*, Toulouse, 2009.
- [MKP09] S. Merzaghi, C. Koechli, and Y. Perriard. Development of a hybrid MEMS BLDC micromotor. *IEEE Energy Conversion Congress and Exposition*, pages 3595–3601, 2009.
- [Ndi09] M. Ndiaye. *Commande prédictive de deux machines synchrones alimentées en parallèle à l'aide d'un convertisseur statique triphasé standard*. Master's thesis, ENSEEIHT, 2009.
- [NFL11] N. L. Nguyen, M. Fadel, and A. Llor. Predictive Torque Control - A solution for mono inverter - dual parallel PMSM system. In *IEEE International Symposium on Industrial Electronics (ISIE)*, pages 697 – 702, 2011.
- [NFL13] N. L. Nguyen, M. Fadel, and A. Llor. A New Approach to Predictive Torque Control with Dual Parallel PMSM System. In *IEEE International Conference on Industrial Technology (ICIT)*, February 2013.
- [Nfo06] G. Nfonguem. *Contribution au développement d'un actionneur plus électrique - Modélisation inverse et composants mécaniques spécifiques à une application aéronautique*. PhD thesis, National Institute for Applied Sciences of Toulouse, 2006.
- [OG05] E. Ortetagan and E. Godoy. RST-Controller design for sine wave references by means of an auxiliary Diophantine equation. In

*Proceedings of the 44th IEEE Conference on Decision and Control, and the European Control Conference, Spain, December 2005.*

- [PBPT03] P. Perera, F. Blaabjerg, J. Pedersen, and P. Thogersen. A sensorless, stable V/f control method for permanent-magnet synchronous motor drives. In *IEEE Transactions on Industry Applications*, volume 39, pages 783 – 791, 2003.
- [PE02] R. Pena-Eguiluz. *Commande algorithmique d'un système mono-onduleur bimachine asynchrone destiné à la traction ferroviaire*. PhD thesis, National Polytechnic Institute of Toulouse, 2002.
- [PEPDRdF02] R. Pena-Eguiluz, M. Pietrzak-David, V. Riga, and B. de Fornel. Comparison of several speed sensorless strategies of two different dual drive induction motor control structures. In *IEEE International Power Electronics Congress*, pages 41–46, 2002.
- [PIS10] A. D. Pizzo, D. Iannuzzi, and I. Spina. High performance control technique for unbalanced operation of single-voltage PM brushless motor drives. In *IEEE International Symposium on Industrial Electronics (ISIE)*, pages 1302 – 1307, July 2010.
- [PPN105] F. Pérez-Pinal, C. Núñez, and R. Álvarez. Multi-motor synchronization technique applied in traction devices. *IEEE International Conference on Electric Machines and Drives*, pages 1542–1548, 2005.
- [PW05] M. Pacas and J. Weber. Predictive direct torque control for the PM synchronous machine. *IEEE Transactions on Industrial Electronics*, 52(5):1350 – 1356, October 2005.
- [QD08] N. P. Quang and J.-A. Dittrich. *Vector Control of Three-Phase AC Machines*. Springer, 2008.
- [Rex02] Rexroth Bosch Group. *Vis à bibles de précision Rexroth Powers d'extrémité et botier*, 2002.
- [RKE<sup>+</sup>10] J. Rodriguez, J. Kolar, J. Espinoza, M. Rivera, and C. Rojas. Predictive torque and flux control of an induction machine fed by an indirect matrix converter. In *IEEE International Conference on Industrial Technology (ICIT)*, pages 1857 – 1863, March 2010.
- [ROAR07] J. Rosero, J. Ortega, E. Aldabas, and L. Romeral. Moving towards a more electric aircraft. *IEEE Aerospace and Electronic Systems Magazine*, 22(3):3–9, 2007.
- [RPS<sup>+</sup>07] J. Rodriguez, J. Pontt, C. Silva, P. Correa, P. Lezana, and P. Cortes. Predictive Current Control of a Voltage Source Inverter. *IEEE Transactions on Industrial Electronics*, 54(1):495 – 503, February 2007.

- [RVAB06] J. Restrepo, J. Viola, J. Aller, and A. Bueno. A Simple Switch Selection State for SVM Direct Power Control. In *IEEE International Symposium on Industrial Electronics (ISIE)*, pages 1112 – 1116, July 2006.
- [Sch08] R. Schroer. Flight control goes digital [ Part Two, NASA at 50]. *IEEE Aerospace and Electronic Systems Magazine*, 33(10):23–28, 2008.
- [SH07] M. Shibata and N. Hoshi. Novel structures topologies for two-wheel drive electric vehicles with two permanent magnet synchronous motors. In *European Conference on Power Electronics and Applications*, pages 1–10, 2007.
- [Sia92] S. Siala. *Motorisation a synchrone d'un robot mobile - Observation et régulation du flux; contrôle de l'alimentation pour le suivi de trajectoire*. PhD thesis, National Polytechnic Institute of Toulouse, 1992.
- [TN86] I. Takahashi and T. Noguchi. A new quick-response and high-efficiency control strategy of an induction motor. In *IEEE Transactions on Industry Applications*, volume IA-22, pages 820 – 827, 1986.
- [VARP08] R. Vargas, U. Ammann, J. Rodriguez, and J. Pontt. Predictive Strategy to Reduce Common-Mode Voltage on Power Converters. In *IEEE Power Electronics Specialists Conference (PESC08)*, June 2008.
- [Vas90] P. Vas. *Vector Control of AC Machines*. Clarendon Press-Oxford, 1990.
- [Vas98] P. Vas. *Sensorless Vector and Direct Torque Control*. Oxford University Press, 1998.
- [VCA<sup>+</sup>07] R. Vargas, P. Cortes, U. Ammann, J. Rodriguez, and J. Pontt. Predictive control of a three-phase neutral-point-clamped inverter. *IEEE Transactions on Industrial Electronics*, 54(5):2697 – 2705, October 2007.
- [VLF<sup>+</sup>09] S. Vazquez, J. Leon, L. Franquelo, J. Carrasco, O. Martinez, J. Rodriguez, P. Cortes, and S. Kouro. Model Predictive Control with constant switching frequency using a Discrete Space Vector Modulation with virtual state vectors. In *IEEE International Conference on Industrial Technology (ICIT)*, pages 1 – 6, 2009.
- [VRAGL12] C. Vlad, P. Rodriguez-Ayerbe, E. Godoy, and P. Lefranc. Explicit model predictive control of buck converter. In *15th International Conference in Power Electronics and Motion Control*, pages 1 – 6, September 2012.
- [VRRE08] R. Vargas, M. Rivera, J. Rodriguez, and J. Espinoza. Predictive Torque Control with Input PF Correction applied to an Induction Machines fed by a Matrix Converter. In *IEEE Power Electronics Specialists Conference (PESC08)*, pages 9 – 14, June 2008.



# Résumé en français

## Introduction

Aujourd'hui, les systèmes embarqués sont de plus en plus nombreux et ils impactent fortement les systèmes de conversion d'énergie. Les contraintes associées concernent la réduction de masse ainsi que la diminution des pertes afin d'améliorer l'efficacité énergétique de la chaîne de conversion. C'est bien sûr le cas dans le domaine aéronautique où le concept de «l'avion plus électrique» devient aujourd'hui une réalité. En conséquence, la machine synchrone à aimant permanent devient un actionneur par excellence grâce à sa forte densité de puissance, son faible coût d'entretien et ses qualités dynamiques.

Lorsque ces machines sont associées pour mener à bien des fonctions coopératives (par exemple les surfaces de vol), la masse embarquée peut encore être réduite par le partage de l'électronique de puissance. C'est précisément dans ce contexte où notre travail a été élaboré, avec l'idée de développer des structures d'électronique de puissance capables d'alimenter deux ou plusieurs machines électriques en parallèle et dotées de lois de contrôle adaptées afin d'améliorer l'efficacité énergétique.

Nous avons travaillé plus spécifiquement sur la commande prédictive de deux machines synchrones connectées en parallèle reliées à un seul convertisseur triphasé. Ces machines ont des caractéristiques identiques et doivent suivre le même profil de vitesse avec un couple de charge qui peut être différent et indépendant dans tous les cas.

Le cadre de travail de ces travaux est présenté en quatre chapitres:

- Le premier chapitre présente les usages de la machine synchrone à aimant permanent (MSAP) dans de nombreux domaines d'application. Les systèmes multi-machines dans le domaine aéronautique ainsi que l'idée de la structure d'électronique de puissance partagée sont ainsi considérés. Les structures typiques du système multi-machine sont alors présentées. Les caractéristiques de chaque structure sont ensuite étudiées.
- Le deuxième chapitre consacre à la description générale d'un système d'entraînement de MSAP et notamment le système d'entraînement des MSAP en

parallèle. Dans cette partie, l'analyse de la stabilité et le principe de commande de la MSAP sont ainsi considérés.

- Le troisième chapitre est la partie principale de cette thèse. La commande prédictive du couple des deux machines synchrones connectées en parallèle, reliées à un seul convertisseur triphasé deux niveaux est ainsi étudiée. Chaque composant de ce système d'entraînement est étudié et expliqué en détail. Deux approches de commande prédictive seront décrites et comparées. Des simulations permettront de vérifier les performances des méthodes de contrôle.
- Le quatrième chapitre présente le banc expérimental qui a été développé au laboratoire LAPLACE avec l'objectif de vérifier le fonctionnement du système avec les stratégies de contrôle proposées. Le banc représente un déplacement hypothétique de deux volets d'un avion. Le système étudié convertit l'énergie électrique fournie par le réseau EDF pour alimenter deux charges mécaniques. Dans ce mécanisme, les deux MSAPs sont connectées en parallèle sur un même onduleur.

### **Machine Synchrone à Aimant Permanent (MSAP)**

La machine synchrone à aimants permanents (MSAP) a émergé comme une solution compétitive dans une large gamme d'applications de contrôle du mouvement. En particulier, la MSAP est largement utilisée dans les machines-outils, la robotique et les actionneurs industriels et elle est également en visagée dans des applications de haute puissance comme la propulsion des véhicules et des entraînements industriels. Elle devient également viable pour des applications commerciales ou résidentielles. La MSAP est connue pour avoir beaucoup d'avantages par rapport à d'autres types de machines électriques:

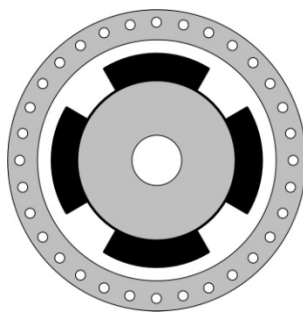
- **Une grande efficacité:** les MSAPs utilisent des aimants permanents pour créer un champ magnétique au rotor constant au lieu d'utiliser un circuit. Par conséquent, il n'y a pas de pertes cuivre. En outre, sans le circuit du rotor, la seule chaleur est produite sur le stator, ce qui est beaucoup plus facile à refroidir.
- **Une haute densité de flux:** Les progrès récents dans les aimants de haute densité énergétique (NdFeB) ont permis la réalisation de très fortes densités de flux. Ces aimants permettent un couple élevé, le développement de machines plus petites et plus légères, une grande longévité et fiabilité. Parce qu'il n'y a pas de commutateurs mécaniques ni de contacts glissants le frottement est plus faible et la durée de vie est plus longue. D'ailleurs, sans ces éléments, le coût d'entretien est réduit et le

risque lié aux courants d'extra-coupure est éliminé ce qui est particulièrement appréciable dans certaines conditions d'utilisation.

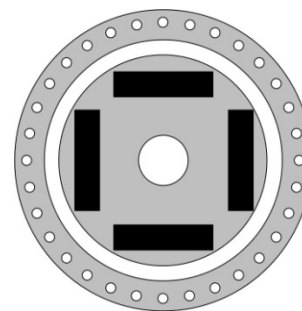
- **Un rapport entre couple et inertie élevé:** En utilisant des aimants permanents, la MSAP aura une faible inertie, ce qui assure une réponse rapide sous un couple électrique donné une densité de puissance élevée (il est représenté par le rapport kW / kg qui traduit la puissance massique)
- ...

Dans les MSAPs, des aimants permanents sont montés à l'intérieur du rotor (machine synchrone à aimants permanents en terres - IMSAP) ou situés en périphérie du rotor (machine synchrone à aimants montés en surface- SMSAP) (Figure 1). Dans tous les cas, la structure du stator est identique aux machines asynchrones comme d'autres types de moteurs à courant alternatif. Les bobinages sont alors construits de manière à produire une densité de flux sinusoïdale dans l'entrefer de la machine.

Aujourd'hui, les MSAPs jouent un rôle important dans les applications à vitesse variable. Ces applications ont la capacité de produire quelques Watts (micro-moteur brushless DC développé en technologie MEMS) à plus d'un GW (générateur synchrone AC). Pour les petites machines électriques, le rotor comporte généralement plusieurs aimants permanents. Ces moteurs synchrones à aimants permanents sont également appelés «*moteur sans balais*» parce que le flux du rotor est toujours créé par les aimants, ils n'ont pas de collecteur et de balais.



a) Machine synchrone à aimants montés en surface  
(SPMSM)



b) Machine synchrone à aimants enterrés (IPMSM)

Figure 1: Deux principaux types de MSAP

Il convient de noter, plusieurs applications à haute performance telles que la robotique et les actionneurs dans l'aérospatiale où le besoin d'un couple élevé par rapport à l'inertie, sont autant d'applications typiques de la MSAP.

## Système multi-machines dans le domaine aéronautique

Dans le cadre de l'avion plus électrique (ou More Electric Aircraft –MEA), la tendance est à l'utilisation de machines de plus en plus électriques, que ce soit pour les actionneurs de commande de vol ou pour les autres équipements tels que le train d'atterrissage, les freins, les pompes à essence, les systèmes de dégivrage, les systèmes de climatisation, ou encore les systèmes de verrouillage. Comme représenté sur la Figure 2, la MSAP peut être utilisée dans de nombreux systèmes de l'avion.

Afin de faire fonctionner de tels ces systèmes, chaque moteur a besoin d'un dispositif d'électronique de puissance qui se compose d'une composante de refroidissement lourde et encombrante. Cet élément va augmenter le poids et la taille de l'ensemble du système de manière significative. De plus, les applications aéronautiques exigent des systèmes à haute sécurité intégrée, il faut donc avoir des systèmes redondants. Ces systèmes servent essentiellement à assurer le fonctionnement continu de l'ensemble du système, même si un problème se produit. Toutefois, ils alourdissent et augmentent le volume du système.

D'ailleurs, pendant chaque phase de vol, un certain nombre de systèmes d'entraînement nécessitent des dispositifs d'électronique de puissance. Ils sont alors utilisés tandis que les autres sont inactifs. Par exemple, les systèmes d'ouverture des portes ne sont utilisés que lorsque l'avion est à l'arrêt. Les systèmes du train d'atterrissage, des volets des ailes ou des ondulateurs de poussée sont également utilisés seulement pour quelques minutes sur l'ensemble du vol. Il est intéressant d'examiner l'utilisation de structures de partage pour exploiter des systèmes individuels en fonction de la disponibilité de séquençage, tout en respectant la continuité de service.

Les systèmes de contrôle de vol sont présentés dans Figure 3, ils se composent de deux parties d'actionnement:

- La partie primaire est l'élément essentiel de chaque vol., Il contrôle l'évolution de l'aéronef selon trois axes: le roulis (par les ailerons sur les bords de fuite des ailes), le tangage (par les gouvernes de profondeur sur le bord de fuite de l'empennage), le lacet (par la gouverne de direction).
- La partie secondaire représente la configuration aérodynamique de l'avion lors de l'atterrissage et du décollage des processus (système de volets, spoilers ...). Il y a deux parties principales dans le système d'actionnement secondaire: les volets 'slat' et 'flap' qui sont utilisés pour le décollage, l'atterrissage et pour l'augmentation de la portance à basse vitesse ; les spoilers qui augmentent la traînée. Ces composants ne sont pas réellement nécessaires pour le vol, mais sont indispensables.

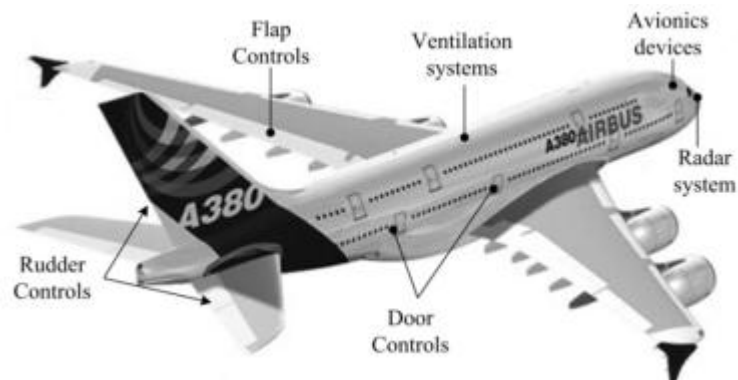


Figure 2: Utilisation des MSAP en aéronautique

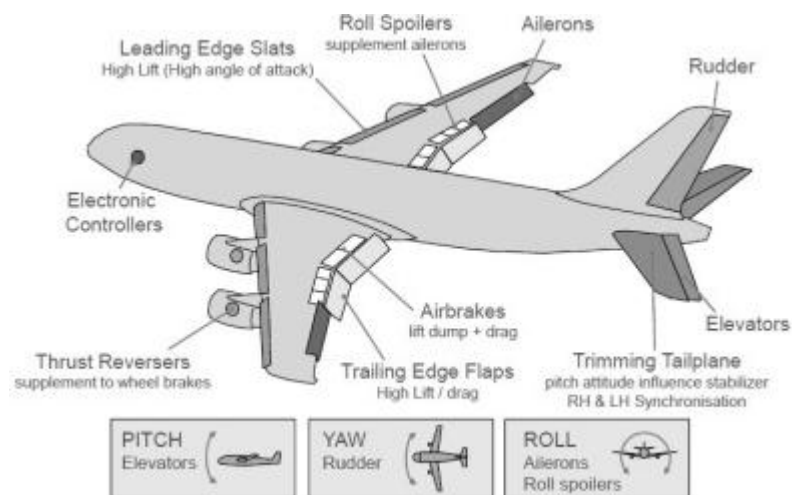


Figure 3: Système de contrôle des surfaces de vol

## La structure classique

Dans la structure classique d'un système multi-machine, chaque phase d'une machine est connectée et commandée par le bras de son propre onduleur. Pour  $n$  machines triphasées, donc  $m=3n$  bras d'onduleur, la structure SM ( $3n, n$ ) est décrite dans la Figure 4.

Dans ce cas, ainsi que dans les cas qui sont mentionnés par la suite, toutes les branches de l'onduleur sont connectées à un bus de courant continu qui fournit la tension  $V_{dc}$ .

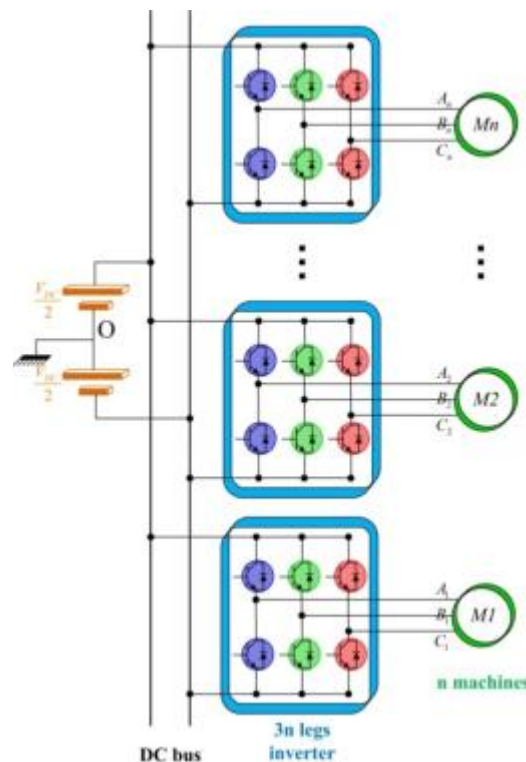


Figure 4: Structure classique multimachine/multionduleur SM( $3n, n$ )

Dans cette configuration, il n'y a pas de contrôle mutuel entre les différents onduleurs. Toutes les machines fonctionnent indépendamment. Le synchronisme de l'installation peut être obtenu facilement. Toutefois, l'utilisation d'un onduleur pour chaque machine ainsi qu'un système d'entraînement nécessite un dispositif de commande individuel. Le système devient alors coûteux et encombrant. Ces problèmes peuvent être considérés comme le point le plus négatif de cette structure.

## Les structures mutualisées

Dans les structures mutualisées, plusieurs machines peuvent avoir des phases communes. Ces phases peuvent être reliées aux mêmes bras d'un onduleur ou au point commun (le point neutre d'une ligne DC). C'est la raison pour laquelle un bras d'onduleur

peut générer une tension alternative, donc un onduleur possédant  $x$  bras peut alimenter  $y$  machines. Ces structures sont marquées comme MS  $(2 \cdot x, y)$ . Les structures typiques se représentent sur Figure 5.

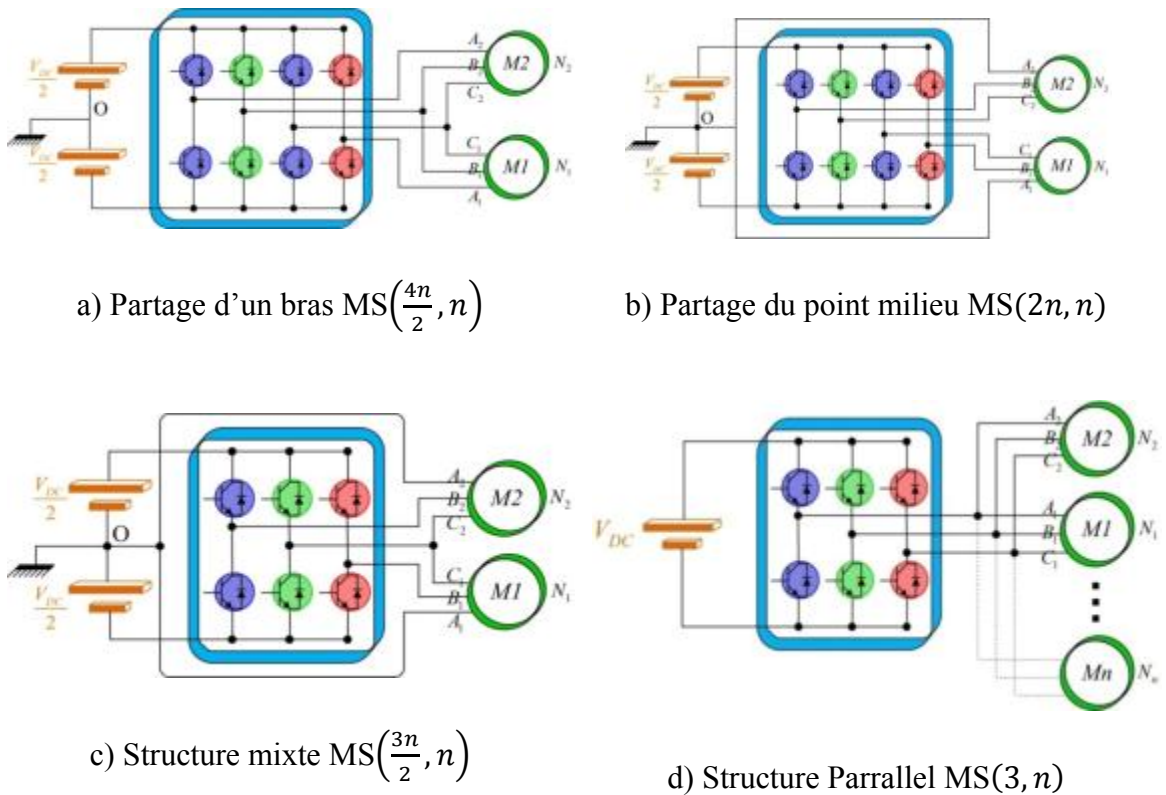


Figure 5: Structure typiques pour les systèmes multimachines

Dans Figure 5a, un onduleur à quatre bras est utilisé pour alimenter deux machines. Les deux phases B et C des deux machines sont connectées à la même branche de l'onduleur. La troisième phase de chaque machine est connectée individuellement à son propre bras. Cette structure est désignée par SP  $\left(\frac{4n}{2}, n\right)$ .

Une autre structure mutualisée est appelée MS  $(2n, n)$  et est illustrée à la Figure 5b. Dans la structure, deux phases de chaque machine sont reliés à deux branches séparées d'un onduleur et la troisième phase de ces deux machines est partagée et connectée au point neutre O du bus DC. Un des avantages de cette structure est que les moteurs peuvent fonctionner indépendamment les uns des autres, tandis que le nombre de composants d'électronique de puissance peut être réduit. Toutefois, pour mettre en œuvre cette structure dans les applications, le point neutre du bus continu DC doit être accessible afin de réguler la tension de référence. Il n'est pas facile de résoudre ce problème, en particulier dans les systèmes aéronautiques.

Sur la base des deux structures ci-dessus, une structure mixte est développée et considérée comme la Figure 5c. Selon cette structure, un onduleur à trois branches est utilisé pour faire fonctionner les deux moteurs. Une phase des deux moteurs sera partagée et connectée à une branche commune de l'onduleur ( $C_1$  et  $C_2$ ), tandis que l'autre phase de deux moteurs ( $A_1$  et  $A_2$ ) est reliée au point neutre O. La troisième phase est reliée à ses propres bras de l'onduleur. Cette structure est nommée  $MS\left(\frac{3n}{2}, n\right)$ .

Une structure parallèle qui appartient au type  $MS(3, n)$  utilise un onduleur à trois bras pour faire fonctionner  $n$  machines simultanément. Cette structure est représentée sur la Figure 5d.

Le Table 1 synthétise l'ensemble des caractéristiques des structures présentées précédemment.

Nom de la structure	MS(m,n)	Nombre de bras par machine	Relation $\frac{(V_{Nk})_{\max}}{(V_{Ok})_{\max}}$	Vitesse	Volume	Notes	
						Avantages	Inconvénients
Classique	$MS(3n, n)$	3	1	indépendant	grand	machines indépendantes	non partagée
Bras commune	$MS\left(\frac{4n}{2}, n\right)$	2	$\frac{2}{3}$	$\Omega_1 = \Omega_2$ or $\Omega_1 = -\Omega_2$	moyen	facile à implanter	sur-courant dans le bras commun
Point milieu	$MS(2n, n)$	2	$\frac{1}{\sqrt{3}}$	indépendant	moyen	applicable à une machine	accès au point neutre
Mix	$MS\left(\frac{3n}{2}, n\right)$	1.5	$\frac{1}{\sqrt{3}}$	$\Omega_1 = \Omega_2$ or $\Omega_1 = -\Omega_2$	petit	Idem	Idem
Parallèle	$MS(3, n)$	$\frac{3}{n}$	1	$\Omega_1 = \Omega_2$	petit	facile à implanter	sur-courants dans tous les bras

Table 1: Résumé des différentes structures

La structure parallèle présente le meilleur avantage de l'utilisation par rapport au nombre possible de bras de l'onduleur. De plus, il n'est pas nécessaire de moduler la tension du bus continu ( $V_{DC}$ ) afin d'obtenir la même tension de la machine par rapport au cas d'une structure classique. Il n'est pas trop difficile d'appliquer cette structure dans des applications réelles. Certaines études ont été élaborées afin de contrôler ce genre de systèmes d'entraînement. Ces études portent sur un système d'entraînement en comprenant deux MS APs connectées à un onduleur triphasé. Ces systèmes sont également appelés mono-onduleur MSAP double-parallèle (Figure 6).

## Mono-onduleur dual-parallèle MSAP

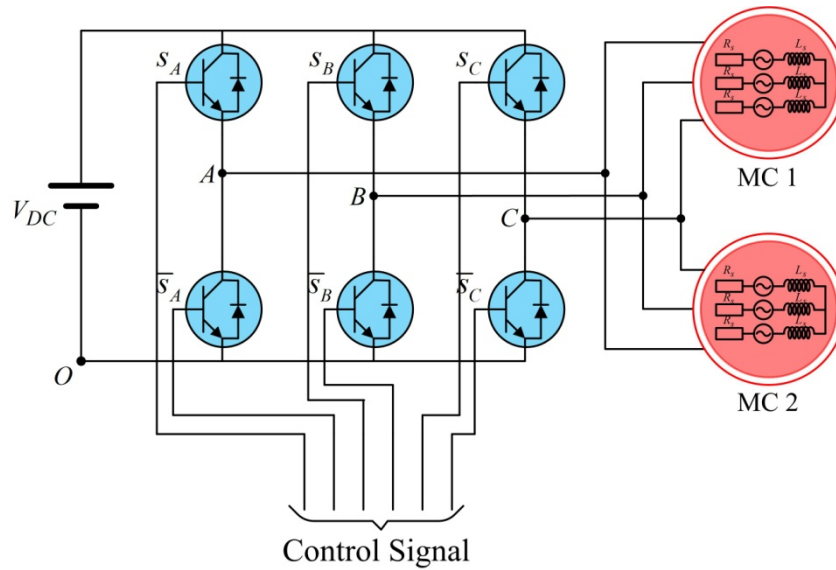


Figure 6: Mono-onduleur dual-parallèle MSAP

Selon la Figure 6, un système d'entraînement en comprenant deux MSAPs connectées en parallèle et alimentées par un onduleur triphasé à deux niveaux est présenté. Dans ce genre de système d'entraînement, les machines doivent être identiques. Cela signifie que tous les paramètres des deux machines sont les mêmes et les deux machines recevront la même tension (en amplitude et en fréquence):

$$\begin{cases} |V_{s1}| = |V_{s2}| = |V_s| \\ \omega_{re1} = \omega_{re2} = \omega_s \end{cases}$$

Pour ce type de système, l'objectif est de maintenir les vitesses des deux machines qui sont égales, de façon à suivre la vitesse de référence dans les différentes conditions de charge:

$$\omega_{re1} = \omega_{re2} = \omega_{ref}$$

$$s.t. T_{load1} \neq T_{load2}$$

### La structure maître/esclave

Une configuration maître/esclave a été appliquée au système d'entraînement mono-onduleur bi-machine MSAP. Dans de tels systèmes, notons que :

- + Les deux machines sont identiques

- + Les deux machines doivent être actionnées à la même vitesse  $\omega_{m1} = \omega_{m2}$
- + Les charges appliquées à chaque machine sont différentes et non liées mécaniquement.

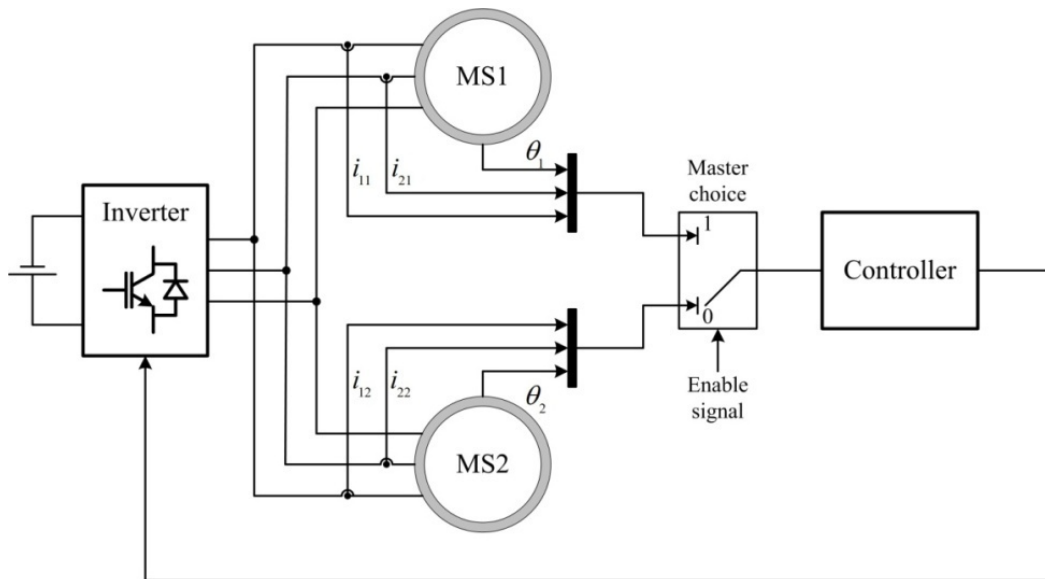


Figure 7: La structure parallèle avec maître/esclave

La Figure 7 illustre la configuration maître/esclave. Un bloc nommé sélecteur est ajouté au système en vue de sélectionner la machine maître. Selon cette configuration, à chaque moment, seule la machine "maître" est contrôlée. L'autre, la machine esclave, fonctionne en boucle ouverte dans le cadre d'une alimentation en tension. Ainsi, la valeur de la tension alimentée par l'onduleur est entièrement due à la commande de la machine « maître ». On remarque que la machine « esclave » n'a aucune influence sur cette valeur. En pratique, le principe de contrôle n'est pas différent par rapport au système d'entraînement de la MSAP. Par conséquent, la stabilité de la machine « maître » est assurée. Toutefois, il est possible que la machine « esclave » qui est en boucle ouverte soit instable. Le problème posé est le suivant : « *comment choisir la machine maître pour que les deux machines restent stables ?* ».

### Commande de couple directe avec mono-onduleur alimentant deux MSAP en parallèle

La méthode Direct Torque Control (DTC) cherche à contrôler directement le couple électromagnétique par action sur le module du flux et l'angle entre le flux rotor et le flux stator.

Dans le cas de deux machines fonctionnant en parallèle, les composantes d'erreur sont  $\Delta T_1, \Delta T_2, \Delta \psi_{s1}$  et  $\Delta \psi_{s2}$ . Quatre comparateurs à hystérésis doivent alors être utilisés. Seize cas peuvent être synthétisés à partir de quatre états de deux machines (Table 2).

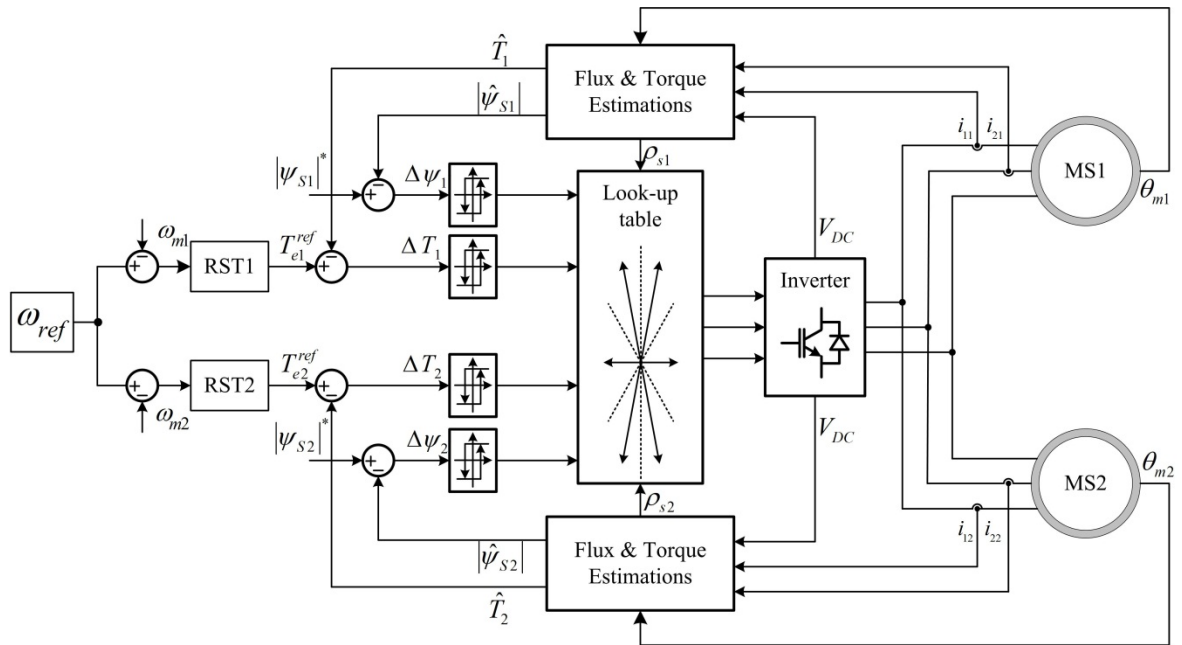


Figure 8: Commande directe de couple

$\Delta \psi_{s1} \Delta \psi_{s2} \backslash \Delta T_1 \Delta T_2$	00	01	11	10
00				
01				
11				
10				

Table 2: Table de correspondance entre le flux et le couple pour 2 machines en parallèle

Selon l'éd TC, chaque paire couple-flux doit être corrélée à un vecteur tension. Toutefois, le choix de ce vecteur dépend aussi de la position spatiale du vecteur flux. Sous

différentes conditions de charge, il est possible que les vecteurs de flux des deux machines puissent être situés dans différents secteurs. Ce problème est illustré sur la Figure 9.

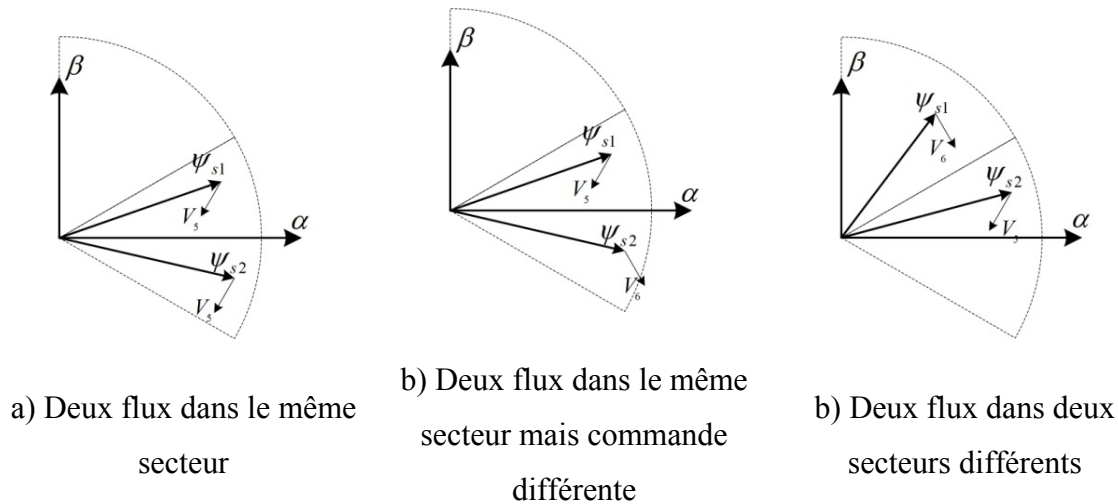


Figure 9: Différents cas pour choisir un vecteur tension adéquat

Sur la Figure 9a, les vecteurs de flux des deux machines sont dans le même secteur. Les si gnoux en p rovenant d e l'ensemble d es co mparateurs à h ystérésis n écessitent l a réduction à la fois du couple et du flux de deux machines. Le vecteur de tension approprié dans ce cas pour les deux machines est le même.

Dans d'autres cas, lorsque la demande de chaque machine est différente (Figure 9b) ou deux vecteurs flux localisés dans des secteurs différents (Figure 9c), il est nécessaire de construire une autre table de consultation pour satisfaire les deux moteurs.

### Commande Prédictive Directe de Couple (DPTC)

Les p remières i dées su r l a co mmande p rédictive a ppliquées a ux co nvertisseurs de puissance ont commencé dans les années 1980. Le principe de cette stratégie est basé sur le calcul d es co mportements futurs du système e t l'utilisation d'une fonction de co ût pou r évaluer c es co mportements. L 'algorithme p rédictif pe ut ê tre di visé e n t rois é tapes principales:

- + Mettre à jour l es é tats du sy stème et l'estimation d es v ariables q ui p euvent être mesurées;
- + Prévoir les comportements futur des systèmes;
- + Optimiser le signal de commande conformément à une fonction de coût.

Basé su r l e p rincipe d e l a co mmande p rédictive e t su r l e D TC, u ne st ratégie d e commande prédictive directe de couple (DPTC) est appliquée au système d'entraînement

mono-onduleur pour deux MSAP en parallèle. Selon cette stratégie, les huit états réels de l'onduleur triphasé à deux niveaux sont considérés séquentiellement afin d'évaluer la fonction coût. Aucune technique de modulation ne doit être utilisée. Chaque configuration élue par la procédure d'optimisation sera appliquée directement à l'onduleur.

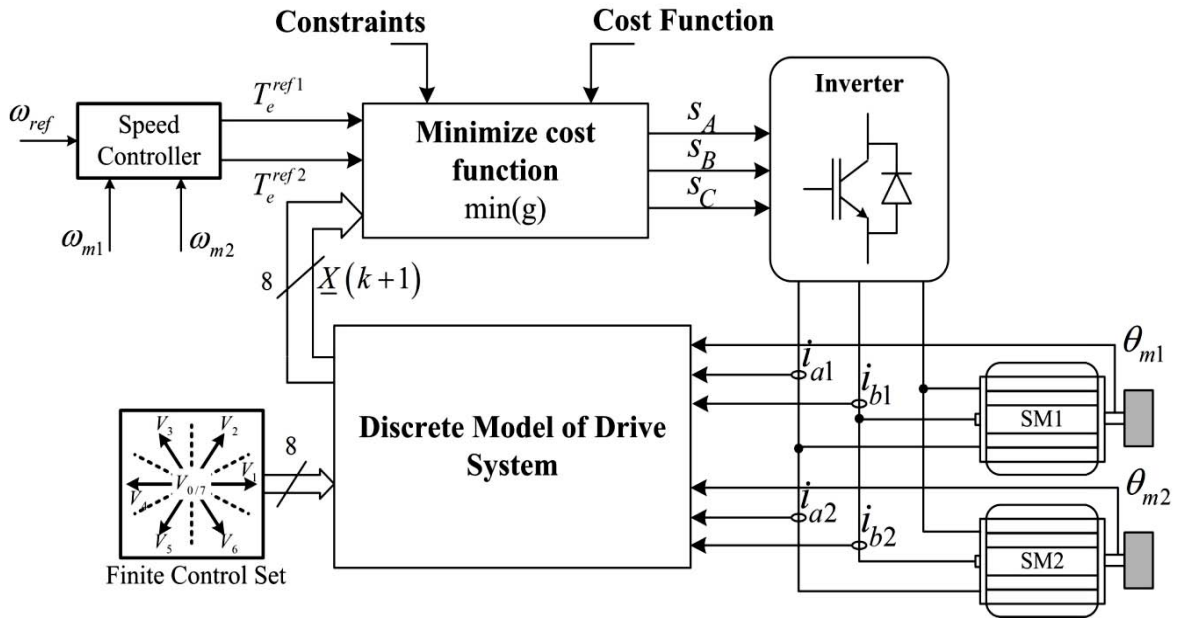


Figure 10: Commande Prédictive Directe de Couple (DPTC)

Les états du système à l'instant  $k$  en fonction de la position  $\theta_m(k)$ , des courants  $i_s(k)$  sont toujours mis à jour. L'ensemble des huit états réels des onduleurs  $\{(s_a, s_b, s_c)\}_{(1 \dots 8)}$  sont mis dans le modèle discret du système d'entraînement afin de prévoir l'évolution possible du système:  $X_i(k+1) = f\{x(k), (s_a, s_b, s_c)_i\}$ , pour  $i = 1 \dots 8$ . Il est noté que cette fonction de prédiction est directement dérivée du modèle discret et de ses paramètres du système. Pour déterminer quelle action de contrôle doit être sélectionnée, la fonction de coût sera évaluée avec toutes les combinaisons de commande possibles et la valeur de référence souhaitée  $x^*(k+1)$ . Les références sont ici les couples souhaités pour les deux machines, fournis par la sortie des régulateurs de vitesse RST. Noter que la valeur de référence future  $x^*(k+1)$  peut-être supposée égale à la valeur réelle  $x^*(k)$  parce que le temps d'échantillonnage  $T_s$  est assez petit et donc la référence peut être considérée comme constante dans ce temps. L'évaluation de la fonction de coût avec les huit prédictions conduira à huit coûts différents. L'action de contrôle correspondant à un coût minimum ( $\min\{g_i\}$ ), pour  $i = 1 \dots 8$ , est sélectionnée pour contrôler le système.

Un schéma de l'algorithme de commande est représenté dans la Figure 11.

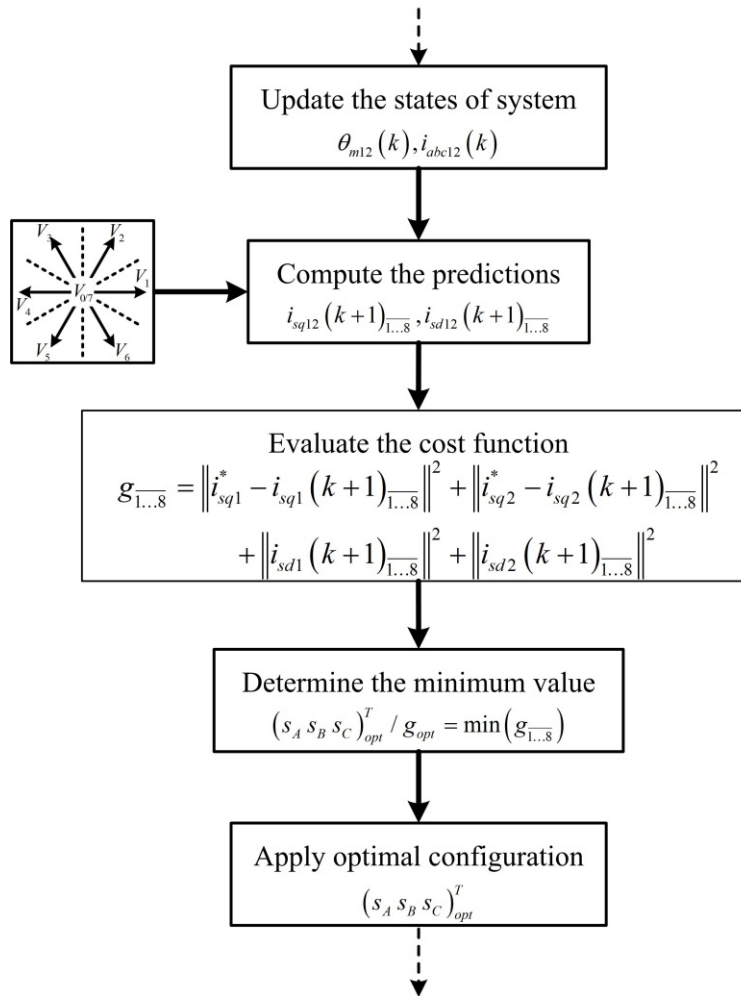


Figure 11: Schéma de l'algorithme de commande

### Commande Prédictive de Couple - “Split and Seek” (PTC “Split and Seek”)

L'idée de l'utilisation non seulement des états réels discrets de l'onduleur mais également des vecteurs de tension virtuels dans l'ensemble de l'espace de commande est considérée ici, afin de réduire l'ondulation de couple Figure 12.

Selon la Figure 12, les vecteurs virtuels de tension peuvent être localisés à n'importe quelle position dans la région de la commande de l'onduleur. Chaque vecteur virtuel est considéré dans le plan  $(\alpha\beta)$  et est représenté par un couple de valeurs, l'angle  $\alpha$  par rapport à l'axe et l'amplitude. Dans cette figure, les véritables vecteurs sont représentés par une ligne continue, les vecteurs virtuels par des lignes en pointillés. La région de commande d'un onduleur à deux niveaux dans l'espace de modulation vectorielle (SVM) est limitée par un cercle dont le rayon est égal à  $\frac{V_{DC}}{\sqrt{3}}$ .

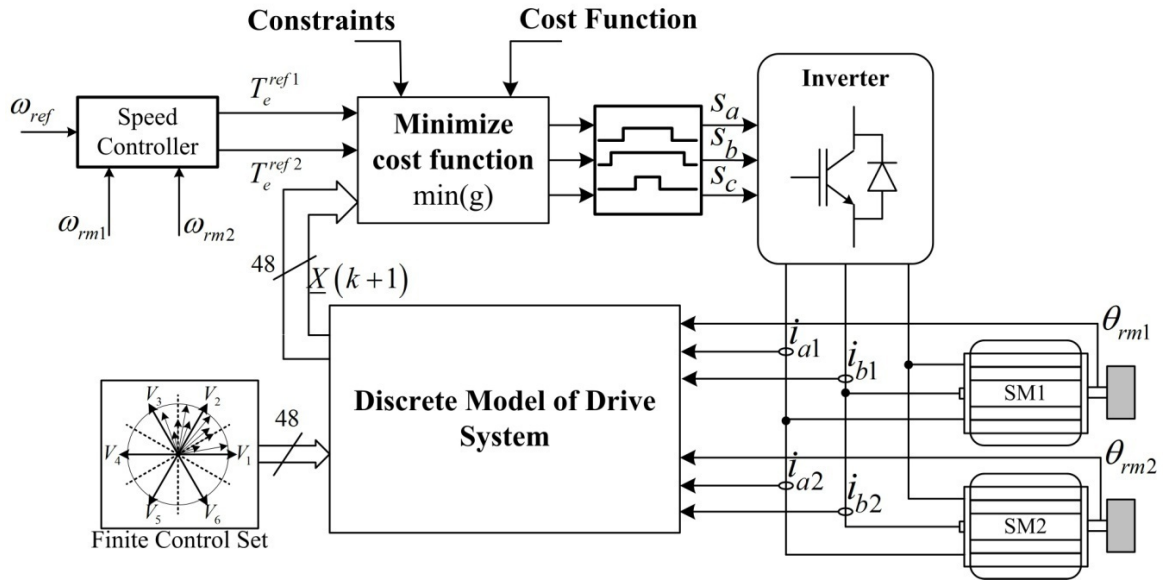


Figure 12: Schéma de la méthode PTC – “Split and Seek”

L'objectif de cette approche est de trouver le vecteur de tension le plus exact à chaque période de commande, tout en bénéficiant de la technique SVM. Grâce à cela, le fonctionnement du système peut être amélioré. Les ondulations de couple et des courants seront donc réduites.

Cependant, la façon de définir ces vecteurs virtuels efficacement est une réelle difficulté. Par conséquent, une méthode appelée "Split and Seek" est étudiée afin de résoudre ce problème. Au lieu de considérer tous les vecteurs virtuels dans chaque cycle de contrôle, le processus de recherche sera divisé en deux étapes: "la recherche de l'angle et la recherche de l'amplitude".

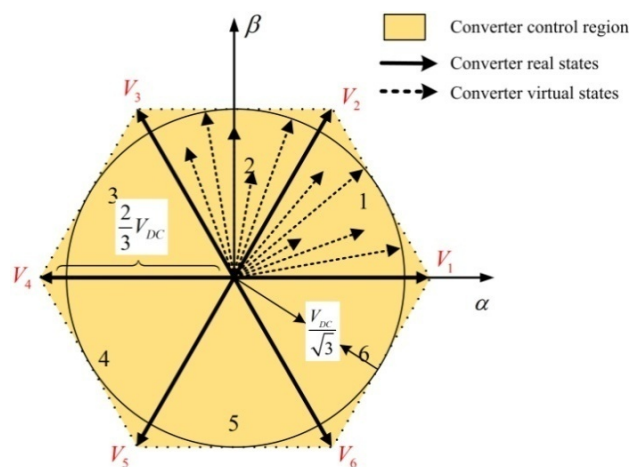


Figure 13: La région de contrôle d'onduleur avec vecteurs virtuels

### *La recherche de l'angle*

Comme pour la méthode directe, l'espace de tension sera d'abord divisé en six secteurs donnant six véritables vecteurs de tension actifs (comme dans la Figure 14). Ces six vecteurs de base sont repérés dans le premier ensemble de commande. Cet ensemble est mis en œuvre lors d'une première évaluation du critère. Une valeur de la fonction de coût qui correspond à chaque vecteur est ainsi obtenue. Le vecteur qui nous donne la valeur minimale de la fonction de coût est choisi comme le point de départ pour la recherche suivante.

A partir du vecteur de base trouvé dans la recherche précédente, un groupe de vecteurs de deux secteurs adjacents de tension virtuelle (à gauche et à droite du vecteur de base) est considéré. Par la mise en place d'un secteur angulaire entre deux vecteurs adjacents de  $\Delta\alpha = 10^\circ$ , nous obtenons un groupe de dix vecteurs de tension (Figure 14). Ces vecteurs ont la même amplitude égale à la valeur maximale de la tension  $V_{max}$ . Nous continuons ensuite à évaluer ces vecteurs pour élire le vecteur de tension rendant la fonction de coût prédéfinie minimale. Ce vecteur va nous donner la meilleure valeur de l'angle.

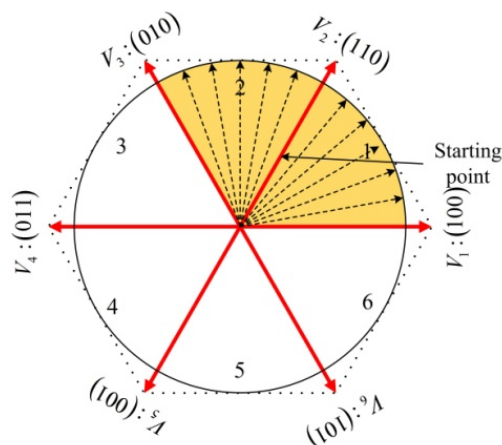


Figure 14: Deux vecteurs adjacents et les vecteurs virtuels

### *La recherche de l'amplitude*

Après avoir défini un vecteur de tension approprié par le processus de recherche de l'angle, nous continuons à moduler l'amplitude de ce vecteur afin de minimiser encore, si possible, la fonction coût.

Par conséquent, le vecteur de tension élu par le processus de recherche de l'angle sera passé par la recherche d'une amplitude optimale. Dans ce processus, un groupe de vecteurs

de tension est représenté par l'angle optimal, on fera varier leur amplitude. Avec la gamme de tension de 0 à  $V_{max}$ , un pas de progression d'amplitude  $\Delta V$  est alors défini.

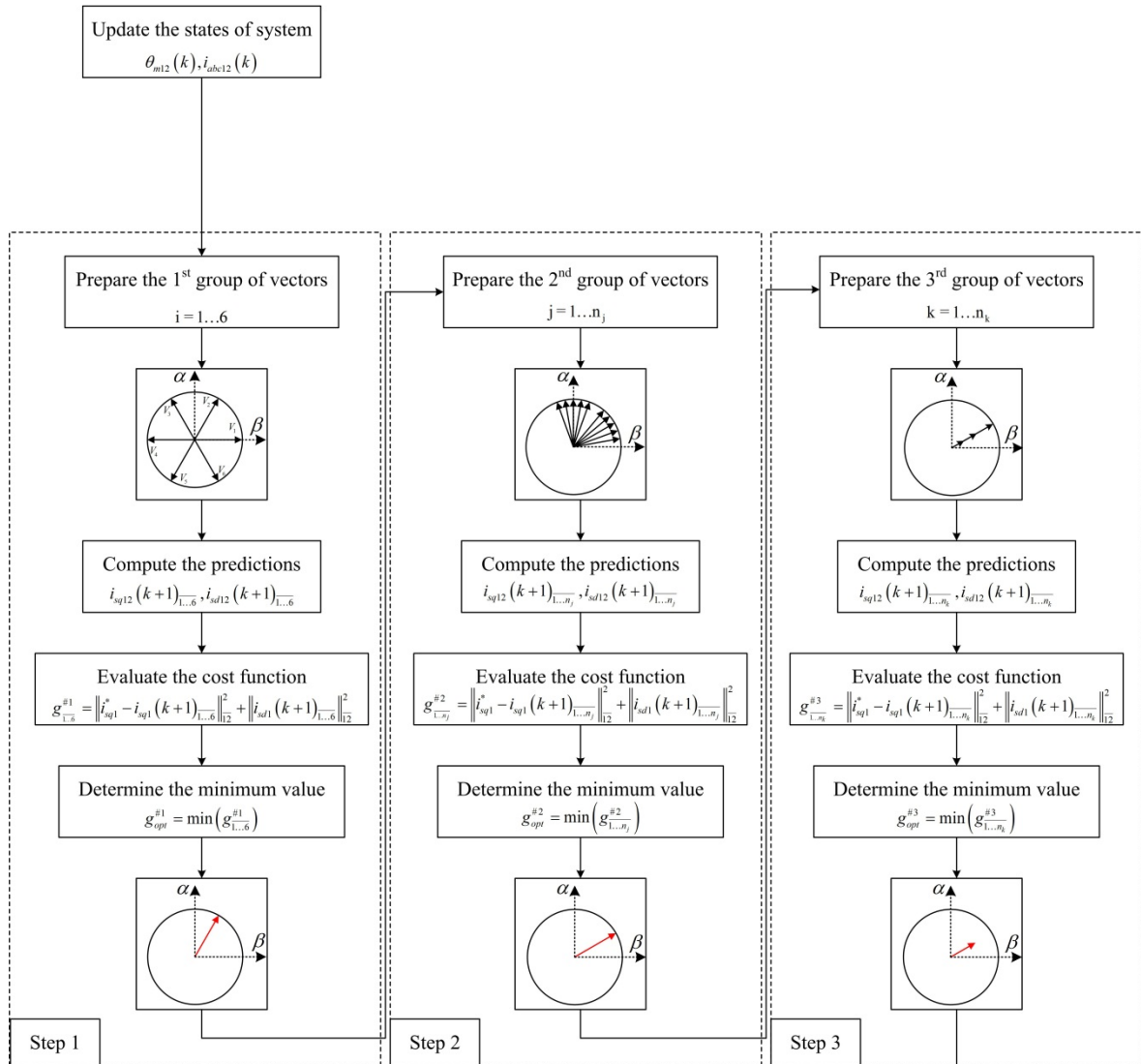


Figure 15: Diagramme de la nouvelle solution

Grâce au processus des deux recherches, un vecteur de tension virtuel approprié est finalement choisi. La technique SVM est chargée de moduler ce vecteur de tension et de générer les impulsions de l'onduleur.

### Le banc expérimental

Un banc expérimental basé sur le principe d'un système de commande électrique à base de DSP est ensuite utilisé pour vérifier les analyses théoriques des chapitres précédents. Ce système se compose de quatre grandes parties: 1) le système de couplage du moteur, 2)

Power Electronics Conseil Drive, 3) une carte dSAPCE DS1103 R & D associée à sa carte CP1103 d'entrées/sorties et 4) MATLAB/Simulink et le bureau de contrôle.

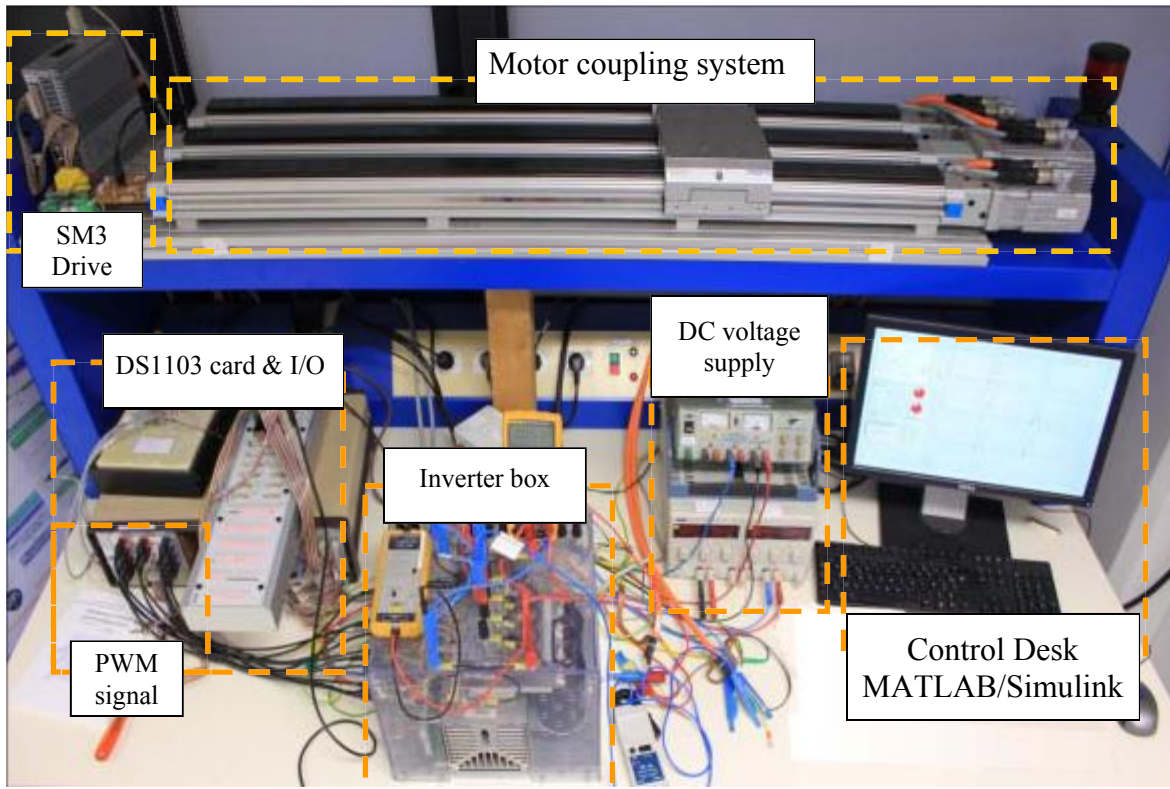


Figure 16: Présentation du banc expérimental

Tous les équipements sont installés et organisés de la manière suivante (Figure 16):

- Système d'accouplement moteur: il se compose de deux MSAPs identiques avec le résolveur déjà installé. Les bobines de résolveur sont disponibles à partir du moteur via un connecteur à 12 broches dans le carter du moteur
- Système de mesure:
  - Les équipements sont alimentés par un courant continu à tension  $\pm 15V$
  - Un capteur à effet Hall de type LEM LA 25-S mesure le courant
  - Le convertisseur à résolveur numérique mesure de la position du rotor
  - Un multimètre affiche le DC bus de tension.
- Système d'alimentation et de commande d'électronique de puissance:
  - Un auto-transformateur commande l'énergie électrique du réseau EDF
  - Une source de tension  $\pm 15V\_DC$  alimente le système de commande de l'onduleur
  - Une source de tension fournit des lignes de courant continu pour l'onduleur
  - L'onduleur à trois bras utilise des commutateurs IGBT à deux niveaux

- Système de contrôle et d'observation: il se compose de
  - Une plaquette CP1103 d SPACE avec des entrées/sorties analogiques et numériques I/O
  - Une plaquette dSPACE CLP1103 avec des LED lumineuses qui montrent l'état des différents signaux
  - L'ordinateur avec MATLAB/Simulink et le logiciel de contrôle.

Ce banc expérimental a été développé dans le laboratoire LAPLACE dans le but de créer un système qui représente de manière fiable la commande de deux volets d'un avion. Dans ce mécanisme, la structure parallèle de deux MSAPs est utilisée.

Plusieurs tests avec PTC-SS ont été développés avec ce banc d'essai. Les résultats transitoires sont présentés au Chapitre 4 de cette thèse.

### Résultats expérimentaux

L'algorithme PTC-SS est choisi pour l'appliquer à un système réel selon trois configurations: avec une machine; avec deux machines en parallèle; avec deux machines en parallèle en config maître/esclave.

#### *Test avec une machine*

Le schéma du mécanisme de commande est représenté sur la Figure 17.

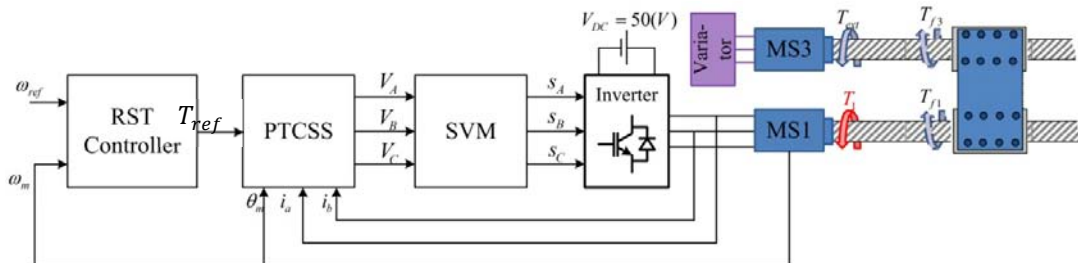


Figure 17: PTC-SS appliqué à une MSAP

Dans ce test, le profil de couple de charge générée par SM3 est mis en place comme suit:

- g. De  $t = 0(s) \rightarrow t = 1.5(s)$  et  $t = 9.0(s) \rightarrow t = 10(s)$ : le couple de charge est fixé à zéro. Cela signifie que la charge totale appliquée à SM1 est  $T_{total} = T_{f1} + T_{f3}$ ;
- h. De  $t = 1.5(s) \rightarrow t = 3.0(s)$ : la charge est fixée à  $T_{ext} = 0.1Nm$ . Ainsi, la charge totale sera réduite:  $T_{total} = T_{f1} + T_{f3} - T_{ext}$ ;
- i. De  $t = 3.0(s) \rightarrow t = 5.0(s)$ : la charge est fixée à  $T_{ext} = -0.1Nm$ . Ainsi, la charge totale sera  $T_{total} = T_{f1} + T_{f3} + |T_{ext}|$ ;

- j. De  $t = 5.0(s) \rightarrow t = 6.5(s)$ : la charge est fixée à  $T_{ext} = -0.1Nm$ , cependant, le moteur est inversé. Ainsi, la charge totale sera  $T_{total} = -(T_{f1} + T_{f3} - |T_{ext}|)$ . La valeur absolue de la charge est la même que pour (b);
- k. De  $t = 6.5(s) \rightarrow t = 9.0(s)$ : la charge est fixée à  $T_{ext} = 0.1Nm$ , cependant, le moteur est inversé. Ainsi, la charge totale aura la valeur absolue obtenue en (c);
- l. De  $t = 9.0(s) \rightarrow 10.0(s)$ : le couple de charge est égal à zéro. La charge totale est la même que pour (a).

La réponse en vitesse de la machine est représentée sur la Figure 18

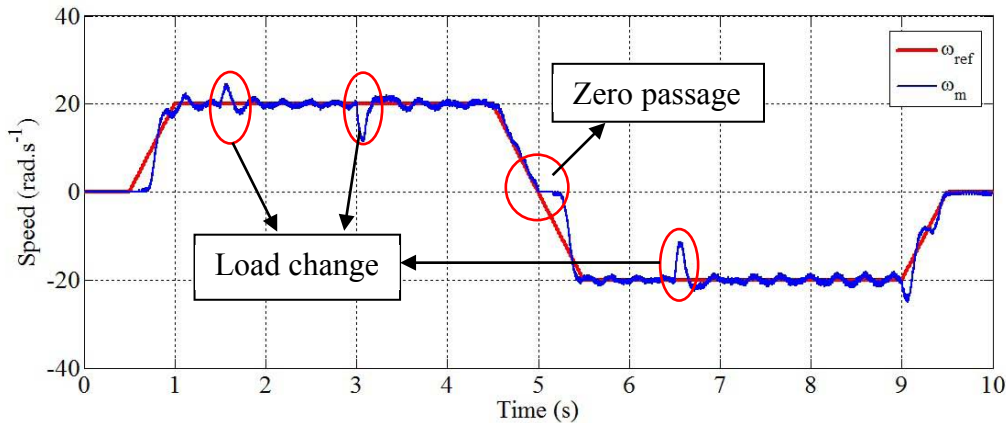


Figure 18: Réponse de vitesse de MSAP

Dans ce test, la fonction de coût est définie comme suit:

$$g = (i_{sq}^{ref} - i_{sq}(k+1))^2 + (i_{sd})^2$$

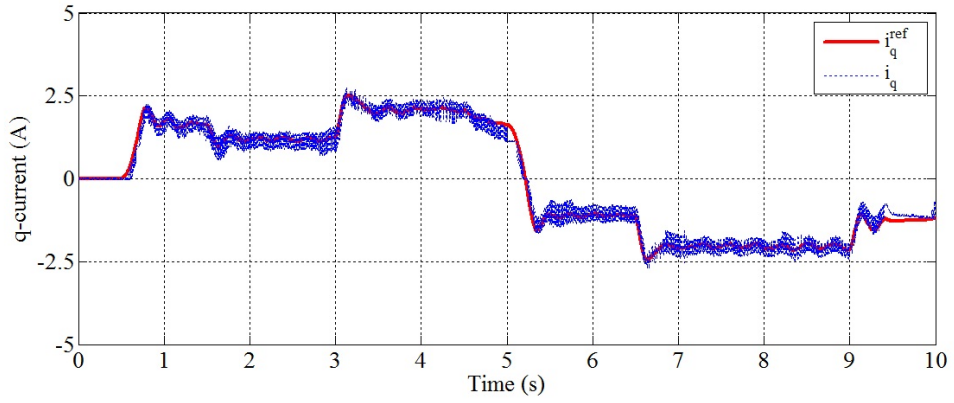
Par conséquent, le courant d-q de la machine est considéré sur la Figure 19.

### **Test avec deux machines en parallèle**

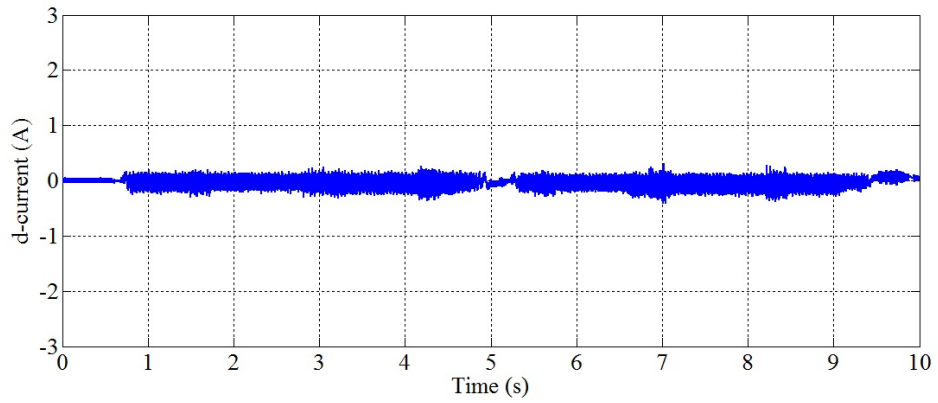
Dans ce test, les informations des deux machines sont considérées dans une seule fonction de coût:

$$g = (i_{sq1}^{ref} - i_{sq1}(k+1))^2 + (i_{sq2}^{ref} - i_{sq2}(k+1))^2 + (i_{sd1}(k+1))^2 + (i_{sd2}(k+1))^2$$

La position et les courants de phase de deux MSAPs sont mis à jour dans le bloc de contrôle PTC-SS chaque temps d'échantillonnage. Ces variables seront utilisées pour prédire l'évolution des deux machines dans la prochaine période. Le schéma du mécanisme de commande est présenté sur la Figure 20.



a) Courant sur l'axe q



b) Courant sur l'axe d

Figure 19: Courant sur les axes dq

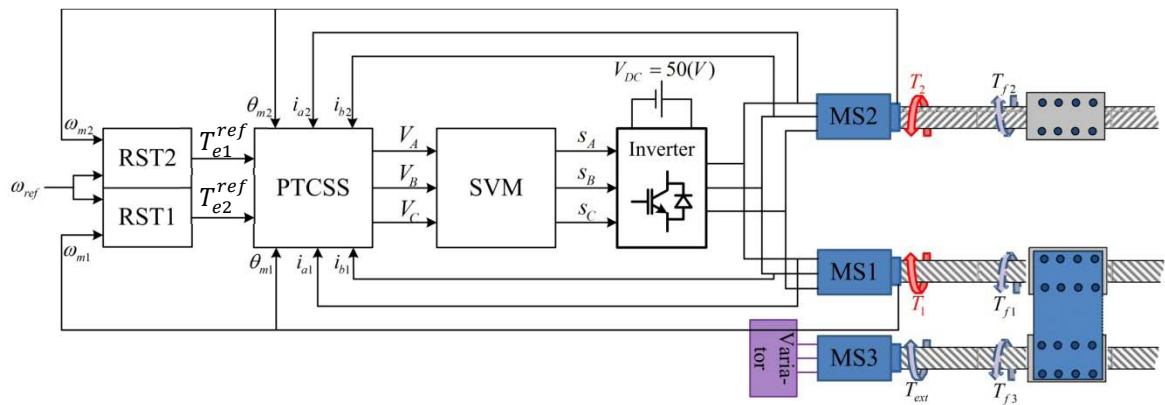


Figure 20: PTC-SS avec les deux MSAPs

D'après la Figure 20, la charge appliquée à SM2 est  $T_{f2}$ . Pendant ce temps la charge appliquée à SM1 est  $T_{f1} + T_{f3}$ . Dans ce test, le couple de SM3 est nul ( $T_{ext} \approx 0Nm$ ). Par conséquent, les charges entre les deux machines sont toujours légèrement différentes. Le test est réalisé avec la même valeur de consigne  $\omega_{ref} = 20(rad.s^{-1})$ . La référence de vitesse est inversée à  $t = 5s$ .

La réponse en vitesse des deux machines est représentée sur la Figure 21

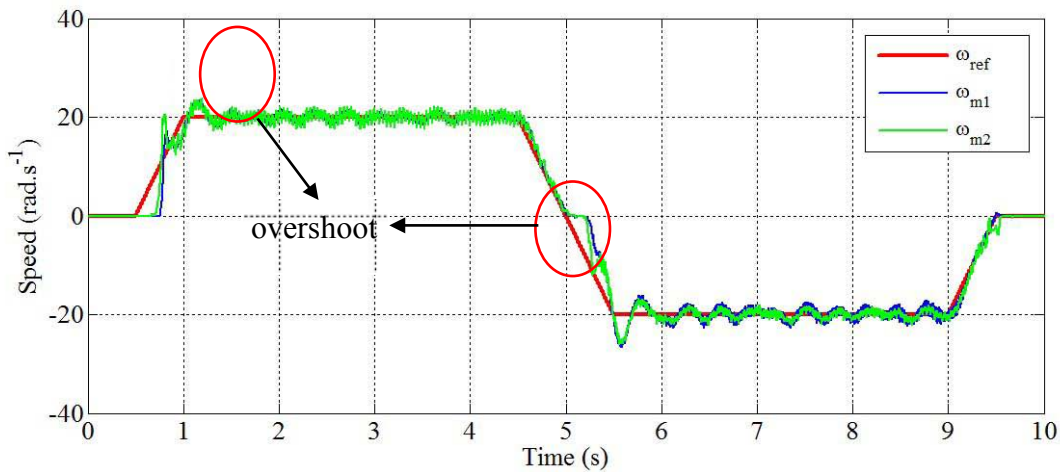


Figure 21: Réponse en vitesse de deux machines

Sur les Figure 23 et Figure 22, le courant dq de deux machines est présentée.

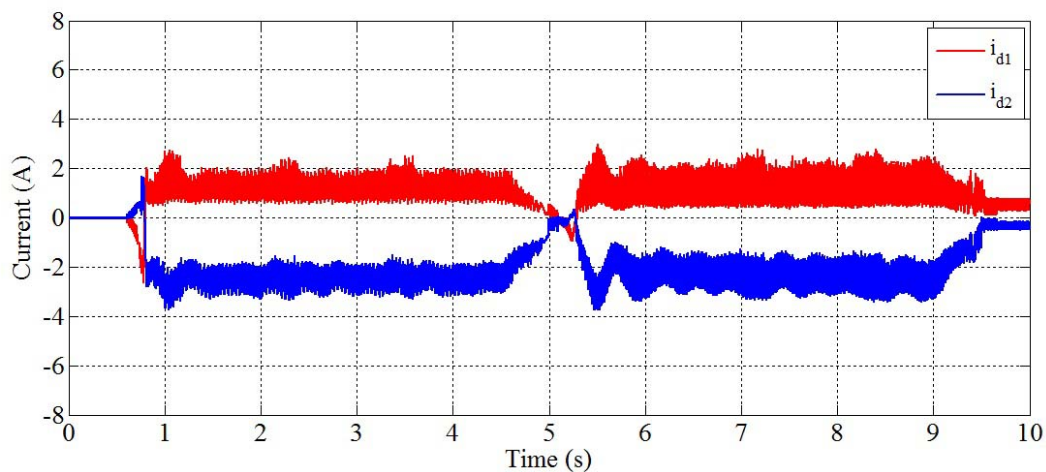


Figure 22: Courant sur l'axe d des deux machines

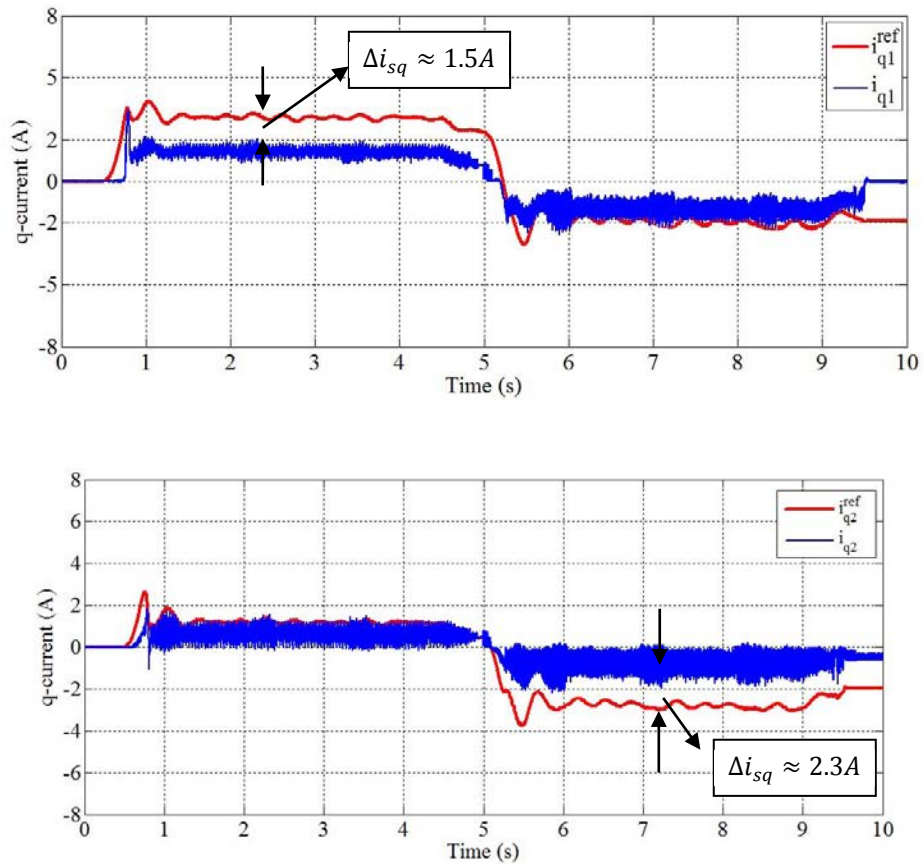


Figure 23: Courants sur l'axe q des deux machines

**Test avec deux machines en parallèle dans une configuration maître / esclave**

Dans ce test, la structure avec la configuration maître/esclave est utilisée avec l'algorithme PTC-SS. Le schéma du mécanisme de commande est indiqué sur la Figure 24.

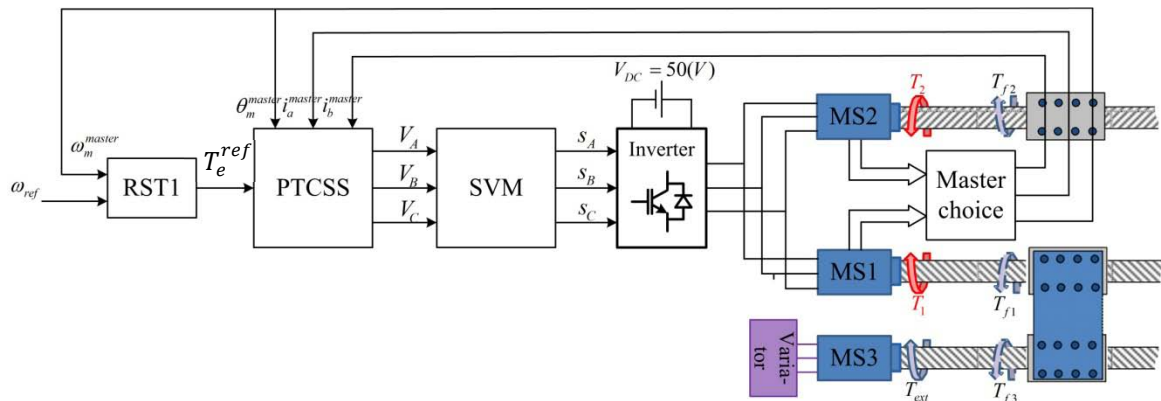


Figure 24: PTC-SS avec deux MSAPs en configuration maître/esclave

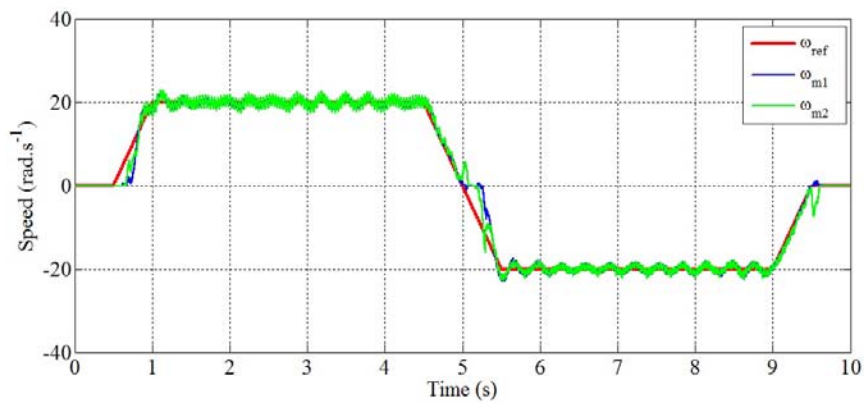


Figure 25: Réponse en vitesse des deux MSAPs en configuration maître/esclave

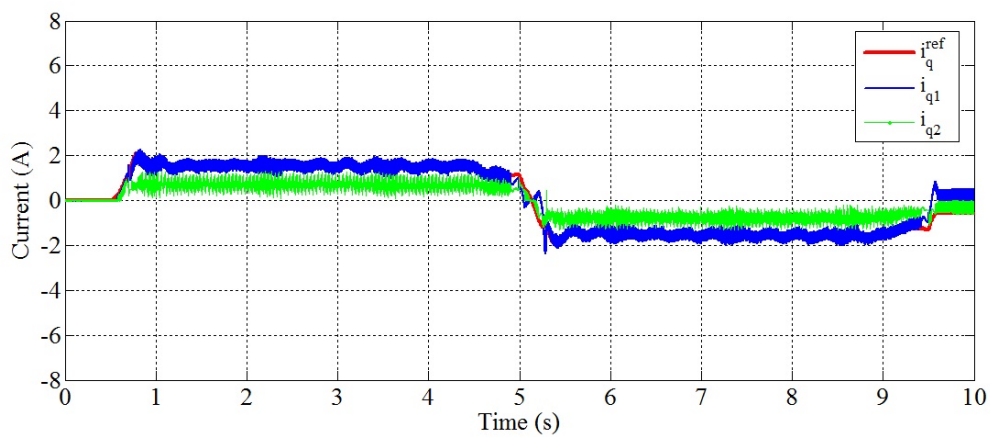


Figure 26: Courants sur l'axe q des deux machines

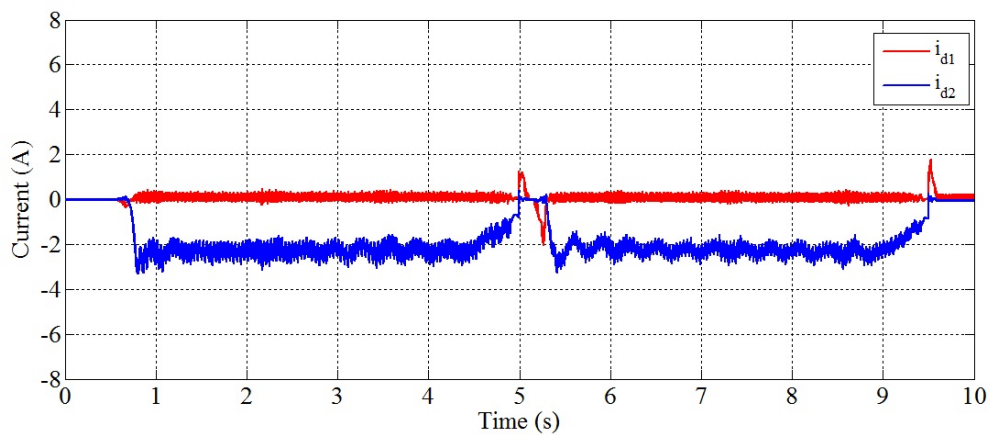


Figure 27: Courants sur l'axe d de deux machines

Selon cette structure, il existe toujours une seule machine commandée, à un instant donné. Par conséquent, le volume de calcul sera le même que dans le cas d'une machine seule et sera plus faible que dans le cas où on pilote les deux machines.

Sur la Figure 25, la réponse en vitesse des deux MSAPs est tracée et comparée avec la valeur de référence.

Les courants  $dq$  des deux machines sont représentées sur les Figure 26 et Figure 27. Parce que seulement la machine maître est contrôlée, la réponse de cette machine est bonne. Nous pouvons voir que le courant sur l'axe  $q$  de MS1. suit toujours la référence, et le courant sur l'axe  $d$  est maintenu proche de zéro.

Cependant, contrairement à la SM1, la machine esclave (SM2) ne respecte pas les références. La valeur du courant sur l'axe  $d$  est différente de zéro aussi.

## Conclusions

L'objectif principal de cette thèse est l'application d'une stratégie de commande prédictive à un système d'entraînement qui se compose de deux machines synchrones à aimants permanents (MSAP) reliées en parallèle alimentées par un onduleur triphasé de l'onduleur à deux niveaux.

Plusieurs analyses théoriques et des résultats de simulation ont été effectués afin de vérifier l'effet de cette approche. Les premiers résultats de l'expérience ont montré que le système d'entraînement peut fonctionner avec cette méthode. Bien que les résultats obtenus puissent être améliorés, la méthode PTC-SS constitue une nouvelle approche de la stratégie de commande prédictive. Sur la base de cette méthode, il est possible de développer une recherche dynamique afin de trouver le vecteur de tension le plus adéquat tout en cherchant à réduire le temps de calcul. Ceci fera l'objet de recherches futures.



## Appendix A

### "FMINCON" and SVM technique

A.1. Using FMINCON to solve the optimal problem:.....	168
A.2. Space vector modulation (SVM).....	169
A.2.1. Determine $V_\alpha$ , $V_\beta$ , $V_{ref}$ and angle $\alpha$ .....	170
A.2.2. Determine time duration $t_1$ , $t_2$ and $t_0$ .....	170
A.2.3. Determine the switching time of $(s_A, s_B, s_C)$ .....	171

## A.1 Using FMINCON to solve the optimal problem:

### Problem:

We need to find the minimum value of the cost function:

$$g = \left(i_{sq1}^{ref} - i_{sq1}(k+1)\right)^2 + \left(i_{sq2}^{ref} - i_{sq2}(k+1)\right)^2 + \left(i_{sd1}(k+1)\right)^2 + \left(i_{sd1}(k+1)\right)^2 \quad (A.1)$$

The constrain condition:

$$\begin{cases} -\frac{V_{DC}}{\sqrt{3}} \leq V_{\alpha} \leq \frac{V_{DC}}{\sqrt{3}} \\ -\frac{V_{DC}}{\sqrt{3}} \leq V_{\beta} \leq \frac{V_{DC}}{\sqrt{3}} \\ 0 \leq V_{\alpha}^2 + V_{\beta}^2 \leq \frac{V_{DC}^2}{3} \end{cases} \quad (A.2)$$

### Implementation:

- + Update the current state of the system:  $\theta_{m1}(k)$ ,  $\theta_{m2}(k)$ ,  $i_{abc1}(k)$ ,  $i_{abc2}(k)$ ;
- + Calculate the predictions
- + Receive the reference value of torque from the speed RST controller;
- + Build the cost function as presented in (A.1);
- + Create the start point for FMINCON function:  $x_0$  ;

### Run FMINCON:

The function which calculates the cost function is built as follow:

```
function [fval] = mf_f(x)
    %MF_F Summary of this function goes here
    % Detailed explanation goes here
    ip = Ad*i + Bd*Vdq + Pd;

    iq1ref = Tref1_image/(p*K*phif);
    iq2ref = Tref2_image/(p*K*phif);

    iref = [0;iq1ref;0;iq2ref];

    fval = sum((iref-ip).^2);
end
```

The constraint conditions are also declared in “mf\_noncons” function:

```
function [c, ceq] = mf_noncons(x)
    %MF_NONCONS Summary of this function goes here
    % Detailed explanation goes here
    c = x(1)^2 + x(2)^2 - E^2/3;
    ceq = [];
end
```

Run “fmincon”:

```
% Star the fmincon
lb = [-E/sqrt(3); -E/sqrt(3)];
ub = [E/sqrt(3); E/sqrt(3)];
Aeq = [];
beq = [];
A = [];
b = [];

opts = optimset('Algorithm', 'interior-point');

[x, fval] = fmincon(@mf_f, x0, A, b, Aeq, beq, lb, ub, @mf_noncons, opts);
```

## A.2 Space vector modulation (SVM)

This technique refers to a special switching sequence of the upper three power electronic components of the inverter. It has been shown to generate less harmonic distortion in the output voltages and/or currents applied to the phases of an AC motor and provide more efficient use of supply voltage compared with sinusoidal modulation technique as shown in Figure A.1.

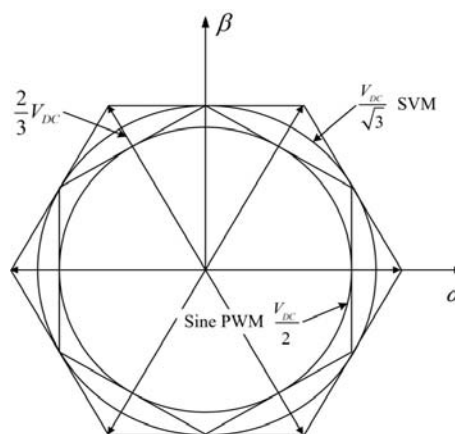


Figure A.1: Maximum voltage in SVM and Sine PWM

To implement the SVM, the voltage equations in the  $(abc)$  reference frame must be transformed into the stationary  $(\alpha\beta)$  reference frame. SVM technique will be implemented by the following steps:

- + Step 1: Determine  $V_\alpha$ ,  $V_\beta$ ,  $V_{ref}$  and the angle  $\alpha$  between the voltage vector and the  $\alpha$ -axis;
- + Step 2: Determine time duration  $t_1$ ,  $t_2$  and  $t_0$ ;
- + Step 3: Determine the switching time of each power electronic switch ( $s_A, s_B, s_C$ )

### A.2.1 Determine $V_\alpha$ , $V_\beta$ , $V_{ref}$ and angle $\alpha$

Considering the  $\alpha\beta$  coordinate, the  $\alpha$ -axis is chosen a lign with the  $a$ -axis. The link between two coordinate is shown in Equation

From this figure, the voltage vector  $\vec{V}_s$  can be represented in  $\alpha\beta$  frame according to the equation in (A.3):

$$\begin{bmatrix} V_\alpha \\ V_\beta \end{bmatrix} = \sqrt{\frac{2}{3}} \begin{bmatrix} 1 & -\frac{1}{2} & -\frac{1}{2} \\ 0 & \frac{\sqrt{3}}{2} & -\frac{\sqrt{3}}{2} \end{bmatrix} \begin{bmatrix} V_A \\ V_B \\ V_C \end{bmatrix} \quad (\text{A.3})$$

Consequently, the magnitude and angle will be obtained:

$$\begin{aligned} |V_{ref}| &= \sqrt{V_\alpha^2 + V_\beta^2} \\ \alpha &= \tan^{-1} \left( \frac{V_\beta}{V_\alpha} \right) \end{aligned} \quad (\text{A.4})$$

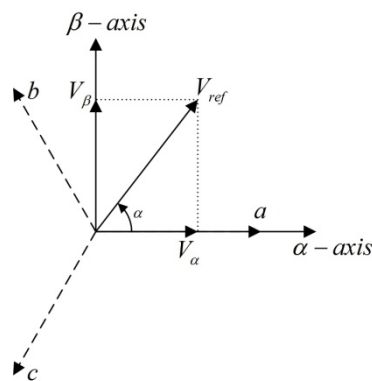


Figure A.2: Voltage space vector and its components in ( $\alpha\beta$ )

### A.2.2 Determine time duration $t_1$ , $t_2$ and $t_0/7$

From the , the switching time duration can be calculated as follows:

$$\begin{aligned}
 t_1 &= \frac{\sqrt{3}T_{pulse}|V_{ref}|}{V_{DC}} \left( \sin \left( \frac{\pi}{3} - \alpha + \frac{n-1}{3}\pi \right) \right) \\
 t_2 &= \frac{\sqrt{3}T_{pulse}|V_{ref}|}{V_{DC}} \left( \sin \left( \alpha - \frac{n-1}{3}\pi \right) \right) \\
 t_{0/7} &= T_{pulse} - t_1 - t_2
 \end{aligned} \tag{A.5}$$

where  $n = 1 \dots 6$  which is represented to sector 1 to 6,  $0 \leq \alpha \leq 60^\circ$ .

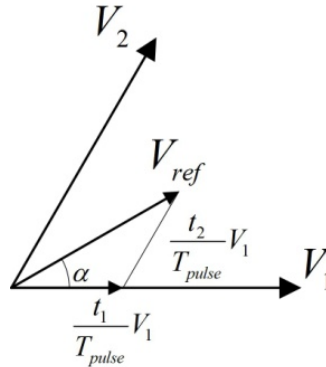
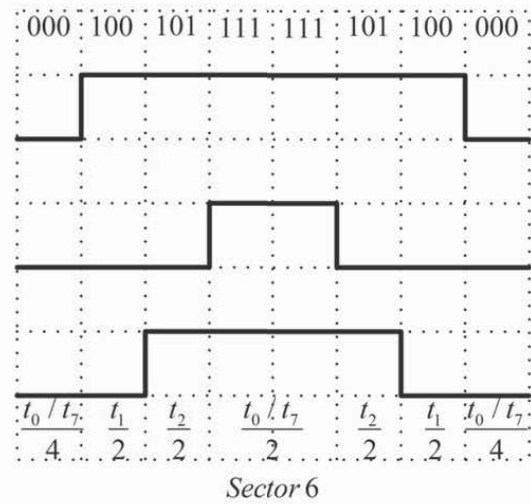
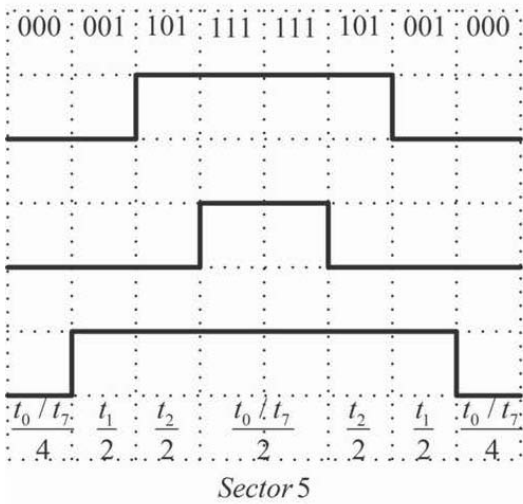
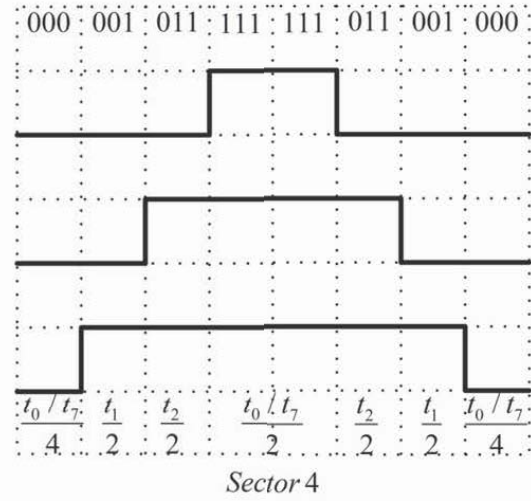
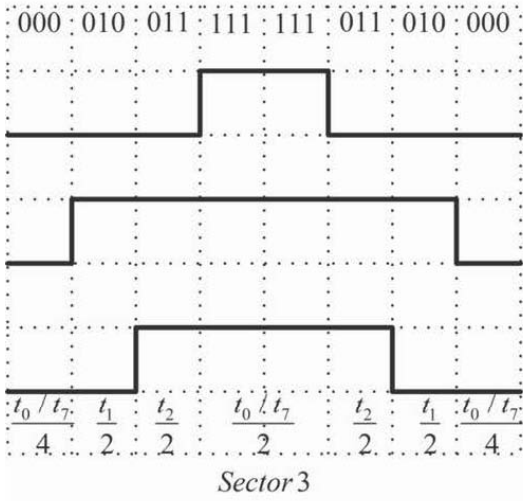
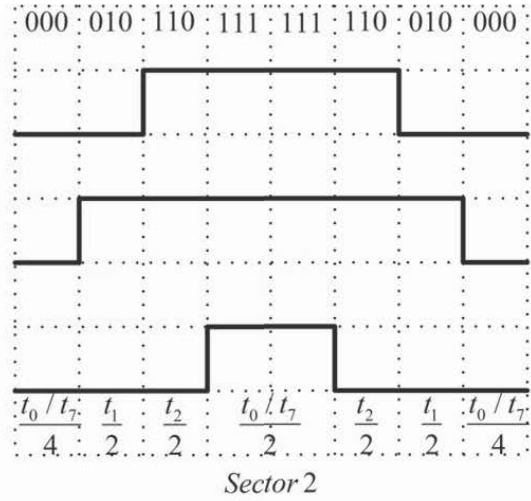
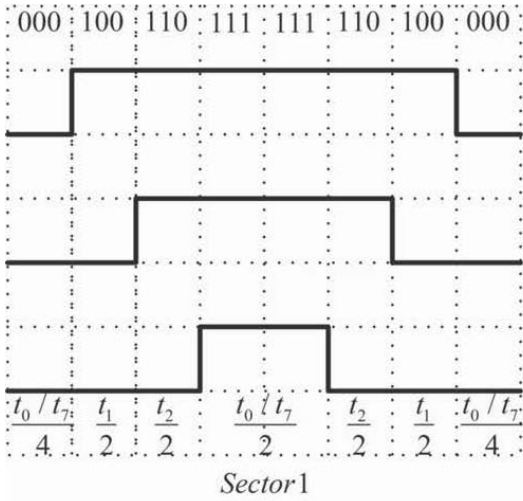


Figure A.3: Reference vector as a combination of adjacent vectors in sector 1

### A.2.3 Determine the switching time of ( $s_A, s_B, s_C$ )

Using the equation in (A.5), the switching time for the inverter's legs correlative with each sector can be calculated before generating to the inverter. This calculation is based on the principle of symmetric sequence in combination of basic voltage vectors.



Sector	Upper Switches ( $s_A, s_B, s_C$ )
<b>1</b>	$s_A = t_1 + t_2 + t_0/2$ $s_B = t_2 + t_0/2$ $s_C = t_0/2$
<b>2</b>	$s_A = t_1 + t_0/2$ $s_B = t_1 + t_2 + t_0/2$ $s_C = t_0/2$
<b>3</b>	$s_A = t_0/2$ $s_B = t_1 + t_2 + t_0/2$ $s_C = t_2 + t_0/2$
<b>4</b>	$s_A = t_0/2$ $s_B = t_1 + t_0/2$ $s_C = t_1 + t_2 + t_0/2$
<b>5</b>	$s_A = t_2 + t_0/2$ $s_B = t_0/2$ $s_C = t_1 + t_2 + t_0/2$
<b>6</b>	$s_A = t_1 + t_2 + t_0/2$ $s_B = t_0/2$ $s_C = t_1 + t_0/2$



## **Appendix B**

### **Technical data of the experimental**

---

B.1. The auto-transformer .....	176
B.2. The SEMIKRON device.....	176
B.2.1 The rectifier .....	176
B.2.2 The inverter .....	176
B.3. The PMSM .....	178
B.3.1 The motor .....	178
B.3.2 The holding brake.....	178
B.3.3 The resolver .....	179
B.4. Mechanical properties.....	180
B.4.1 Load machine .....	180
B.4.2 The SEC-AC-305 (Smart Electromotor Controller).....	180
B.4.3 Spindle axes with recirculating ball bearing guide.....	183
B.5. Hardware part of the control.....	185
B.5.1 DS1103 PPC Controller Board.....	185
B.5.2 Current sensors .....	188

---

B.5.3	Limit switches.....	190
B.6	The Human-Machine Interface.....	191

---

## B.1 The auto-transformer

The auto-transformer used is a TC 400/ 450/20 which is a product of Automelec society. This is a variable three-phase autotransformer, whose purpose is to:

- Adjust the value of the DC voltage  $V_{DC}$  imposed on the DC bus;
- Avoid a sudden change in voltage on the capacitors during startup.

In addition, thanks to its inductive nature, the auto-transformer smoothes the current which is returned to the EDF network.

The characteristics of this device are given in Table B.1

Parameters	Value	Unit
Primary voltage	400	V
Secondary voltage	0 – 450	V
Capacity	15600	VA
Intensity	20	A

Table B.1: Technical parameters of the auto-transformer

A three-phase voltage, whose amplitude is controlled by a control knob, can then be supplied to the rectifier device of SEMIKRON.

## B.2 The SEMIKRON device

### B.2.1 The rectifier

The rectifier is a three-phase diode rectifier type. In order to eliminate all harmonics, this rectified voltage is filtered immediately before putting into the inverter by two capacitors  $1\mu F$ . The inverter is powered by a DC voltage ranging from 0 to 400V.

### B.2.2 The inverter

The voltage inverter is composed of three legs. Each leg uses two IGBT switches, which are bidirectional in current, controllable. SKHI22 drivers which control each leg of

the inverter are supplied with a DC voltage of 15V. The control signals for drivers that provide switching commands use the C-MOS technology (0 – 15V).

In case of lack of power or an error occurring on one of the control signals, operating systems are blocked and an error signal is generated. If the error signal is not canceled, the inverter is blocked and the security of the system is assured. The driver is able to detect a short circuit in approximately 4 $\mu$ s, the IGBT can withstand a short circuit current up to 10 times the maximum current value (10  $\times$  50A), with a voltage 1200V for 10 $\mu$ s.

In order to protect the inverter against short circuits when IGBT of the same leg closes or opens, the device is integrated to another security module that generates a dead time ( $t_{dead} \approx 6\mu$ s) for each status change. The control signals applied to the drivers are inhibited during this time. The switching period is chosen  $T_{sw} = 100\mu$ s, the dead time corresponds to 6% of this period. It has no influence on the mechanical part of the system and few harmonics induced on the electrical quantities also do not play a role with regard to the study.

Parameters	Value	Unit
Nominal voltage	325	V
Rated current	4.3	A
Rated Torque	1.4	Nm
Rated speed	6250	rpm
Motor constant	0.32	Nm. A <sup>-1</sup>
EMF constant	0.27	Vs. rad <sup>-1</sup>
Resistance	0.955	$\Omega$
Inductance	1.65	mH
Peak current	10	A
Peak torque	3.1	Nm
Maximum speed	11640	rpm
Pairs of poles	4	

Table B.2: Technical parameters of PMSM (given by manufacturer)

In addition, the power modules that contain the IGBTs are protected against surges through resistance  $R_g$ . Settling speed of the current is then limited, which significantly reduces surges induced by parasitic inductances due to the cables.

The DC voltage bus is then transformed into a system of three-phase voltage  $V_{a,b,c}$  which is applied to both permanent magnet synchronous machines.

### B.3 The PMSM

The two PMSM used, denoted as SM1 and SM2 in this thesis, is a model of Festo manufacturer (motor MTR-AC-70-3S-AB).

These models are composed of a synchronous motor, a brake and a holding position sensor encoder type resolver.

#### B.3.1 The motor

It is a permanent magnet synchronous machine comprising a rotor and a stator. The characteristics of this motor is given by the manufacturer and shown in Table B.2

#### B.3.2 The holding brake

On machines “MTR-AC-70-3S-AB”, a failsafe brake holding current spring is built. To unlock the brake, a DC voltage  $U_{br}$  whose value is given in Table B.3 must be applied to the terminals of the electromagnet. This voltage, which is identical for the two motors, is created by a power supply and applied to the two brakes of the desired motor rotation.

Parameters	Value	Unit
Braked voltage	24	V
Braked power	11	W
Holding torque of the brake	1.5	Nm

Table B.3: Characteristics of holding brake

The power supplying to both the two motors and brakes is carried out by means of two shielded cables.

### B.3.3 The resolver

The absolute position of the rotor is achieved by a brushless resolver encoder. The absence of the electronic sliding contact can integrate the sensor directly into the machine, which gives it a long life.

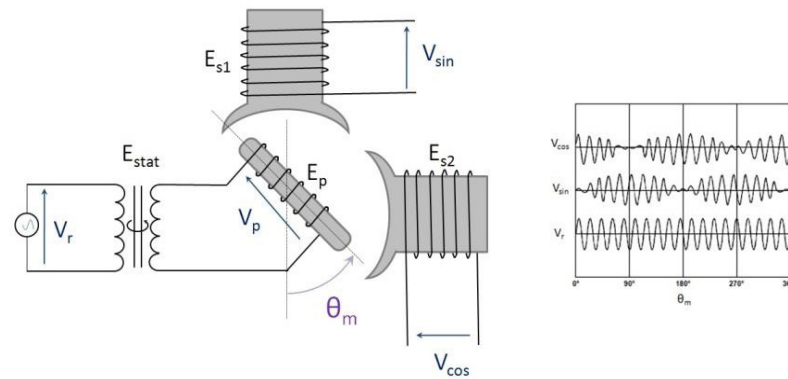


Figure B.1: Diagram of an encoder brushless resolver

Resolver operates as a rotary transformer: transformation ratio between the primary and secondary varies with the position of the primary windings, this position is related to the position  $\theta$ . As shown in Figure B.1, the brushless resolver comprises a primary winding to the rotor ( $E_p$ ) and two secondary windings ( $E_{s1}$ ,  $E_{s2}$ ), placed to the stator and mechanically shifted by  $90^\circ$ . A further winding ( $E_{stat}$ ) is placed on the stator.

Parameters	Value	Unit
Nominal voltage	325	V
Nominal current	5	A
Nominal torque	3.53	Nm
Nominal speed	4300	rpm
Peak current	20	A
Peak torque	12.2	Nm
Maximum speed	5320	rpm

Table B.4: Characteristics of the load machine

On  $E_{stat}$ , a reference sinusoidal voltage  $V_r$  with high frequency (10 kHz in the case of study) is applied. A magnetic field is created and an induced voltage appears across the primary winding ( $V_p$ ). Across  $E_{s1}$ ,  $E_{s2}$ , two signals of the same frequency and amplitude varying according respectively  $\cos \theta$  and  $\sin \theta$  are then induced.

These signals denoted  $V_{cos}$  and  $V_{sin}$  are analyzed by an analog device AD2S1200. This component, which also creates the signal  $V_r$ , is located on a card called “resolver card”. Signals are transferred to the two resolver card by two shielded cables.

## B.4 Mechanical properties

### B.4.1 Load machine

Load machine SM3 is the “MTR-AC-100-3S-AB” motor type from Festo company. This is a permanent magnet synchronous machine which is chosen from the series models like MS1 and MS2. Besides, a brake and a holding position sensor resolver are thus included in the model. The main features of the machine are given in Table B.4.

This machine is controlled by current (and thus torque) to produce an extra torque  $T_{ext}$  to SM1. The current control of SM3 is carried out by an industrial variable speed drive.

### B.4.2 The SEC-AC-305 (Smart Electromotor Controller)

The used controller, shown in Figure B.2, is the “SEC-AC-305” developed by Festo company. It has been designed for use in control cabinets for supplying AC servo motors and for controlling their torque (current), speed and position.

All technical specifications of this device is summary in Table B.5



Figure B.2: Variable speed drive SEC-AC-305 (Festo)

SEC-AC-305	
Power supply <ul style="list-style-type: none"> <li>• <math>V_{rated}</math></li> <li>• <math>V_{CC}</math></li> <li>• Current consumption 24 V</li> </ul>	<ul style="list-style-type: none"> <li>• 230 <math>V_{AC}</math>, 50/60 Hz or 310 <math>V_{DC}</math> with <math>U_{ZK}</math> supply</li> <li>• 24 <math>V_{DC} \pm 20\%</math> (Power supply of the electronics)</li> <li>• Approx. 0.35A</li> </ul>
Rated output <ul style="list-style-type: none"> <li>• With DC supply</li> <li>• With AC supply</li> </ul>	1500 VA 1000 VA
Peak power max. 10s	3000VA
Intermediate circuit voltage	Max. 340 V DC, 5 A
Rated current per phase	5 $A_{eff}$
Peak current per phase max. 10s	10 $A_{ff}$
Braking chopper Internal resistor (external extension only via additional braking module) <ul style="list-style-type: none"> <li>• Pulse output</li> <li>• Continuous output</li> <li>• Response threshold</li> <li>• Load tolerance</li> </ul>	100 $\Omega$ 1,3 kVA 25 W 375 0.5 : 25 s
Ambient temperature	0°C bis 50°C At rated output 1kW; motor current 5 $A_{eff}$ under following conditions: output reduction 30W/°C as from 35°C
Storage temperature	-25°C bis 60°C
Connecting cable to motor	Max. 50m, screened cable $C' < 200\text{pF/m}$ Depending on the system additional external

	mains filtes may be necessary in the power supply cables in order to comply with the EMC guidelines. By experience this applies to motor cable lengths > 5m.
Voltage endurance for cable	Min. 1500V
Nominal value inputs for speed and current	
• Ain0, Ain0/	$\pm 10V$ , $R_i = 20 k\Omega$ , offset adjust $\pm 0.1 V$
• Ain1, Ain1/	$\pm 10V$ , $R_i = 20 k\Omega$ , offset adjust $\pm 0.1 V$
Monitor settings	2 analogue outputs with 8-bit resolution at X1
• Output level	$\pm 10V$ voltage output, short-circuit resistant
• Representable variables	Freely standardized, e.g nominal and actual current values, rotary angle electric or mechanical, nominal and actual speed value
General logic inputs	Isolated, 12 ...30 V, active high
• Dino	• Bit 0 \
• Din1	• Bit 1, \ target selection for positioning
• Din2	• Bit 2, /16 destinations can be selected
• Din3	• Bit 3/ from destinations window
• Din4	• Control input for final output stage enable at high
• Din5	• Regulator enable at high, quit at low
• Din6	• Limit switch input 1
• Din7	• Limit switch input 2
• Din8	• Control signal start positioning
• Din9	• Control signal Sync for coupling in master-slave mode
• Reset (electrically)	Reset button on the front

General logic output	Electrically isolated
<ul style="list-style-type: none"> <li>• Dout0: ready-to-operate</li> <li>• Dout1: freely configurable</li> <li>• Dout2: freely configurable</li> <li>• Dout3: freely configurable</li> <li>• Dout4: holding brake</li> </ul>	<ul style="list-style-type: none"> <li>• 24 V, 100 mA via external 24 V supply</li> <li>• 24 V, 100 mA via external 24 V supply</li> <li>• 24 V, 100 mA via external 24 V supply</li> <li>• 24 V, 100 mA via external 24 V supply</li> <li>• 24 V, 500 mA via external 24 V supply</li> </ul>
Monitor settings	
<ul style="list-style-type: none"> <li>• Overvoltage in intermediate circuit</li> <li>• Undervoltage in intermediate circuit</li> <li>• Overcurrent in intermediate circuit</li> <li>• Thermo-protection of motor</li> <li>• Thermo-protection of final output stage</li> <li>• Fault in rotary angle sensor</li> </ul>	<ul style="list-style-type: none"> <li>• Approx. 400 V</li> <li>• Programmable, can be switched off</li> <li>• Short-circuit monitoring</li> <li>• Normally-closed contact</li> <li>• 100°C heat sink temperature</li> <li>• Common error</li> </ul>
Displays on device	
<ul style="list-style-type: none"> <li>• Ready-to-operate</li> <li>• Error and status messages</li> </ul>	<ul style="list-style-type: none"> <li>• LED</li> <li>• Seven-segment display</li> </ul>
Terminal interface	Serial
<ul style="list-style-type: none"> <li>• Level</li> <li>• Plug connector</li> </ul>	<ul style="list-style-type: none"> <li>• RS 232, 9600 ... 57600 bit/s</li> <li>• 9-pin. D-sub</li> </ul>
Interference emission	EN 50 081 part 2, basic standard industrial area
Immunity to interference	EN 50 081 part 2, basic standard industrial area

Table B.5: Technical parameters of PMSM (given by manufacturer)

### B.4.3 Spindle axes with recirculating ball bearing guide

Three axes used in this work are standard spindle axes with recirculating ball bearing guide (DGE-40-1000-SP-KG-KF-GK-SH) made by Festo company. This type of axis has a stroke-lengths from 100 to 2000 mm. It has some basic characteristics:

- Guides on these DGEs provides superior load and moment capacity;

- Use when medium to high loads need to be moved;
- Wide range of options for third-party motor mounting kits
- Comprehensive range of mounting accessories for multi-axis combinations.

The components of this axis are shown in Figure B.3 and the brief descriptions are pointed out in Table B.6

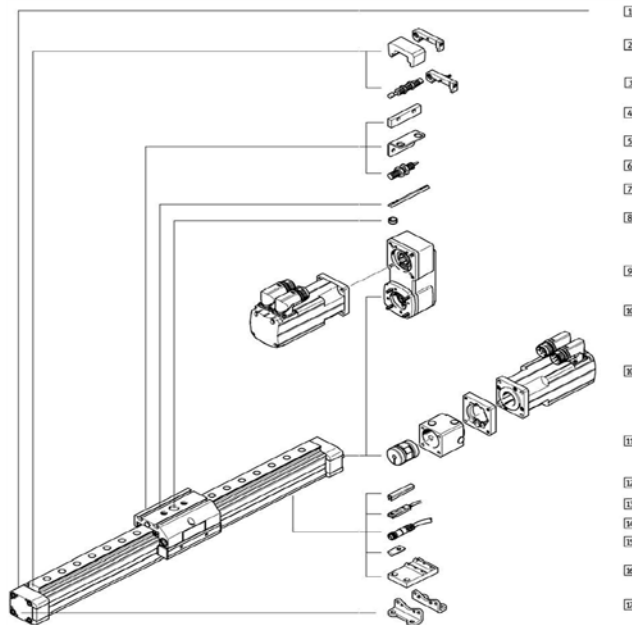


Figure B.3: A brief description of a ballscrew axis

Type	Brief description
[1] Spindle axis DGE-SP-KF	Electromechanical axis with spindle and recirculating ball bearing guide
[2] Emergency buffer with retainer A	For avoiding damage at the end stop in the event of malfunction
[3] Shock absorber kit C	For avoiding damage at the end stop in the event of malfunction
[3] Shock absorber kit E	For avoiding damage at the end stop in the event of malfunction
[4] Switching lug L	For sensing the slide position
[5] Sensor bracket T	Adapter for mounting the inductive proximity sensors on the axis
[6] Inductive proximity sensor O/P/R/W	For use as a signal generator and safety monitoring
[7] Slot nut for slide X	For mounting loads and attachments on the slide
[8] Centring pins/sleeves Z	For centring loads and attachments on the slide
[9] Parallel kit	For parallel motor attachment

EAMM-U	(consisting of: housing, clamping component, clamping sleeve, toothed belt gearwheel, toothed belt)
[10] Motor EMMS	Motors specially matched to the axis, with or without gearing, with or without brake
[11] Axial kit EAMM-A	For axial motor attachment (consisting of: coupling housing, clamping component, motor flange)
[12] Slot cover B/S	For protecting against the ingress of dirt
[13] Proximity sensor G/H/I/J/N	For use as a signal or safety check
[14] Cable with socket V	For proximity sensors
[15] Slot nut for mounting slot Y	For mounting attachments
[16] Central support M	For mounting the axis
[17] Foot mounting F	For mounting the axis

Table B.6: Brief description of a ballscrew axis

## B.5 Hardware part of the control

### B.5.1 DS1103 PPC Controller Board

The control board used in this work is DS1103 PPC Controller Board developed by dSPACE.

All technical specifications of this board is summarized in Table B.7

Parameter		Specification	
Processor	PowerPC Type	<ul style="list-style-type: none"> <li>• PPC 750GX</li> </ul>	
	CPU clock	<ul style="list-style-type: none"> <li>• 1 GHz</li> </ul>	
	Cache		<ul style="list-style-type: none"> <li>• 32 KB level 1 (L1) instruction cache</li> </ul>
			<ul style="list-style-type: none"> <li>• 32 KB level 1 (L1) data cache</li> </ul>
			<ul style="list-style-type: none"> <li>• 1 MB level 2 (L2)</li> </ul>
	Bus frequency	<ul style="list-style-type: none"> <li>• 133 MHz</li> </ul>	
Temperature sensor	<ul style="list-style-type: none"> <li>• Reads actual temperature at the PPC</li> </ul>		
Memory	Local memory	32 MB application SDRAM as program memory, cached	
	Global memory	96 MB communication SDRAM for data storage and data exchange with host	
2 general-purpose timers		<ul style="list-style-type: none"> <li>• One 32-bit down counter</li> <li>• Reload by software</li> <li>• 15-ns resolution</li> </ul>	
		<ul style="list-style-type: none"> <li>• One 32-bit up counter with compare register</li> <li>• Reload by software</li> <li>• 30-ns resolution</li> </ul>	

	1 sampling rate timer (decrementer)	<ul style="list-style-type: none"> <li>• 32-bit down counter</li> <li>• Reload by software</li> <li>• 30-ns resolution</li> </ul>
	1 timer base counter	<ul style="list-style-type: none"> <li>• 64-bit up counter</li> <li>• 30-ns resolution</li> </ul>
Interrupt controller		<ul style="list-style-type: none"> <li>• 3 timer interrupts</li> <li>• 7 incremental encoder index line interrupts</li> <li>• 1 UART (universal asynchronous receiver and transmitter) interrupt</li> <li>• 1 CAN interrupt</li> <li>• 1 slave DSP interrupt</li> <li>• 2 slave DSP PWM interrupts</li> <li>• 1 host interrupt</li> <li>• 4 external interrupts (user interrupts)</li> </ul>
A/D Converter	Channel	<ul style="list-style-type: none"> <li>• 16 multiplexed channels equipped with 4 sample &amp; hold A/D converters(4 channels belong to one A/D converter. 4 consecutive samplings are necessary to sample all channels belonging to one A/D converter.)</li> <li>• 4 parallel channels each equipped with one sample &amp; hold A/D converter</li> <li>• Note: 8 A/D converter channels (4 multiplexed and 4 parallel) can be sampled simultaneously</li> </ul>
	Resolution	<ul style="list-style-type: none"> <li>• 16-bit</li> </ul>
	Input voltage range	<ul style="list-style-type: none"> <li>• <math>\pm 10V</math></li> </ul>
	Overvoltage protection	<ul style="list-style-type: none"> <li>• <math>\pm 15V</math></li> </ul>
	Conversion time	<ul style="list-style-type: none"> <li>• Multiplexed channels: <math>1\mu s</math></li> <li>• Parallel channels: 800 ns</li> </ul>
	Offset error	<ul style="list-style-type: none"> <li>• <math>\pm 5\text{ mV}</math></li> </ul>
	Gain error	<ul style="list-style-type: none"> <li>• <math>\pm 0.25\%</math></li> </ul>
	Offset drift	<ul style="list-style-type: none"> <li>• <math>40\ \mu V/K</math></li> </ul>
	Gain drift	<ul style="list-style-type: none"> <li>• 50 ppm/K</li> </ul>
	Signal-to-noise ratio	<ul style="list-style-type: none"> <li>• <math>&gt;83\text{ dB}</math></li> </ul>
D/A Converter	Channels	<ul style="list-style-type: none"> <li>• 8 channels</li> </ul>
	Resolution	<ul style="list-style-type: none"> <li>• 16-bit</li> </ul>
	Output range	<ul style="list-style-type: none"> <li>• <math>\pm 10V</math></li> </ul>
	Settling time	<ul style="list-style-type: none"> <li>• <math>5\ \mu s</math> (14-bit)</li> </ul>
	Offset error	<ul style="list-style-type: none"> <li>• <math>\pm 1\text{ mV}</math></li> </ul>
	Gain error	<ul style="list-style-type: none"> <li>• <math>\pm 0.5\%</math></li> </ul>
	Offset drift	<ul style="list-style-type: none"> <li>• <math>30\ \mu V/K</math></li> </ul>
	Gain drift	<ul style="list-style-type: none"> <li>• 25 ppm/K</li> </ul>
	Signal-to-noise ratio	<ul style="list-style-type: none"> <li>• <math>&gt;83\text{ dB}</math></li> </ul>
	$I_{max}$	<ul style="list-style-type: none"> <li>• <math>\pm 5\text{ mA}</math></li> </ul>
	$CI_{max}$	<ul style="list-style-type: none"> <li>• 10 nF</li> </ul>
Digital I/O	Channels	<ul style="list-style-type: none"> <li>• 32-bit parallel I/O</li> <li>• Organized in four 8-bit groups</li> <li>• Each 8-bit group can be set to input or output</li> </ul>

		(programmable by software)
	Voltage range	<ul style="list-style-type: none"> <li>TTL input/output levels</li> </ul>
	$I_{out,max}$	<ul style="list-style-type: none"> <li><math>\pm 10</math> mA</li> </ul>
Digital incremental encoder interface	Channels	<ul style="list-style-type: none"> <li>6 independent channels</li> <li>Single-ended (TTL) or differential (RS422) input (software programmable for each channel)</li> </ul>
	Position counters	<ul style="list-style-type: none"> <li>24-bit resolution</li> <li>Max. 1.65 MHz input frequency, i.e., fourfold pulse count up to 6.6 MHz</li> <li>Counter reset or reload via software</li> </ul>
	Encoder supply voltage	<ul style="list-style-type: none"> <li>5 V/1.5 A</li> <li>Shared with analog incremental encoder interface</li> </ul>
Analog incremental encoder interface	Channels	<ul style="list-style-type: none"> <li>1 channel</li> <li>Sinusoidal signals: 1 Vpp differential or 11 <math>\mu</math>App differential (software programmable)</li> </ul>
	Position counters	<ul style="list-style-type: none"> <li><math>&lt; 5^\circ</math> resolution</li> <li>32-bit loadable position counter</li> <li>Max. 0.6 MHz input frequency, i.e., fourfold pulse count up to 2.4 MHz</li> </ul>
	A/D converter performance	<ul style="list-style-type: none"> <li>6-bit resolution</li> <li>10 MSPS</li> </ul>
	Encoder supply voltage	<ul style="list-style-type: none"> <li>5 V/1.5 A</li> <li>Shared with digital incremental encoder interface</li> </ul>
CAN interface	Configuration	<ul style="list-style-type: none"> <li>1 channel based on SAB 80C164 microcontroller</li> <li>ISO DIS 11898-2 CAN high-speed standard</li> </ul>
	Baud rate	<ul style="list-style-type: none"> <li>Max. 1 Mbit/s</li> </ul>
Serial interface	Configuration	<ul style="list-style-type: none"> <li>TL6C550C single UART with FIFO</li> <li>PLL-driven UART for accurate baud rate selection</li> <li>RS232/RS422 compatibility</li> </ul>
	Baud rate	<ul style="list-style-type: none"> <li>Up to 115.2 kbd (RS232)</li> <li>Up to 1 Mbd (RS422)</li> </ul>
Slave DSP	Type	<ul style="list-style-type: none"> <li>Texas Instruments TMS320F240 DSP</li> </ul>
	Clock rate	<ul style="list-style-type: none"> <li>20 MHz</li> </ul>
	Memory	<ul style="list-style-type: none"> <li>64Kx16 external code memory</li> <li>28Kx16 external data memory</li> <li>4Kx16 dual-port memory for communication</li> <li>32 KB flash memory</li> </ul>
	I/O channels	<ul style="list-style-type: none"> <li>16 A/D converter inputs</li> <li>10 PWM outputs</li> <li>4 capture inputs</li> <li>2 serial ports</li> </ul>
	Input voltage range	<ul style="list-style-type: none"> <li>TTL input/output level</li> <li>A/D converter inputs: 0 ... 5 V</li> </ul>
	Output current	<ul style="list-style-type: none"> <li>Max. <math>\pm 13</math> mA</li> </ul>
Host interface		<ul style="list-style-type: none"> <li>Plug &amp; Play support</li> <li>Requires a full-size 16-bit ISA slot</li> </ul>

Table B.7: Technical specification of DS1103 PPC Controller Board

The architecture of the card DS1103 with the link to the input/output of other devices is shown in Figure B.4.

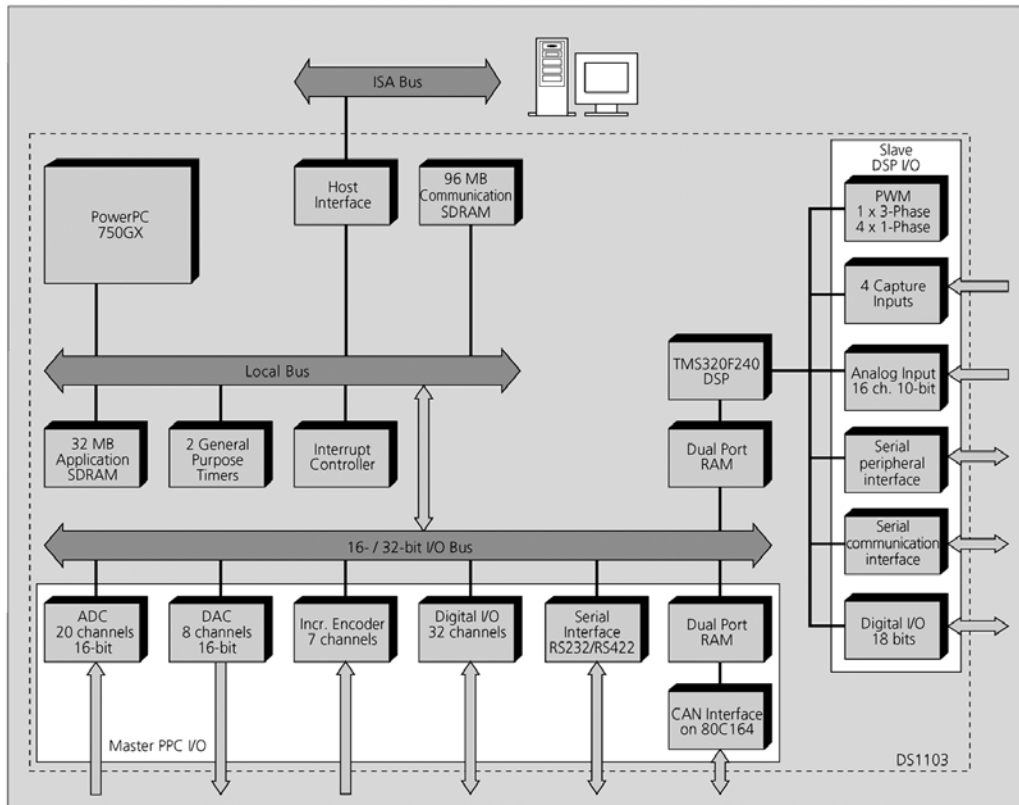


Figure B.4: Architecture of the card DS1103

### B.5.2 Current sensors

Instantaneous measurements of stator current are carried out by Hall sensor type LEM LA25-P.

During operation, these sensors provide an voltage correlated with the current according to the rate  $1V/A$ . The bandwidth of this sensor type is 150 kHz. The outputs of the sensors are connected to an analog input of the control board by the shielded coaxial cables. CAN bus accept a voltage between  $\pm 10V$  and a reduction ratio of ten. The digital signal is created under 12-bit and changing between -1 and +1.

The parameters of this sensor are presented below.



## Current Transducer LA 25-P

$I_{PN} = 25\text{ A}$

For the electronic measurement of currents : DC, AC, pulsed..., with a galvanic isolation between the primary circuit (high power) and the secondary circuit (electronic circuit).



### Electrical data

$I_{PN}$	Primary nominal r.m.s. current	25	A				
$I_p$	Primary current, measuring range	0 .. $\pm 55$	A				
$R_M$	Measuring resistance @	$T_A = 70^\circ\text{C}$		$T_A = 85^\circ\text{C}$			
			$R_{Mmin}$	$R_{Mmax}$	$R_{Mmin}$	$R_{Mmax}$	
		with $\pm 12\text{ V}$	@ $\pm 25\text{ A}_{max}$	10	280	60	275
			@ $\pm 55\text{ A}_{max}$	10	80	60	75
	with $\pm 15\text{ V}$	@ $\pm 25\text{ A}_{max}$	50	400	135	395	
		@ $\pm 55\text{ A}_{max}$	50	140	135	135	
$I_{SN}$	Secondary nominal r.m.s. current	25	mA				
$K_N$	Conversion ratio	1 : 1000					
$V_C$	Supply voltage ( $\pm 5\%$ )	$\pm 12 \dots 15$	V				
$I_C$	Current consumption	10 (@ $\pm 15\text{ V}$ ) + $I_S$	mA				
$V_S$	R.m.s. voltage for AC isolation test, 50 Hz, 1 mn	3	kV				

### Features

- Closed loop (compensated) current transducer using the Hall effect
- Printed circuit board mounting
- Insulated plastic case recognized according to UL 94-V0.

### Advantages

- Excellent accuracy
- Very good linearity
- Low temperature drift
- Optimized response time
- Wide frequency bandwidth
- No insertion losses
- High immunity to external interference
- Current overload capability.

### Accuracy - Dynamic performance data

$X$	Accuracy @ $I_{PN}$ , $T_A = 25^\circ\text{C}$	@ $\pm 15\text{ V}$ ( $\pm 5\%$ )	$\pm 0.95$	%
		@ $\pm 12 \dots 15\text{ V}$ ( $\pm 5\%$ )	$\pm 1.25$	%
$\epsilon_L$	Linearity error		< 0.15	%
$I_0$	Offset current @ $I_p = 0$ , $T_A = 25^\circ\text{C}$	Typ	Max	
$I_{OM}$	Residual current <sup>1)</sup> @ $I_p = 0$ , after an overload of $3 \times I_{PN}$		$\pm 0.2$	mA
$I_{OT}$	Thermal drift of $I_0$	0°C .. +70°C	$\pm 0.1$	$\pm 0.5$
		-25°C .. +85°C	$\pm 0.1$	$\pm 0.6$
$t_{90}$	Reaction time @ 10 % of $I_{p,max}$	< 500		ns
$t_r$	Response time @ 90 % of $I_{p,max}$	< 1		$\mu\text{s}$
$di/dt$	di/dt accurately followed	> 200		A/ $\mu\text{s}$
$f$	Frequency bandwidth (-1 dB)	DC .. 200		kHz

### Applications

- AC variable speed drives and servo motor drives
- Static converters for DC motor drives
- Battery supplied applications
- Uninterruptible Power Supplies (UPS)
- Switched Mode Power Supplies (SMPS)
- Power supplies for welding applications.

### General data

$T_A$	Ambient operating temperature	-25 .. +85	°C
$T_S$	Ambient storage temperature	-40 .. +90	°C
$R_S$	Secondary coil resistance @	$T_A = 70^\circ\text{C}$	80
		$T_A = 85^\circ\text{C}$	85
$m$	Mass Standards		24
			EN 50178 : 1997

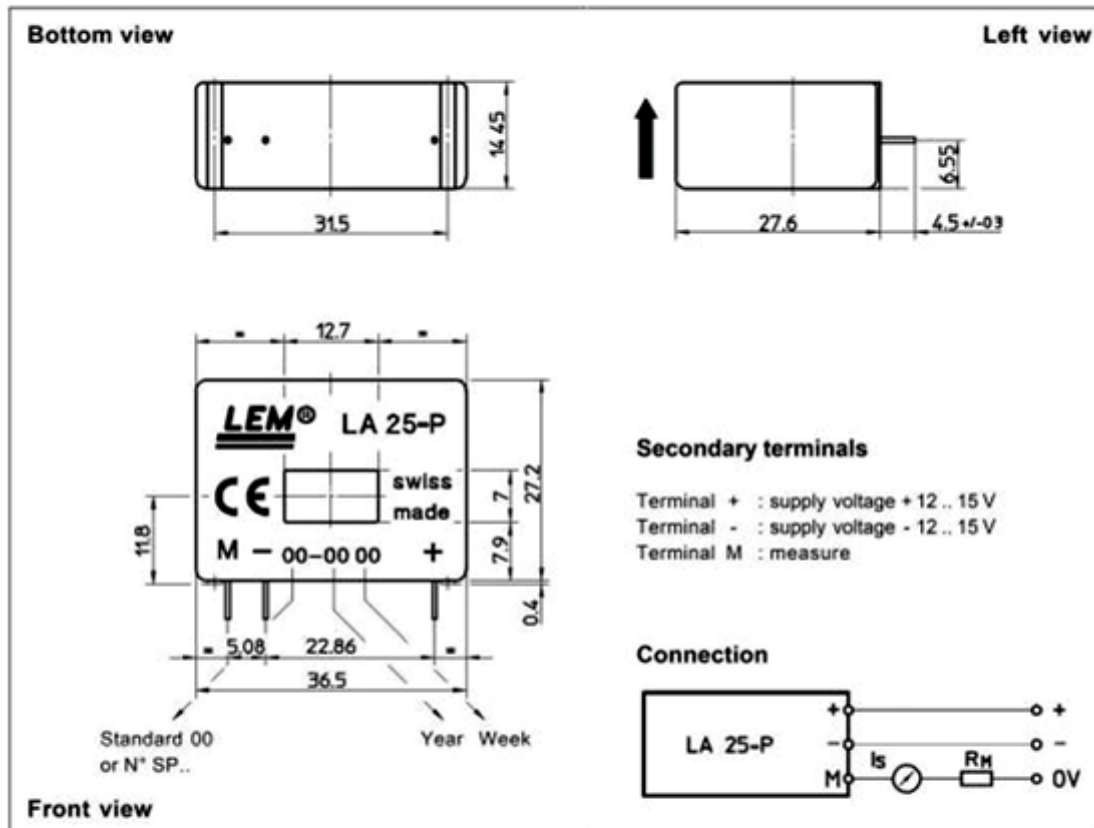
Notes : <sup>1)</sup> Result of the coercive field of the magnetic circuit.

LEM reserves the right to carry out modifications on its transducers, in order to improve them, without previous notice.

060303/2  
page 1/2

LEM

www.lem.com


**Dimensions LA 25-P** (in mm, 1 mm = 0.0394 inch)

**Mechanical characteristics**

• General tolerance	± 0.2 mm
• Primary through-hole	12.7 x 7 mm
• Fastening & connection of secondary	3 pins
	0.63 x 0.56 mm
Recommended PCB hole	0.9 mm

**Remarks**

- $I_p$  is positive when  $I_p$  flows in the direction of the arrow.
- Temperature of the primary conductor should not exceed 90°C.
- Dynamic performances (di/dt and response time) are best with a single bar completely filling the primary hole.
- In order to achieve the best magnetic coupling, the primary windings have to be wound over the top edge of the device.
- This is a standard model. For different versions (supply voltages, turns ratios, unidirectional measurements...), please contact us.

### B.5.3 Limit switches

In order to limit the end positions of the axes of an uncontrolled overflow, sensors are placed at the end of the race trucks. If one of these sensors is activated (when one of the carriages reaches to the end of an axis), the command is configured to turn off the power immediately.

The used sensors are inductive typed position sensors (HIS-M8BPO-SL from Festo), powered by a DC voltage of 24V. At its end, the coil of such a sensor creates an oscillating magnetic field (generated by a coil and a capacitor connected in parallel). As the field

oscillates, the sensor is considered “active” and delivers a DC voltage ( $f_{dc} = 1$ ). When the metal plate enters this field, it is disturbed and then reduced. The attenuation of this field then disables the sensor. No voltage produces ( $f_{dc} = 0$ ). Four digital input are then reserved for these sensors. A logic circuit allows the power delivery until all sensors are activated to the high state.

## B.6 The Human-Machine Interface

As explained in the thesis, the programming of the DS1103 card is carried out through the use of RTI library compatible with Matlab/SIMULINK.

After compiling the program to this card, ControlDesk interface software will be used to build a human-machine interface (HMI). The HMI will provide all the necessary functions for controlling, data acquisition and modification of the parameters of Simulink block in real time. The acquired data can then be saved as “.mat” data file and processed by Matlab.

A screenshot of HMI is presented in Figure B.5.

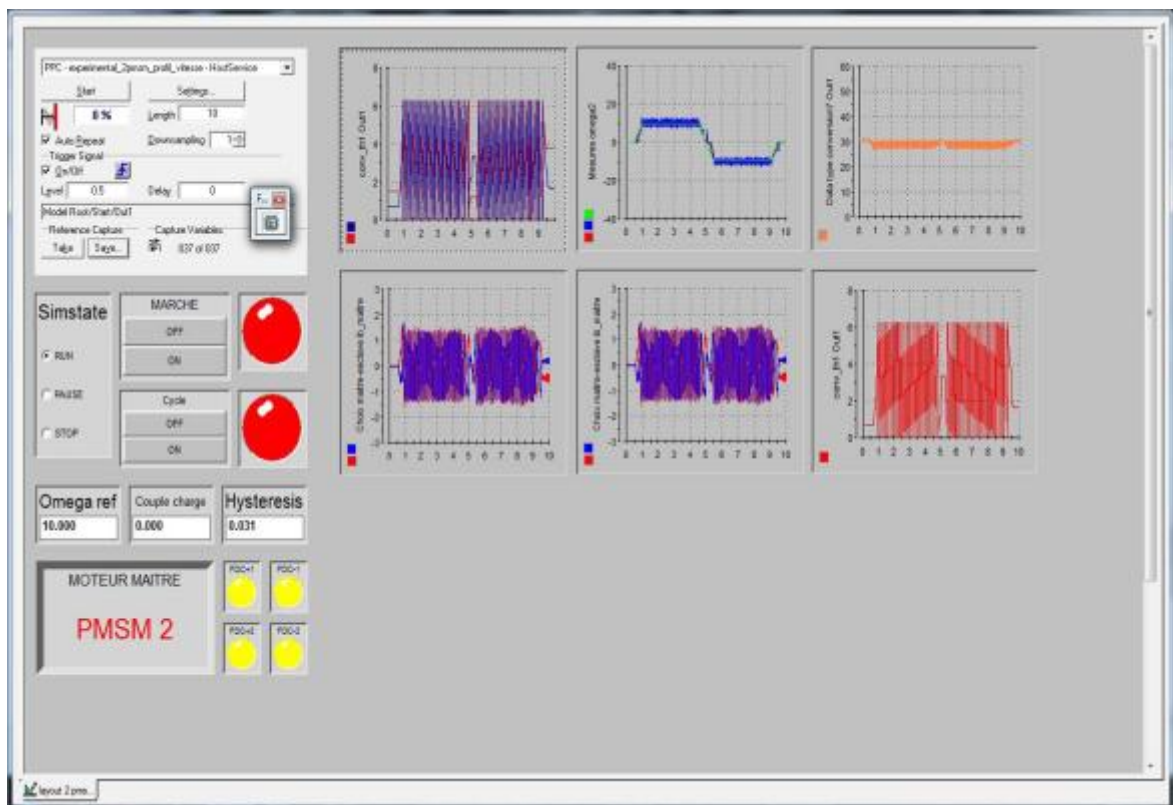


Figure B.5: Human-machine interface



# List of figures

## Main parts

Figure 1.1: Multi-Machine System MS(m,n) .....	6
Figure 1.2: Two main types of PMSM .....	8
Figure 1.3: Examples of application of brushless motors in small power range .....	9
Figure 1.4: Examples of applications of brushless motors in medium power range .....	10
Figure 1.5: Examples of applications of brushless motors in high power range .....	11
Figure 1.6 The possibility of using PMSM in aeronautics [All95] .....	13
Figure 1.7: Flight control actuation systems [Nfo06] .....	13
Figure 1.8: Wing of an airbus A300 .....	14
Figure 1.9: An advanced Motor Device EMA .....	14
Figure 1.10: Direct drive architecture for EMA [ROAR07] .....	16
Figure 1.11: The classical structure multi-machine multi-inverter MS(3n,n) .....	17
Figure 1.12: Diagram of voltage vectors under structure MS(3n,n) .....	18
Figure 1.13: The structure using a common leg $MS\left(\frac{4n}{2}, n\right)$ .....	19
Figure 1.14: Diagram of voltage vectors under structure $MS\left(\frac{4n}{2}, n\right)$ .....	19
Figure 1.15: The structure sharing the midpoint MS(2n, n) .....	21
Figure 1.16: Diagram of voltage vectors under the structure MS(2n, n) .....	21
Figure 1.17: Mixed structure $MS\left(\frac{3n}{2}, n\right)$ .....	22
Figure 1.18: Diagram of voltage vectors under mixed structure: $MS\left(\frac{3n}{2}, n\right)$ .....	23
Figure 1.19: Parallel structure MS(3, n) .....	24
Figure 2.1: Mono-inverter dual-parallel PMSM drive .....	28
Figure 2.2: Structure of a PMSM drive system .....	29
Figure 2.3: Stator windings of a three-phase PMSM 2 pole pairs .....	30
Figure 2.4: Two-pole three-phase PMSM .....	32
Figure 2.5: Electrical model of one phase of PMSM .....	33
Figure 2.6: Equivalent circuit of a PMSM in d-q frame .....	36
Figure 2.7: Evolution of $T_e = f(\delta)$ with the consideration of $R_s$ .....	37
Figure 2.8: Evolution of $T_e = f(\delta)$ without consideration of $R_s$ .....	38
Figure 2.9: Diagram of a three-phase two-level inverter .....	39
Figure 2.10: General scheme of FOC for a PMSM .....	40

Figure 2.11: General scheme of DTC for a PMSM .....	41
Figure 2.12: The basic voltage vectors and six sectors.....	42
Figure 2.13: Circular trajectory of stator flux linkage in DTC .....	42
Figure 2.14: The evolution of torque under DTC .....	43
Figure 2.15: General scheme of DPTC for PMSM.....	44
Figure 2.16: Parallel structure under master/slave configuration .....	46
Figure 2.17: Evolution of system under master/slave configuration with different loads..	49
Figure 2.18: Voltage vector diagram of two PMSM under different loads .....	51
Figure 2.19: Master choice block.....	50
Figure 2.20: General scheme of DTC for dual-parallel PMSM drive system .....	53
Figure 2.21: Different situation for selecting a suitable voltage vector.....	55
Figure 2.22: Average rule .....	56
Figure 2.23: Two vectors are adjacent.....	56
Figure 2.24: The evolution of reference value.....	61
Figure 2.25: The variation of load of each machine in simulation .....	62
Figure 2.26: Responses of system under DTC.....	63
Figure 3.1: dq-current at steady state of a PMSM .....	70
Figure 3.2: Load angle at steady state.....	71
Figure 3.3: Limit in operation of a PMSM .....	71
Figure 3.4: Map of roots of $P_s$ .....	73
Figure 3.5: Example of limitation of stable zone of a PMSM .....	74
Figure 3.6: PTC for Mono-Inverter Dual-parallel PMSM drive system.....	74
Figure 3.7: The R-S-T digital controller [Lan98] .....	75
Figure 3.8: RST anti-windup Speed/Torque controller for a PMSM .....	77
Figure 3.9: A standard three-phase two-level inverter.....	80
Figure 3.10: Two strategies for predictive control [LKKS10].....	84
Figure 3.11: Direct predictive torque control (DPTC) scheme.....	85
Figure 3.12: Flow chart of direct predictive control algorithm.....	86
Figure 3.13: The evolution of reference value.....	87
Figure 3.14: The variation of load of each machine in simulation .....	87
Figure 3.15: Speed of two machines .....	88
Figure 3.16: Electromagnetic torque of two machines .....	89
Figure 3.17: Currents in d-q frame for two machines.....	89
Figure 3.18: Ripple in torque under different sampling time for DPTC.....	90
Figure 3.19: “FMINCON” procedure .....	92

List of figures	195
Figure 3.20: Simulation results after optimization process	93
Figure 3.21: Control region of a three-phase two-level inverter including the virtual states	95
Figure 3.22: PTC – “Split and Seek” approach	97
Figure 3.23: Two adjacent sectors with virtual voltages	98
Figure 3.24: Diagram of the new solution	98
Figure 3.25: Responses of system under PTC-SS	100
Figure 3.26: A-phase current of two machines	103
Figure 3.27: Spectrum of A-phase current of machine 1	104
Figure 3.28: Spectrum of A-phase current of machine 2	104
Figure 4.1: Presentation of the experimental bench	108
Figure 4.2: Motor coupling system	110
Figure 4.3: Structure of a ballscrew axis	111
Figure 4.4: Power supply system	112
Figure 4.5: Reading of $\theta_{m1}$ and $\theta_{m2}$ : Hardware part	114
Figure 4.6: Example of filtering speed	115
Figure 4.7: Interrupt signal	117
Figure 4.8: RST controller block with anti-windup	118
Figure 4.9: PTC-SS applied to one PMSM	120
Figure 4.10: Variation of load during the test	120
Figure 4.11: Speed response of PMSM	121
Figure 4.12: Current in q-axis	121
Figure 4.13: Current in d-axis	122
Figure 4.14: PTC-SS with two PMSMs	123
Figure 4.15: Speed response of two PMSMs	123
Figure 4.16: Current in q-axis of both machines	124
Figure 4.17: Current in d-axis of both machines	124
Figure 4.18: PTC-SS with two PMSMs under master/slave	125
Figure 4.19: Speed response of two PMSMs under master/slave configuration	126
Figure 4.20: Current in q-axis of both machines	126
Figure 4.21: Current in d-axis of both machines	126

### **Résumé en français**

Figure 1: Deux principaux types de MSAP	143
Figure 2: Utilisation des MSAP en aéronautique	145
Figure 3: Système de contrôle des surfaces de vol	145

Figure 4: Structure classique multimachine/multionduleur SM(3n,n).....	146
Figure 5: Structure typiques pour les systèmes multimachines.....	147
Figure 6: Mono-onduleur dual-parallèle MSAP.....	149
Figure 7: La structure parallèle avec maître/esclave.....	150
Figure 8: Commande directe de couple.....	151
Figure 9: Different cases for selecting a suitable voltage vector.....	152
Figure 10: Commande Directe de Couple (DPTC).....	153
Figure 11: Schéma de l'algorithme de commande.....	154
Figure 12: PTC – “Split and Seek” schema.....	155
Figure 13: La région de contrôle d’onduleur avec vecteurs virtuelles.....	155
Figure 14: Deux vecteurs adjacents et vecteurs virtuels.....	156
Figure 15: Diagramme de la nouvelle solution.....	157
Figure 16: Présentation du banc expérimental.....	158
Figure 17: PTC-SS appliqué à une MSAP.....	159
Figure 18: Réponse de vitesse de MSAP.....	160
Figure 19: Courant dans dq-axes.....	161
Figure 20: PTC-SS avec les deux MSAPs.....	161
Figure 21: Speed response of two PMSMs.....	162
Figure 22: Courant dans l'axe q de deux machines.....	163
Figure 23: Courant dans l'axe d de deux machines.....	162
Figure 24: PTC-SS avec deux PMSMs sous maître / esclave.....	163
Figure 25: Réponse de vitesse de deux MSAPs sous configuration maître / esclave.....	164
Figure 26: Courant dans l'axe q de deux machines.....	164
Figure 27: Courant dans l'axe d de deux machines.....	164

## Appendix

Figure A.1: Maximum voltage in SVM and Sine PWM.....	169
Figure A.2: Voltage space vector and its components in $(\alpha\beta)$ .....	170
Figure A.3: Reference vector as a combination of adjacent vectors in sector 1.....	171
Figure B.1: Diagram of an encoder brushless resolver.....	179
Figure B.2: Variable speed drive SEC-AC-305 (Festo).....	180
Figure B.3: A brief description of a ballscrew axis.....	184
Figure B.4: Architecture of the card DS1103.....	188
Figure B.5: Human-machine interface.....	191

# List of tables

## Main parts

Table 1.1: Summary of different structures .....	26
Table 2.1: Optimal switching table for DTC control.....	43
Table 2.2: Table of the evolution of torque and flux of two PMSMs in parallel .....	54
Table 2.3: Table of optimal voltage vectors for two PMSMs .....	57
Table 2.4: Table of optimal voltage vectors for two PMSMs ( $S_{12} \rightarrow S_{34}$ ).....	59
Table 2.5: Table of optimal voltage vectors for two PMSMs ( $S_{43} \rightarrow S_{65}$ ).....	60
Table 2.6: Parameters of machine using in simulation.....	61
Table 3.1: Parameters of PMSM.....	68
Table 3.2: Eight real states of a three-phase two-level inverter.....	80
Table 3.3: Cost functions with secondary terms.....	82
Table 3.4: The total losses of two machines.....	102
Table 3.5: The fundamental and THD values.....	105
Table 4.1: Parameters of speed controller .....	119

## Résumé en français

Table 1: Résumé des différentes structures .....	148
Table 2: Table de correspondance entre le flux et le couple pour 2 machines en parrallèle .....	151

## Appendix

Table B.1: Technical parameters of the auto-transformer.....	176
Table B.2: Technical parameters of PMSM (given by manufacturer).....	177
Table B.3: Characteristics of holding brake .....	178
Table B.4: Characteristics of the load machine.....	179
Table B.5: Technical parameters of PMSM (given by manufacturer).....	183
Table B.6: Brief description of a ballscrew axis.....	185
Table B.7: Technical specification of DS1103 PPC Controller Board.....	187